MICHIGAN STATE UNIVERSITY

CYCLOTRON LABORATORY

ENERGETIC PARTICLE EMISSION IN NUCLEAR REACTIONS

DAVID H. BOAL

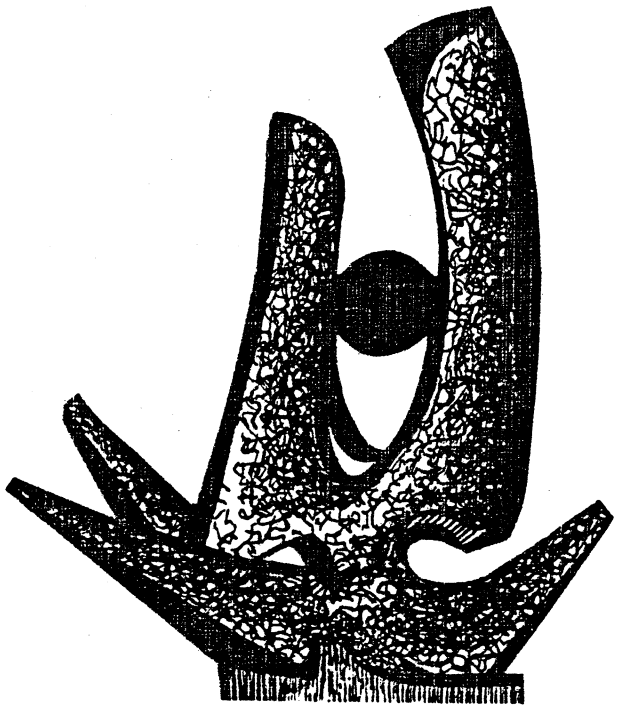

FEBRUARY 1984

MSUCL-451

MSUCL-451
February 1984

ENERGETIC PARTICLE EMISSION IN NUCLEAR REACTIONS*

by

David H. Boal

National Superconducting Cyclotron Laboratory
Michigan State University
East Lansing, Michigan 48824, USA

and

Department of Physics†
Simon Fraser University
Burnaby, B.C., Canada

*To be published in Advances in Nuclear Physics, J.W. Negele and E. Vogt, editors.

†Permanent address

Table of Contents

1. Introduction 1

2. Direct Interactions in the Nucleus
   2.1 Quasi-elastic Scattering 7
   2.2 Theoretical Models 10
   2.3 Coincidence Experiments as a Probe of Reaction Mechanisms 18

3. Thermalization and Multiple Scattering in Nucleon Emission
   3.1 The Approach to Thermal Equilibrium 25
   3.2 Is Chemical Equilibrium Achieved? 34
   3.3 Cascade and Hydrodynamics 44
   3.4 A Limiting Temperature in the Hadronic Medium? 48
   3.5 Hanbury-Brown/Twiss Effect in the Nucleus 51

4. Light Fragment Formation
   4.1 Overview 59
   4.2 Coalescence and Pickup Models 61
   4.3 Statistical Models 69
   4.4 Nuclear Entropy 73
   4.5 Results from Coincidence Experiments 75

5. Production of Intermediate Mass Fragments
   5.1 Statistical Approach 79
   5.2 Reaction Rates 85
   5.3 Liquid-Vapor Phase Transitions 89

6. Summary 99

7. Acknowledgments 104

8. Appendix 105

9. References 111

1. Introduction

When a projectile with several hundred MeV kinetic energy per nucleon interacts with a target nucleus, a very large number of final states are available in the interaction. A significant fraction of the reaction products will be ejectiles of more than a few nucleons. Certainly nucleon emission dominates, but the yields of higher mass fragments are also substantial. Further, a large portion of the integrated cross section comes from emission of particles with more than a few MeV per nucleon of kinetic energy, that is, with energies beyond those associated with emission from a large system of nucleons in thermal and chemical equilibrium. For example, shown in Fig. 1 is a recent analysis of proton induced fragment emission from a silver target at 480 MeV (GKJ 83). Shown is the percentage of the reaction products which these authors estimate arises from non-evaporative processes, (that is, an evaporation model fit is made to the evaporative part of the light ion differential cross section, the resulting prediction for heavy fragments then being compared with the data) processes which will be called pre-equilibrium here. Because energetic fragment production is such a common reaction channel for both proton and heavy ion induced reactions, it has become a currently popular area of study from both experimental and theoretical viewpoints.

For the experimentalist, the cross sections are large and hence an extensive body of data for a wide variety of projectile-target-ejectile combinations has been collected. Many different experimental techniques have been used as well. Among the earliest of these was the nuclear chemistry approach, which gave the total yield of various nuclei in a reaction. Of course, the technique has its greatest strength in the higher mass fragments since it generally involves either measuring some decay mode of a particular product nucleus after the reaction, or determining via chemical separation

techniques the absolute yield of a particular species. Although much of the work done using these methods involves total cross section measurement, it can be extended to determine differential cross sections by the use of catcher foils. A description of many of the techniques involved can be found in MH 59.

A somewhat more modern approach uses solid state detectors to identify and measure the energy of ejectiles. Differential cross section data as a function of energy and angle of the ejectile are now becoming quite extensive for both proton and heavy ion induced reactions thanks to this development. Data on electron induced reactions are more sparse because of the low electromagnetic cross sections. Data on particle emission following a weak interaction are available from muon capture and even neutrino reactions, the latter involving proton emission. As we will discuss in more detail below, reactions induced by electromagnetic and weak probes, and to a degree, protons, will yield information on nucleon reactions at lower particle number densities than what can be obtained in heavy ion physics, and so are a necessary part of the data set.

As data from single arm experiments began to accumulate as rapidly as theoretical interpretations of them, it became clear that less inclusive measurements were required to help determine the reaction mechanisms involved. At the time of writing, the first results from two- (and in a few cases three-) particle coincidence experiments have become available. Of course, there is always the danger that the coincidence data will simply show (and, indeed, seem to be showing) that there are several mechanisms operating in a given inclusive process, just as both the equilibrium and pre-equilibrium processes are known to contribute to the integrated cross sections. However, at least the possibility is opening up that kinematical regions and

projectile-target-ejectile combinations will be found wherein a particular reaction pathway is the dominant component.

Theoretical interest in fragment formation first centered on its mere existence: if so much of the reaction cross section arose from fragment formation, what was the reaction mechanism? As we shall see, much of the inclusive cross section data involving projectiles ranging from electrons to heavy ions had the same general features when plotted semilogarithmically as a function of ejectile kinetic energy K: they could be approximately fitted by a function of the form $\exp(-\beta(\theta)K)$ where $\beta(\theta)$ was in general smaller at forward angles and larger at backward angles. Such apparent simplicity in the data prompted the construction of equally simple models, most of which could handily fit the data, especially if they were plotted logarithmically. The assumptions of these models were often very different. For example, the direct interaction model most often used in describing the (p,p') reaction assumes a long mean free path, λ, of the reaction participants compared with the nuclear radius R. In contrast, the hydrodynamics approach assumes $\lambda \ll R$. With time, some of the models have evolved to include more complicated effects so that their underlying physics is no longer as easily segregated as it once was.

Hope seems to be rapidly fading that a simple model can be found to describe inclusive reactions encompassing the wide range of conditions over which they currently have been measured. However, it may be possible to find regions in which the dynamics simplify sufficiently that one can use the experimental data to test or determine the theory incorporated in the phenomenology. For example, under conditions in which multiple scattering is minimal, say electron scattering to specific nuclear states, one can learn about the behavior of the nuclear wave function at various momentum transfers.

At the other extreme, if one can produce a thermalized system of nucleons which is sufficiently large and long lived, one can learn about the nuclear equation of state. Hence, there is important physics to be learned by determining the mechanism applicable to these reactions.

The approach which will be taken in this review will be to examine the experimental data by means of a few very simple models, and then contrast the results obtained thereby. In other words, we will be using experiment to delineate theory, rather than explain in detail several (often fairly sophisticated) models and compare their calculational results. This is not to say that these simple models will work at anything better than the factor-of-two level, but they will allow the extraction of at least part of the physics involved in a straightforward manner. We will be concentrating on the emission of energetic ejectiles (more than five or ten MeV per emitted nucleon) into the continuum region. Reactions involving discrete final states are discussed at length in other reviews (for example CR 75 and RC 75) and will not be considered here. Similarly, the low energy "evaporation" of particles also will not be discussed. Again, they are well described elsewhere (for example Ale 68 and BW 52). Lastly the projectile energy under consideration will generally be above 100 MeV per nucleon, to at least partially avoid certain Coulomb and Pauli blocking effects. As a consequence, the exciton model and others which are used to describe the lower kinematical region will not be covered. The interested reader is referred to the literature (Bla 75 and references in the Appendix).

In Section 2, we consider the evidence for direct nucleon-nucleon interactions in those reactions responsible for the emission of energetic nucleons. Data discussed include not only the double differential cross sections, but also analyzing powers, n/p ratios <u>etc</u>. Our conclusion is that

there is evidence for both direct interaction and multiple scattering components to the reaction mechanism. Information about the magnitudes of these components can be found in the (p,2p) coincidence experiments which have recently been performed. Such experiments point to the presence of a surprising amount of multiple scattering even in as light a target as beryllium.

Section 3 investigates multiple scattering effects further and examines the approach followed towards thermal and chemical equilibrium among the reaction participants. This may allow a description of heavy ion and perhaps even certain proton-induced reactions in terms of statistical or hydrodynamical ideas. The temperatures, reaction volumes, densities etc. which are obtained in the models are presented. Finally, the concept of a possible limiting temperature in hadronic matter is dealt with.

The actual formation of a nuclear fragment must also involve some multiple interaction among it constituents, so Section 4 treats the question of how energetic light fragments are emitted. There are many different models for this process and at present one cannot get a definitive answer as to which better approximates the true mechanism. The possibilities include statistical emission from a hot region in chemical equilibrium as well as coalescence of a hot nucleon gas. Nuclear phase transitions begin to play a theoretical role here as light and intermediate mass fragment yields are used to estimate the entropy change in a nuclear reaction.

Theoretical interest in the intermediate mass fragment region ($10 \leq A_F \leq 30$) has currently revived with the discovery of systematics in the fragment yields. Several approaches to this mass region are presented in Section 5, including the possibility that these fragments result from the condensation of

a hadronic vapor during a phase transition. As yet, this remains an area requiring far more theoretical and experimental effort.

A summary of our current view of these pre-equilibrium phenomena is given in Section 6. As in every review of this type, one of the goals which the author wishes to accomplish is to produce a guide to the literature. The references are arranged alphabetically (by acronym) at the end of the review although not all of them are referred to in the main text. Rather, in the Appendix some effort is made to provide an index to the references for the use of the interested reader. In this article, the reviewer reached a point of saturation after reading some 500 articles of relevance to the subject area, so this limited the number of topics covered. In particular the author regrets that the production of pions and heavy mass fragments (mass number greater than 30) is only briefly mentioned, although introductory references are given in the Appendix.

2. Direct Interactions in the Nucleus

2.1 Quasi-elastic Scattering

We will begin our discussion of direct interaction effects in inclusive reactions by looking at the (p,p') reaction. In free elastic nucleon-nucleon scattering, one expects to find a locus of allowed values for the momentum of the scattered nucleon as shown by the dashed curve in Fig. 2. The locus is simple, of course, since the final state contains only two particles. When the target nucleon is placed inside a nucleus, the kinematical situation is changed dramatically since the residual nucleus can carry off considerable momentum but not necessarily a large amount of energy. In the limit of a very heavy target, the allowed energy of the struck nucleon can be almost as great as that of the projectile changed only by the Q value of the reaction. This situation is shown as the solid curve in Fig. 2. The central problem addressed in (p,p') reaction studies is how does this newly available phase space become filled.

A first question is whether any vestige of the quasi-elastic scattering process remains in a nuclear reaction (Ben+ 67, Che+ 81, CHM 52, Chr+ 80, Cor+ 72, Tan+ 81, WR 66). Shown in Fig. 3 are data from the (p,p') reaction at 800 MeV (Tan+ 81). At forward angles, one can clearly see a peak corresponding to quasi-elastic proton-proton scattering. At wide angles, the peak is no longer visible above the continuum. This is as one would expect from the elementary NN elastic cross sections. Such cross sections are often parametrized as being of the form

$$\frac{d\sigma}{dt} = Ae^{bt} \qquad (1)$$

where t is the squared four-momentum transfer in the NN collision given by $t=-2p_{cm}^2(1-\cos\theta)$, p_{cm} being the center-of-mass momentum. Small t corresponds to forward scattering ($\theta\approx 0$), while large (negative) t corresponds to wide angle scattering ($\theta >> 0$). One can see from Fig. 4, (after PDG 70) which shows the parameter b plotted as a function of bombarding energy in the lab frame, that b is reasonably large at 800 MeV, indicating a strong forward peaking. A large value for b shows that the quasi-elastic cross section decreases rapidly at wide angles and may be buried in the continuum. At lower bombarding energies, a quasi-elastic peak does not stand out above the continuum (Seg+ 82). Again, one sees from Fig. 4 that b is small in this region. Hence, Fermi motion of the struck nucleons and multiple scattering of the ejectile will easily obscure the quasi-elastic scattering.

In summary, we see that quasi-elastic scattering is clearly discernible in the (p,p') reaction under certain conditions. However, as one moves away from the quasi-elastic region, one finds that the inclusive cross section does not drop off as rapidly as one might expect (Ala+75, Bay+ 79, BP 73, Bro+ 77, Bur+ 76, Bur+ 79, Coc+ 72a, FMP 62, Fra+ 76, Fra+ 78b, Gea+ 80, Kom+ 77, Pee+ 68, Seg+ 82, Shi+ 83, ST 56, and WCH 79c). For example, suppose that the observed nucleon is actually one which was struck by the projectile, as shown in Fig. 5. Then the Fermi motion of the struck nucleon will smear out the quasi-elastic scattering region. Assuming that the momentum distribution is of the zero-temperature Fermi gas form and performing the calculation in a plane wave impulse approximation (PWIA) sense, one finds (Hat 79) that the calculations begin to underpredict the observed cross sections as one moves further away from the quasi-elastic region, especially at wide angles and high energies. (For a comparison in

the quasi-elastic region, see Ale+ 80.) Hence, the mechanism or mechanisms which account for the inclusive spectra must involve more physics than single scattering from a zero-temperature Fermi gas of nucleons.

Before we move on to discuss the models which have been proposed for nucleon emission, it is worthwhile pointing out two pieces of information which are useful to keep in mind in evaluating those models. The first is the (p,n) to (p,p') ratio (And+ 81, Bon+ 78, Kal+ 83, WBG 67, WGB 72). After correcting for the N/Z ratio of the target nuclei, this ratio was measured (And+ 81, Kal+ 83) to be on the order of two for a wide range of ejectile energies, angles and targets (Al being the lightest) for a bombarding energy of 100 MeV. This is certainly not what would be expected in a model in which there have been a very large number of collisions and all species are present with the abundance expected at chemical equilibrium. Such a model would predict the ratio to be much closer to unity. We will return to a more detailed discussion of the (p,n)/(p,p') ratio later.

The other observation worth commenting on is the analyzing power. The analyzing power in an experiment with polarized protons is defined by the polarization dependent counting rate

$$N \propto 1 + A\vec{o}\cdot\vec{n} \qquad (2)$$

where $\vec{o}$ is the projectile polarization and $\vec{n}$ is the unit vector in the $\vec{p}_{in}\times\vec{p}_{out}$ direction. This quantity was measured at 65, 500 and 800 MeV bombarding energies (KSW 78a, Sak+ 80, Roy+ 81 and Fra+ 78a) and a variety of angles. In almost all experiments, the analyzing power was observed to be non-zero, an example being shown in Fig. 6. The fact that the analyzing

powers are so different from zero argues (FW 77) that the ejectile may not be too many N-N collisions away from the projectile: it has some knowledge of the original spin. On the other hand, the elementary p+p analyzing power has an approximately constant value with no sign reversal in this energy range. Due to their inherent difficulty, convincing calculations of these analyzing power measurements are not easy to come by. It is clear that the sign reversal of the analyzing power shown in Fig. 6 does not seem to emerge easily in a single scattering model involving only p+p collisions. In a thermal model analysis, one would have to postulate that the thermal source would have to be given a directional preference determined early in the thermalization process. These analyzing power measurements will not be investigated further in this review, but it is worthwhile remembering that they yield a non-zero value.

2.2 Theoretical Models

We showed in the previous section that neither single scattering from a zero temperature Fermi gas of nucleons nor emission from an ensemble of nucleons in thermal and chemical equilibrium can account for all of the observations in inclusive nucleon production. Modifications of these simple schemes are in order therefore, and we will discuss the following possibilities:

i) Single scattering from a single particle momentum distribution which is larger in magnitude at large momenta than that of the zero temperature Fermi gas. This is shown schematically in Fig. 7a.

ii) Single scattering from a correlated cluster of nucleons, the observed nucleon being either the projectile or a member of the cluster (Fig. 7b).

iii) Multiple scattering of the projectile and ejectile (Fig. 7c).

Of course, these possibilities have large regions of overlap and all will be present in the real reaction mechanism to varying degrees. For example, the high momentum components of the nuclear wave function needed for the first possibility may be generated by short range NN interactions, implying that the projectile actually scatters off a two nucleon cluster, as in ii). Similarly, unless the target nucleus is very light indeed, there will be multiple scattering of both projectile and ejectile, as in iii). Naturally, there are many more possibilities than what have been given here, but these examples will be used as a basis for discussion.

We begin by looking at the first possibility. Detailed calculations of the single particle momentum distribution show (Ama 76, AW 76a, AW 77c, CG 61, VTB 80, ZE 78) that inclusion of the short range nucleon-nucleon interaction will substantially increase the high momentum components over what one expects from the ideal gas results (Mon+ 71, Whi+ 74, and references therein). An example of these calculations is shown in Fig. 8. Historically, most of these results emerged after model calculations along the lines of i) were performed (for example AW 76b). Hence, the comparisons with data using mechanism i) were made with a phenomenological momentum distribution adjusted to fit the data. We will describe these phenomenological results first, then contrast the momentum distribution so determined with the calculated one. The role of momentum distributions in heavy ion collisions has also been investigated (BH 80, FH 80, HN 81).

In plane wave impulse approximation language, the differential cross section for the (p,p') reaction can be written as (for a general discussion of this approach, see AW 77a, AW 77b, CDG 83, Fra 78, Jac 71)

$$\frac{d^2\sigma}{d\Omega_q dE_q} = \frac{M_p^*}{2(2\pi)^5}\frac{q}{p}\int \frac{d^3p_f}{E_f \epsilon_k}\left[n_p(k)|T_{pp}|^2 + n_n(k)|T_{pn}|^2\right] \tag{3}$$

$$\times\ \delta(E_i + M_A - E_f - E_q - E_k)$$

where the kinematic labels are as in Fig. 5 except that $\epsilon_k = (k^2 + M_p^2)^{1/2}$. The target has a mass M_A while the proton has mass M_p. The elementary N+N transition matrix elements are denoted by T_{NN}, while the momentum distribution is n(k). Most of the work done in applying this approach to the inclusive spectra concentrated on kinematic areas away from the quasi-elastic region so that the phase space integral contained only a monotonic function of k, i.e. $\vec{k}=0$ in the quasi-elastic region was not included. For large k (corresponding to the wide angle, large ejectile energy region) one can see from Fig. 8 that n(k) is a steeply falling function.

This behavior of n(k) tempts one to factorize Eq. (3) into a part which varied rapidly with k, and a part which varied slowly. The rapidly varying part is most sensitive to the minimum value of k (k_{min}) which is found when $\vec{k}$ and $\vec{p}_f$ are parallel and point along the $\vec{p}$-$\vec{q}$ direction (the so-called quasi-two body scaling angle, θ_{QTBS}). Thus, much of the early phenomenology worked on testing the hypothesis (Fra 77, Fra+ 78c, Wal+ 79) that the differential cross sections obeyed

$$\frac{d^3\sigma}{d^3q} \propto G(k_{min}) \tag{4}$$

where the function G was determined from experiment. (Many tests of this proposal can be found in Gur 81, Gur 82a, Gur 82b. See also FF 77.)

The success of the tests in finding a universal function G (on a logarithmic scale) does not imply that the mechanism is knockout in origin, however. A number of other models, often emphasizing very different aspects of the scattering problem but still being nonstatistical, have also been advanced (Bay+ 73, BLT 77, Cha+ 80, FH 79, FS 77, FS 79, Fuj 77, Fuj 79, WM 77, Wol 78, Wu 80, YF 79b). For example, the phase space available to the recoiling system will also depend on k_{min}, and hence a model in which the inclusive spectrum depends on the phase space available at any given energy and angle will also be described in terms of some $G(k_{min})$, although the functional form may be different. Better tests of mechanism i) must involve testing the normalization of n(k).

Two data-to-data tests which were performed involved fitting the (p,p') data, then taking the momentum distribution so obtained and predicting the rate of nucleon emission in a reaction induced by a different projectile. The first test was performed (SMA 79) on neutron emission following π^- or μ^- capture. In both of these reactions, the (isotropic) cross section is describable in the knockout model by an equation similar to Eq. 3, only with the T_{NN} replaced by the appropriate πN or μN matrix element. While it was found that the shape of the spectra (that is, the slope of the rates when plotted logarithmically) were well reproduced, their normalizations were not. In other words, if the (μ^-,n) reaction were entirely attributable to μ^- capture on a high momentum proton, then only a fraction of the (p,p') cross section could be attributed to the same mechanism.

A second test (BW 81) was made on the (γ,p) reaction, for which a large body of experimental data exists (ADS 75, Ant+ 71, DS 73, Fel+ 54, Kim+ 63, Mat+ 76, MT 66, Ste+ 60, VL 73, Whi+ 58). Again, n(k) was

determined by analysis of the (p,p') reaction, then applied to a (γ,p) model in which the incident photon is directly captured on a nucleon which is subsequently ejected. This method was also used in electron scattering in VV 69. For tagged photons, this would predict a proton spectrum with a peak centered at the incident photon energy and a width determined by the distribution of excitation energies carried off by the residual nucleus. Unfortunately, tagged photon data was not available for this test, and the calculations were compared with photons from a bremsstrahlung source instead. (Subsequent experimental results with quasi-monochromatic photons appear to be consistent with the cascade approach. See Bab+ 82.) First, it was found (BW 81) that the data could not be reproduced if the coherently recoiling nucleus assumption implicit in Eq. 3 was kept: the recoiling system had to carry off excitation energy and break up. When this assumption was dropped and the (p,p') data were fit with a model incorporating such a residual energy distribution, the (γ,p) data could be reproduced at the factor of two level. An example of the comparison between the data and the prediction is shown in Fig. 9. (The quantity Q is the expectation value of the photon energy integrated over the bremsstrahlung energy spectrum and divided by the end point energy. See LS 51, Sch 51.) In general, the (γ,p) data were overpredicted by a factor of two or more, particularly for lower photon energies, again indicating that n(k) as deduced from the (p,p') reaction was too large.

The study of the (γ,N) reaction by itself (without reference to the (p,N) reaction) began several decades ago. A model widely used to describe this reaction is the quasi-deuteron model, (Lev 51, see also Gab 76, GH 74, HWG 76 and WC 77) in which the photon is captured on a transient proton-neutron pair in the nucleus. Such a model has experimental support

in the study of p,n coincidences following photon absorption (BS 54, BS 58, FM 71, GA 69, Gar+ 65, Mye+ 54, Odi+ 56, Smi+ 67, Wat+ 56. See also WM 53). This has similarities to the direct knockout model in the sense that the high momentum components of the momentum distribution required for the success of the knockout model presumably arise from short range NN interactions, as in the correlated cluster (FH 79, Fuj 77) approach.

A theoretical test can be made by comparing n(k) from the naive treatment of (p,p') with the calculated values from many-body theory. Of course, even if the model is correct, the n(k) determined from the continuum region may not be the same as that found in the bound state PWIA analysis (in, for example ARW 77, KW 70). As is clear from Fig. 8, there is some spread in the predictions according to the model chosen for the short range part of the NN interaction. There is a similar spread in the phenomenologically determined value according to what prescriptions are used for estimating the off-shell extrapolation of T_{NN} (among many other things). But, in general, the theoretical n(k) is a factor of two to five below the phenomenological one.

To summarize, the data indicate that only a fraction, probably one-half at the most, of inclusive proton production arises from a direct knockout of a high momentum off shell nucleon. As will be shown below, the remainder probably arises after some multiple scattering of either the projectile or ejectile, as one would expect in mechanism iii) (see Ch 81b for example). This does not mean that mechanism ii) is absent, however. As indicated above, the high momentum components which are required for mechanism i) to operate would arise from the sort of short range correlations envisaged in the second mechanism (FH 79, Fuj 77, Fuj 79) and so in some sense mechanism i) is actually one term in mechanism ii). At

present, it is difficult to disentangle experimentally two possible contributions: low momentum transfer scattering from a highly off-shell nucleon in a correlated cluster (the projectile emerging in the forward direction) versus high momentum transfer scattering from a transient cluster (with the projectile becoming the observed particle). In the former case, n(k) is small but $|T_{NN}|^2$ is large because of the low momentum transfer. In the latter case, n(k) is large while $|T|^2$ is small because of the large momentum transfer. There has been considerable theoretical debate as to the relative contribution of each of these terms. Experiment indicates that the high momentum transfer process cannot be the only one since the (γ,p) cross sections are as large as they are (roughly, $(\gamma,p)/(p,p') \approx \alpha_{em}$, the electromagnetic coupling constant). Obviously, the observed proton can't be the incident photon. Similarly, even if the (p,n)/(p,p') ratio is of the order one-half, the observed neutron will not arise from p+p scattering at large t if a small momentum transfer charge exchange reaction is available.

Most of the discussion of multiple scatterng will be left to Section 3, where the cascade, statistical and hydrodynamical models will be presented. However, it is worthwhile presenting a simple calculation here to illustrate the importance of multiple scattering as a function of target. Imagine that the projectile, in this case with a radius r_p, sweeps out a volume at impact parameter b along a straight line trajectory through the nucleus, as shown in Fig. 10. Assuming a uniform density nucleus of radius R, the path length L(b) of the projectile in traversing the nucleus at impact parameter b is

$$L(b) = 2(R^2-b^2)^{1/2} \qquad (5)$$

Then the impact parameter averaged number of mean free paths will be roughly

$$n_\lambda \equiv \frac{2\pi}{\lambda} \frac{\int_0^R L(b) b db}{\pi R^2} = \frac{4}{3} \left(\frac{R}{\lambda}\right) \quad (6)$$

(A proper counting of the number of collisions can be found in KK 68.) Now, taking $\lambda = 1/\rho\sigma$, $\sigma = \pi r_p^2$ and $\rho = (\frac{4}{3}\pi r_0^3)^{-1}$, we find

$$n_\lambda = (r_0/r_p)^2 A^{1/3} \quad (7)$$

which for $r_0 \simeq r_p$ becomes

$$n_\lambda = A^{1/3} \quad (8)$$

This result can also be obtained by purely geometric considerations (BR 84).

For light targets such as Be, one then estimates n_λ to be about 2, while for heavy targets in the mass 200 range, n_λ may be as large as 6. Hence, multiple scattering will be present in small amounts in a light target and it is here that one should look for experimental signatures of direct interactions. For heavy targets, multiple scattering may begin to smear out some of the direct interaction effects. Of course, this is an energy dependent statement in that the NN cross sections are strongly forward peaked at large incident energies as indicated by Fig. 4 so that multiple scattering may not significantly effect the trajectory of a high energy nucleon. However, the struck nucleons, which have much lower energy, will be far more susceptible to the effects of multiple scattering. As was indicated above, further discussion of multiple scattering effects

will be postponed until after the discussion of the coincidence experiments' results.

2.3 Coincidence Experiments as a Probe of Reaction Mechanisms

The coincidence experiments performed thus far to clarify the mechanism for pre-equilibrium particle emission fall into two broad groups. The first group, which we will defer presenting until Section 3.4, utilizes the nuclear version of the Hanbury-Brown/Twiss effect used in astronomy to estimate stellar sizes. This type of experiment looks for correlations between identical particles observed in coincidence with low relative momentum. Such analysis presumes an equilibrated source for the particles.

The second group of experiments (Bho+ 76, Cia+ 83, Cow+ 80, Fra+ 81, Gre+ 83, Kom+ 78, Kom+ 79a, Kom+ 79b, Sim+ 70, Tan+ 81) chooses kinematical regions which are expected to be important in direct interaction models. In general, an event is triggered by the observation of a wide angle energetic proton, and then a search is made for another energetic proton in the forward direction. Conservation of momentum leads to a momentum vector diagram such as the one shown in Fig. 11, where the kinematic labels from Fig. 5 have been used. The vector $\vec{p}-\vec{q}$ is specified by the momentum of the projectile and trigger respectively, implying $\vec{p}_f$ and $\vec{k}$ must sum to $\vec{p}-\vec{q}$. If the inclusive spectrum is knockout in origin with k_{min} determining its magnitude, then one would expect the coincidence rate to be peaked along the $\vec{p}-\vec{q}$ direction (θ_{QTBS}) near the kinematic limit. If the mechanism involved backscattering from a cluster in the nucleus, as in Fig. 7b), then one would not expect to see such a peak, but rather a peak at about half of this energy or less, arising from the scattering of the cluster into the forward direction and its subsequent breakup.

The first two pioneering attempts at these difficult experiments which were performed to distinguish between these mechanisms did not provide a solution. In one case (Kom+ 79a) such a large energy cut in the detectors was required in order to give a high enough event rate that unambiguous interpretation of the data was difficult. The experiment was oriented toward searching for cluster emission, and events were observed. The second experiment (Fra+ 81) observed forward peaking, but the coincidence rate was much lower than expected in the knockout model. Kinematically more complete experiments (Gre+ 83, Tan+ 81) performed subsequent to these in a similar energy range confirms a forward peaking at an event rate much higher than Fra+ 81, as well as other contributions to the inclusive spectra. It is these latter experiments upon which we will concentrate.

Shown in Fig. 12 is a plot of constant coincidence rate contours as a function of summed trigger plus forward proton kinetic energies, for 300 MeV protons on a beryllium target. The trigger energy was fixed at 70 MeV in this figure. A leading particle effect is clearly visible at an angle outside of the QTBS angle, which is marked by an arrow (we will return to this latter point momentarily). It is also clear from this data that the coherent recoil assumption implicit in Eq. (3) is not supported: the events should be concentrated on a line in a plot such as Fig. 12 if the system recoiled coherently to a specific state (Boa 80b).

As the trigger energy is raised, the peak gradually vanishes and one is left with only the smooth continuum region, with a maximum very close to the QTBS angle. Is this continuum region merely phase space? Such an interpretation of the inclusive spectra of both proton and heavy ion induced reactions has been proposed (see Section 3), but certainly for these small targets it does not appear to be the dominant mechanism. Our

argument goes as follows: Since the energies of the residual system are not particularly relativistic, use will be made of the non-relativistic expression for N-body phase space:

$$R_N \equiv \int \prod_{i=1}^{N} \frac{d^3p_i}{2E_i} \delta^4(k^\mu - \Sigma_i p_i^\mu) \tag{9}$$

where k^μ is the overall four-momentum of the N particles. This becomes

$$R_N \propto \frac{(2\pi^3)^{(N-1)/2} \left(\prod_{i=1}^{N} m_i\right)^{1/2}}{2\Gamma[3(N-1)/2]\left(\sum_{i=1}^{N} m_i\right)^{3/2}} \left(M_k - \sum_{i=1}^{N} m_i\right)^{(3N-5)/2} \tag{10}$$

where M_k is the invariant mass of the N particle system of total energy E_k and momentum $\vec{k}$. Taking as a special case the situation in which all of the recoiling objects are nucleons of mass m, then

$$R_N = \frac{(2\pi^3)^{(N-1)/2}}{2N^{3/2}\Gamma[3(N-1)/2]} m^{(N-3)/2} (M_k - Nm)^{(3N-5)/2} \tag{11}$$

For a model, suppose that the coincidence rate is proportional to the phase space of the residual N-body system (N to be determined). Obviously this expression will not reproduce the peaking in the data near the kinematic limit, so we will concentrate on the continuum region. Shown in Fig. 13 is a comparison (BR 84) of the phase space calculation with the data for the forward angle fixed and the forward energy varying. The phase space calculation is normalized at 75 MeV forward kinetic energy. The data would seem to require that the recoil system contain only a very few particles.

Yet, even in the continuum region the data is not well reproduced by the phase space approach, as shown (Gre+ 83) in Fig. 14. In this figure, the forward angle is varied while the energy is held fixed. The agreement is not good, even for a small recoil system. In other words, the continuum region is more like one would expect from a direct interaction with some multiple scattering. Of course, for thicker targets one would anticipate more multiple scattering and hence phase space to play a larger role.

The direct knockout model developed in the (p,p') and (γ,p) reactions (BW 81) can be applied directly to the coincidence data (after a very minor adjustment in the parameters found in analyzing 800 MeV inclusive (p,p') data was made to insure the 300 MeV inclusive data were properly fit) and an example of the results is shown in Fig. 15. The theoretical curve is a prediction in the sense that the parameters were fixed by previous analyses. The agreement is surprisingly good, but still does not reproduce the data on anything better than the factor of two level. (The bumps in the model prediction are an artifact of the manner in which the calculation was performed. See Gre+ 83.) Again, our conclusion is that there is a knockout component but that it is somewhat smeared by multiple scattering.

Before leaving this experiment, the shift in the peak to an angle beyond the QTBS angle should be commented upon. Eq. (3) contains two functions, n(k) and T_{NN}, which depend on $\vec{k}$ and $\vec{p}$. The first function is peaked at k_{min}, which will push the maximum in the concidence rate towards the QTBS angle, while the second function is peaked at small momentum transfer, which will push the maximum in the rate towards θ=0. Hence, one would expect the actual maximum to be between 0° and the QTBS angle, depending on the value of b from Fig. 4 relevant at this energy. For 300 MeV, this predicts a maximum slightly inside the QTBS angle. Multiple

scattering, however, can shift it to larger values. For example, if the trigger proton were produced initially with a higher energy than that with which it actually emerges (the reduction caused by multiple scattering) then the relevant QTBS angle would be shifted to a larger value. A similar situation would arise if the projectile momentum were reduced before the collision. Although this is no guarantee that multiple scattering of the knockout component will reproduce the data, it does point in the right direction. This experiment did not observe an enhancement in the coincidence rate at an energy expected from the breakup of a two nucleon cluster scattered into the forward direction (which would show up at an energy of about 180 MeV in Fig. 15). If such a cluster were present, it would have to either contain more nucleons or be multiply scattered itself to lower energies in order to pass below the low energy cutoff of the experiment.

Turning now to the last coincidence experiment (Tan+ 81) which we wish to consider, and a different approach to short range correlations. This experiment was performed at a higher energy (800 MeV) than the previous one, but also on a light target (carbon) to minimize multiple scattering effects. The data have been analyzed in several ways, only one of which will be summarized here.

The experimental layout was basically the same as the 300 MeV experiment. A trigger proton was detected at 118° while a forward angle on the other side of the beam was searched for proton (and deuteron) coincidences. The same forward peaking as in the 300 MeV experiment was observed, but so was an enhancement around the region expected for deuteron breakup. Unfortunately, the forward angle was fixed at 15° so it is not known how the relative magnitudes of rates in these regions change with

energy. The forward peaking near the kinematic limit was observed to decrease with respect to the continuum just as it did in the 300 MeV experiment.

Figure 16 shows the effect, although in a slightly different fashion. Here, the backward proton (θ_q=118°) spectrum is shown for a forward trigger in the peak region (denoted by QES), elsewhere in the reaction plane formed by the $\vec{p}$ and $\vec{q}$ vectors (denoted by non-QES) and, finally, out of the reaction plane. The falloff of the peak contribution with respect to the continuum is clear. Some caution should be exercised in comparing Fig. 16 with other scatter plots since a KCl target was used here (vs. carbon and beryllium in the other experiments) and this will result in more multiple scattering.

These authors also found that backward angle protons were also not infrequently accompanied by deuterons in the forward direction. The spectrum of the deuterons was peaked around maximum momentum. The interpretation of this effect is not completely clear at this time, since some of the deuterons may be forward scattered clusters, as in Fig. 7b) while others will result from forward scattered nucleons picking up another nucleon on their way out of the nucleus to form a deuteron. The authors (Tan 83) treat their data as representing the interaction of the incident proton with a pn pair in the nucleus, as in the correlated cluster model, with the proton in the pair being ejected at wide angle, the incident proton then emerging with the neutron as a deuteron at forward angles. Using an argument of Goldhaber's (Gol 74) they estimate the value of $\langle p_p p_n \rangle$ (the momenta in the pn pair) to be -910 MeV/c.

To summarize, the coincidence experiments, as well as comparisons among inclusive experiments involving different non-composite projectiles,

demonstrate that part of the nucleon inclusive spectra involves direct emission of a nucleon, most likely from a few particle cluster providing a high momentum component to the single particle momentum distribution. Probably this direct contribution is at the 50% level at the most, even in a light target, the rest arising from some amount of multiple scattering. The number of secondary scatters is not large, however, and does not produce a thermal distribution in light targets. Coincidence experiments are currently underway in heavy targets to see how rapidly these wide angle two particle correlations are washed out.

3. Thermalization and Multiple Scattering in Nucleon Emission

3.1 The Approach to Thermal Equilibrium

Since even light targets show evidence of multiple scattering in nucleon emission, then as one goes to heavier targets and projectiles, the reaction should look ever more statistical. Indications that there is an increased contribution from multiple scattering in heavy targets can be found in Fig. 17, where the (p,p') inclusive cross section per target nucleon is shown. The differential cross section per target nucleon is observed to increase with target mass particularly for high energy ejectiles.

Statistical models have been used for many years in the study of low energy reactions (see, for example AWM 75, FKS 80, HF 52, Vog 68). In applying thermal concepts to higher energies, one must be more concerned with whether all available nucleons are participating in the thermalization process (Bet 38, SW 81, Wei 78), whether finite particle number effects are phenomelogically important in evaluating the appropriate phase space (for example, BK 81, GK 78a, JSD 81, Kno 79, Man 78), and whether the system cools off too fast for there to be measurable effects (BR 84, Koh 82, MZ 79, Wei 76, WW 75, WW 77). Despite these possible difficulties the thermal model approach has been successful in describing a wide variety of data (see Appendix for references by application).

To be convinced that the reactions are really entering into the statistical domain, however, one has to show that the nucleon's mean free path in the nucleus is small. An experimental attempt (Tan+ 81a) to determine the mean free path involved a comparison of the inclusive and (p,2p) coincidence data in the quasi-elastic region with the free nucleon-nucleon cross sections. There are a number of assumptions which go into this calculation, which we will not dwell on here, but the basic idea is to introduce an attenuation

factor into an expression for the measured nuclear cross sections. For example, the inclusive cross section in the quasi-elastic region is expressed as

$$\frac{d\sigma}{d\Omega} = \frac{1}{A}\left(Z\,\frac{d\sigma_{pp}^{el}}{d\Omega} + N\,\frac{d\sigma_{pn}^{el}}{d\Omega}\right)\int \rho dV\, \exp\left(-\frac{\ell^{in}}{\lambda^{in}}\right)\exp\left(-\frac{\ell^{out}}{\lambda^{out}}\right) \qquad (12)$$

where the free particle cross sections bear the NN subscripts. An integration is performed over the possible incoming and outgoing distances ℓ^{in}, ℓ^{out} that the projectile covers in traversing the nucleus. A similar expression can be written for the coincidence cross sections. A comparison with the data for several choices of mean free path is shown in Fig. 18. One can see that λ^{in}= 2.4 fm does a good job in reproducing both the trend and the magnitude of the target dependence. How large an error is to be associated with this estimate is not yet clear, but one can see that the value of λ^{in} is of the same order as the internucleon spacing.

This value for λ must be regarded as an effective mean free path, since it entered into Eq. (12) as an absortion-like term. At this energy (800 MeV), the NN cross sections are strongly forward peaked, meaning that there will be scatterings of the projectile which do not result in a significant change in its momentum, or its contribution to the quasi-elastic region. Hence, it is no surprise that the λ obtained in this experiment is larger than the value of $1/\rho\sigma$ =1.4 fm (with ρ = 0.17 fm^{-3}) which one might otherwise expect at this energy.

At much lower energies, the mean free path should increase due to Pauli blocking. An estimate of the magnitude of this effect is made in KK 68. They

express the mean free path in terms of the free NN cross sections σ_{pp} and σ_{pn} for a Z=N nucleus by

$$\lambda = [\tfrac{1}{2} \rho (\sigma_{pp} + \sigma_{pn}) P(\xi)]^{-1} \qquad (13)$$

where the Pauli blocking factor is given as

$$P(\xi) = 1 - \tfrac{7}{5}\xi \qquad \text{for } \xi < 1/2 \qquad (14)$$

and

$$\xi = E_F/K_N \qquad (15)$$

The nucleon kinetic energy K_N is measured from the bottom of the Fermi sea, E_F being the kinetic energy at the top of the sea. Their results are shown in Fig. 19.

One can see from the above that λ is of the order of the internucleon separation. While models which require $\lambda \ll r_{pp}$ or $\lambda \gg r_{pp}$ therefore will not be expected to describe completely the reaction mechanism certain elements of the models will present themselves in the data. This was shown to be the case in the analysis of the light target (p,p') reaction, in which there was both a direct interaction and a multiple scattering component. In heavier targets, there should be more multiple scattering, and the reaction participants should begin to approach thermal and chemical equilibrium.

One approach in the problem of thermalization would be to find kinematic and other regions in which the direct interaction is a significant factor in the mechanism, and modify the direct interaction model by adding some amount

of multiple scattering (Ber 77, Che 79, CHH 82, CS 80, GDA 79, GM 70, Gur 80a, Gur 80b, HK 79, Jai 80, Koo 77a, LG 79, SB 77, SC 80, Tam+ 77, TB 78, SS 75). To keep the discussion simple, except for an overview of the cascade calculations,we will instead concentrate on finding out how far from thermal or chemical equilibrium a given process is, rather than how far from a direct reaction it is. Similarly, the transport approach to these reactions will not be reviewed (HP 80, Mal 80, PS 79, Ran 79, Rem 75, Rem 79, Sch 79, SM 82).

First, a quick review of some statistical ideas which will be useful. (For a more general review, see DM 81). For a system in thermal equilibrium, the number density of a particle species i is given by

$$n_i = \frac{g_i}{(2\pi)^3} \int \frac{d^3q}{e^{(E-\mu_i)/T} \pm 1} \qquad (16)$$

where the ± sign refers to fermions (bosons). For the time being, finite particle number effects will be ignored. In Eq. (16), $E = (q^2 + m^2)^{1/2}$. The chemical potential is associated with a conserved quantum number, and may even manifest itself for bosons, depending on the quantum number involved (e.g. a gas of pions with a net charge). If the system under consideration is in chemical as well as thermal equilibrium, then the ratios of various particle species can also be determined. Only the question of thermal equilibrium will be dealt with for the moment.

In the non-relativistic regime, Eq. (16) will be simplified by adopting Maxwell-Boltzmann statistics and dropping the ±1, so that the chemical potential can be easily replaced by the total number of particles of species i present:

$$\frac{dN_i}{dK_q} = \frac{4\pi}{(2\pi mT)^{3/2}} N_i qm \exp(-K_q/T) \qquad (17)$$

where the subscript on the kinetic energy K shows with which momentum it is associated and serves to distinguish it from the temperature T. Hence, in the system's rest frame, the energy spectrum of particles emitted will be exponential with slope equal to T^{-1}. The energy spectrum associated with this hot source (the word source will be used in place of system or ensemble for the remainder of this review) is shown schematically in Fig. 20a). The low energy "evaporation" region is similar to this in that the emission is approximately isotropic and the spectra have an exponential shape.

If the source is moving with respect to the laboratory frame then emission will not appear to be isotropic in the lab frame. For example, if the motion is along the beam direction, then one might expect to see an energy distribution as shown in Fig. 20 b), each curve being at fixed angle. This form is reminiscent of what is observed in the pre-equilibrium region, and hence prompted reseachers to consider a thermal equiblibrium model (involving an equilibrium among a subset of the target nucleons, but not the nucleus as a whole) as being appropriate to describe the pre-equilibrium region. A knockout model can also reproduce the same gross features of this region as will now be shown.

As an application of the statistical approach, proton emission from heavy targets will be examined. Although the conventional thermal model approach has been to fit the data explicitly with an expression like Eq. (17), it is instructive to use a somewhat different approach which transforms the data before analysis. In particular suppose that contours of constant cross section are plotted as a function of perpendicular and parallel velocity, for non-relativistic emission in the source's rest frame. Then the curves would

be semi-circular, with the origin at zero. Now, if the source is moving with a velocity v_s with respect to the lab, then the shape of an invariant cross section curves will still be circular, but shifted by the source velocity. Relativistically, it is preferrable to deal with the perpendicular component of momentum, $q_\perp$, and the rapidity, y, defined in terms of the parallel component of momentum, $q_{||}$, as

$$y = \frac{1}{2} \ln \frac{E+q_{||}}{E-q_{||}} \qquad (18)$$

The shape of the contours of constant Lorentz invariant cross section will no longer be semi-circular in the relativistic domain as a function of these variables (usually $q_\perp/m$ is used as the ordinate so that $q_\perp/m, y \to v_\perp, v_{||}$ non-relativistically) but the shape will be preserved in a moving frame.

An illustration of what is observed experimentally is shown in Fig. 21, a plot of U(p,p')X data taken at T_p = 1041 MeV. One can see that the contours are roughly semi-circular, but the centers of the circles (indicated by the arrows) are at increasingly large y the lower the cross section. We will return to this shifting source velocity later in section 4.1; for the time being it will be assumed that the shapes are sufficiently close to what one can expect from a thermally equilibrated source that it is worthwhile pursuing the analysis.

Thermal model analysis (the type performed here is often referred to as a single source analysis) have been performed for many projectile-target-ejectile combinations. Shown in Fig. 22 are the source rapidities found in proton emission in heavy ion and proton induced reactions, plotted as a function of incident kinetic energy per nucleon. Presuming that the source gets its momentum from the projectile, it is apparent that a

nucleon in a heavy ion projectile spreads its momentum over fewer target nucleons than does a single incident proton. This is as one would expect from geometrical considerations. Fig. 23 shows the temperatures found in the same analysis. Again, the higher temperatures observed in the heavy ion reactions are an indication that an average nucleon in a heavy ion projectile spreads its energy over fewer nucleons than does a single incident proton.

Several detailed versions of the thermal model make specific assumptions about the collision geometry to determine the source size (fireball and firestreak model: MDJ 83, MJD 81, Mye 78, Wes+ 76, Wes+ 82 for example; collective tube model: BDE 76, Men 77, Men 79, MM 78a, MM 78b, Var 78). However, one can test the geometry by using several different methods of calculating the source size, and then seeing if they are self-consistent. It was argued in Section 2 on the basis of geometry that about $A^{1/3}$ nucleons should be expected to participate in the interaction region, (which is almost 6 for the heavy targets under consideration here) for a proton induced reaction. Suppose now that the projectile loses all of its momentum, p, to the source. Then the number of nucleons N_s, in this non-relativistic source which take up the momentum will be

$$N_s = \frac{p}{mv_s} \qquad (19)$$

Source sizes calculated by this method are referred to as the momentum dump calculation in Fig. 24. A similar calculation can be done using the kinetic energy of the projectile being transformed into the kinetic energy of the source as a whole, plus thermal energy. This is referred to as the energy dump calculation in Fig. 24. Aside from being somewhat crude, these calculations are over-estimates in the sense that the projectile does not have

to lose all of its energy to the source. In fact, at high energies there is direct evidence that the projectile does not lose all of its energy in the target region. Correcting for the incomplete stopping of the projectile will result in a smaller source size.

A different approach is to fit the absolutely normalized (p,p') data and determine N_s via Eq. (17) (multiplying by 2 to include the (p,n) contribution). One needs a reaction cross section to go from the inclusive cross section to a number density, and the simple geometrical reaction cross section has been used in obtaining Fig. 24. Since not all source nucleons will ultimately emerge in the pre-equilibrium stage, and since some of the source nucleons will emerge as fragments, this is an underestimate of the source size. In summary, all of these calculations give a source in the 4-10 nucleon range, agreeing with the geometrical argument. An interaction volume, and hence a freeze out density, can be found by analysis of (p,π) data (Coc+ 72b). Typical values found for the freeze out density are 1/4 to 1/2 ρ_o (BR 84).

Similar calculations have been performed for heavy ion reactions (Jac 83). There, substantially larger sources were found. For example, in a 137 MeV/nucleon Ar + Au experiment, the momentum dump calculation gave a source size of about 90 nucleons, while the energy dump calculation gave a smaller value of about 70 nucleons. The proton normalization calculation gave a much smaller number, about 19, similar to the behavior observed in the analysis of proton induced reactions. Again the thermal model analysis yielded approximately self-consistent source size estimates, which were in the range expected from geometrical considerations. Freeze out densities similar to those found for the (p,π) reacton can also be obtained from the havy ion data (Ben+ 79, Fra+ 82, Fun+ 78a, Nag+ 81, Nag+ 82, Sul+ 82, Wol+ 79, Wol+ 82)

Hence, a reasonably self-consistent thermal model description of nucleon emission emerges for both heavy ion collisions and p-nucleus collisions. Of course, there will still be direct interaction effects from peripheral collisions (large impact parameter) although these may be less important in heavy ion collisions than in proton induced reactions. Particularly with the small source size which the thermal model analysis gives for p-nucleus reactions, some caution must exercised in disregarding direct interaction effects completely. The same caveat must be applied to nucleus-nucleus collisions with light nuclei. For example, direct interaction effects have been observed in $^{12}C + {}^{12}C$ reactions (Nag+ 79, Tan+ 80), and in quasi-elastic neutron emission in heavy ion reactions (Cec+ 81, Sch+ 79a).

With such a small source size for the interaction region in proton induced reactions, one can question whether thermal equilibrium is achieved at all. The answer lies in the fact that the initial interactions of the projectile alone produce a spectrum of particles which looks roughly thermal, indicating that not a great deal of multiple scattering would be required to "thermalize" the spectrum. This effect can be illustrated with a simple calculation (Boa 84), although it is known already that since the cascade calculations reproduce the nucleon emission data, an approximately thermal spectrum will result from only a few NN collisions per particle.

Suppose the cross section expression in Eq (3) is simply approximated by

$$E \frac{d^3\sigma}{d^3q} \propto \exp(-k_{min}/k_o) \qquad (20)$$

Demanding constant cross section, as is done for the rapidity plot analysis, gives a relationship between $q_\perp$ and $q_{||}$ for a given fixed k_{min}. An example is shown for K_p = 500 MeV in Fig. 25. In heavy targets, there will be several

collisions of the projectile, each having a set of curves like Fig. 28 and each contributing to the observed cross section. To gain some feeling for how this multiple projectile scattering will change the shape of the curves, a summation is made of the exponentials for a succession of three collisions in which the incident proton loses one third of its original energy per collision. A value for k_o is necessary to perform the summation, and this is set at 100 MeV. The result is shown on Fig. 26. The contours have a familiar circular shape, with an apparent center around y = 0.4. Clearly, it will not take a great deal of multiple scattering of the ejectiles to produce a spectrum which looks roughly thermal.

3.2 Is Chemical Equilibrium Achieved?

This question is more difficult to answer than the previous one about thermal equilibrium because one must have a system whose particle ratios change with time in a well defined way and are experimentally determinable to good accuracy. As an example, Mekjian (Mek 82) has looked at the problem of kaon production in heavy ion collisions. There it is observed that kaons are not as plentiful as a chemical equilibrium model would predict using parameters determined from proton and pion yields. He concludes that the temperature and density regions from which kaons emerge are not long lived enough to come into chemical equilibrium.

At lower temperatures, the number of particle species available for such calculations is more limited. The π^+/π^- ratio in proton induced reactions (Coc+ 72b) could also be used in a similar manner as kaons (unless one has a model for the interaction volume or density, one cannot use the pion yield itself as a prediction: it is used as an input). For proton induced reactions at lower energies, one possibility is to use the (p,n)/(p,p') ratio.

Experimentally, this ratio is measured to be about 1/2 (for observed energies away from the evaporative region) for light targets, although the ratio increases somewhat as one goes to very neutron rich targets (And+ 81, Bon+ 78, Kal+ 83, WBG 67, WGB 72). In a direct interaction model, one would expect that the ratio is of the order of 1/2 if only the first proton-nucleon scattering is considered. Calculations using approximations to Eq. (3) have been performed (Boa 82) at both 400 MeV and 1 GeV incident proton energy, and are shown in Fig. 27. The observed ratios are somewhat higher than this, indicating some multiple scattering which would move the ratio closer to the statistical value of about unity (dependent upon Z/N, Q-values etc.). Because the observed values are so close to the knockout prediction, the system has obviously not evolved for a sufficiently long time before emitting nucleons.

If the initial conditions (that is, the initial interaction step) were known very well, then one could follow the time evolution of the system as it moves toward chemical equilibrium. As it is, the $(\mu^-,p)/(\mu^-,n)$ ratio has a slightly better defined initial stage and so will be used as an example (Boa 84). In μ^- capture, (for a review see Sin 74) one knows that the elementary weak interaction must involve

$$\mu^- + p \rightarrow n + \nu_\mu \qquad (21)$$

The neutrino carries off most of the energy, but there is usually enough left to emit at least one nucleon. Hence, one would expect to see only neutrons emerging if capture took place on a free gas of neutrons and protons. Experimentally (Kra+ 79), the ratio of $(\mu^-,p)/(\mu^-,n)$ for nucleons emitted with energies greater than 15 MeV is observed to be about 1/2 for light targets such as Al or Cu (what is usually measured is the charged particle spectrum

rather than (μ^-,p). Since the alpha yield is smaller than the proton yield (Bud+ 71), we will equate the charged particle spectrum with the proton spectrum). The individual (μ^-,p) and (μ^-,n) reactions have energy spectra which are both exponential in shape and have similar slopes.

In muon capture by a free proton, most of the energy released is carried off by the neutrino, as a consequence of momentum conservation. The recoiling neutron will have a unique energy of 5 MeV. When the capture takes place in a nucleus, an energy spectrum is observed for the emitted neutrons (BE 77, Bud+ 71, Sch+ 74, SE 73, VKR 70). At low neutron kinetic energy, the spectrum falls steeply and is describable in terms of evaporation from a source with a small temperature, on the order of an MeV. Above a neutron kinetic energy of about 5 MeV, the falloff is less steep, corresponding to an apparent temperature of 7-14 MeV (data with better statistics tend to favor the lower end of the temperature range, see Sch+ 74). In a thermal model description, the "hot" interaction region cannot be the entire nucleus, since there is only about 100 MeV of energy available for thermalization to begin with.

The reason that there is a spread in energy, of course, is that the residual nucleus can carry away momentum which the neutrino would otherwise have to carry, without carrying off much energy. Imagine that the muon is captured on a zero temperature Fermi gas of protons. Then integrating over the momenta $\vec{k}$ of the capturing protons (kinematic labels are shown in fig. 28) would give an average kinetic energy to the neutron produced in the reaction of about 25 MeV, assuming a separation energy of 10 MeV. Identifying this energy with (3/2)T would give a temperature of 17 MeV, not far removed from the range of temperatures indicated by experiments. Hence, the produced neutron would only have to share its energy with one other nucleon to give an average energy consistent with experiment.

The Fermi gas approach will not, however, reproduce the energy spectrum without multiple scattering. It is easily calculated that if the maximum momentum available in the nucleus is 270 MeV/c (corresponding to a Fermi energy of 38 MeV) then the maximum neutron energy will be 50 MeV. Such a sharp cut off is not observed experimentally. In a calculation which uses an effective vertex function to account for both multiple scattering, and a less sharp momentum distribution than the zero temperature Fermi gas, Singer, Mukhopadhyay and Amado (SMA 79) are able to reproduce a temperature of 12 MeV easily. (For other theoretical work on this problem, see BEJ 77, BPV 65, Ish 59, LS 78, Muk 77, Ube 65.) Both of these approaches, then, indicate that only a small amount of multiple scattering is required to produce an apparently thermal spectrum with a temperature of 7-10 MeV.

The normalization of the thermal model approach can be checked by calculating the neutron energy spectrum with a temperature of 7 MeV and a total of 2 neutrons in the source. Since it is estimated (Sin 74) that about half of the captured neutrons go through giant resonance absorption, rather than the direct mechanism under consideration here, then the calculated thermal model normalization should be divided by perhaps a factor of 2 since the data is quoted per capture. The data are about a factor of two below the result so obtained. Again, this is about what one would expect since not all of the hot zones will emit a neutron in the cooling time covered by the 17-7 MeV temperature range.

To estimate the time scale involved, one approximate method would be to follow the time evolution of a system which is initially entirely neutrons as the neutrons charge exchange with protons in the Fermi sea. Then the rate equations for the number densities of "hot" nucleons n_i, will be of the form:

$$\frac{dn_n(t)}{dt} = (-n_n(t) + n_p(t))\lambda_{cx}$$

$$\frac{dn_p(t)}{dt} = (+n_n(t) - n_p(t))\lambda_{cx} \qquad (22)$$

The charge exchange reaction rate λ_{cx} should involve integrating the number densities of a finite temperature nucleon system with a zero temperature one, including Pauli blocking. An approximation that has been used to this is the classical expression for a particle A reacting with a gas of particles B

$$\lambda_{AB} = n_B\, 4\pi \left(\frac{\mu}{2\pi T}\right)^{3/2} \int v^3\, \sigma_0(v) \exp\left(-\frac{\mu v^2}{2T}\right) dv \qquad (23)$$

where μ is the reduced mass. For a cross section of the form

$$\sigma(v) = \sigma^0/v^2 \qquad (24)$$

this expression becomes

$$\lambda_{AB} = \left(\frac{2\mu}{\pi T}\right)^{1/2} n_B\, \sigma^0 \qquad (25)$$

An example of the magnitude that one would expect for the reaction rates is shown in Fig. 29. The n→n rate is a combination of nn (≡pp) and pn elastic scattering (θ_{cm} in the forward direction) while the n→p rate is from pn scattering with θ_{cm} in the backward direction. These rates can be substituted into Eqs. (22) to give the time evolution of the "hot" p/n ratio. The result is shown in Fig. 30 for $\lambda_{cx} = 1.0\ (10^{-23}\text{sec})^{-1}$. One can see that it takes

about 0.7×10^{-23} sec, in this calculation, for the p/n ratio to evolve to the 0.6 observed in muon capture.

The actual lifetime of the hot zone may be longer than this estimate for several reasons:

i) This estimate does not include the effects of Pauli blocking, which could lower the reaction rate by a factor of 2 or more at these temperatures.

ii) The lifetime is for nucleon emission only, and fragment formation, which necessarily involves more NN interactions, should take corresponding more time.

iii) The reactions considered will have a surface component to it, and many of the outgoing nucleons that are not absorbed in the nuclear core may not have much nuclear matter to scatter from.

Hence, collisions of heavy ions in which there are more nucleons available for multiple scattering may be correspondingly more thermalized. This is illustrated in Fig. 31 in which the charge exchange rate for heavy ion reactions (at normal nuclear density) is contrasted with the rate for proton induced reactions (at half nuclear density) at the same incident energy per nucleon. The temperatures were parameterized from the thermal model results:

$$T = 1.9\ K_i^{0.46}\ \text{MeV} \tag{26}$$

for proton induced reactions (BR 84) and

$$T = 2.1\ K_i^{0.52}\ \text{MeV} \tag{27}$$

for heavy ion reactions (Jac 83), where K_i is the incident kinetic energy per nucleon in MeV. Of course, the test which has been applied here to muon and proton reactions is generally not available for heavy ion reactions since the latter systems usually involve N=Z targets and projectiles.

Now that a time scale has been determined "experimentally" for energetic nucleon emission, one can check whether the result is in agreement with theoretical estimates. One approach is to use the classical diffusion equation to estimate the time evolution of the system (BR 84):

$$C_p \frac{\partial T}{\partial t} = \text{div}\ (\frac{\kappa}{\rho}\ \text{grad}\ T) \tag{28}$$

where C_p is the specific heat at constant pressure, ρ is the density and κ is the thermal conductivity. The temperature T is, of course, allowed to be a function of position and time, while C_p, ρ and κ are, in general, a function of T. Since our attention will be focussed on the central region of the hot zone it will be assumed here that the latter quantities are sufficiently slowly varying with position that Eq. (28) can be approximated by

$$\frac{\partial T}{\partial t} = \frac{\kappa}{\rho C_p} \nabla^2 T \tag{29}$$

Lastly, parameterizing T(r) in a gaussian form

$$T(r) = T_o \exp\ (-(r/r_o)^2) \tag{30}$$

one has at $r = 0$

$$\left.\frac{\partial T}{\partial t}\right|_o = -6 \frac{\kappa}{\rho C_p r_o^2} T_o \qquad (31)$$

In general, the diffusion equation will have to be solved numerically, although analytical expressions are available at high and low temperatures. At high temperatures, one can use the results from the classical theory of gases, in which the thermal conductivity at zero pressure κ_0 is

$$\kappa_o = \frac{25}{32} \sqrt{\frac{T}{\pi m}} \frac{C_v}{d^2} \qquad (32)$$

where d is the rigid sphere diameter (taken to be 1 fm in the calculations below). The specific heats, of course, are C_p=5/2, C_v=3/2 (as above, Boltzmann's constant has been absorbed into T). In Enskog's theory of transport phenomena in dense gases, correction terms to the thermal conductivity have the form:

$$\kappa/\kappa_o = (b_o/\tilde{V}) \left[\frac{1}{y} + 1.2 + 0.755\ y\right] \qquad (33)$$

where $\tilde{V}$ is the molar volume

$$y = \left(\frac{P\tilde{V}}{RT} - 1\right) \qquad (34)$$

and b_o is the second virial coefficient. At moderate densities (HCB 54)

$$y = \left(\frac{b_o}{\tilde{V}}\right) + 0.625 \left(\frac{b_o}{\tilde{V}}\right)^2 + 0.287 \left(\frac{b_o}{\tilde{V}}\right)^3 + 0.115 \left(\frac{b_o}{\tilde{V}}\right)^4 \qquad (35)$$

For a hard sphere gas,

$$\frac{b_o}{\tilde{V}} = \frac{2}{3} \pi p d^3 \qquad (36)$$

The high temperature part of the curve shown in Fig. 32a is calculated using this approach. For temperatures around the Fermi energy, we estimate the rate of cooling from the numerical solutions found in (Koh 82). At low temperatures, the expression for the thermal conductivity found by Tomonaga can be used :

$$\kappa = \frac{7}{48\pi\sqrt{2}} \frac{E_F^{3/2}}{m^{1/2} T Q_k} \qquad (37)$$

where Q_k will be chosen to be 1.35 fm² after Kohler (Koh 82). The specific heat at low temperature is given by

$$C_p = 4.8 \left(\frac{T}{E_F}\right) \qquad (38)$$

This calculation was used in estimating the low temperature part of Fig. 32. The three regions were joined together smoothly by eye. A slightly more useful version of Fig. 32a is shown in Fig. 32b where $T_o/(\partial T/\partial t)_o$ is shown. Evidently the high temperature hot spots should cool very fast, on the time scale of 10^{-23} sec, while the intermediate temperatures show a slower cooling rate. The cooling rate of the low temperature regime shown in the figure is not the calculated lifetime of a compound nucleus, but rather the time scale for the dissipation of energy of a small, cool area of the nucleus. A

compound nucleus would have a similar temperature throughout the nucleus, and would include coulomb tunnelling effects etc. in the calculation of the lifetime. Clearly, both effects would increase the time scale shown on Fig. 32.

The lifetime shown in Fig. 32 is larger than that found in the $(\mu,p)/(\mu,n)$ analysis, although as was shown in that analysis, such a difference is to be expected. It should also be pointed out that, if the nuclear density is reduced by half in the theoretical calculation of the cooling rate, then the estimated lifetimes of the hot spots will be correspondingly shorter. In summary, the estimated time from the chemical potential argument is in coarse agreement with the estimated time from the diffusion equation approach; corrections to both calculations will lessen the disagreement.

If one really can apply statistical mechanics ideas to these reactions, then it would be interesting to know if there is any way of obtaining independent information on the temperature profile assumed in Eq. (30). It has been pointed out (Nag 82b, Sch+ 82) that in heavy ion collisions the apparent temperatures (defined as the inverse slope of the inclusive cross section at 90° in the c.m. frame) found for different ejectiles vary with their mean free path in nuclear matter. Specifically, the pion, proton and kaon temperatures were found to be ordered as $T_\pi > T_p > T_K$, while their mean free paths are $\lambda_\pi < \lambda_p < \lambda_K$. Hence, one can imagine that short mean free path ejectiles sample the temperature of the nuclear surface while long mean free path ejectiles sample the nuclear interior, although there are other interpretations of this effect.

Results from proton induced reactions are not necessarily in disagreement with this hypothesis. Here, it is found that $T_\pi \approx T_p$ (see Fig. 23) in contrast

with the heavy ion results. However, the hot zone is substantially smaller in proton induced reactions, so much so that it is almost entirely "surface" and hence mean free path effects may be minimal. It is also worthwhile pointing out that in $p + \bar{p}$ reactions, the reversed order is obtained: $T_K < T_\pi$. However, this is almost entirely attributable to the difference in phase space available, since much less of the center of mass energy is available as kinetic energy in a final state involving kaons.

3.3 Cascade and Hydrodynamics

Up until this point, we have been approaching the data with two simple models, direct knockout and thermal, which have very different assumptions, in order to extract the gross features of the reaction mechanism involved in certain kinematical regimes. Here, we will try to summarize more sophisticated approaches: intranuclear cascade and hydrodynamics. Because these models are computer based, they are not as immediately accessible to the reader as the simple models described previously. Of course, one could take the approach of looking at all of the reactions considered herein through the eyes of a particular model, but such a viewpoint is not required here as it has been adopted in other reviews (for example, Sto+ 80b). Because several different computer codes, each with its own assumptions, have evolved for both the cascade and hydrodynamic models, the features of the models will only be discussed from a general point of view, rather than dealing with the specific predictions of each code. The list of references to cascade and hydrodynamics calculations is rather lengthy. Rather than repeat them here, they have been compiled in the Appendix.

The most general classical approach to the multiple collision problem would be to integrate the equations of motion, assuming some form for the

nucleon-nucleon potential. While this, in fact, has been attempted (BM 77, BP 77, BP 81, BPM 80, CWY 79, WYC 78), the more extensive calculations involve simplifying assumptions about the mean free path: short mean path compared to the size of the interaction region leads to hydrodynamics while long mean free path compared to the range of the nucleon-nucleon interaction is required for the intranuclear cascade. As was shown above, neither relationship is really satisfied in these reactions, so neither model can describe all of the data. However, the mean free path requirements, while not being satisfied, are neither grossly violated, so that elements of each model are likely present in the reaction mechanism.

Although some advances have been made recently on this problem, in general the cascade approach uses only free nucleon-nucleon scattering cross sections and neglects the many-body effects which would manifest themselves in the nuclear equation of state. The interaction of an incident nucleon is then treated as a sequence of independent nucleon-nucleon scatterings, it being hoped that the scatterings are sufficiently far apart that the cross sections can be approximated by their asymptotic (i.e. free) values. This approximation may be better for the high energy incident particle than it will be for multiple scatterings of the lower energy struck nucleons. As would be expected, then, the cascade approach is in better agreement with the inclusive cross section data at forward angles than it is at wider angles, where multiple scattering and the Fermi motion of the target nucleons will be more important. Of course, the predictions of the codes will be less accurate at wide angles as well, because of the lower predicted cross sections and hence poorer statistical accuracy.

Similarly, the cascade model predictions for the (p,n)/(p,p') ratio discussed previously are closer to unity than are the data (Ber 67, Kal+ 83).

This may be a Pauli blocking effect, the neglect of which would tend to overestimate the amount of multiple scattering of the struck target nucleons. While it is not an immediate topic of this review, the cascade approach also has difficulty predicting the pion yield in heavy ion collisions (BKD 84). Nevertheless, the cascade approach does reproduce much of the inclusive proton data, and demonstrates that after only a few collisions of the projectile nucleons (3 seems to be an average), the spectrum of secondaries looks surprisingly thermal.

At the other extreme is the hydrodynamics approach which requires a short mean free path compared with the scale of the interaction region. This is not likely to be satisfied in peripheral collisions, where only a few nucleons are interacting, so that a comparison of the model predictions for inclusive cross sections, which include a significant peripheral component, may not be the best test of the model.

In order to make a comparison with inclusive cross sections, the behavior of the nuclear fluid is followed as a function of time, then stopped at a freezeout density corresponding to the system going out of thermal equilibrium. A typical value for the freezeout density is about 1/2 ρ_o, similar to what is found in thermal models. A recent three dimensional hydrodynamical calculations (Buc+ 83) which includes the viscosity and thermal conductivity of nuclear matter, shows good agreement with the shape of the high energy tails of the inclusive proton spectrum (^{12}C + ^{197}Au at 84 A MeV) at forward angles, but poorer agreement at angles wider than 90°. However, the overall normalization is too low by a factor of six. Part of this discrepancy will be rectified by the inclusion of the decay of nuclear and hadronic excited states, although it's not clear whether the spectral shape will be preserved when these decays are taken into account.

A more likely arena for the testing of hydrodynamical ideas would be in the central collisions of heavy ions (Sto+ 81). In such collisions, the densities achieved should be substantially larger than normal nuclear density. Shown in Fig. 33 is a hydrodynamical estimate of the temperatures and densities reached in a central collision. These estimates depend upon the nuclear equation of state since the internal energy per nucleon $W(\rho,T)$ enters into the relativistic Rankine-Hugoniot equation

$$W^2 - W_0^2 + p(W/\rho - W_0/\rho_0) = 0 \qquad (39)$$

where p is the pressure and W_0 and ρ_0 are put equal to 931 MeV and 0.17 fm^{-3} respectively, in front of the shock zone. Two dependences of the compression term in W on the density are shown in Fig. 33: linear and quadratic. In either case, one can see that the densities which are potentially achievable are fairly high. Correspondingly, this will decrease the mean free path and provide a regime in which hydrodynamics can be used more justifiably. As illustrated by the box labelled "Fluid 1" in Fig. 34, the compression of nuclear matter in the fluid dynamical calculations causes a sideways flow of the reaction participants. This is in contrast to many cascade calculations which tend to lead to forward peaking in the angular distributions of the reactant nucleons. This is illustrated by two cascade calculations shown (with labels "Casc 1" and "Casc 2") in the same figure. The data (Sto+ 80a) from a reaction involving the bombardment of U by 393 A MeV Ne ions and triggered on high multiplicities seem to show sideways peaking at low ejected proton energies. While this is by no means proof of collective flow it is suggestive. On the other hand, impact parameter averaging of the hydrodynamic

results tends to wash out the sideways flow, so that one does not expect to see much of an effect in inclusive measurements.

In summary, efforts to bridge the gap between hard scattering models and statistical models by following the multiple collision process numerically have met with at least partial success in providing a more detailed view of the data. The interested reader is referred to the Appendix for further references. We will return to the use of these models for interpreting fragment production in later sections.

3.4 Limiting Temperature in the Hadronic Medium?

In the target fragmentation region under consideration in this review, there appears to be an asymptotic regime above a few GeV incident kintic energy per nucleon where the cross sections for many processes flatten out. For example, shown in Fig. 35 is the behavior of the differential cross section per target nucleon for the (p,p') reaction on heavy targets. One sees that the asymptotic regime in this reaction sets in by about 10 GeV bombarding energy. As can be seen from Figs. 22 and 23, this implies that the temperature and source rapidity associated with the reaction have also reached asymptotic values. (For a critique of the temperature measurement process, see SOG 81.) Is there a novel phenomenon behind this effect?

The exciting physics which could result in such apparently asymptotic features would be a limit to the hadronic temperature (see, for example GK 78c and references therein) perhaps from a phase transition. For example, a quark-hadron phase transition may occur in infinite nuclear matter for a temperature in the 100 MeV range for the densities under consideration here (for a recent summary, see BW 83). Such a transition should have a transition temperature which decreases with increasing net baryon number density (or

chemical potential) (for example, BSW 82). This would lead one to expect a higher transition temperature in proton induced reactions than in heavy ion reactions, since the densities achieved in the former reaction are likely to be lower than in the latter. Unfortunately, experiment would appear to indicate that the reverse is true, as can be partially seen from Fig. 23.

This variability of the temperature would also seem to argue against an interpretation of the effect in terms of the Hagdorn statistical bootstrap model. In that model, the density of states $\sigma(E)$ has the form

$$\sigma(E) = cE^a e^{bE} \tag{40}$$

where a, b and c are parameters. Substituting such a density of states into the partition function

$$Z(T) = \int dE\, e^{-E/T}\, \sigma(E) \tag{41}$$

leads to a singularity at

$$T_c = b^{-1}. \tag{42}$$

The parameters of Eq. (40) which fit the known hadron spectrum gives T_c a value of about 140 MeV, around the range indicated in Fig. 23. But again, one would not expect the limiting temperature to change with projectile.

The cause of the effect probably lies in somewhat more mundane physics. Without question, part of the cause lies in the hadronic density of states: that it requires increasingly more energy to raise the temperature by an equal amount the higher the temperature is. However, the main cause probably has

more to do with the dynamics of NN collisions. For the moment, consider the energy dependence of elastic scattering only. As the incident energy increases, the elastic scattering cross section becomes increasingly forward peaked, as shown by the behavior of the slope parameter b in Fig. 4. This indicates that, at low bombarding energies, an incident nucleon would lose, on average, a substantial amount of its energy in an elastic collision, while as the energy increases, the projectile would be more strongly forward scattered and hence lose less energy as a fraction of its initial energy.

As a simple calculation, define $\bar{t}$ as that 4-momentum transfer in an elastic NN collision such that half of the cross section has a momentum transfer greater than $\bar{t}$ and half less. The energy lost in the lab frame corresponding to this 4-momentum transfer is then an estimate of the mean energy loss, and is shown in Fig. 36. At low incident energies, the fractional energy loss is roughly constant, it taking about 3 collisions to stop an incident nucleon. At higher energies, the fractional energy loss decreases and the amount lost per elastic collision becomes constant. Hence, for a constant number of nucleons in the source (as indicated by geometry) one would expect the temperature to increase roughly linearly with incident energy and then become constant.

Of course, this calculation does not include pion production which will become increasingly important at high energies. However, not all of the energy dissipated into pions will wind up in the target rapidity region. Many of the pions will be emitted "downstream", outside of the target, as it takes a finite time in the projectile's rest frame for the pion to be produced (see article by M. Gyulassy in BW 83). Hence, while inclusion of pion production will allow a greater degradation of the projectile's energy in the multi-GeV

region, the flattening of the temperature in the target rapidity region can still be expected to occur.

It should be pointed out that the direct knockout component should also exhibit asymptotic cross sections, but for a different reason. As the incident momentum becomes very large compared to the measured momentum q, then the minimum momentum k_{min} in the vector diagram Fig. 11 tends to a constant. Hence, the cross sections should also tend to a constant if they depend strongly on k_{min}. Detailed calculations show that the transition to the asymptotic regime is not as sharp as it is experimentally (Fig. 35), but it is still amusing to note that the same general trend is expected as in a thermal model.

To summarize, while aspects of the hadronic density of states may play a role in the asymptotic behavior of the cross sections, a large part of the effect probably arises from simple NN dynamics: the constancy of the energy deposited per collision or the constancy of the internal momentum required to expel a wide angle nucleon.

3.5 Hanbury-Brown/Twiss Effect in the Nucleus

Section 2.3 dealt with two particle correlation experiments as a probe of the reaction mechanism for inclusive measurements. In general, the particles detected were at large momentum difference with respect to each other, in an attempt to separate knockout from statistical effects. Here, we wish to deal with correlations at small momentum difference, in an attempt to determine the space-time dimensions of the source of the particles. For identical particles at small momentum difference, spin-statistics arguments requiring the symmetrization (antisymmetrization) of the two particle wavefunction of bosons (fermions) will lead to correlations between the particles, the magnitude of

the correlations depending on, among other things, the spatial size of the emitting region. This effect was first used in astronomy to estimate stellar sizes and goes under the name of the Hanbury-Brown/Twiss effect (HT 56, Gol+ 60).

In astronomy, correlations between photons are measured. Because the photons have such a low cross section for scattering from each other, and can be emitted from regions of the star which are widely separated, difficulties arising from final state interactions between the photons, and coherence effects in the source, can be minimized. Extending the technique into the hadronic domain (Coc 74, Kop 74) raises the possibility that these effects could be much larger and could substantially alter what one expects on the basis of statistics arguments alone (Biy 83, GKW 79, Gyu 82).

In order to avoid dealing with these problems immediately, we will begin our discussion with pion interferometry involving π^- correlations. The experiments which are interpreted in terms of this effect are generally performed at sufficiently high energy that the particle multiplicity is usually larger than ten so as to minimize coherence in the source region. Pions are measured far enough from the kinematic limits such that modification of the correlation function arising from conservation laws such as conservation of energy, are small.

In π^- interferometry, a correlation function can be defined as (GKW 79)

$$R(p_1,p_2) = \frac{\langle n_{\pi^-}\rangle^2}{\langle n_{\pi^-}(n_{\pi^-}-1)\rangle} \frac{\sigma_{\pi^-} d^6\sigma/d^3p_1 d^3p_2}{(d^3\sigma/d^3p_1)(d^3\sigma/d^3p_2)} \qquad (43)$$

for pions of momenta $\vec{p}_1$ and $\vec{p}_2$. The total negative pion production cross section is denoted by σ_{π^-}, while the momenta of the π^- multiplicity distribution are normalized by

$$\int d^3p_1\, d^3p_2 (d^6\sigma(\pi^-\,\pi^-)/d^3p_1\, d^3p_2) = \langle n_{\pi^-}(n_{\pi^-}-1)\rangle\, \sigma_{\pi^-} \qquad (44)$$

and

$$\int d^3p\, (d^3\sigma(\pi^-)/d^3p) = \langle n_{\pi^-}\rangle\, \sigma_{\pi^-} \qquad (45)$$

Not all authors choose the normalization used above.

If the pions originate from source points $\vec{x}_1$ and $\vec{x}_2$ which are randomly distributed in a region of space specified by a density distribution $\rho(x)$, then the probability $P(\vec{p}_1,\vec{p}_2)$ of observing two pions with momenta $\vec{p}_1$ and $\vec{p}_2$ can be obtained from

$$P(\vec{p}_1,\vec{p}_2) \propto \int d^3x_1 d^3x_2 \rho(\vec{x}_1)\rho(\vec{x}_2)|\Phi_{12}|^2 \qquad (46)$$

where Φ_{12} is the amplitude for observing the two pions. A plane wave form for Φ is assumed:

$$\Phi_{12} \propto \frac{1}{\sqrt{2}} (e^{-i\vec{p}_1\cdot\vec{x}_1} e^{-i\vec{p}_2\cdot\vec{x}_2} + e^{-i\vec{p}_1\cdot\vec{x}_2} e^{-i\vec{p}_2\cdot\vec{x}_1}) \qquad (47)$$

Two terms are required because one does not know whether a given pion originated at $\vec{x}_1$ or $\vec{x}_2$. The plus sign is imposed by Bose-Einstein statistics. With this choice of Φ, Eq. (46) becomes

$$P(\vec{p}_1,\vec{p}_2) \propto 1 + |\rho(\vec{p}_1-\vec{p}_2)|^2 \qquad (48)$$

where $\rho(\vec{p})$ is the Fourier tranform of $\rho(\vec{x})$. In general the pions are allowed to be emitted at different times as well as different spatial points, so that ρ is made to be a function of $\vec{x}$ and t, and the correlation function becomes a function of $\Delta\vec{p}$ and ΔE. If the density be assumed to be a guassian in both space and time,

$$\rho(r,t) \propto \exp(-r^2/r_0^2 - t^2/\tau^2) \qquad (49)$$

where r_0 and τ measure the space-time volume of the emitting region, then the correlation function becomes

$$R(q_0,\vec{q}) \propto \exp(-\vec{q}^2 r_0^2/2 - q_0^2\tau^2/2) \qquad (50)$$

Here, $\vec{q}=\vec{p}_1-\vec{p}_2$ and $q_0=E_1-E_2$.

On the experimental side, a function form such as Eq. (50) is often assumed, and the parameters r_0, τ and the normalization are varied to obtain a best fit to the data. The normalization can be used a check on the incoherence assumption used in the derivation of Eq. (50) (Gyu 82). Corrections are often made for the mutual coulomb interaction of the two pions, but the changes in r_0 determined by the fitting procedure are usually not large once these corrections are incorporated (YK 78, Bea+ 83a). The fits were not as sensitive to τ as they were to r_0, so the lifetime remains a less well determined quantity.

Preliminary experimental work with a 1.8 A GeV Ar beam on heavy targets gave r_0 in the 3 fm region (Lu+ 81, Fun+ 78, Zaj+ 81). More recent work (Bea+ 83a) with 1.5 A GeV ^{40}Ar on KCl gave larger values, namely r_0~5 fm with

τ fixed at 5×10^{-24} sec. in the fit. These authors also tried a fit to the function

$$\exp(-\vec{q}_{||}^{\,2}r_{||}^{2}/2 - \vec{q}_{\perp}^{\,2}r_{\perp}^{2}/2 - q_0^2\tau^2/2) \qquad (51)$$

to see if there was a difference between the transverse and longitudinal dimensions of the pion source. No significant deviations were observed.

The dependence of the source size on the observed pion momentum in the center of mass frame p_{cm}, was also investigated in Bea+ 83. They found R=6.0±1.1 fm in the case where both pions had p_{cm}<150 MeV/c and R=4.1±0.5 fm when both pions had p_{cm}>150 MeV/c. In other words, higher energy pions came from smaller sources. This may be a reflection of the cooling down of the pion source during expansion, or of the distribution of the fluctuations in energy density during source formation.

One can use the estimated size to obtain a density for the source. By equating the root mean square radii for a uniform spherical density distribution with a sharp edge at radius R_S, and for the gaussian form assumed above, one finds $R_S=\sqrt{5/2}\ r_o$. Taking the value of r_o=5 fm found above, and assuming that the source contains 80 nucleons, the corresponding density is ρ=0.04 fm^{-3}, which is somewhat less than 1/4 ρ_o. A more recent analysis (Bea+ 83b) of 1.2 A GeV Ar+KCL collisions gives a somewhat lower r_o than the 1.5 A GeV data, namely 3.8±0.5 fm, corresponding to a density of 0.09 fm^{-3} in the calculation outlined above. Both of these results are comparable to what one finds in a thermal model analysis of inclusive pion production (BR 84).

Because a fairly large energy per nucleon is required for $2\pi^{\pm}$ interferometry, the technique is not so useful at lower bombarding energies. Here, where nucleon multipllicity is still large, 2p interferometry can be

used (Koo 77b, NY 81). However, for two proton correlations at small relative momenta final state interactions are much more important than they are for the two pion sysem. A convention often taken for the two proton correlation function is (Koo 77b)

$$1 + R(\vec{p}_1,\vec{p}_2) = \frac{\sigma_p d^6\sigma/d^3p_1 d^3p_2}{(d^3\sigma/d^3p_1)(d^3\sigma/d^3p_2)} \qquad (52)$$

Assuming a gaussian form for the source region in space and time, the correlation function can be written as (Koo 77b)

$$R(\vec{p}_1,\vec{p}_2) = \frac{1}{(2\pi)^{3/2}r_o^3 D}\int d^3r\ \exp\left[-\left[r^2-(\vec{r}\cdot\vec{V}'\tau/D)^2\right]/2r_o^2\right]$$

$$\times\left\{\frac{1}{4}\left|{}^1\psi(\vec{q},\vec{r})\right|^2 + \frac{3}{4}\left|{}^3\psi(\vec{q},\vec{r})\right|^2 - 1\right\} \qquad (53)$$

where $\vec{V}'=\vec{V}-\vec{V}_o$, $\vec{V}$ being the lab velocity of the 2p center of mass and $\vec{V}_o$ the lab velocity of the emitting region. The quantity D is not really a free parameter, since it depends upon V' through $D=(r_o^2+(V'\tau)^2)^{1/2}$. The singlet and triplet p+p scattering wavefunctions are denoted by ${}^1\psi$ and ${}^3\psi$.

Equation (53) is evaluated numerically. Both coulomb and nuclear effects must be taken into account in evaluating the wave functions. An example of such a calculation is shown in Fig. 37. The Reid soft core central, spin orbit and diagonal tensor potentials were used to generate the nuclear part of the wave functions (restricted to $\ell\leq2$). The nuclear part is responsible for the peak around Δp=20 MeV. The trough at small Δp arises from the coulomb contribution. The parameters r_o and τ were fixed at 4 fm and 0 sec. respectively. As the source size or the lifetime increases, the nuclear peak decreases.

This predicted form for the correlation function has been observed experimentally for both high and low energy heavy ion reactions. In high energy (1.8 A GeV Ar + KCl) experiments (Zar+ 81) with no multiplicity cut, the parameter r_o was found to have a value of 2.2 fm for two protons in the beam rapidity (y_B) region, and a smaller value of 1.75 fm in the mid rapidity ($y_B/2$) region. Their analysis assumed that τ=0; relaxation of this assumption would lower the r_o required to fit the data. The source sizes so obtained are significantly smaller than those found in 2π interferometry perhaps reflecting the fact that the protons observed in this experiment, which had an energy of more than 200 MeV, came from an earlier stage of the reaction.

An experiment was performed at lower energies with 25 A MeV ^{16}O on ^{197}Au. Preliminary results (Lyn+ 83) for the correlation function found in this experiment are shown in Fig. 38. The value of r_o extracted from this data is 4 fm assuming τ=0. This value decreases with increasing proton energy. For example, taking a subset of the data with summed proton kinetic energy above 90 MeV gives a value to r_o of 3.1 fm. These results are more in line with the high energy $2\pi^-$ results. Taking r_o=4 fm, and assuming that the source has twice as many nucleons as the projectile, gives a density of 0.03 fm^{-3}.

To summarize, the nuclear Hanbury-Brown/Twiss effect may be able to provide us with much needed information about the space-time evolution of nuclear reactions involving the emission of energetic ejectiles, although the interpretation of the data may be hampered by spurious correlations caused by partial coherence of the source or other effects (GKW 79, Gyu 82). The first results from heavy ion experiments indicate that the more energetic the particles, the smaller the source. The source sizes extracted so far are neither outrageously small or large. Usually, the time scale is a fixed input parameter, although a recent analysis of $2\pi^-$ interferometry which fitted the

lifetime gave $\tau=1.8\pm0.6\times10^{-23}$ sec (Bea+ 83b). Lastly, experiments are now also underway in proton induced reactions, and these should presumably show smaller source sizes than the heavy ion reactions give.

4. Light Fragment Formation

4.1 Overview

Although free nucleons represent the most likely product of a nuclear reaction in the intermediate and high energy range, nuclear fragment production is also common. Typically, the yield of deuterons (integrated over energy and angle) is fairly large, being about one-third of the proton yield. The yields of heavier mass fragments are less, but the decrease with increasing mass is not precipitous. For example, shown in Fig. 39 are the cross sections observed for fragments in the target rapidity region, and one can see that these cross sections are substantial.

Not only have total yields been measured, but the inclusive cross sections of a wide range of projectiles have been obtained as well: pions (for example Ama+ 75), photons (HPU 66, KP 63, MV 65), electrons (Flo+ 78, Flo+ 79, MGS 77, Mur+ 78), protons (Ala+ 75, Bog+ 76, BP 73, Che+ 75, FMP 62, Fra+ 76, Fra+ 79, GK 78b, GK 80, Kom+ 76, Nak+ 82, PBH 71, Pos+ 75, Rai+ 75, Seg+ 82, Sut+ 67, Vol+ 75, WCH 79c, Wes+ 78, Zeb+ 75), light ions (Doe+ 78, Sch+ 79b, Tho+ 79, WCH 79a, WCH 79b, Zeb+ 75) and heavy ions (Aub+ 82, Awe+ 81, Awe+ 82, Gos+ 77, Gut+ 83, Ho+ 77, Lem+ 79, Nat+ 81, Pos+ 75, San+ 80b, Wes+ 83). They show the same general behavior as a function of ejectile energy as do the nucleon spectra, namely an exponentially decreasing function. An example is shown in Fig. 40. The differential cross sections seem to decrease smoothly with fragment mass A_F up to about mass 10, at which point there may be a qualitative change in the data (depending, of course, upon how it is plotted). Certainly, below mass 10 there is more variation in the cross sections from one mass to the next, while above mass 10 the decrease is smoother and less steep. For this reason, light mass fragments ($2 \leq A_F \leq 10$ will be the operative definition here) will be treated separately in this review, followed by a

section on intermediate mass fragments ($10 \leq A_F \leq 30$ here). Heavy fragment production, which includes fission, will not be dealt with in this review. (See Appendix for introductory references. Some of the systematics of heavy fragment production can be found in Win 80a, Win 80b.) This delineation of mass range is more for the convenience of the author than does it represent a fundamental shift in the physics of the reaction mechanism, although certainly it is difficult to imagine that a pick-up mechanism which might be important for deuteron production also being applicable to silicon emission.

The fact that we are dealing with energetic fragment emission presumably means that the time for the reaction which produced these fragments to occur is longer than that for nucleon emission; more target nucleons must undergo a change in momentum to form an energetic fragment (implying multiple NN collisions) than would be required for energetic nucleon emission. One can test this idea at least in part by examining the data from the standpoint of a cluster knockout model, similar to the direct knockout model of proton emission. In such a model, the projectile strikes a preformed cluster near the nuclear surface, ejecting it with a large amount of kinetic energy. Such models had been used in low energy reactions (Ari+ 72, MB 73, MBS 76, Mil+ 74, SBM 77) where the energy transfer is much less, and in reactions involving specific states (for example CR 77, Dol+ 79).

Part of the motivation for this approach comes from the similarity of scaling behavior observed in heavy ion collisions (PSF 77) and proton induced reactions as well as the non-zero analyzing power observed in some (Sak+ 80, TLU 81) but not all (GJK 82) (p,α) experiments. Calculations for cluster knockout in intermediate energy proton induced reactions have been successful in fitting the data (BW 79, Boa+ 81), as shown in Fig. 40. The normalization of the model depends upon the effective number of transient clusters on the

surface, n_{eff}. Phenomenologically what one does is determine n_{eff} by fitting the data. The numbers of clusters so determined, while not outrageous, show behavior which is difficult to understand. For example, in the (p,α) reaction, one would expect that light targets (such as Be or C) which are largely surface and may have a large alpha particle component to their ground state wave functions, actually show a smaller n_{eff} for alpha particles (compared to $A_{TARGET}/4$) than does a heavy target such as silver (Boa+ 81). Attempts to test the normalization of the cluster knockout model by comparing (e,α) with (p,α), as was done with (γ,p) and (p,p'), were inconclusive (BW 81). Because of the peculiar behavior of n_{eff}, the idea of cluster knockout will not be pursued in this review, but rather models with multiple nucleon-nucleon scattering will be concentrated on. As was stated before, a non-zero analyzing power can arise even in a thermal model if the source formation depends sensitively on the first NN interaction.

4.2 Coalescence and Pickup Models

The cluster knockout model described above represents one extreme of the model spectrum, namely that the mechanism is dominated by the dynamics of the direct projectile-cluster interaction. At the other extreme are statistical models in which the dominant effect is phase space. In some sense, in between these extremes lie pickup and coalescence models, to which we will turn our attention now. Statistical models will be dealt with in Sections 4.3 and 4.4.

One can imagine that in high multiplicity reactions, such as would be expected in heavy ions, clusters could be forming and breaking up during the expansion phase of the reaction. Depending on how fast these reactions proceed, there may be simplifications in the description of the mechanism. For example, if the formation and break up are very fast compared to the

expansion rate then one could imagine that a chemical equilibrium is achieved, and statistics play a dominant role. If fragment formation occurs more towards the end of the expansion phase, and fragment breakup is less likely, then a coalescence or condensation description might be more important: fragments are formed near freezeout only when nucleons are sufficiently close in phase space. This is illustrated in Fig. 41b.

For low multiplicities such as are often found in proton induced reactions there are fewer nucleons close enough together in phase space to coalesce compared to a heavy ion reaction. Then, a pickup model in which an outgoing nucleon picks up a few nucleons as it nears the nuclear surface, would be an approximate description. This is shown in Fig. 41a. As in the case of energetic nucleon emission, several mechanisms are probably at work simultaneously so our task will be to find which are important in which kinematic etc. regime.

In principle, what one would want to do is use the actual nuclear wave functions to determine whether a group of nucleons occupying a particular configuration in phase space can form a fragment. Approaches to fragment production along this line have generally been limited to deuteron production because of the computational difficulties (BP 61, BP 62, BP 63, SZ 63, Kap 80, BC 81, SY 81, GFB 83, Aic 83). For heavier fragments, drastic simplifications are made, as will be outlined below.

The pickup model, or snowball model as its Canadian practitioners have called it (HCH 80, Boa+ 81, see also Boa 80a), will be treated first. According to Fig. 41a, the differential cross section for fragment emission, $d^2\sigma(p,F)/dE d\Omega$, should be proportional to the differential cross section $d^2\sigma(p,n)/dE d\Omega$ for the first scattering in which the "snowballing" nucleon is produced at the angle and energy (on the average) of the observed fragment.

This differential cross section must be multiplied by a probability P that in a subsequent scattering, the secondary struck nucleon will be scattered into a momentum space volume V_S. For small P, the cross section expression becomes (Boa+ 81, BS 82, Boa 82b):

$$\frac{d^2\sigma}{dEd\Omega}(p,F) = C_{FT}\frac{d^2\sigma}{dEd\Omega}(p,N)\,P^{A_F-1} \qquad (54)$$

for a fragment of mass A_F. Combinatoric factors are incorporated in C_{FT} while impact parameter averaging, and mean path length effects (of the snowballing nucleon) are omitted. This expression is in rough agreement with the observed (Flo+ 78, Flo+ 79, WCH 79c) ratio of the (e,α)/(p,α) reactions (See BS 82). Assuming P is constant along the outgoing trajectory, then a plot of log $C_{FT}^{-1}d^2\sigma(p,F)/dEd\Omega$ vs A_F-1 at constant fragment energy and angle should yield a straight line whose slope is log P. Such a plot is shown in Fig. 42. The straight line behavior extends to a fragment mass of ~9, probably larger than what one would expect for a pickup mechanism, given the limit on the number of collisions that can realistically take place in the target nucleus. The momentum space volue V_S,

$$V_S = \frac{4\pi}{3}P_S^3 \qquad (55)$$

can be found from the value of P extracted from the graph

$$P = \frac{1}{\bar{M}}\frac{1}{\sigma_R}\frac{d^3\sigma(p,N)}{d^3q}V_S \qquad (56)$$

where $\bar{M}$ is the mean multiplicity and σ_R is the p-nucleus reaction cross section. Of course, the differential cross section used in Eq. (56) is for a much lower incident energy that that in Eq. (54), since it involves the rescattering of a secondary nucleon. Values for p_S obtained in analysis (BS 82) of data on Ag targets were in the 155-170 MeV/c range. For uranium targets, the values were about 180 MeV/c, probably reflecting the larger path length available for pickup rather than a real change in p_S. This number should be comparable to the average momentum per nucleon in a light target (and not to the Fermi momentum) and indeed it is, experimentally (Whi+ 74). A crude attempt at including Pauli blocking (BS 82) raised the phenomenological value of p_S to ~200 MeV/c, which can then be compared to the Fermi momentum for light targets.

The target dependence of the fragment cross section can be used to extract an accumulation length D for the fragment to form (BS 82). It was mentioned above that alpha production decreased for light targets faster than the target mass. Suppose that a nucleon must traverse a minimum average distance D in reaching the nuclear surface to pick up enough nucleons to form for example, an alpha particle. The number of target nucleons available for initiating alpha production (i.e., are more than a distance D away from the surface facing the detector) is

$$A_{eff} = A_T\left[1 + \frac{1}{2}(\xi^3 - 3\xi)\right] \equiv A_T G(\xi) \qquad (57)$$

where ξ D/2R, R being the nuclear radius. A comparison of this functional form to the data is shown in Fig. 43. What has been plotted is the ratio of the differential cross sections for the (p,α) reaction at fixed α energy and angle to the same value for uranium. This hopefully cancels any target dependence in the (p,N) cross section which appears in Eq. (54). The solid curve shows G(ξ) with D=4 fm. In other words, in order for a nucleon to pick

up enough other nucleons to form an alpha, it must start out 4 fm from the surface, on average. This number is about what one would intuitively expect.

Other tests to which the pickup model can be put involve the projectile energy dependence of the differential cross section (Boa 82a). As was indicated in the discussion of the limiting temperature behavior of the (p,p') reaction, the differential cross section increases with bombarding kinetic energy K_p in a simple power law form K_p^{δ}. In fact, this behavior appears to be valid for a number of reactions, as shown in Fig. 44. Now, from Eq. (54) the exponent for fragment production δ_F should be equal to δ_p in the snowball model. As will be shown below, for the coalescence model, one should find $\delta_F = A_F \delta_p$. A comparison of the predictions is given in Table 1. One can see that the snowball model is reasonably successful in describing proton or alpha induced reactions, which have low multiplicity. (It fails for heavy ion reactions, see Boa 82a.) Similarly, the coalescence model at least passes this test for heavy ion reactions, but fails for proton induced reactions. Even though the snowball model is in not too serious disagreement for proton induced reactions, there must be other reaction paths which compete with it. For example, shown in Fig. 45 are some possible contributors to alpha emission. The pure snowball is labelled I, but other contributors must be present as well. Diagrams II and III will raise δ_F for (p,α) in Table I to 1.6, in agreement with experiment, and are probably more likely than I or V on mean free path arguments.

We expect, then, that as we increase the mass of the projectile there should be a shift in the reaction mechanism (Boa 82b). Deuteron induced reactions seem to be similar to proton induced reactions, in that (Zeb+ 75)

$$\frac{d^2\sigma(d,F;2.1\ \text{GeV/nucleon})/dE d\Omega}{d^2\sigma(p,F;4.9\ \text{GeV/nucleon})/dE d\Omega} \sim 1.5 \qquad (58)$$

independent of fragment energy and angle for a variety of light fragments. If one estimates a correction for the differing energies (per nucleon) of the p and d projectiles, then the ratio is raised to 2.5±0.5. This is in the range which one would expect if the deuteron were behaving like two independent nucleons.

For proton emission in alpha induced reactions, the same appears to be true. An example of the ratio of (α,F) to (p,F) data (San+ 80b) for F=p,d and t is plotted in Fig. 46. Independent of angle, the (α,p)/(p,p') ratio is observed to be about 3.0. If the incident alpha were behaving like four independent nucleons, one would expect (Boa 82b)

$$\frac{(\alpha,p)}{(p,p')} = 2\left[1 + \frac{(n,p)}{(p,p')}\right] = 3.0 \qquad (59)$$

as is indeed observed. However, this simple behavior is not observed for deuteron or triton emission, perhaps because of the higher nucleon multiplicities making the coalescence or other contributors more important than they are in proton induced reactions.

In its simplest form, the coalescence expression for fragment emission is (Gut+ 76, Gos+ 77, Mac 79, Mek 77. See also Mac 80, Sch+ 83)

$$\frac{d^3\sigma}{d^3p_N}(p,F) = \frac{d^3\sigma}{d^3p_N}(p,n)\,\frac{1}{A_F!}\left[\frac{1}{\sigma_R}\frac{d^3\sigma}{d^3p_N}(p,N)\,V_o\right]^{A_F-1} \qquad (60)$$

where p_N is the average momentum per nucleon in the fragment. Again, V_o will represent a momentum space volume within which a given nucleon must lie in order to be part of the fragment. Clearly, plots similar to Fig. 42 are to be expected, as in the pickup model. As it is, this type of plot has not been emphasized in heavy ion reactions, perhaps because many of the data sets

measure only Z=1 and 2 fragments. What is often made, therefore, is a comparison of the differential cross sections over a wide range of p_N, the normalization then determining p_o in

$$V_o = \frac{4\pi}{3} p_o^3 \qquad (61)$$

An example of such a comparison is shown in Fig. 47 for the low energy heavy ion reaction 310 MeV $^{16}O+^{197}Au$, where the fragment differential cross section is compared with the proton cross section raised to the appropriate power (Awe+ 82). The curves are surprisingly similar, although the logarithmic scale helps suppress the differences. The values of p_o which are extracted from the data appear to be a function of both energy and target. In early work (Gut+ 76, Gos+ 77) performed using Eq. (60), the values ranged from 106 to 147 MeV/c, the fragment mass dependence being the strongest variable. These values are certainly fairly small compared to what one would expect for the average Fermi momentum. Of course, not only have spin and Pauli blocking been ignored, as was done in the snowball model, but also coordinate space correlations have been neglected. In the snowball model, this is probably not too serious, as any nucleons which the "seed" nucleon picks up must be struck by this primary nucleon and hence be in reasonably close proximity to it. However, since Eq. (60) uses differential cross sections which measure all protons, regardless of where in the target nucleus region they originated, this correction should be more substantial. Since these coordinate space effects will tend to reduce the number of nucleons available for fragment formation, the p_o required to fit the data will increase and be in better agreement with what one expects from a Fermi gas model. (See JDM 82 for further discussion of coordinate space effects in the coalescence model.)

A more extensive compilation of p_o's has been obtained using the definition (Lem+ 79)

$$\frac{d^3N(Z,N)}{d^3p_N} = \left(\frac{N_t+N_p}{Z_t+Z_p}\right)^{N_F} \frac{1}{Z_F!N_F!} \left(\frac{4\pi}{3} p_o^3\right)^{A_F-1} \left(\frac{d^3N}{d^3p_N}\right)^{A_F} \qquad (62)$$

where $p_{A_F} = A_F p_N$ and N and Z represent the neutron and proton numbers respectively of the target (t) and projectile (p). The values of p_o so obtained show substantial variation with projectile, target, fragment and energy. Mekjian (Mek 78a) has pointed out that if one takes spin and other factors into account, p_o is reduced from those values found using Eq. (62), by about 30%. Pauli blocking and other corrections still have not been taken into account, however, so the values of p_o cannot be directly compared with Fermi gas results. However, the momentum radii do show a surprisingly large target dependence for a given fragment type, changing by up to 50% in some cases. Hence, there are probably other significant contributions to light fragment formation in heavy ion collisions beyond just the coalescence contribution.

Both of these models have used rather drastic assumptions in order to obtain analytic expressions which can be used for analyzing a variety of data. A more exact approach has recently been developed (GFR 83) which uses a cascade code to calculate a position and momentum space distribution of nucleons. Extraction of the fragment (in this case deuteron) differential cross sections is then made using a technique advanced by Remler (RS 75, RS 78, Rem 81, Rem 82). The method is in effect parameter free: no arbitrary coalescence radii, source volumes or breakup densities appear. The agreement

with the data from heavy ion experiments over a wide range of angles is remarkably good.

4.3 Statistical models

If the (p,p') reaction on heavy targets exhibits statistical behavior, then it should come as no surprise that fragment production does also. Shown in Fig. 48 is the usual $q_\perp/m$ versus y plot for several fragments measured in the reaction of 480 MeV protons on silver (GKJ 83). The appearance of the curves is similar to that observed for U(p,p') in Fig. 21. As before, the centers of the circles appear to change with observed energy: the larger the radial velocity (V_r) the larger the apparent source velocity (V_s). This feature is shown on Fig. 49 in a representation advanced by Price and Stephenson (PS 78). Such behavior might be expected if a similar amount of energy and momentum were deposited into a source of variable size, smaller sources then having a larger T and V_s than larger ones.

Even electron induced fragment emission (Flo+ 78, Flo+ 79) can be analyzed in terms of the thermal model. However, a comparison (BW 81) of the electron to proton-induced cross sections argues that only a single scattering of the electron is required to initiate thermalization. The ratio shown in Fig. 50 would be much smaller than α_{em}^2 if multiple scatterings of the electron were required.

It was shown in Sections 3.1 and 3.2. that the lifetime of reactions which involve heavy targets may be long enough to produce thermal equilibrium, but may not be long enough to establish chemical equilibrium. These conclusions were based on the study of nucleon emission. Fragments, as we have argued, probably involve a larger number of NN scatterings in their formation and emission, so their measurement may, on the average, sample a

later stage in the reaction than nucleon emission does. Hence, it is tempting to assume that the system has achieved chemical as well as thermal equilibrium. This allows the elimination of the chemical potentials in the expression for the fragment abundances, leaving only the volume of the emitting region as a parameter (as was seen in pion emission). The kinetic model approach has been applied to a wide variety of systems: see Bec+ 81, Bon+ 77, Cse+ 83, GK 81, GKW 78, GW 79, Mek 77, Mek 78b, Mek 80, RK 81, SWW 82. The geometrical and other assumptions used in thermal model approaches can be found in CDM 80, JDM 82, Kap 80. Specifically, for a given fragment characterized by Z_F, N_F, A_F and ground state energy E_o emitted from an N=Z region of volume V, one has (Mek 77):

$$\frac{d^3N(Z_F,N_F)}{d^3p_N} = \frac{A_F^{3/2}}{2^{A_F}} f(Z,N) \left(\frac{(2\pi)^3}{V}\right)^{A_F-1} \left(\frac{d^3N_N}{d^3p_N}\right)^{A_F} \tag{63}$$

The quantity f(Z,N) is given by

$$f(Z,N) = A_F^{3/2} \exp(E_o/T) \sum_i (2S_j+1) \exp(-E_j/T) \tag{64}$$

where the sum extends over the ground and excited states of the fragment with S_j being the spin of these states and E_j being their excitation mesured from E_o. One can see immediately that a similar power law dependence of the fragment cross sections on the nucleon cross section as was observed in the snowball and coalescence models is also observed here. Further, one can make a formal identification between V and p_o in Eq. (62) (where $N_t+N_p=Z_t+Z_p$) when there is only one state in the summation in Eq. (64):

$$V = (Z_F!N_F!e^{E_o/T})^{1/(A_F-1)} \left(\frac{3(2\pi)^3}{4\pi\bar{p}_o^3}\right) \tag{65}$$

where $\hbar$ has been put equal to unity. The quantity $\bar{p}_o$ is related to p_o via

$$(p_o^3)^{A_F-1} = A_F^3 \frac{2S+1}{2^{A_F}} (\bar{p}_o^3)^{A_F-1} \tag{66}$$

Some typical values found for p_o, $\bar{p}_o$ and R $\left[R \equiv (\frac{3V}{4\pi})^{1/3}\right]$ have been taken from Lem+ 77 and are summarized in Table II. Of course, R still varies from one target-fragment combination to the next, but now such a variation is not unexpected in principle. In fact, R appears to increase with the mass of the reactants for fixed fragment mass, as one would expect. The only troublesome aspect (aside from the energy dependence) seems to be their magnitude: their values appear to be smaller than comparable radii found in the Hanbury-Brown/Twiss experiments. Of course, if more excited states could be summed over in Eq. (64), V would be correspondingly larger.

To summarize, the parameters extracted from the thermal model analysis appear to be better behaved than those of the coalescence model, on the basis of the approximations made to the models thus far. The projectile energy dependence tests which the coalescence model successfully passed in Section 4.2 will also be passed by the thermal model.

Before leaving this section, the question of time scales should be addressed. We will deal with the times appropriate for heavy fragment formation in Section 5. Here we wish to deal only with light fragments, namely deuterons. A gas which is composed initially only of nucleons can form deuterons via many reaction paths, for example

$$\begin{matrix} n + p + N \rightarrow d + N \\ \\ n + p + d \rightarrow d + d \end{matrix} \tag{67}$$

<u>etc</u>. If one knows the cross sections for these processes, then a set of coupled rate equations can be solved to follow the deuteron abundance as a function of time (Mek 78b, Kap 80). The particle number densities ρ_i will approach their equilibrium values $\rho_{i,eq}$,

$$\left(\frac{\rho_d}{\rho_n\rho_p}\right)_{eq} = \frac{3}{4}\left(\frac{4\pi}{mT}\right)^{3/2} \tag{68}$$

at a rate determined from

$$\frac{d\rho_d}{dt} = \left[\rho_p\rho_n\left(\frac{\rho_d}{\rho_p\rho_n}\right)_{eq} - \rho_d\right]\rho_N\langle v\sigma(N+d\rightarrow N+p+n)\rangle \tag{69}$$

Here, only the first process in Eq. (67) is being considered in the thermal average of the product of the relative N-d velocity with the cross section σ. By using a simple analytic hydrodynamic model (BGZ 78) for the expansion of the hot zone, Kapusta (Kap 80) calculated the rate of approach of the deuteron abundance to its value at chemical equilibrium. Two examples of starting conditions which one might expect to find were considered, and in both cases the abundance had evolved to close to its equilibrium value in less that 10^{-23} sec. Hence, the application of statistical models to light fragments may not be inappropriate. Cugnon and Jaminon (CJ 83) exercise more caution on the chemical equilibrium question, based on cascade model calculations.

Another approach which is currently being developed is the extension of the evaporation formulation of particle emission (HF 52) used to describe the low energy part of the particle spectrum (see GK 81 for example). This technique (FL 83) follows the time evolution of a source emitting particles statistically, assuming that the source can re-equilibrate rapidly after each particle is emitted. Good agreement is obtained with the data. Lastly, Bertsch and Siemens (BS 83) have proposed that there may be kinematic domains where the breakup of nuclear matter arises from mechanical instability (see Section 5 as well).

4.4 Entropy in the Nucleus

The fact that the thermodynamic approach to the nuclear reactions which we have been considering works as well as it does, leads us to try to use these reactions to investigate the nuclear equation of state. In particular, since the hydrodynamic approach assumes isentropic expansion of the reacting region, and this assumption is supported by cascade calculations (BC 81), then one may be able to measure the entropy in the early stages of the reaction by finding a way to determine it from the final debris of the reaction.

Such an approach was put forward by Siemens and Kapusta (SK 79) who proposed using the deuteron to proton ratio as a measure of the entropy. For a dilute system in chemical equilibrium, the entropy is given by the Sackur-Tetrode formula

$$S = \sum_i N_i \left[\frac{5}{2} + \ln \frac{g_i}{\rho_i} \left(\frac{m_i T}{2\pi}\right)^{3/2}\right] \qquad (70)$$

where N_i is the number of particles of species i, with density, mass and statisitical degeneracy ρ_i, m_i, and g_i respectively. For temperatures large compared to the deuteron binding energy this leads to the simple expression

$$S/A = 3.95 - \ln d/p. \qquad (71)$$

Since the observed d/p ratios are typically in the 1/3 range, then S/A calculated from this expression will have a value of about 5. This value is surprisingly large compared to what would be expected in hydrodynamics, for example. There, estimates (Sto 81) are in the 3-3 range for a reaction involving a projectile of energy 800 A MeV, about two units below what is found from Eq. (71).

The presence of extra entropy in the final products of a reaction might be an indication of a nuclear phase transition (a topic to which we will return in Section 5) so the determination of the entropy is a significant problem. Somewhat more sophisticated calculations which drop the dilute limit assumption of Eq. (70) have been performed (Kap 83) and lower S/A somewhat but not down to the hydrodynamic results. A cascade calculation has been performed (BC 81) which calculates the nucleon occupation probability of phase space f, and then obtains the entropy through the dilute limit expression

$$S/A = 1 - \langle \ln f \rangle. \qquad (72)$$

The calculation was performed for a $^{40}Ca+^{40}Ca$ collision at 800 A MeV, and gave S/A of about 4.4. It also showed that S/A was roughly constant after the nuclei has been in collision for about 3×10^{-23} sec.

At this point, it is not perfectly clear whether the assumptions made in the various formula for extracting the entropy are causing the apparent

disagreement. Stöcker (Sto 81) has argued that one should include the decay of higher mass nuclei into deuterons and protons, so that the true entropy is not given by Eq. (71). He is able to reproduce the observed d/p ratio with a much smaller S/A by incorporating such decays, although the calculation depends on the breakup density and viscosity assumed. Other recent work relevant to the entropy question can be found in Bir+ 83, Kno+ 82, KS 81 and MMS 80. One complication of the entropy interpretation has been the recent observation (Gut+ 83) that cluster production appears to be a function of the multiplicity of the reaction.

4.5 Results from Coincidence Experiments

Just as in the study of inclusive proton reactions, one needs to go to coincidence experiments to further elucidate the reaction mechanism for fragment production. (For coincidence experiments involving specific states, see Bac+ 76, Roo+ 77, for example.) Currently, these studies are in their infancy, although enough new data have been taken recently that some issues can be at least partly resolved (Bac+ 80, Bin+ 80, Cra+ 84, Hel+ 83, Mey+ 80, Tan 83).

One such study (Hel+ 83) looked for direct interaction effects in proton induced reactions. A light target was chosen, and coincidences between wide angle (90° in the lab) energetic deuterons on one side of the beam and fast forward protons on the other side were sought. The results of the experiment were surprisingly similar to the (p,2p) results found with the same experimental setup.

Shown in Fig. 51 is the behavior of the differential multiplicity as a function of forward proton energy and angle for two deuteron trigger momenta. For the lower of the two momenta (q=517 MeV/c) a strong enhancement is

observed near the kinematic limit (the differential multiplicity shown is integrated over the highest 25 MeV of forward proton energy.) For the next highest energy interval shown, namely 75 to 25 MeV of the maximum, there is still a peak in angle, but the coincidence rate is reduced. At higher deuteron trigger momentum (q=588 MeV) the angular peak remains but the peak near the kinematic limit has decreased. This behavior is quite similar to that shown for the (p,p') reaction considered in Section 2.

In the (p,p') reaction, the peaks in the angular distributions were observed to be slightly outside of the QTBS angle (which is defined as the angle between the vectors $\vec{p}-\vec{q}$ and $\vec{p}$, where $\vec{p}$ and $\vec{q}$ are the projectile and deuteron momenta, respectively). In this experiment, similar behavior is observed, as is shown in Fig. 52. By assuming that the differential mean multiplicity is symmetric in angle around the QTBS angle, one can integrate over forward proton energies and angle to determine the percentage of time that a wide angle deuteron is accompanied by a forward proton. As with the (p,2p) reaction, the percentage decreases with trigger momentum, an average being in the 25% range. The forward proton multiplicity is shown as a function of trigger momentum in Fig. 5.

These observations certainly argue against a thermal model being the sole contributor to the deuteron formation mechanism here, since such a large fraction of the deuteron triggers are accommpanied by a forward proton which has lost only enough energy to produce the deuteron. The fact that the forward proton angular distributions show a peak around the QTBS angle for the deuteron momentum can be interpreted to mean that contributors to the mechanism such as are shown in Fig. 54 may be important. The term "coalescence" is applied loosely to contribution III in Fig. 54, since the original coalescence model makes no assumption about the origin of the

coalescing nucleons. In each of these contributors, the momentum of the observed deuteron plays a central role in determining the scattering angle of the forward proton, so we expect them all to give a forward proton peak in the neighborhood of the QTBS angle.

One can try to use the forward proton multiplicities associated with the deuteron trigger to distinguish between these mechanisms, but only in one case is there a strong test as yet. That is for the pickup model. Since this model contains the emission of an energetic nucleon as the first step, then one can relate the forward multiplicity for a deuteron trigger with that for a proton trigger. Since the incident nucleon must lose at least as much kinetic energy to nucleon A in II as the observed deuteron gains (neglecting binding energy effects), then one test would be to compare the two multiplicities at the same trigger kinetic energy. To do this, a fit was made to the forward multiplicities with proton triggers; a function of the form

$$m_f = 13.2 \exp(-q/103 \text{ MeV/c}) \qquad (73)$$

described the data reasonably well. This is compared to the deuteron data at the same kinetic energy in Fig. 53. The agreement is not spectacular, but better than might be expected. It should be pointed out, however, that if the primary struck nucleon in the pickup mechanism (II) is on the mass shell with the deuteron's observed energy, then the corresponding QTBS angle would be smaller than the peak position in the multiplicity. For example, a deuteron with momentum 600 MeV, and kinetic energy 93 MeV, will have a QTBS angle of 37°, as shown in Fig. 52. A proton emitted at 90° with a kinetic energy of 93 MeV will have a momentum of 429 MeV/c and a QTBS angle of 28°. This value is substantially inside the peak value, although one can see from Fig. 51 that

the peak is not particularly narrow. In the (p,2p) studies, the peaking of the differential multiplicities at an angle larger than the QTBS angle was in fact observed, an effect which has a possible origin in multiple scattering.

While this coincidence experiment appears to show evidence for a direct interaction mechanism for light fragment production in proton induced reactions on light targets, we expect different behavior for heavy ion reactions involving heavy targets. Preliminary data which can be compared to the (p,pd) data is shown in Fig. 55 for the Ar+Au reaction at 100 MeV/nucleon (Cra+ 84). In this case, the deutron trigger is still at 90°, but a much lower trigger energy, namely 20 to 40 MeV, was chosen in order to provide reasonable statistics. The coincidence cross sections would appear to be falling off more rapidly as a function of forward proton angle than is observed in the (p,pd) experiment, and little structure is discernible. Presumably this reflects the greater degree of thermalization expected with a much heavier projectile and target. Clearly, the study of reaction mechanisms through coincidence experiments will expand significantly in the coming years.

5. Production of Intermediate Mass Fragments

5.1 Statistical Approach

Because the target-projectile mass combinations which are generally chosen for the measurement of intermediate mass fragment production usually involve heavy nuclei, a discussion of possible direct interaction effects will be omitted. We adopt this approach partly because statistical models appear to play a large role in the reaction mechanism for heavy nuclei, and partly because almost all of the theoretical analysis has been performed with such models.

In general, the yield of a particular species decreases with increasing mass of the species, except, of course, as the target mass region and the fission region are approached (Chi+ 83, Fin+ 82, GKJ 83, HBP 71, Hir+ 83, Jac+ 83, KTH 73, Min+ 82. See Appendix for further related references). Shown in Fig. 56 are the intermediate mass fragment production cross sections for the p+Ag reaction at 480 MeV (GKJ 83). The plot is fully logarithmic, so a straight line on the graph corresponds to a power law in fragment mass for the yield. [Of course, this parametrization is not unique.] The exponent τ of this power law, as we will return to in later subsections, is generally in the 2 to 4 range, and it decreases with increasing bombarding energy, on the average. For very low bombarding energies (Chi+ 83), the yields appear to increase again beyond Z=12 as shown in Fig. 57. At present, the origin of this increase is not completely clear, although it may reflect the fact that binding energies play a much more important role at these energies.

Substantial information on intermediate mass fragment production is available: both forward/backward ratios (see, for example CHH 81) and differential cross sectons have been measured (for a review, see GH 78). The differential cross sections show the usual semi-circular behavior when

contours of constant invariant cross section are plotted as a function of $q_\perp/m$ and y. (Some novel sideways peaking shows up at higher energies, but we will not deal with that aspect here. See RP 75, Urb+ 80). An example is shown in Fig. 58 for several carbon isotopes observed in the p+Ag reaction. One can see that the source rapidities are fairly small, probably less than 0.04 c for the data shown (see also SPF 77). This is a continuation of a trend in proton induced reactions that the heavier the ejectile, the slower the source. Before drawing a conclusion from this, the corresponding temperatures should be examined.

In the analysis of the (p,p') reaction on heavy targets, it was found (BR 84) that the source size was fairly small, less than ten nucleons. Obviously, we must be dealing with a larger thermal model source here since mass 30 fragments are being considered. If the source is, say, on the order of twice the size of the fragment, then there may be a significant recoil effect present which would effect the inferred temperatures. That is, if the source has to recoil with as much kinetic energy in the lab as the fragment is measured to have, then the "real" temperature will be higher than the observed one. A way of taking recoil effects into account by measuring the temperature with respect to the kinetic energy in the center of mass frame was used by Hir+ 83 (see references therein). The real temperature T_o was related to the lab temperature for a given fragment T_F via

$$T_F = T_o\left(1 - \frac{A_F}{A_S}\right) \qquad (74)$$

where A_S is the source mass, including the fragment mass. (Note that it is the mass which appears, not the charge.) If the source mass is constant as a function of A_F, then a plot of T_F vs. A_F should yield a straight line whose

intercept is T_o and slope $-T_o/A_S$. Such a plot is shown in Fig. 59 for the p+Ag data mentioned above where the temperatures used are simply the average for a given isobar. The assumption of the universal source size appears to be satisfied only for fragments in the mass 12 to 25 range. For these fragments, the value of A_S is determined to be 43, about double to triple the size of the fragment, on average. For higher energies, the source size appears to be higher, about 75 for p+Kr and 110 for p+Xe at 80-350 GeV proton energy.

A similar conclusion can be reached by reversing the assumptions, namely making the source size a function of fragment mass (as is indicated by a thermal model analysis of the differential cross sections) but dropping the recoil assumption. For example, suppose there is a constant amount of energy E_o in the thermal energy of the source. Assume that the conditions are such that this energy gives an approximate temperature of

$$E_o = \frac{3}{2} TA_S. \qquad (75)$$

If A_S is proportional to A_F, say $A_S = xA_F$, then a plot of T vs. A_F^{-1} should show a straight line through the origin with slope $\frac{2}{3x} E_o$. Such a plot is shown in Fig. 60. In fact, this functional form seems to describe a wider range of A_F than Eq. (74), since this function may be applicable down to $A_F = 7$. In any event, assuming $E_o = 400$ MeV for this reaction (the remaining 100 MeV going into translational kinetic energy of the source plus providing any necessary energy to overcome binding energies) the slope of 100 MeV corresponds to a value of x of 8/3; the source is between double and triple the fragment size. The fact that these two calculations, with differing assumptions, give about the same value of the source size indicates that a more complete analysis incorporating both effects would give similar results.

One can check the source size by doing a "momentum dump" calculation as was performed for the (p,p') reaction. Using Fig. 58 for example, a typical source velocity is about 0.03 C. If this source has absorbed all of the projectile's momentum, then the number of nucleons in the source would have to be ~40, similar to that found from the recoil analysis of the temperature.

There are several explanations for the observation that the apparent source size increases, and the temperature decreases, with increasing fragment mass. One explanation is that one is looking at an impact parameter averaging effect: small sources in peripheral collisions and large sources in central collisions. Another explanation is that one is observing the time evolution of the source: small at earlier stages of the reaction, then becoming larger as the source "heats up" the surrounding nuclear matter.

If this latter effect were significant, then presumably the temperature dependence would be less pronounced in heavy reactions than in the proton induced reactions considered above. Analyses (Jac+ 83) of energetic fragment emission in low energy heavy ion collisions (42-137 A MeV Ar+Au) provides some evidence that this is the case. Shown in Fig. 61 are the apparent temperatures extracted from a single source fit to the data. Although there is some scatter in the temperatures, they are closer to a constant value as a function of fragment mass than are the temperatures extracted in proton induced reactions. The fragment energies measured in the heavy ion reactions are higher than those measured in the proton reactions, however, and this may complicate their comparison. Lastly, the fact that the behavior of the temperatures is different does not by itself rule out impact parameter averaging effects.

Previously, we dealt with the use of composite particles, namely deuterons, as a measure of entropy production. Such an analysis has been made

of the intermediate mass fragment data as well (Jac+ 83, JSW 83). The entropy was extractd by comparing the data with a quantum statistical calculation in which the distribution of fragment species was calculated as a function of S/A and the breakup density ρ. The results were not particularly sensitive to the value of ρ chosen in the expected range $0.3\ \rho_o \leq \rho \leq 0.7\ \rho_o$, so the S/A determined within the context of this model is reasonably unique. The model (Sto+ 83) includes π's, Δ's, both stable and γ-unstable nuclei up to mass 20, and the known particle unstable nuclear states up to mass 10. Whether chemical equilibrium among all of these states is actually achieved has not yet been shown, so this calculation may be underestimating the entropy.

The results of such an analysis (JSW 83) for fragments emitted in the target rapidity region of heavy ion collisions are shown by the histograms in Fig. 39. The breakup density was fixed at $\rho_o/2$, and the average value of the extracted entropy is 1.84±0.16. These values are in contrast with the substantially larger values of S/A found in fits to light fragments. For example, shown in Fig. 62 is a comparison of the fit made to the light fragment data ($1 \leq A_F \leq 4$ are used for (a) and (b), while $1 \leq A_F \leq 3$ are used for (c)) with the full range of intermediate rapidity data. One can see that a higher entropy (few composites) is implied by the light fragment data; in fact S/A=4.2±0.3 is found for the $1 \leq A_F \leq 3$ data set while S/A=3.6±0.1 is found for $1 \leq A_F \leq 4$.

Clearly, S/A depends upon the technique used to extract it. Not only does it decrease with fragment mass, but it also depends on the rapidity region considered: intermediate rapidity entropies appear to be higher (2.2 to 2.4 for the intermediate rapidity heavy ion data (Jac+ 83) discussed above) than the 1.8 found in the target rapidity region. The results of the analysis of many data sets are summarized in Fig. 63 (from JSW 83). What is striking

is the independence of the extracted entropy from projectile energy or projectile mass. The curves labelled 1.0-3.0 show the entropy calculated in a model which uses fireball geometry for the interaction region and assumes the particles form a Fermi gas. The densities used are 1.0, 2.0 and 3.0 times ρ_o. The entropies so calculated are fairly similar to those found in the intermediate mass fragment analysis.

A different type of model, still employing statistical assumptions, has also been advanced (AH 83, AHI 83) to account for heavy fragment emission. In this model, the fragments do not come from the hot interacting zone, but rather the cold spectator matter. (For other applications of this idea, see AF 83, BFN 78, BHN 83, FH 73, Gol 74, HSS 75.) The pressure of the expanding hot zone then imparts extra kinetic energy to the cold region. The cold matter is assumed to break up statistically. The model has been used successfully to fit a fairly broad range of data, including isotopic yields.

A source of confusion in knowing which of these mechanisms is closer to the truth arises from knowing the temperature of the quantity being examined. A temperature can be assigned to the high energy tails fairly easily. However, the yield, which integrates over the low energy part of the differential cross section as well, may well contain or even be dominated by a low temperature component. For example, analyzing the yields for a group of isobars, which should be sensitive to binding energy effects, gives a much lower temperature than is typically found in the tails. Successful analyses which use these low temperatures include not only the studies mentioned above, but also CH 81a and Gro+ 82.

5.2 Reaction Rates

In the study of nucleon emission, the importance of the time scale for the reaction has been emphasized: there may be sufficient time for the system to come to kinetic equilibrium, but not to chemical equilibrium. One method of determining the time scale involved is to find a system with a well defined starting condition and then follow its time evolution. A comparison with some measurable quantity may then allow the determination of the time scale. This method has been used to analyze light fragment and kaon production (HM 82, Mek 78a, Mek 82).

One such approach (Boa 83a) to heavy fragment emission has been to assume that the initial system is a hot gas of free nucleons and then follow its time development as the nucleons combine into fragments. The time development is illustrated schematically in Fig. 64. At early times, the system is mainly nucleons which then interact and combine so that an abundance of heavy fragments begins to accumulate. If the system were to remain in chemical equilibrium for a long period as it cooled, then the abundances would be dominated by binding energy effects and would be peaked around iron. This is shown as the "late time" curve in Fig. 64. The form of the "late time" curve depends on the temperature, density etc. of the system when it goes out of thermal equilibrium. For example, in the entropy calculations outlined in the previous section, the high mass states present as the system nears the breakup density are allowed to subsequently decay as the system cools off, thus shifting the yield curve to lower masses. In contrast, for the low temperatures and densities considered in, for example, stellar evolution calculations, far fewer excited states will be involved and ground state properties (as opposed to level densities of excited states) of the heavy nuclei will play a more prominent role.

Before presenting a simplified rate equation approach to intermediate mass fragment emission, it should be pointed out that several potentially important contributions to fragment production have been omitted in this approach. One is the cold matter breakup contribution from the spectator nucleons, investigated by Aichelin, Hüfner, and Ibarra (AHI 83). Another is the role of density fluctuations originally present in the participant region which would ultimately emerge as fragments. In a sense, then, the rate equation approach will only give one a bound on the time required for fragment formation: the presence of other contributions would decrease the time needed to go from the early to intermediate time curves of Fig. 64 (assuming that the reaction rates employed are correct).

We will assume that at the beginning of the fragment formation epoch, the initial hot zone (which has a temperature of 75 MeV for proton induced reactions (BR 84) in the multi-GeV incident energy range) has cooled and expanded such that the temperature has dropped to about 1/3 its initial value. (This fractional decrease appears in the analysis of 500 MeV proton induced reactions.) At this time, which we define as t=0, the distribution of number densities N_i of the species present will be assumed to be of the form

$$N_1(t=0) \equiv \rho$$

$$N_i(t=0) = 0 \qquad 2 \leq i \leq A_T \tag{76}$$

At this point we will not distinguish between protons and neutrons. At the freeze-out point for pions, the density of nucleons has already decreased (BR 84) to at least 1/2 nuclear matter density or one nucleon per 12 fm^3. Hence only two body interactions will be considered in the rate equations.

For early times, the breakup of heavy nuclei will be assumed to be slow compared to the formation rate, although, as equilibrium is approached these rates will become comparable. Then the rate equations have the form:

$$\frac{dN_k(t)}{dt} = + \sum_{i,j} \frac{N_i(t)N_j(t)}{1+\delta_{ij}} \bar{o}_{ij}\delta_{i+j,k} - \sum_i N_i(t)N_k(t)\bar{o}_{ik} \qquad (77)$$

Here, $\bar{o}$ is the thermal averaged cross section

$$\bar{o} \equiv 4\pi \left(\frac{\mu}{2\pi T}\right)^{3/2} \int v^3\, o(v)\, e^{-(\mu v^2/2T)}\, dv \qquad (78)$$

where μ is the reduced mass and v is the relative velocity. For simplicity it has been assumed that the main contribution to fragment formation is two particle fusion. The omission of more complicated processes will partly compensate for the omission of breakup reactions in these equations.

To actually extract an estimate of the reaction time, we will compare with the p+Kr data (Hir+ 82) at 80-350 GeV. For simplicity the integrated reaction cross section in the energy range of interest will be parametrized as (Data from DP 79 were used to obtain this form):

$$o_{AB} = \pi(r_o(A+B)^{1/3}+\lambda\!\!\!^{-})^2 \qquad (79)$$

where $\lambda\!\!\!^{-}$ is the reduced de Broglie wavelength, r_o=1.2 fm and A and B are the mass numbers of the fusing nuclei. Of course, not all of the total reaction cross section results in fusion. We estimate the relevant part by inserting o_{AB} in Eq. (78) but truncating the integral at the Fermi velocity, v_{max} of nuclear matter at normal density. In other words, a pair of nuclei whose relative velocity is less than v_{max} will fuse, while those with velocity

greater than v_{max} will not. This is an obvious oversimplification but will suffice for our purposes here. Lastly, the temperature and initial density ρ will be taken to be 25 MeV (1/3 of the initial proton temperature) and 1/2 ρ_o respectively. Again, a more sophisticated calculation would allow these to change as the system expands. This temperature justifies in part the use of Eq. (78) which assumes Maxwell-Boltzmann statistics.

The result of the numerical integration is shown in Fig. 65. To obtain an absolute yield, the calculated number densities must be multiplied by a volume. Here this will be neglected since the data are arbitrarily normalized. The predicted yields match the data well, with deviations occurring at the expected masses. Masses 5 and 8 have not been suppressed in the calculation, so they are necessarily overpredicted. Similarly, these two isobars will enhance mass 4 in their decay, so the underprediction of mass 4 is anticipated. That masses 5 and 8 are suppressed by binding energy considerations during the formation period is probably also responsible for the decrease in isobars immediately above them, i.e. 6 and 9, from the prediction. Lastly, although a specific data set has been chosen, the predicted falloff of the mass yield with A should be roughly universal in this calculation, as the formation times should not depend sensitively on the projectile energy or target involved.

The formation time required to produce the observed distribution is 4×10^{-23} seconds. This estimate is in accord with what is required to explain the (p,p')/(p,n) ratio, and with the estimated rate of cooling of the hot zone, namely about 1×10^{-23} sec. One would expect the fragment time to be longer than this as the cross sections involved are larger than (p,p') and therefore the heavy fragments go out of equilibrium somewhat later. It is interesting to note that in their investigation of deuteron production in

heavy ion collisions, Bertsch and Cugnon (BC 81) find that S/A decreases to a constant value in $\sim 3\times10^{-23}$ sec, although this time should not be compared directly with the reaction rate time estimated here.

A different approach which also follows the time evolution of a system of nucleons initially at an elevated temperature has been pursued by Friedman and Lynch (FL 83, see also DFR 60). In this model, the emitting region is assumed to be in kinetic and chemical equilibrium and the Hauser-Feshbach (HF 52) formalism for particle evaporation is used to estimate the particle emission rate. The emitting region is allowed to cool and evolve with time. Detailed results from this calculation have not yet been published, but the preliminary application of this model to fragment emission showed surprisingly good agreement with the yield data (FL 83) as shown in Fig. 57. It could well be that even if the equilibration time assumptions inherent in the model are not satisfied, that the phase space, coulomb, impact parameter averaging and other effects in the model so dominate the yield curves that the model will provide a good descripton of the data.

5.3 Liquid-Vapor Phase Transitions

The fact that statistical ideas appear to have such wide applicability in the mechanism of energetic particle emission opens up the possibility that these reactions can be used to study the thermodynamics of nuclear matter. (As well as the references on hydrodynamics, see Buc+ 83b, Gar+ 80, GGK 79, Hof+ 76, Sco 80, Sco 81, Sob+ 75, Sto+ 83. For a discussion of the role of the equation of state in pion production, see BKD 84.) The role of transport properties of nuclear matter such as thermal conductivity and viscosity have been discussed in prevous sections. Another aspect of the equation of state which might be accessible experimentally would be a phase transition: nucleon

liquid-vapor transition, pion condensation or hadronic to quark-gluon matter. Only the first of these will be considered here. For reviews of the other transitions, see, for example, NG 83 and Boa 83c, respectively, and RMS 82, Rop+ 83 for a discussion of Mott transitions.

The interparticle separation dependence of the nucleon-nucleon force has many gross similarities to that of the intermolecular force: attraction at long distances and repulsion at short distances. Such behavior is known to result in a liquid-gas phase transition for molecules, and so it is worthwhile investigating whether the same feature holds for nuclear matter. As a coarse calculation, one can try the following approach (Boa 83c):

Assume that the NN force can be approximated by a square well form as shown in Fig. 66, with a hard core internucleon separation of $2r_0$ and a limit to the attractive well (depth W) of $2r_1$. Neglecting the fact that the nucleons are fermions, then the equation of state which this potential generates has the van der Waal's form:

$$\left(P + \frac{a}{\tilde{V}^2}\right)(\tilde{V} - b) = T \tag{80}$$

where

$$a = \frac{V_1 - V_0}{2} W \qquad b = \frac{V_0}{2} \qquad V_1 = \frac{4\pi}{3}(2r_1)^3 \tag{81}$$

As before, Boltzmann's constant has been absorbed into T, and $\tilde{V}$ is the volume per particle. A plot of this equation of state is shown on Fig. 67. The parameters chosen for this plot are $2r_0$=1 fm, $2r_1$=1.64 fm and W=10 MeV. Particularly since the Fermi-Dirac nature of the nucleon has been neglected, (forcing the unusual choice for W), this equation of state will not be useful at temperatures much less than the critial temperature. The important point is that the equation of state exhibits a critical point, given by

$$T_c = \frac{8}{27} \frac{V_1 - V_o}{V_o} W \quad (82)$$

and

$$\bar{V}_c = \frac{3}{2} V_o. \quad (83)$$

For the parameters chosen, this corresponds to T_c=10 MeV and ρ_c=0.16 fm^{-3}. More sophisticated calculations using a Skyrme effective interaction in a finite temperature Hartree-Fock theory have recently been performed (JMZ 83). Depending upon the parameters chosen, these calculations yield a critical temperature in the 22-28 MeV range for infinite nuclear matter, and 16-20 MeV for finite nuclei. The critical density in either case is about 1/2 ρ_o. The remaining part of the phase diagram can also be calculated (for example, by using the Maxwell construction in the van der Waal's example) and give a form shown schematically in Fig. 68. The regions marked superheated and supercooled are metastable regions which are not thermodynamically favored but nevertheless may be accessible depending upon the time scales involved.

Clearly, the range of temperatures and densities associated with the phase transition region can easily be attained in both heavy ion and proton induced reactions. If the reaction region is sufficiently large, long lived and uniform, then it may pass through the phase transition region as it expands and cools. Before looking at the question of what the experimental signatures will be, we will first check to see whether the "large and long lived" conditions are met.

Since data from proton induced reactions have figured prominently in the search for experimental signatures of phase transitions, they will also be dealt with at length here. In the thermal model analyses of the source size in intermediate mass fragment emission considered above, it was shown that typically about 40-60 nucleons were involved in proton induced reactions,

somewhat more in heavy ion reactions. Density fluctuations for such a small number of particles are quite substantial, and will certainly tend to soften the sharpness of the transition. Consider, for example, a part of the van der Waals-like equation of state shown in the inset of Fig. 69. In the Maxwell construction, states A are thermodynamically favored over states B and C. In a recent paper, Goodman, Kapusta and Mekjian (GKM 83) provide a thorough review of phase transition phenomena, including an estimate of the sharpness of the transition. The probability of being in states B or C compared to A is shown in Fig. 69 for a 40 nucleon system and, for comparison, a 10,000 nucleon system. Clearly, one must go to temperatures well below the critical temperature before the transition becomes at all sharp for small systems.

Similarly, the time scale involved is fairly short. As was indicated above, hydrodynamical and other calculations give estimates for the lifetime of the hot region in the 10 to 20 MeV temperature range of 5 to 10×10^{-23} sec. These results are supported by the analysis (Boa 84) of nucleon emission in muon and proton induced reactions. This time scale should be contrasted to that of Curtin, Toki and Scott (CTS 83b) for the time required for the phase transition to take place. Using an argument based on the frequency of the monopole oscillation, they estimate times in the 10^{-22} sec range.

The facts that the system may be too small or short lived for there to be a sharp transition, or that the transition occurs at the same density range ($\rho_o/2$) as it was previously estimated that the reaction region goes out of thermal equilibrium, may mean that the phase transition idea may not be cleanly applied to fragment production. Nevertheless, reaction conditions may be close enough to those required for a phase transitiion that there may be some experimental effect.

One of the first observations put forward as possible evidence of phase transition effects was the form of the mass yield curve. In the thermal liquid drop model of droplet formation (Fis 67, for another approach, see Sta 79), it is found that at the critical point, the distribution of droplets has the simple form

$$Y(A) \propto A^{-\tau} \tag{84}$$

As shown on Figs. 56, 57, 62 and 65, the yields do fall with increasing fragment mass, and the power law fit can be applied to the intermediate mass fragment region. The exponent τ is related to the critical exponent δ used in the equation of state near the critical point by (see GKM 83)

$$\tau = 2 + \delta^{-1} \tag{85}$$

Since δ has the range $2<\delta<\infty$, then $2<\tau<2.5$. In fact, τ determined phenomenologically for high energy reactions is typically in this range. Away from the critical point, the predicted mass distribution is more complicated:

$$Y(A) = Y_0 \exp\left[\frac{\mu_B-\mu_A}{T} A - \frac{4\pi r^2 o}{T} A^{2/3} - \tau \ln A\right] \tag{86}$$

where Y_0 is an undetermined parameter and the chemical potentials $\mu_{A,B}$ are for a droplet containing A particles of the liquid being surrounded by B particles of the gas phase. The surface free energy is denoted by o, while the radius of the drop has been assumed to be of the form $rA^{1/3}$. Eq. (86) has been used to successfully describe the experimentally measured yield curves, the parameters being determined phenomenologically. It has been checked that the

values of the parameters so determined do fall in the theoretically expected range.

Of course, the droplet model approach is only one of several models which have been used successfully to describe the same data, so it cannot yet be taken as proof of a phase transition. It has been argued by Pan+ 83 that the temperature dependence of τ (now taken as a parameter to represent all of the terms in Eq. 86) may be evidence of a phase transition. They determine τ by the analysis of several different data sets, and find apparently discontinuous behavior in τ around a temperature of 12 MeV. The results of their analysis, as well as some extra data points which will be discussed momentarily, are shown in Fig. 70a.

Not only have several different data sets been used in generating Fig. 70a, but also data from targets with very different Q-values for fragment production have been employed (particularly uranium vs. silver targets). The author feels Fig. 70b represents a more consistent data set than that used in Fig. 70a (Boa 83b). There are also difficulties in determining the relevant temperature to be used. The temperature used in plotting points P_1 (which was not included in Pan+ 83; see Hir+ 83) and P_2 are the quantity T_0 in Eq. (68). The actual average fragment temperatures, labelled P_1 and P_2, are much lower. However, this method of determining the temperature has not been used uniformly. For example, if the intercept temperature method is applied to data point S, it moves to point S' (with the inclusion of new data [GKJ 83] not available at the time Pan+ 83 was prepared) using the authors' own fits (of temperature and τ, see Fig. 56) to their data. Similarly, in some instances the intercept temperature was determined by plotting T vs. Z_F, rather than T vs. A_F. This causes a 20% error in the temperature. We belabor

this point to illustrate the difficulty in performing a consistent analysis of the yield data.

Replotting the data points from Fig. 70a in 70b, the discontinuity is much less evident. Nevertheless, the interesting rise in the exponent at low temperatures remains. Is this evidence for a phase transition, or is it explicable in terms of more conventional ideas? The yield curves used in determining the exponents in Fig. 70 are found by numerically integrating the inclusive differential cross section $d^2\sigma/dEd\Omega$. The differential cross section has its largest value at relatively low energies, in the region of the coulomb barrier. For example, GKJ 83 show that coulomb effects strongly cut off their heavy fragment yields in this energy region. Plotted in Fig. 71 are the differential cross sections for ^{7}Li and ^{7}Be production at the same angle in p+Ag collisions at 480 MeV. Combinatorial and binding energy differences can account for about a factor of 2 difference in the spectra, and this seems to be the difference observed in the high energy tails. However in the low energy region around the coulomb barrier, the ^{7}Li differential cross section greatly exceeds the ^{7}Be one. The yields, which are strongly affected by this region, are observed to differ by about a factor of five, not the factor of two expected from the tails.

To see if coulomb effects can quantitatively explain the behavior shown in Fig. 70, we perform the following simple calculation. Suppose that there is a mass distribution given by $Y(A_F)=CA_F^{-\tau}$ (where C is a normalization constant) which describes the yield independent of temperature before coulomb effects are included. The individual fragment spectra we will characterize by a Maxwell-Boltzmann distribution in energy. Now, at high temperatures, the existence of the coulomb barrier will only have a major effect on the lowest energy part of the fragment spectrum. As the temperature is lowered, an

increasing fraction of the large Z fragments will be subject to a coulomb barrier in leaving the nucleus. The calculation consists of taking the spectrum inside the coulomb barrier and modifying it by multiplying by a barrier penetration factor $P_A(q)$, where q is the fragment momentum. In other words,

$$\left.\frac{d^3\sigma_A}{d^3q}\right|_{outside} = P_A(q)\left.\frac{d^3\sigma_A}{d^3q}\right|_{inside} \qquad (87)$$

where the integral of the "inside" distribution obeys $Y=CA_F^{-\delta}$. The integral of the left hand side then gives the yield. The penetration factor will be approximated by $\exp(-2\int\kappa dx)$ where $\kappa=\sqrt{2\mu(V(x)-K)}$, V(x) being the coulomb barrier and K the kinetic energy.

The change in the apparent exponent for the $10\leq A_F\leq 20$ region is shown as the curve on Fig. 70b. The high temperature exponent is chosen as $\tau\equiv 2.2$ here. The results depend upon the charge and mass of the emitting system, chosen to be 25 and 50 respectively here, similar to what is found in analysis of the fragment differential cross sections (Hir+ 83, GK 80, GKJ 83). No attempt was made to tailor the coulomb barrier to get a "best fit" to the data. It is evident that the magnitude of the changes in the yield curve observed at low temperatures is similar to what one expects from coulomb barrier effects. Again it is worth mentioning that the temperatures extracted from the high energy tails of the differential cross sections may not be the ones appropriate to the yield curve. If Fig. 70 really is evidence for a phase transition, the temperature may have to be much lower than 12 MeV (see Gro+ 82).

It is also worth commenting on that it had been expected that there would be entropy generated during the collision, and this entropy would be seen in the analysis of the intermediate mass fragments. Yet, as was shown above, the entropy extracted from these fragments by JSW 83 is about 2-2.5, below the value of 3.3±0.3 expect (Kap 83) from the phase transition. However, the entropy analysis itself is somewhat puzzling, since the entropy obtained is nearly independent of bombarding energy.

Bertsch and Siemens have pointed out (BS 83) that even if the system enters the unstable region without establishing chemical equilibrium or going through a phase transition, there may be observable effects. In particular, they suggest that the yield of light fragments might be enhanced in this region. The possible role of the liquid-gas transition in light fragment production has also been investigatd by CTS 83a.

In summary, in spite of the impressive calculational evidence that nuclear gas to liquid phase transitions should be expected in large, long lived assemblies of nucleons, there are indications that the nuclear interaction region involved in intermediate mass fragment emission may be both too small and too short lived to support a sharp transiton. The mass yield curves themselves can be explained by several models which do not invoke a phase transition. The change of the yield curves with temperature is approximately what one expects from the necessity of the higher Z fragments to tunnel through a substantial coulomb barrier at low temperatures.

Better experimental signatures (or disproof of the alternate models proposed for the current signatures) are required before phase transitions can be said to be established. Perhaps using centrally triggered heavy ion reactions, to insure a large number of nucleons in the transition region, or comparing the yields as calculated by fitting only the high energy tails of

the fragment energy spectra (to avoid the strong coulomb influence on the lower energy part of the spectrum) would help eliminate some of the complicating effects.

6. Summary

This review has concerned itself principally with attempting to determine the mechanism for the emission of energetic particles in reactions which involve projectiles with more than 100 MeV per nucleon in kinetic energy. Because the evaporative emission of low energy particles is well understood, emphasis has been placed here on the mechanism of the emission of energetic ejectiles, mainly protons and fragments but occasionally other debris (such as pions) from the reaction. The intermediate and high energy region has been chosen for study so as to minimize quantum effects and maximize the use of classical ideas which might provide more intuitive and less calculationally complex insight into the mechanism. In order to be able to use the widest data set available for model testing, our attention has been largely restricted to particles emitted with a rapidity closer to the target than the projectile, since it is this region which has been most thoroughly explored experimentally.

Until fairly recently, the greater part of the experimental observations in this kinematic domain has consisted of measurements of the single particle inclusive cross sections. Because these cross sections show such simple apparent form when plotted semi-logarithmically, they have been fitted with a variety of models, many containing mutually contradictory hypotheses. With the availability of a larger data set, the dependence of the models on target mass number, bombarding energy etc., could be tested to delimit the applicability of certain models. The arrival of coincidence experiments has greatly accelerated the process of finding these domains of applicability. As the measurements become less inclusive, they become more sensitive to the details of the reaction mechanism.

Of course, what has emerged from these experiments is the finding that there may be several mechanisms contributing to a given inclusive process. The relative importance of each contributor appears to depend upon many factors, including projectile, target and ejectile mass number. The general trend which has been observed is that the larger any of these quantitites is, the more important will be the role of statistics.

The prospect that one could find in inclusive measurements a means of cleanly accessing the short distance behavior of nucleons in the nucleus, by simply knocking them out with a high energy projectile, now looks fairly remote. Coincidence studies have shown evidence for direct knockout contributions to energetic particle emission, but the target and projectile must be light to avoid having the direct interaction effect washed out by multiple scattering. Even in as light a target as beryllium, the (p,2p) studies showed evidence for a surprising amount of multiple scattering. In collisions of heavy projectiles and targets, a knockout component will still be present at large impact parameter, but the inclusive measurements will probably be dominated by less peripheral reactions which involve the interaction of a much larger number of nucleons.

The fact that the strong interaction is, indeed, strong, tells us that the mean free path of nucleons in the intermediate energy range is not particularly long: even a proton projectile can undergo several scatterings in an average transit of a heavy nucleus. Cascade simulations have shown that the energy spectrum of the struck particles in such a traversal looks remarkably thermal. Self-consistency tests performed on data from reactions with heavy targets do not contradict the assumptions of thermal equilibrium, although they do not unambiguously rule out knockout contributions. These tests do show that the source region is fairly small, less than ten nucleons

in the first stages of the reaction for proton induced reactions, larger for heavy ion reactions.

The hot interaction region produced in intermediate energy reactions may emit mainly nucleons (or pions and perhaps kaons) during its early life, with fragments only separating out at a later stage after more nucleon-nucleon collisions have occurred. Thus, while thermal equilibrium may be achieved fairly early on in the reaction, chemical equilibrium may not appear until much later. The study of nucleon, pion and kaon emission seems to support this view, that chemical equilibrium among these species may not be established on the time scale ($\sim 10^{-23}$ sec) associated with their emission.

Complete chemical equilibrium itself may also not be fully established in the reaction, although equilibrium among a subset of the reaction products may be established. For example, analysis of the p/n ratio in proton and muon induced reactions argues that chemical equilibrium is not established for the emission of nucleons. However, the ^{3}He/t or ^{7}Be/^{7}Li ratios may be much closer to their values at chemical equilibrium if they are emitted from a later stage in the reaction. Analysis of intermediate mass fragment data tends to argue that the overall time scale is still relatively short, since a reaction rate analysis (admittedly subject to considerable uncertainty in the rate constants) gives a time of about $1/2 \times 10^{-22}$ sec.

The obvious role that statistics plays in reactions of heavy projectiles and targets leads one to the prospect that the thermodynamic properties of nuclear matter - transport coefficients, phase transitions, etc. - might be accessible in these experiments. The idea that one can at last investigate the nuclear equation of state is certainly seductive. But while we now know that multiple scattering can wash out direct interaction effects in these reactions, we must also exercise some caution that the finite particle numbers

and short lifetimes inherent in heavy ion collisions do not wash out information about the equation of state.

The possibility that these effects may be important is evident in the study of the limiting temperature behavior observed in the thermal model analysis of high energy inclusive reactions. The variability of the limiting temperature with projectile mass surely must be an indication that NN dynamics still play a strong role in source properties. It may take experiments with better defined initial conditions (for example, tagged electron scattering where the amount of energy deposited in the nucleus is accurately known) to answer the limiting temperature question.

The same conclusion may be true for the study of the liquid-vapor phase transition. While the theoretical evidence for liquid-vapor transitions is convincing in infinite nuclear matter, the finite size and short lifetime of the interaction region in a nuclear reaction lie uncomfortably close to the regions where the phase transition should be washed out. Similarly, the temperature region wherein the transition may cause rapid variation in phenomenological quantities such as the apparent power law behavior of mass yield curves, is also the region where more mundane effects such as Coulomb tunnelling become important. More precise experimental signatures must be sought.

As always in a review such as this, one concludes that much experimental and theoretical work needs to be done. But it should be emphasized that progress in our understanding of the mechanisms involved in these reactions has advanced significantly in the past several years. The current generation of coincidence experiments is beginning to allow us to identify the kinematic (and other variable) domains where our knowledge of the interaction region is reasonably accurate. This, is an essential step if we are going to access new

properties of nuclear matter by experiment. It is required by theoreticians for an accurate application of infinite nuclear matter ideas to finite systems, and provides us with different experimental domains where equation of state effects should and, equally importantly, should not appear.

7. Acknowledgments

The author has benefitted from discussions about the topics covered in this review with a considerable number of colleagues, chief among them his associates at Simon Fraser University and TRIUMF. He wishes to thank the theory group of the Nuclear Science Division at Lawrence Berkeley Laboratory, who extended their hospitality to him while this work was begun, and the theory group of the National Superconducting Cyclotron Laboratory, where he completed the project while on sabbatical leave. The author also wishes to thank all of those who permitted their figures to be used in this review, and in some cases even provided photographic prints. Lastly, he is grateful to the National Research Council of Canada for financial support. This work was supported in part by the U.S. Department of Energy under contract DE-AC03-76SF00098 and the National Science Foundation through grant no. 83-12245.

8. Appendix

Because of the large number of references in this review, it is useful to have a "guide to the literature" wherein references on related topics are listed together for easier identification. This index contains about 60 categories under which the references are listed. In many cases, a given reference will be listed under more than one category. Each category also contains references which are not directly in the subject area under consideration, but are frequently cited by researchers in that field (for example, a theoretical technique not originally applied to a particular reaction, but subsequently used for it). The categories are fairly broad, particularly those dealing with models for reaction mechanisms, and often contain approaches which differ significantly in detail, although they share many general characteristics. The author thought this was more appropriate than generating an index whose entries were comparable in number to the number of references. Lastly, time and exhaustion limited the literature search, so areas only mentioned in passing in the review (for example, pion production) will only contain references familiar to the author. These classifications are meant only as an introduction to the literature rather than a survey of it. Naturally, the author apologizes to those whose work he has overlooked. The masses referred to in the titles are approximately: light fragment (LF), $2 \leq A \leq 10$, intermediate mass fragment $10 \leq A \leq 30$, heavy fragment $A \geq 30$, heavy ion projectile (HI) $A \geq 2$.

Cascade calculations
  general
    CKR 81, Coh 66, Gab 76, Met+ 58, Ser 47,

  in heavy ion reactions
    Ams+ 77, BC 81, BGS 74, Bon+ 76a, Bon+ 76b, BSH 76, CMV 81, Cug 80, GFR 83, GFS 82, GIT 79, GT 78, Hal 81, HK 77, Iwe 79, Kod+ 82, KR 79, KR 81, Mor+ 79, Nix+ 82, Ran 78, Ste 78, Ste 80, Sto+ 81, YF 79a, YF 81

  in proton induced reactions

    Aba+ 61, Ber 63, Ber 67, Ber 69, BP 73, Che+ 68, BG 77, Hat 79, HH 81, KP 81

Direct interaction models
  general (including PWIA etc.)
    Ale+ 80, ARW 77, AW 77a, AW 77b, Bho+ 76, BLT 77, Boa 84a, CDG 83, Cha+ 80, FF 77, Fra 78, Jac 71, KW 70, Whi+ 74, WM 77

  in electromagnetic reactions
    BW 81, FM 71, Lev 51, Mon+ 71, SMA 79, VV 69

  in fragment emission
    BW 79, BW 81, CR 77, Dol+ 79, MB 73, MBS 76, Mil+ 74, SBM 77

  in heavy ion reactions
    Ber 77, Che 79, HK 79, Jai 80, Koo 77a, LG 79, MJD 81, SB 77

  in (p,N)
    AW 76b, Bay+ 73, Boa 82b, BW 81, CH 81b, FH 79, Fra 77, Fra+ 78c FS 77, Fuj 77, Fuj 79, Gur 81, Gur 82a, Gur 82b, Wal+ 79, Wol 78, Wu 80

  in (p,2p)
    Boa 80b, CR 83, Gre+ 83

  in weak reactions
    FS 77, SMA 79, YF 79b

Direct interaction with multiple collisions
    BFN 78, CHH 82, CS 80, FS 79, GDA 79, GM 70, Gur 80a, Gur 80b, HSS 75, Mor+ 79, Rem 75, RS 78, SC 80, Sch 79, SS 75, Tam+ 77, TB 78, TLU 81

Equation of state, transport and other properties of nuclear matter
    BKD 84, Boa 83c, BS 83, Buc+ 81, Buc+ 83b, CB 80, CTS 83a, CTS 83b, Gar+ 80, GGK 79, GKM 83, Hof+ 76, JMZ 83, Koh 82, KS 81, NS 81, Sob+ 75, Sto+ 83, SWW 82, Wei 76

Equations of motion calculations
    BM 77, BP 77, BPM 80, BP 81, CWY 79, WYC 78

Exciton and related models
    Akk 79, BL 70, Bla 68, Bla 71, Bla 72, Bla 73, Bla 74, Bla+ 76, BM 72, Bra+ 72, CB 71, Cli 72, Den 54, Gad+ 76, GMT 83, Gri 66, HM 71, LS 78, Mac 80, Mac 83, MAW 75, MAW 76, MBS 76, RO 73, WC 76, WC 77, WC 78

Hanbury-Brown/Twiss effect
  Theory
    Biy 83, Coc 74, GKW 79, Gol+ 60, Gyu 82, HT 56, Koo 77b, Kop 74, Lyn+ 83, NY 81, YK 78

  Experiment
    Bea+ 83a, Bea+ 83b, Fun+ 78b, Lu+ 81, Zaj+ 81, Zar+ 81

Heavy fragment emission
Ale+ 81, BHN 83, BP 71, BP 79, CAH 63, CCP 68, CHF 58, Cra+ 75, CS 74, Cum+ 64, FP 78, FP 80a, FP 80b, FP 80c, HBM 69, HS 83, Hud 68, Kau+ 76, Kau+ 80, KC 67, KC 70a, KC 70b, KH 64, KK 70, KSW 78b, KW 75, Lov+ 77, Lov+ 81, MLS 78, Mor+ 78, Mor+ 80, Por+ 79a, Por+ 79b, PS 57, PT 64, SCW 56, Shi+ 78, SP 76, Sug+ 66, War+ 83, Wil+ 79, Win 80a, Win 80b

(HI,N) reactions (experiment)
Awe+ 81, Awe+ 82, Bro+ 77, Cec+ 81, Gea+ 80, Gos+ 77, Jak+ 81, Kal+ 83, Kas+ 81, Nag+ 79, San+ 80b, Sch+ 79a, SG 66, Tho+ 79, WCH 79a, WCH 79b, Wes+ 82

(HI,π) reactions (experiment)
Ben+ 79, Fra+ 82, Fun+ 78a, Nag+ 81, Nag+ 82, Pap+ 75, Sch+ 82, Sul+ 82, Wol+ 79, Wol+ 82

Hydrodynamics
AHN 77, Ams+ 75, Ams+ 77, Bau+ 75, BCG 82, BGZ 78, Buc+ 81, Buc 83a, CB 80, CG 81, CLZ 80, Cse+ 82, Dan 79, KMS 76, KS 75a, KS 75b, Nix+ 82, NS 81, Rem 82, SGB 81, SMG 79, SMG 80, SN 80, SR 79, Sto 81, Sto+ 80c, Sto+ 81, Sto+ 82, TW 80, WMW 75

Intermediate mass fragment emission (experiment)
heavy ion reactions
CHH 81, Chi+ 83, FS 81, Jac+ 83, Mey+ 80, Ols+ 83, SPF 77

proton induced reactions
BLY 79, Fin+ 82, GKJ 83, HBP 71, Hir+ 82, KTH 73, Min+ 82, PBH 71, PT 64, PT 65, RP 75, Urb+ 80, Win+ 80

Intermediate mass fragment emission (theory)
liquid-gas phase transitions
Boa 83b, CTS 83b, GKM 83, Pan+ 83

non-equilibrium model
Boa 83a

spectator breakup
AF 83, AH 83, AHI 83, BFN 78, BHN 83, HSS 75

statistical approach
Aic 83, CH 81a, DFR 60, FL 83, Gro+ 82, JSW 83

Light fragment emission (experiment)
coincidence experiments
Bac+ 76, Bac+ 80, Bin+ 80, Cra+ 84, Hel+ 83, Mey+ 80,Roo+ 77, Tan 83

electromagnetic reactions
Ant+ 71, Flo+ 78, Flo+ 79, HPU 66, KP 63, MGS 77, Mur+ 78, MV 65

heavy ion reactions
Aub+ 82, Awe+ 82, Bin+ 80, Che+ 75, Doe+ 78, Dol+ 79, Gos+ 77, Gut+ 83, Ho+ 77, Jac+ 83, Lem+ 79, Mey+ 80, Nag+ 81, Nat+ 81, Nom+ 78, Pos+ 75, San+ 80b, Sch+ 79b, Tho+ 79, WCH 79a, WCH 79b,

Wes+ 82, Wes+ 83, Zeb+ 75

proton induced reactions
Ala+ 75, Bog+ 76, BP 73, Che+ 75, FMP 62, Fra+ 76, Fra+ 79, GJK 82, GK 78b, GK 80, Kom+ 76, Nak+ 82, PBH 71, Pos+ 75, Rai+ 75, Sak+ 80, Seg+ 82, Sut+ 67, SZ 63, Tan 83, Vol+ 75, WCH 79c, Wes+ 78, Zeb+ 75

Light fragment emission (theory)
cluster knockout
BW 79, BW 81, CR 77, Dol+ 79, MB 73, MBS 76, Mil+ 74, SBM 77

coalescence model
Boa 82b, BP 61, BP 62, BP 63, Gos+ 77, Gut+ 76, JDM 82, Kap 80, Mac 79, Mac 80, Mek 80, Sch+ 83, Ste 80, SY 81, SZ 63

entropy
BC 81, Bir+ 83, CJ 83, JSW 83, Kno+ 82, KS 81, MMS 80, SK 79, Sto 81

pickup model
Boa+ 81, Boa 82b, BS 82, HCH 80

statistical models
Bec+ 81, Bon+ 77, BS 83, CJ 83, Cse+ 83, FL 83, GK 81, GKW 78, GW 79, JDM 82, Kap 80, Mek 77, Mek 78a, Mek 78b, PS 78, RK 81, RMS 82, Rop+ 83, SWW 82

other
CDM 80, CTS 83a, DJK 82, GFR 83, PSF 77, Rem 81, Rem 82, Roo+ 77, RS 75, RS 78, TLU 81

Momentum distributions (theory)
Ama 76, AW 76a, AW 77c, BH 80, CG 61, FH 73, FH 80, HN 81, VTB 80, ZE 78

μ^--induced particle emission
experiment
BE 77, Bud+ 71, Kra+ 79, Sch+ 74, SE 73, VKR 70, Wyt+ 78

theory
BEJ 77, BPV 65, Ish 59, LS 78, Muk 77, Ube 65

Multiparticle production in heavy ion reactions
Bar 80, Bha+ 79, Che+ 77, Hec+ 78, Jak 78, Lu+ 81, Nag+ 80, San+ 80, Sto+ 80a, Tan+ 80

Nucleon emission in electromagnetic reactions
experiment
ADS 75, Ant+ 71, Bab+ 82, BS 54, BS 58, DS 73, Fel+ 54, GA 69, Gar+ 65, Kim+ 63, LS 51, Mat+ 76, Mon+ 71, Mye+ 54, Odi+ 56, Smi+ 67, Ste+ 60, VL 73, Wat+ 56, Whi+ 58, WM 53

theory
Bog+ 80, BW 81, DT 76, FM 71, Gab 76, GH 74, HWG 76, Lev 51, Mon+ 71, MT 66, Sch 51, VV 69, WC 77

π-induced particle emission
  experiment
    Ama+ 75, Lev+ 81, Shi+ 83

(p,N) reactions (experiment)
  analyzing power
    Fra+ 78a, FW 77, KSW 78a, Roy+ 81, Sak+ 80

  free NN scattering
    Pal+ 67, PDG 70

  (p,n)/(p,p') ratio
    And+ 81, Bon+ 78, Kal+ 83, WBG 67, WGB 72

  quasi-elastic scattering
    Ben+ 67, Che+ 81, CHM 52, Chr+ 80, Cor+ 72, WR 66

  wide angle scattering
    Ala+ 75, Bay+ 79, BP 73, Bro+ 77, Bur+ 76, Bur+ 79, Coc+ 72a,
    Fra+ 76, Fra+ 78b, Gea+ 80, Kom+ 77, Kom+ 79a, Pee+ 68, Roy+ 81,
    Seg+ 82, Shi+ 83, ST 56, WBG 67, WCH 79c, WGB 72

(p,π) and (p,K) reactions (experiment)
    Coc+ 60, Coc+ 72b, FF 77, FMP 62, Pap+ 75, Sch+ 82

(p, 2p) reaction (experiment)
    Cia+ 83, Cow+ 80, Fra+ 81, Gre+ 83, Kom+ 78, Kom+ 79a, Kom+ 79b
    Sim+ 70, Tan+ 81

Reviews and lectures
    Ale 68, Ari+ 72, AWM 75, Bal 77, Ben 83, Bla 75, Boa 80a, Boa 82a,
    Boa 83c, BW 52, CR 75, DM 81, FKS 80, Foa 75, GH 78, Gyu 81, KK 68,
    MH 59, Muk 77, Nag 80, Nag 81, Nag 82, NG 83, Nix 80, RC 75, Sco 80,
    Sco 81, Sin 74, Sto+ 80b, Vog 68, Wei 78

Thermal and statistical models
  collective tube model
    BDE 76, Men 77, Men 79, MM 78a, MM 78b, Var 78

  explicit phase space calculations
    BK 81, GK 78a, Gre+ 83, Kno 79

  firestreak model
    GKW 78, MDJ 83, Mye 78, Wes+ 82

  general
    Bet 38, DL 79, JSD 81, KHB 78, Man 78, Mek 80, MJD 81, MZ 79,
    Nag 82b, RK 81, SR 79, Sub+ 81, Wei 76, WW 75, WW 77

  in fragment emission
    AH 83, Bon+ 77, Cse+ 83, FL 83, GK 81, Gol 74, Gos+ 77, Gro+ 82,
    GW 79, HF 52, JSW 83, Kap 80, Mek 77, Mek 78a, Mek 78b, RMS 82,
    Rop+ 83, SWW 82

  in nucleon emission

    Boa 84, Bog+ 80, BR 84, Das 78, Gos+ 77, Hoa 77, Kap 77, SW 81,
    Wal+ 79, Wes+ 76

  limiting temperature behavior
    BR 84, GK 78c, SOG 81

Transport approach to reactions

    HP 80, Mal 80, PS 79, Ran 79, Rem 75, Rem 79, RS 75, SGB 81, SM 82,
    SN 80

Others references cited
    BSW 82, BW 83, DP 79, Fis 67, HCB 54, HM 82, Kap 83, Mek 82, Sta 79

9. References

Aba+ 61 E. Abate, G. Bellini, E. Fiorini, and S. Ratti, Nuovo Cimento 22, 1206 (1961).

ADS 75 G. Andersson, P. Dougan, and W. Steifler, Z. Physik A272, 263 (1975).

AF 83 H. Araseki and T. Fujita, Nucl. Phys. A399, 434 (1983).

AH 83 J Aichelin and J. Hüfner, Phys. Lett. B (in press).

AHI 83 J. Aichelin, J. Hüfner, and R. Ibarra, submitted to Phys. Rev. C.

AHN 77 A.A. Amsden, F.H. Harlow and J.R. Nix, Phys. Rev. C15, 2059 (1977).

Aic 83 J. Aichelin, Nucl. Phys. A411, 474 (1983).

Akk 79 J.M. Akkermans, Phys. Lett. 82B, 20 (1979).

Ala+ 75 J.P. Alard, A. Baldit, R. Brun, J.P. Costilhes, J. Dhermain, J. Fargeix, L. Fraysse, J. Pellet, G. Roche, J.C. Tamain, A. Cordaillat, and A. Pasinetti, Nuovo Cimento A30, 320 (1975).

Ale 68 J.M. Alexander in Nuclear Chemistry, Vol. 1, L. Yaffe, editor, (Academic, New York, 1968), p. 273.

Ale+ 80 Y. Alexander, J.W. Van Orden, E.F. Redish, and S.J. Wallace, Phys. Rev. Lett. 44, 1579 (1980).

Ale+ 81 K. Aleklett, D.J. Morrissey, W. Loveland, P.L. McGaughey, and G.T. Seaborg, Phys. Rev. C23, 1044 (1981).

Ama+ 75 J.F. Amann, P.D. Barnes, M. Doss, S.A. Dytman, R.A. Eisenstein, J. Penkrot, and A.C. Thompson, Phys. Rev. Lett. 35, 1066 (1975).

Ama 76 R.D. Amado, Phys. Rev. C14, 1264 (1976).

Ams+ 75 A.A. Amsden, G.F. Bertsch, F.H. Harlow, and J.R. Nix, Phys. Rev. Lett. 35, 905 (1975).

Ams+ 77 A. Amsden, J.N. Ginocchio, F.H. Harlow, J.R. Nix, M. Danos, E.C. Halbert, and R.K. Smith, Jr., Phys. Rev. Lett. 38, 1055 (1977).

And+ 81 B.D. Anderson, A.R. Baldwin, A.M. Kalenda, R. Madey, J.W. Watson, C.C. Chang, H.D. Holmgren, R.W. Koontz, and J.R. Wu, Phys. Rev. Lett. 46, 226 (1981).

Ant+ 71 Yu. P. Antuf'ev, V.L. Agranovich, V.B. Ganenko, V.S. Kuz'menko, I.I. Microshnichenko, and P.V. Sorokin, Yad. Fiz. 13, 473 (1971) [Sov. J. Nucl. Phys. 13, 265 (1971)].

Ari+ 72 A. Arima, H. Horiuchi, K. Kubodera, and N.Takigawa, in Advances in Nuclear Physics, Vol.5, M. Baranger and E.W. Vogt, editors, (Plenum, New York, 1972), p. 345.

ARW 77 Y. Alexander, E.F. Redish, and N.W. Wall, Phys. Rev. C16, 526 (1977).

Aub+ 82 R.L. Auble, J.B. Ball, F.E. Bertrand,C.B. Fulmer, D.C. Hensley, I.Y. Lee, R.L. Robinson, P.H. Stelson, D.L. Hendrie, H.D. Holmgren, J.D. Silk, and H. Breuer, Phys. Rev. Lett. 49, 441 (1982).

AW 76a R.D. Amado and R.M. Woloshyn, Phys. Lett. 62B, 253 (1976).

AW 76b R.D. Amado and R.M. Woloshyn, Phys. Rev. Lett. 36, 1435 (1976).

AW 77a R.D. Amado and R.M. Woloshyn, Phys. Lett. 69B, 400 (1977).

AW 77b R.D. Amado and R.M. Woloshyn, Phys. Rev. C16, 1255 (1977).

AW 77c R.D. Amado and R.M. Woloshyn, Phys. Rev. C15, 2200 (1977).

Awe+ 81 T.C. Awes, G. Poggi, S. Saini, C.K. Gelbke, R. Legrain, and G.D. Westfall, Phys. Lett. 103B, 417 (1981).

Awe+ 82 T.C. Awes, S. Saini, G. Poggi, C.K. Gelbke,D. Cha, R. Legrain, and G.D. Westfall, Phys. Rev. C25, 2361 (1982).

AWM 75 D. Agassi, H.A. WeidenmÜller, and G. Mantzouranis, Phys. Rep. 22C, 145 (1975).

Bab+ 82 K. Baba, I. Endo, H. Fukuma, K. Inoue, T. Kawamoto, T. Ohsugi, Y. Sumi, T. Takeshita, S. Uehara, Y.Yano, and K. Maki, Phys. Lett.

113B, 459 (1982).

Bac+ 76 D. Bachelier, J.L. Boyard, T. Hennino, H.D. Holmgren, J.C. Jourdain, P. Radvanyi, P.G. Roos, and M. Roy-Stephan, Nucl. Phys. A268, 488 (1976).

Bac+ 80 B.B. Back, K.L. Wolf, A.C. Mignerey, C.K. Gelbke, T.C. Awes, H. Breuer, V.E. Viola, Jr., and P. Dyer, Phys. Rev. C22, 1927 (1980).

Bal 77 A.M. Baldin, Fiz. Elem. Chastits At. Yadra 8, 429 (1977).

Bar 80 J. Bartke, Nucl. Phys. A335, 481 (1980).

Bau+ 75 H.G. Baumgardt, J.U. Schott, Y. Sakamoto, E. Schopper, H. Stöcker, J. Hofmann, W. Scheid, and W. Greiner, Z. Phys. A273, 360 (1975).

Bay+ 73 Yu.D. Bayukov, L.S. Varob'ev, G.A. Lesin, V.L. Stolin, V.B. Fedorov, and V.D. Khovanskii, Yad. Fiz. 18, 1246 (1973) [Sov. J. Nucl. Phys. 18, 639 (1974)].

Bay+ 79 Y.D. Bayukov, V.I. Efremenko, S. Frankel, W. Frati, M. Gazzaly, G.A. Leksin, N.A. Nikiforov, C.F. Perdrisat, V.I. Tchistilin, and Y.M. Zaitsev, Phys. Rev. C20, 764 (1979).

BC 81 G. Bertsch and J. Cugnon, Phys. Rev. C24, 2514 (1981).

BCG 82 H.W. Barz, L.P. Csernai, and W. Greiner, Phys. Rev. C26, 740 (1982).

BDE 76 G. Berlad, A. Dar, and G. Eilam, Phys. Rev. D13, 161 (1976).

BE 77 Yu. A. Batusov and R.A. Eramzhyan, Fiz. Elem. Chastits At. Yadra 8, 229 (1977) [Sov. J. Part. Nucl. 8, 95 (1977)].

Bea+ 83a D. Beavis, S.Y. Fung, W. Gorn, A. Huie, D. Keane, J.J. Lu, R.T. Poe, B.C. Shen, and G. Van Dalen, Phys. Rev. C27, 910 (1983).

Bea+ 83b D. Beavis, S.Y. Chu, S.Y. Fung, W. Gorn, D. Keane, R.T. Poe, G. VanDalen, and M. Vient, Phys. Rev. C28, 2561 (1983).

Bec+ 81 R. Beckmann, S. Raha, N. Stelte, and R.M. Weiner, Phys. Lett. 105B, 411 (1981).

BEJ 77 J. Bernabeu, T.E.O. Ericson, and C. Jarlskog, Phys. Lett. 69B, 161 (1977).

Ben+ 67 G.W. Bennett, J.L. Friedes, H. Palevsky, R.J. Sutter, G.J. Igo, W.D. Simpson, G.C. Phillips, R.L. Stearns, and D.M. Corley, Phys. Rev. Lett. 19, 387 (1967).

Ben+ 79 W. Benenson, G. Bertsch, G.M. Crawley, E. Kashy, J.A. Nolen, Jr., H. Bowman, J.G. Ingersoll, J.O. Rasmussen, J. Sullivan, M. Koike, M. Sasao, J. Peter, and T.E. Ward, Phys. Rev. Lett. 43, 683 (1979).

Ben 83 W. Benenson in Pion Production and Absorption in Nuclei - 1981, H.C. Wolfe, editor, AIP (1982), p. 381.

Ber 63 H.W. Bertini, Phys. Rev. 131, 1801 (1963) and Phys. Rev. 138, AB2(E) (1965).

Ber 67 H.W. Bertini, Phys. Rev. 162, 976 (1967).

Ber 69 H.W. Bertini, Phys. Rev. 188, 1711 (1969).

Ber 77 G. Bertsch, Phys. Rev. C15, 713 (1977).

Bet 38 H. Bethe, Phys. Rev. 53, 675 (1938).

BFN 78 J.P. Bondorf, G. Fai, and O.B. Nielsen, Phys. Rev. Lett. 41, 391 (1978).

BGS 74 H.W. Bertini, T.A. Gabriel, and R.T. Santoro, Phys. Rev. C9, 522 (1974).

BGZ 78 J.P. Bondorf, S.I.A. Garpman, and J. Zimanyi, Nucl. Phys. A296, 320 (1978).

BH 80 O. Bohigas and J. Hüfner, Phys. Lett. 95B, 9 (1980).

Bha+ 79 K.B. Bhalla, S. Hertzman, A. Oskarsson, I. Otterlund, and B. Jakobsson, Phys. Lett. 82B, 216 (1979).

BHN 83 S. Bohrmann, J. Hüfner, and M.C. Nemes, Phys. Lett. 120B, 59 (1983).

Bho+ 76 R.K. Bhowmik, C.C. Chang, J.-P. Didelez, and H.D. Holmgren, Phys.

Rev. C13, 2105 (1976).

Bin+ 80 M. Bini, C.K. Gelbke, D.K. Scott, T.J.M. Symons, P. Doll, D.L. Hendrie, J.L. Laville, J. Mahoney, M.C. Mermaz, C. Olmer, K. Van Bibber, and H.H. Wieman, Phys. Rev. C22, 1945 (1980).

Bir+ 83 T. Biro, H.W. Barz, B. Lukacs, and J. Zimanyi, Phys. Rev. C27, 2695 (1983).

Biy 83 M. Biyajima, Phys. Lett. 132B, 299 (1983).

BK 81 S. Bohrmann and J. Knoll, Nucl. Phys. A356, 498 (1981).

BKD 84 G.F. Bertsch, H. Kruse, and S. Das Gupta, Phys. Rev. C (in press).

BL 70 M. Blann and F.M. Lanzafame, Nucl. Phys. A142, 559 (1970).

Bla 68 M. Blann, Phys. Rev. Lett. 21, 1357 (1968).

Bla 71 M. Blann, Phys. Rev. Lett. 27, 337 (1971).

Bla 72 M. Blann, Phys. Rev. Lett. 28, 757 (1972).

Bla 73 M. Blann, Nucl. Phys. A213, 570 (1973).

Bla 74 M. Blann, Nucl. Phys. A235, 211 (1974).

Bla 75 M. Blann, Ann. Rev. Nucl. Sci 25, 123 (1975).

Bla+ 76 M. Blann, R.R. Doering, A. Galonsky, D.M. Patterson, and F.E. Serr, Nucl. Phys. A257, 15 (1976).

BLT 77 V.V. Burov, V.K. Lukyanov, and A.I. Titov, Phys. Lett. 67B, 46 (1977).

BLY 79 V.I. Bogatin, O.V. Lozhkin, and Yu.P. Yakovlev, Nucl. Phys. A326, 508 (1979).

BM 72 M. Blann and A. Mignerey, Nucl. Phys. A186, 245 (1972).

BM 77 A.R. Bodmer and C.N. Panos, Phys. Rev. C15, 1342 (1977).

Boa 80a D.H. Boal, in Proc. Intermediate Energy Nuclear Chemistry Workshop, available as Los Alamos Report No. LA-8835-C.

Boa 80b D.H. Boal, Phys. Rev. C21, 1913 (1980).

Boa+ 81 D.H. Boal, R.E.L. Green, R.G. Korteling, and M. Soronshian, Phys. Rev. C23, 2788 (1981).

Boa 82a D.H. Boal, in Proceedings of the Relativistic Heavy Ion Winter School (Banff, 1982).

Boa 82b D.H. Boal, Phys. Rev. C25, 3068 (1982).

Boa 83a D.H. Boal, Phys. Rev. C28, 2568 (1983).

Boa 83b D.H. Boal, Michigan State University Report MSUCL-443.

Boa 83c D.H. Boal, Michigan State University Report MSUCL-419.

Boa 84 D.H. Boal, Phys. Rev. C (in press).

Bog+ 76 V.I. Bogatin, V.F. Litvin, O.V. Lozhkin, N.A. Perfilov, and Yu.P. Yakovlev, Nucl. Phys. A260, 446 (1976).

Bog+ 80 I.G. Bogatskaya, C.B. Chiu, M.I. Gorenstein, and G.M. Zinovjev, Phys. Rev. C22, 209 (1980).

Bon+ 76a J.P. Bondorf, H.T. Feldmeier, S. Garpman, and E.C. Halbert, Pnys. Lett. 65B, 217 (1976).

Bon+ 76b J.P. Bondorf, P.J. Siemens, S. Garpman, and E. Halbert, Z. Phys. 279, 385 (1976).

Bon+ 77 R. Bond, P.J. Johansen, S.E. Koonin, and S. Garpman, Phys. Lett. 71B, 43 (1977).

Bon+ 78 B.E. Bonner, J.E. Simmons, C.R. Newsom, P.J. Riley, G. Glass, J.C. Hiebert, M. Jain, and L.C. Northcliffe, Phys. Rev. C18, 1418 (1978).

BP 61 S.T. Butler and C.A. Pearson, Phys. Rev. Lett 7, 69 (1961).

BP 62 S.T. Butler and C.A. Pearson, Phys. Lett. 1, 77 (1962).

BP 63 S.T. Butler and C.A. Pearson, Phys. Rev. 129, 836 (1963).

BP 71 K. Beg and N.T. Porile, Phys. Rev. C3, 1631 (1971).

BP 73 F.E. Bertrand and R.W. Peelle, Phys. Rev. C8, 1045 (1973).

BP 77 A.R. Bodmer and C.N. Panos, Phys. Rev. C15, 1342 (1977).

BP 79 S. Biswas and N.T. Porile, Phys. Rev. C20, 1467 (1979).

BP 81 A.R. Bodmer and C.N. Panos, Nucl. Phys. A356, 517 (1981).

BPM 80 A.R. Bodmer, C.N. Panos, and A.D. MacKeller, Phys. Rev. C22, 1025 (1980).

BPV 65 M. Bertero, G. Passatore, and G.A. Viano, Nuovo Cimento 38, 1669 (1965).

BR 84 D.H. Boal and J.H. Reid, Phys. Rev. C (in press).

Bra+ 72 G.M. Braga-Marcazzan, E. Gadioli-Erba, L. Milazzo-Colli, and P.G. Sona, Phys. Rev. C6, 1398 (1972).

Bro+ 77 H. Brody, S. Frankel, W. Frati, D. Yang, C.F. Perdrisat, J.C. Comiso, and K.O.H. Ziock, Phys. Lett. 71B, 79 (1977).

BS 54 M.Q. Barton and J.H. Smith, Phys. Rev. 95, 573 (1954).

BS 58 M.Q. Barton and J.H. Smith, Phys. Rev. 110, 1143 (1958).

BS 82 D.H. Boal and M. Soroushian, Phys. Rev. C25, 1003 (1982).

BS 83 G. Bertsch and P.J. Siemens, Phys. Lett. 126B, 9 (1983).

BSH 76 H.W. Bertini, R.T. Santoro and O.W. Hermann, Phys. Rev. C14, 590 (1976).

BSW 82 D.H. Boal, J. Schachter and R.M. Woloshyn, Phys. Rev. D25, 3245 (1982).

Buc+ 81 G. Buchwald, L.P. Csernai, J.A. Maruhn, W. Greiner, and H. Stöcker, Phys. Rev. C24, 135 (1981).

Buc+ 83a G. Buchwald, G. Graebner, J. Theis, J.A. Maruhn, W. Greiner, and H. Stöcker, Phys. Rev. C28, 1119 (1983).

Buc+ 83b G. Buchwald, G. Graebner, J. Theis, J. Maruhn, W. Greiner, H. Stöcker, K. Frankel and M. Gyulassy, Phys. Rev. C28, 2349 (1983).

Bud+ 71 Yu.G. Budyashov, V.G. Zinov, A.D. Konin, A.I. Mukhin, and A.M. Chatrchyan, Zh. Eksp. Teor. Fiz. 60, 19 (1971) [Sov. Phys.-JETP 33, 11 (1971)].

Bur+ 76 N.A. Burgov, M.K. Vlasov, L.S. Vorob'ev, S.A. Gerzon, Yu.T. Kiselev, M.V. Kosov, G.A. Leksin, A.N. Martem'yanov, N.A. Pivnyuk, V.L. Stolin, Yu.V. Terekhov, and V.I. Ushakov, Yad. Fiz. 24, 1183 (1976) [Sov. J. Nucl. Phys. 24, 620 (1976)].

Bur+ 79 N.A. Burgov, M.K. Blasov, L.S. Vorob'ev, S.A. Gerzon, Yu.T. Kiselev, G.A. Leksin, A.N. Martem'yanov, N.A. Pirnyuk, V.L. Stolin, Yu.V. Terekhov, V.I. Ushakov, and M.M. Chumakov, Yad. Fiz. 30, 720 (1979) [Sov. J. Nucl. Phys. 30, 371 (1979)].

BW 52 J.M. Blatt and V.F. Weisskopf, in Theoretical Nuclear Physics, Wiley and Sons (1952).

BW 79 D.H. Boal and R.M. Woloshyn, Phys. Rev. C20, 1878 (1979).

BW 81 D.H. Boal and R.M. Woloshyn, Phys. Rev. C23, 1206 (1981).

BW 83 D.H. Boal and R.M. Woloshyn, eds. Short Distance Phenomena in Nuclear Physics (Plenum, New York, 1983).

CAH 63 V.P. Crespo, J.M. Alexander, and E.K. Hyde, Phys. Rev. 131, 1763 (1963).

CB 71 C.K. Cline and M. Blann, Nucl. Phys. A172, 225 (1971).

CB 80 L.P. Csernai and H.W. Barz, Z. Phys., A296, 173 (1980).

CCP 68 V.P. Crespo, J.B. Cumming, and A.M. Poskanzer, Phys. Rev. 174, 1455 (1968).

CDM 80 G. Cecil, S. Das Gupta, and W.D. Myers, Phys. Rev. C22, 2018 (1980).

CDG 83 G. Cannata, J.D. Dedonder, and S.A. Gurvitz, Phys. Rev. C27, 1697 (1983).

Cec+ 81 R.A. Cecil, B.D. Anderson, A.R. Baldwin, R. Madey, W. Schimmerling, J.W. Kast, and D. Ortendahl, Phys. Rev. C24, 2013 (1981).

CG 61 W. Czyz and K. Gottfried, Nucl. Phys. 21, 676 (1961).

CG 81 L.P. Csernai and W. Greiner, Phys. Lett. 99B, 85 (1981).

CH 81a X. Campi and J. Hüfner, Phys. Rev. C24, 2199 (1981).

CH 81b H.C. Chiang and J. Hüfner, Nucl Phys. A352, 442 (1981).

Cha+ 80 Chao Wei-qin, C.B. Chiu, He Zuoxiu, and Don M. Tou, Phys. Rev. Lett. 44, 518 (1980).

Che+ 68 K. Chen, Z. Fraenkel, G. Friedlander, J.R. Grover, J.M. Miller, and Y. Shimamoto, Phys. Rev. 166, 949 (1968).

Che+ 75 A. Chevarier, N. Chevarier, A. Demeyer, G. Hollinger, P. Pertosa, and Tran Minh Duc, Phys. Rev. C11, 886 (1975).

Che+ 77 G.M. Chernov, K.G. Gulamov, U.G. Gulyamov, S.Z. Nasyrov, and L.N. Svechnikova, Nucl. Phys. A280, 478 (1977).

Che 79 M. Chemtob, Nucl. Phys. A314, 387 (1979).

Che+ 81 T. Chen, R.E. Segal, P.T. Debevec, J. Wiggins, P.P. Singh, and J.V. Maher, Phys. Lett. 103B, 192 (1981).

CHF 58 A.A. Caretto, J. Hudis, and G. Friedlander, Phys. Rev. 110, 1130 (1958).

CHH 81 J.B. Cumming, P.E Haustein and H-C. Hseuh, Phys. Rev. C24, 2162 (1981).

CHH 82 W.Q. Chao, F. Hachenberg, and J. Hüfner, Nucl. Phys. A384, 24 (1982).

Chi+ 83 C.B. Chitwood, D.J. Fields, C.K. Gelbke, W.G. Lynch, A.D. Panagiotou, M.B. Tsang, H. Utsunomiya, and W.A. Friedman, Phys. Lett. 131B, 289 (1983).

CHM 52 J.B. Cladis, W.N. Hess, and B.J. Moyer, Phys. Rev. 87, 425 (1952).

Chr+ 80 R.E. Chrien, T.J. Krieger, R.J. Sutter, M. May, H. Palevsky, R.L. Stearns, T. Kozlowski and T. Bauer, Phys. Rev. C21, 1014 (1980).

Cia+ 83 G. Ciangaru, C.C. Chang, H.D. Holmgren, A. Nadasen, P.G. Roos, A.A.

Cowley, S. Mills, P.P. Singh, M.K. Saber, and J.R. Hall, Phys. Rev. C27, 1360 (1983).

CJ 83 J. Cugnon and M. Jaminon, Phys. Lett. 123B, 155 (1983).

CKR 81 J. Cugnon, J. Knoll, and J. Randrup, Nucl. Phys. A360, 444 (1981).

Cli 72 C.K. Cline, Nucl. Phys. A193, 417 (1972).

CLZ 80 L.P. Csernai, B. Lukacs, and J. Zymanyi, Nuovo Cimento Lett. 27, 111 (1980).

CMV 81 J. Cugnon, T. Mizutani, and J. Vandermeulen, Nucl. Phys. A352, 505 (1981).

Coc+ 60 V.T. Cocconi, T. Fazzini, C. Fidecaro, M. Legros, N.H. Lipman, and A.W. Morrison, Phys. Rev. Lett 5, 19 (1960).

Coc+ 72a D.R.F. Cochran, P.N. Dean, P.A.M. Gram, E.A. Knapp, E.R. Martin, D.E. Nagle, R.B. Perkins, W.J. Shlaer, H.A. Thiessen, and E.D. Theriot, LAMPF report La-5083-MS (1972) unpublished.

Coc+ 72b D.R.F. Cochran, P.N. Dean, P.A.M. Gram, E.A. Knapp, E.R. Martin, D.E. Nagle, R.B. Perkins, W.J. Shlaer, H.A. Thiessen, and E.D. Theriot, Phys. Rev. D6, 3085 (1972).

Coc 74 G. Cocconi, Phys. Lett. 49B, 459 (1974).

Coh 66 J.P. Cohen, Nucl. Phys. 84, 316 (1966).

Cor+ 72 D.M. Corley, N.S. Wall, H. Palevsky, J.L. Friedes, R.J. Sutter, G.W. Bennett, W.D. Simpson, G.C. Phillips, G.W. Igo, and R.L. Stearns, Nucl. Phys. A184, 437 (1972).

Cow+ 80 A.A. Cowley, C.C. Chang, H.D. Holmgren, J.D. Silk, D.L. Hendrie, R.W. Koontz, P.G. Roos, C. Samanta, and J.R. Wu, Phys. Rev. Lett. 45, 1930 (1980).

CR 75 N.S. Chant and P.G. Roos in Proceedings of the Second International Conference on Clustering Phenomena in Nuclei, College Park, 1975,

D.A. Goldberg, J.B. Marion and S.J. Wallace, editors, (Oak Ridge, 1975).

CR 77 N.S. Chant and P.G. Roos, Phys. Rev. C15, 57 (1977).

CR 83 N.S. Chant and P.G. Roos, Phys Rev. C27, 1060 (1983).

Cra+ 75 H.J. Crawford, P.B. Price, J. Stevenson, and L.W. Wilson, Phys. Rev. Lett. 34, 329 (1975).

Cra+ 84 G.M. Crawley, J.P. Dufour, L.H. Harwood, B.E. Hasselquist, B.V. Jacak, Z.M. Koenig, T.J.M. Symons, R.S. Tickle, and G.D. Westfall, (private communication).

CS 74 S.K. Chang and N. Sugarman, Phys. Rev. C9, 1138 (1974).

CS 80 M. Chemtob and B. Schürmann, Nucl. Phys. A336, 508 (1980).

Cse+ 82 L.P. Csernai, W. Greiner, H. Stöcker, I. Tanihata, S. Nagamiya, and J. Knoll, Phys. Rev. C25, 2482 (1982).

Cse+ 83 L.P. Csernai, H. Stöcker, P.R. Subramanian, G. Buchwald, G. Graebner, A. Rosenhauer, J.A. Maruhn, and W. Greiner, Phys. Rev. C28, 2001 (1983).

CTS 83a M.W. Curtin, H. Toki, and D.K. Scott, Phys. Lett. 123B, 289 (1983).

CTS 83b M.W. Curtin, H. Toki, and D.K. Scott, Michigan State University Report MSUCL-426.

Cug 80 J. Cugnon, Phys. Rev. C22, 1885 (1980).

Cum+ 64 J.B. Cumming, R.J. Cross, Jr., J. Hudis, and A.M. Poskanzer, Phys. Rev. 134, B167 (1964).

CWY 79 D.J.E. Callaway, L. Wilets, and Y. Yariv, Nucl. Phys. A327, 250 (1979).

Dan 79 P. Danielewicz, Nucl. Phys. A314, 465 (1979).

Das 78 S. Das Gupta, Phys. Rev. Lett. 41, 1450 (1978).

Den 54 D.M. Dennison, Phys. Rev. 96, 378 (1954).

DFR 60 I. Dostrovsky, Z. Fraenkel, and P. Rabinowitz, Phys. Rev. 118, 791 (1960) and references therein.

DJK 82 S. Das Gupta, B.K. Jennings, and J.I. Kapusta, Phys. Rev. C26, 274 (1982).

DL 79 S. Das Gupta and C.S. Lam, Phys. Rev. C20, 1192 (1979).

DM 81 S. Das Gupta and A.Z. Mekjian, Phys. Rep. 72, 131 (1981).

Doe+ 78 R.R. Doering, T.C. Schweizer, S.T. Thornton, L.C. Dennis, K.R. Cordell, K.O.H. Ziock, and J.C. Comiso, Phys. Rev. Lett. 40, 1433 (1978).

Dol+ 79 W.E. Dollhopf, C.F. Perdrisat, P. Kitching, and W.C. Olsen, Nucl. Phys. A316, 350 (1979).

DP 79 R.M. DeVries and J.C. Peng, Phys. Rev. Lett. 43, 1373 (1979).

DS 73 P. Dougan and W. Stiefler, Z. Phys. 265, 1 (1973).

DT 76 E.T. Dressler and E.L. Tomusiak, Nucl. Phys. A273, 383 (1976).

Fel+ 54 B.T. Feld, R.D. Godbole, A. Odian, F. Scherb, P.C. Stein, and A. Wattenberg, Phys. Rev. 94, 1000 (1954).

FF 77 S. Frankel and W. Frati, Phys. Rev. C16, 1499 (1977).

FH 73 H. Feshbach and K. Huang, Phys. Lett. 47B, 300 (1973).

FH 79 T. Fujita and J. Hüfner, Nucl. Phys. A314, 317 (1979).

FH 80 T. Fujita and J. Hüfner, Nucl. Phys. A343, 493 (1980).

Fin+ 82 J.E. Finn, S. Agarwal, A. Bujak, J. Chuang, L.J. Gutay, A.S. Hirsch, R.W. Minich, N.T. Porile, R.P. Scharenberg, B.C. Stringfellow, and F. Turkot, Phys. Rev. Lett. 49, 1321 (1982).

Fis 67 M.E. Fisher, Physics 3, 255 (1967).

FKS 80 H. Feshbach, A. Kerman, and S. Koonin, Ann. Phys. (NY) 125, 429 (1980).

FL 83 W.A. Friedman and W.G. Lynch, Phys. Rev. C28, 16, 950 (1983).

Flo+ 78 A.G. Flowers, A.C. Shotter, D. Branford, J.C. McGeorge, and R.O. Owens, Phys. Rev. Lett. 40, 709 (1978).

Flo+ 79 A.G. Flowers, D. Branford, J.C. McGeorge, A.C. Schotter, P. Thornley, C.H. Zimmerman, R.O. Owens, and J.S. Pringle, Phys. Rev. Lett. 43, 323 (1979).

FM 71 Y. Futami and T. Miyajima, Prog. Theor. Phys. 46, 802 (1971).

FMP 62 V.L. Fitch, S.L. Meyer, and P.A. Piroue, Phys. Rev. 126, 1849 (1962).

Foà 75 L. Foà, Phys. Rep. 22C, 1 (1975).

FP 78 D.R. Fortney and N.T. Porile, Phys. Lett. 76B, 553 (1978).

FP 80a D.R. Fortney and N.T. Porile, Phys. Rev. C21, 664 (1980).

FP 80b D.R. Fortney and N.T. Porile, Phys. Rev. C22, 670 (1980).

FP 80c D.R. Fortney and N.T. Porile, Phys. Rev. C21, 2511 (1980).

Fra+ 76 S. Frankel, W. Frati, O. Van Dyck, R. Werbeck, and V. Highland, Phys. Rev. Lett. 36, 642 (1976).

Fra 77 S. Frankel, Phys. Rev. Lett. 38, 1338 (1977).

Fra 78 S. Frankel, Phys. Rev. C17, 694 (1978).

Fra+ 78a S. Frankel,W. Frati, M. Gazzaly, G.W. Hoffman, O. Van Dyck, and R.M. Woloshyn, Phys. Rev. Lett. 41, 148 (1978).

Fra+ 78b S. Frankel, W. Frati, G. Blanpied, G.W.Hoffmann, T. Kozlowski, C. Morris, H.A. Thiessen, O. Van Dyck, R. Ridge, and C. Whitten, Phys. Rev. C18, 1375 (1978).

Fra+ 78c S. Frankel, W. Frati, R.M. Woloshyn, and D. Yang, Phys. Rev. C18, 1379 (1978).

Fra+ 79 S. Frankel,W. Frati, M. Gazzaly, Y.D. Bayukov, V.I. Efremenko, G.A. Leksin, N.A. Nikiforov, V.I. Tchistilin, Y.M. Zaitsev, and C.F. Perdrisat, Phys. Rev. C20, 2257 (1979).

Fra+ 81 S. Frankel, W. Frati, C.F. Perdrisat, and O.B. Van Dyck, Phys. Rev. C24, 2684 (1981).

Fra+ 82 K.A. Frankel, J.A. Bistirlich, R. Bossingham, H.R. Bowman, K.M. Crowe, C.J. Martoff, D. Murphy, J.O. Rasmussen, J.P. Sullivan, W.A. Zajc, J.P. Miller, O. Hashimoto, M. Koike, J. Peter, W. Benenson, G.M. Crawley, E. Kashy, J.A. Nolen, Jr., and J. Quebert, Phys. Rev. C25, 1102 (1982).

FS 77 L.L. Frankfurt and M.I. Strikman, Phys. Lett. 69B, 93 (1977).

FS 79 L.L. Frankfurt and M.I. Strikman, Phys. Lett. 83B, 407 (1979).

FS 81 K.A. Frankel and J.D. Stevenson, Phys. Rev. C23, 1511 (1981).

Fuj 77 T. Fujita, Phys. Rev. Lett. 39, 174 (1977).

Fuj 79 T. Fujita, Nucl. Phys. A324, 409 (1979).

Fun+ 78a S.Y. Fung, W. Gorn, G.P. Kiernan, F.F. Liu, J.J. Lu, Y.T. Oh, J. Ozawa, R.T. Poe, L. Schroeder, and H. Steiner, Phys. Rev. Lett. 40, 292 (1978).

Fun+ 78b S.Y. Fung, W. Gorn, G.P. Kiernan, J.J. Lu, Y.T. Oh, and R.T. Poe, Phys. Rev. Lett. 41, 1592 (1978).

FW 77 S. Frankel and R.M. Woloshyn, Phys. Rev. C16, 1680 (1977).

GA 69 T.A. Gabriel and R.G. Alsmiller, Phys. Rev. 182, 1035 (1969).

Gab 76 T.A. Gabriel, Phys. Rev. C13, 240 (1976).

Gad+ 76 E. Gadioli, E. Gadioli-Erba, G. Tagliaferri, and J.J. Hogan, Phys. Lett. 65B, 311 (1976).

Gar+ 65 J. Garvey, B.H. Patrick, J.G. Rutherglen, and I.L. Smith, Nucl. Phys. 70, 241 (1965).

Gar+ 80 S.I.A. Garpman, S.K. Samaddar, D. Sperber, and M. Zielinska-Pfabe, Phys. Lett. 92B, 56 (1980).

GB 77 J. Ginocchio and M. Blann, Phys. Lett. 68B, 405 (1977).

GDA 79 S.A. Gurvitz, J.-P. Dedonder, and R.D. Amado, Phys. Rev. C19, 142 (1979).

Gea+ 80 J.V. Geaga, S.A. Chessin, J.Y. Grossiord, J.W. Harris, D.L. Hendrie, L.S. Schroeder, R.N. Treuhaft, and K. Van Bibber, Phys. Rev. Lett. 45, 1993 (1980).

GFR 83 M. Gyulassy, K. Frankel, and E.A. Remler, Nucl. Phys. A402, 596 (1983).

GFS 82 M. Gyulassy, K.A. Fraenkel, and H. Stöcker, Phys. Lett. 110B, 185 (1982).

GGK 79 S.I.A. Garpmann, N.K. Glendenning, and Y.J. Karant, Nucl. Phys. A322, 382 (1979).

GH 74 M. Gari and H. Hebach, Phys. Rev. C10, 1629 (1974).

GH 78 A.S. Goldhaber and H.H. Heckmann, Ann. Rev. Nucl. Part. Sci. 28, 161 (1978).

GIT 79 K.K. Gudima, H. Iwe, and V.D. Toneev, J. Phys. G5, 229 (1979).

GJK 82 R.E.L. Green, K.P. Jackson, and R.G. Korteling, Phys. Rev. C25, 828 (1982).

GK 78a M. Gyulassy and S.K. Kauffmann, Phys. Rev. Lett. 40, 298 (1978).

GK 78b R.E.L. Green and R.G. Korteling, Phys. Rev. C18, 311 (1978).

GK 78c N.K. Glendenning and Y. Karant, Phys. Rev. Lett. 40, 374 (1978).

GK 80 R.E.L. Green and R.G. Korteling, Phys. Rev. C22, 1594 (1980).

GK 81 R.E.L. Green and R.G. Korteling, Nucl. Inst. Meth. 185, 195 (1981).

GKJ 83 R.E.L. Green, R.G. Korteling, and K.P. Jackson, TRIUMF Report TRI-PP-83-116.

GKM 83 A.L. Goodman, J.I. Kapusta, and A.Z. Mekjian, Lawrence Berkeley Laboratory Report LBL-16471.

GKW 78 J. Gosset, J.I. Kapusta, and G.D. Westfall, Phys. Rev. C18, 844 (1978).

GKW 79 M. Gyulassy, S.K. Kauffmann, and L.W. Wilson, Phys. Rev. C20, 2267 (1979).

GM 70 R.J. Glauber and G. Matthiae, Nucl. Phys. B21, 135 (1970).

GMT 83 K.K. Gudima, S.G. Mashnik, and V.D. Toneev, Nucl. Phys. A401, 329 (1983).

Gol+ 60 G. Goldhaber, S. Goldhaber, W. Lee, and A. Pais, Phys. Rev. 120, 300 (1960).

Gol 74 A.S. Goldhaber, Phys. Lett. 53B, 306 (1974).

Gos+ 77 J. Gosset, H.H. Gutbrod, W.G. Meyer, A.M. Poskanzer, A. Sandoval, R. Stock, and G.D. Westfall, Phys. Rev. C16, 629 (1977).

Gre+ 83 R.E.L. Green, D.H. Boal, R. Helmer, K.P. Jackson, and R.G. Korteling, Nucl. Phys. A405, 463 (1983).

Gri 66 J.J. Griffin, Phys. Rev. Lett 17, 478 (1966).

Gro+ 82 D.H.E. Gross, L. Satpathy, Meng Ta-Chung, and M. Satpathy, Z. Phys. A309, 41 (1982).

GT 78 K.K. Gudima and V.D. Toneev, Yad. Fiz. 27, 658 (1978) [Sov. J. Nucl. Phys. 27, 351 (1978)].

Gur 80a S.A. Gurvitz, Phys. Rev. C22, 725 (1980).

Gur 80b S.A. Gurvitz, Phys. Rev. C22, 964 (1980).

Gur 81 S.A. Gurvitz, Phys. Rev. Lett. 47, 560 (1981).

Gur 82a S.A. Gurvitz, Weizmann Institute Report No. WIS-81/29.

Gur 82b S.A. Gurvitz, Weizmann Institute Report No. WIS-82/7.

Gut+ 76 H.H. Gutbrod, A. Sandoval, P.J. Johansen, A.M. Poskanzer, J. Gosset, W.G. Meyer, G.D. Westfall, and R. Stock, Phys. Rev. Lett. 37, 667 (1976).

Gut+ 83 H.H. Gutbrod, H. Löhner, A.M. Poskanzer, T. Renner, H. Riedesel, H.G. Ritter, A. Warwick, F. Weik, and H. Wieman, Phys. Lett. 127B, 317 (1983).

GW 79 P.-A. Gottschalk and M. Weström, Nucl. Phys. A314, 232 (1979).

Gyu 81 M. Gyulassy, Nucl. Phys. A354, 395 (1981).

Gyu 82 M. Gyulassy, Phys. Rev. Lett. 48, 454 (1982).

Hal 81 E.C. Halbert, Phys. Rev. C23, 295 (1981).

Hat 79 R.L. Hatch, Ph.D. thesis, California Institute of Technology, 1979 (unpublished).

HBM 69 J.R. Huizenga, A.N. Behkami, and L.G. Moretto, Phys. Rev. 177, 1826 (1969).

HBP 71 E.K. Hyde, G.W. Butler, and A.M. Poskanzer, Phys. Rev. C4, 1759 (1971).

HCB 54 J.O. Hirschfelder, C.F. Curtiss, and R.B. Bird, Molecular Theory of Gases and Liquids (Wiley, New York, 1954).

HCH 80 F. Hachenberg, H.C. Chiang, and J. Hüfner, Phys. Lett. 97B, 183 (1980).

Hec+ 78 H.H. Heckman, H.J. Crawford, D.E. Greiner, P.J. Lindstrom, and L.W. Wilson, Phys. Rev. C17, 1651 (1978).

Hel+ 83 R.L. Helmer, R.E.L. Green, K.P. Jackson, and R.G. Korteling, Phys. Rev. C (in press).

HF 52 W. Hauser and H. Feshbach, Phys. Rev. 87, 366 (1952).

HH 81 M.K. Hegab and J. Hüfner, Phys. Lett. 105B, 103 (1981).

Hir+ 83 A.S. Hirsch, A. Bujak, J.E. Finn, L.J. Gutay, R.W. Minich, N.T. Porile, R.P. Scharenberg, B.C. Stringfellow, and F. Turkot, to be published.

HK 77 J. Hüfner and J. Knoll, Nucl. Phys. A290, 460 (1977).

HK 79 R.L. Hatch and S.E. Koonin, Phys. Lett. 81B, 1 (1979).

HM 71 G.D. Harp and J.M. Miller, Phys. Rev. C3, 1847 (1971).

HM 82 T.R. Halemane and A.Z. Mekjian, Phys. Rev. C25, 2398 (1982).

HN 81 J. Hüfner and M.C. Nemes, Phys. Rev. C23, 2538 (1981).

Ho+ 77 H. Ho, R. Albrecht, W. Dünnweber, G. Graw, S.G. Steadman, J.P. Wurm, D. Disdier, V. Rauch, and F. Scheibling, Z. Phys. A283, 235 (1977).

Hoa 77 T.F. Hoang, Phys. Rev. D15, 2533 (1977).

Hof+ 76 J. Hofman, H. Stöcker, U. Heinz, W. Scheid, and W. Greiner, Phys. Rev. Lett. 36, 88 (1976).

HP 80 P. Hecking and H. Pirner, Nucl. Phys. A333, 514 (1980).

HPU 66 H. Hoffman, B. Prowe, and H. Ullrich, Nucl Phys. 85, 631 (1966).

HS 83 J. Hufner and H.M. Sommermann, Phys. Rev. C27, 2090 (1983).

HSS 75 J. Hüfner, K. Schafer, and B. Shurmann, Phys. Rev. C12, 1888 (1975).

HT 56 R. Hanbury-Brown and R.Q. Twiss, Nature 178, 1046 (1956).

Hud 68 J. Hudis, Phys. Rev. 171, 1303 (1968).

HWG 76 H. Hebach, A. Wortberg, and M. Gari, Nucl. Phys. A267, 425 (1976).

Ish 59 C. Ishii, Prog. Theor. Phys. 21, 663 (1959).

Iwe 79 H. Iwe, J. Phys. G5, 1405 (1979).

Jac 71 D.F. Jackson, Nucl. Phys. A173, 225 (1971).

Jac 83 B.V. Jacak, private communication.

Jac+ 83 B.V. Jacak, G.D. Westfall, C.K. Gelbke, L.H. Harwood, W.G. Lynch, D.K. Scott, H. Stöcker, M.B. Tsang, and T.J.M. Symons, Phys. Rev. Lett. 51, 1846 (1983).

Jai 80 B.K. Jain, Phys. Rev. C22, 583 (1980).

Jak 78 B. Jakobsson, Physica Scripta 17, 491 (1978).

Jak+ 81 B. Jakobsson, L. Carlen, P. Kristiansson, J. Krumlinde, A. Oskarsson, I. Otterlund, B. Schroder, H.A. Gustafsson,

T. Johansson, H. Ryde, G. Tibell, J.P. Bondorf, G. Fai, A.O.T. Karvinen, O.B. Nielsen, M. Buenerd, J. Cole, D. Lebrun, J.M. Loiseaux, P. Martin, R. Ost, P. de Saintignon, C. Guet, E. Monnard, J. Mougey, H. Nifenecker, P. Perrin, J. Pinston, C. Ristori, and F. Schussler, , Phys. Lett. 102B, 121 (1981).

JDM 82 B.K. Jennings, S. Das Gupta, and N. Mobed, Phys. Rev. C25, 278 (1982).

JMZ 83 H. Jaqaman, A.Z. Mekjian, and L. Zamick, Phys. Rev. C27, 2782 (1983).

JSD 81 B.K. Jennings, L. Satpathy, and S. Das Gupta, Phys. Rev. C24, 440 (1981).

JSW 83 B.V. Jacak, H. Stöcker, and G.D. Westfall, MSUCL Report (1983).

Kal+ 83 A.M. Kalend, B.D. Anderson, A.R. Baldwin, R. Madey, J.W. Watson, C.C. Chang, H.D. Holmgren, R.W Koontz, J.R. Wu, and H. Machner, Phys. Rev. C28, 105 (1983).

Kap 77 J.I. Kapusta, Phys. Rev. C16, 1493 (1977).

Kap 80 J.I. Kapusta, Phys. Rev. C21, 1301 (1980).

Kap 83 J.I. Kapusta, private communication.

Kas+ 81 J. Kasagi, S. Saini, T.C. Awes, A. Galonsky, C.-K. Gelbke, G. Poggi, D.K. Scott, K.L. Wolf, and R.L. Legrain, Phys. Lett. 104B, 434 (1981).

Kau+ 76 S.B. Kaufman, M.W. Weisfield, E.P. Steinberg, B.D. Wilkins, and D. Henderson, Phys. Rev. C14, 1121 (1976).

Kau+ 80 S.B. Kaufmann, E.P. Steinberg, B.D. Wilkins, and D.J. Henderson, Phys. Rev. C22, 1897 (1980).

KC 67 R.G. Korteling and A.A. Caretto, Jr., J. Inorg. Nucl. Chem. 29, 2863 (1967).

KC 70a R.G. Korteling and A.A. Caretto, Jr., Phys. Rev. C1, 193 (1970).

KC 70b R.G. Korteling and A.A. Caretto, Jr., Phys. Rev. C1, 1960 (1970).

KH 64 R.G Korteling and E.K. Hyde, Phys. Rev. 136, B425 (1964).

KHB 78 J. Knoll, J. Hüfner, and A. Bouyssy, Nucl. Phys. A308, 500 (1978).

Kim+ 63 Y.S. Kim, F.F. Liu, F.J. Loeffler, and T.R. Palfrey, Jr., Phys. Rev. 129, 1362 (1963).

KK 68 K. Kikuchi and M. Kawai, Nuclear Reactions at High Energy, (North-Holland, Amsterdam, 1968).

KK 70 R. Korteling and R. Kiefer, Phys. Rev. C2, 957 (1970).

KMS 76 Y. Kitazoe, K. Matsuoka, and M. Sano, Prog. Theor. Phys. 56, 860 (1976).

Kno 79 J. Knoll, Phys. Rev. C20, 773 (1979).

Kno+ 82 J. Knoll, L. Münchow, G. Röpke, and H. Schulz, Phys. Lett. 112B, 13 (1982).

Kod+ 82 T. Kodama, S.B. Duarte, K.C. Chung, and R.A.M.S. Nazareth, Phys. Rev. Lett. 49, 536 (1982).

Koh 82 H.S. Kohler, Nucl. Phys. A378, 159, 181 (1982).

Kom+ 76 V.I. Komarov, G.E. Kosarev, E.S. Kuzmin, A.G. Molokanov, G.P. Reshetnikov, O.V. Savchenko, and S. Tesch, Nucl. Phys. A256, 362 (1976).

Kom+ 77 V.I. Komarov, G.E. Kosarev, H. Muller, D. Netzband, and T. Stiehler, Phys. Lett. 69B, 37 (1977).

Kom+ 78 V.I. Komarov, G.E. Kosarev, H. Muller, D. Netzband, T. Stiehler, and S. Tesch, Phys. Lett. 80B, 30 (1978).

Kom+ 79a V.I. Komarov, G.E. Kosarev, H. Müller, D. Netzband, V.D. Tonnev, T. Stiehler, S. Tesch, K.K. Gudima, and S.G. Mashnik, Nucl. Phys. A326, 297 (1979).

Kom+ 79b V.I. Komarov, G.E. Kosarev, H. Müller, D. Netzband, T. Stiehler, and S. Tesch, J. Phys. G5, 1717 (1979).

Koo 77a S.E. Koonin, Phys. Rev. Lett. 39, 680 (1977).

Koo 77b S.E. Koonin, Phys. Lett. 70B, 43 (1977).

Kop 74 G.I. Kopylov, Phys. Lett. 50B, 472 (1974).

KP 63 M. Kregar and B. Povh, Nucl. Phys. 43, 170 (1963).

KR 79 J. Knoll and J. Randrup, Nucl. Phys. A324, 445 (1979).

KR 81 J. Knoll and J. Randrup, Phys. Lett. 103B, 264 (1981).

Kra+ 79 K.S. Krane, T.C. Sharma, L.W. Swenson, D.K. McDaniels, P. Varghese, B.E. Wood, R.R. Silbar, H.D. Wohlfahrt, and C.A. Goulding, Phys. Rev. C20, 1873 (1979).

KS 75a Y. Kitazoe and M. Sano, Nuovo Cimento Lett. 14, 400 (1975).

KS 75b Y. Kitazoe and M. Sano, Prog. Theor. Phys. 54, 1575 (1975).

KS 81 J.I. Kapusta and D. Strottman, Phys. Rev. C23, 1282 (1981).

KSW 78a J. Källne, A.W. Stetz, and R. M. Woloshyn, Phys. Lett. 74B, 170 (1978).

KSW 78b S.B. Kaufman, E.P. Steinberg, and M.W. Weisfield, Phys. Rev. C18, 1349 (1978).

KTH 73 R.G. Korteling, C.R. Toren, and E.K. Hyde, Phys. Rev. C7, 1611 (1973).

KW 70 F.R. Kroll and N.W. Wall, Phys. Rev. C1, 138 (1970).

KW 75 S.B. Kaufman and M.W. Weisfield, Phys. Rev. C11, 1258 (1975).

Lem+ 79 M.C. Lemaire, S. Nagamiya, S. Schnetzer, H. Steiner, and I. Tanihata, Phys. Lett. 85B, 38 (1979).

Lev 51 J.S. Levinger, Phys. Rev. 84, 43 (1951).

Lev+ 81 S.M. Levenson, D.F. Geesaman, E.P. Colton, R.J. Holt, H.E. Jackson, J.P. Schiffer, J.R. Specht, K.E. Stephenson, B. Zeidman,

R.E. Segal, P.A.M. Gram, and C.A. Goulding, Phys. Rev. Lett. 47, 479 (1981).

LG 79 R.H. Landau and M. Gyulassy, Phys. Rev. C19, 149 (1979).

Lov+ 77 W. Loveland, R.J. Otto, D.J. Morrissey, and G.T. Seaborg, Phys. Lett. 69B, 284 (1977).

Lov+ 81 W. Loveland, D.J. Morrissey, K. Aleklett, G.T. Seaborg, S.B. Kaufman, E.P. Steinberg, B.D. Wilkins, J.B. Cumming, P.E. Haustein, and H.C. Hseuh, Phys. Rev. C23, 253 (1981).

LS 51 C. Levinthal and A. Silverman, Phys. Rev. 82, 822 (1951).

LS 78 M. Lifshitz and P.Singer, Phys. Rev. Lett. 41, 18 (1978).

Lu+ 81 J.J. Lu, D. Beavis, S.Y. Fung, W. Gorn, A. Huie, G.P. Kiernan, R.T. Poe, and G. VanDalen, Phys. Rev. Lett. 46, 898 (1981).

Lyn+ 83 W.G. Lynch, C.B. Chitwood, M.B. Tsang, D.J. Fields, D.R. Klesch, C.K. Gelbke, G.R. Young, T.C. Awes, R.L. Ferguson, F.E. Obenshain, F. Plasil, R.L. Robinson, and A.D. Panagiotou, Phys. Rev. Lett. 51, 1850 (1983).

Mac 79 H. Machner, Phys. Lett. 86B, 129 (1979).

Mac 80 H. Machner, Phys. Rev. C21, 2695 (1980).

Mac 83 H. Machner, Phys. Rev. C28, 2173 (1983).

Mal 80 R. Malfliet, Phys. Rev. Lett. 44, 864 (1980).

Man 78 G. Mantzouranis, Phys. Rev. C18, 2227 (1978).

Mat+ 76 J.L. Matthews, D.J.S. Findlay, S.N. Gardiner, and R.O. Owens, Nucl. Phys. A267, 51 (1976).

MAW 75 G. Mantzouranis, D. Agassi, and H.A. Weidenmüller, Phys. Lett. 57B, 220 (1975).

MAW 76 G.M. Mantzouranis, D. Agassi, and H.A. Weidenmüller, Z. Phys. A276, 145 (1976).

MB 73 L. Milazzo-Colli, and G.M. Braga-Marcazzan, Nucl. Phys. A210, 297 (1973).

MBS 76 A. Mignerey, M. Blann, and W. Scobel, Nucl. Phys. A273, 125 (1976).

MDJ 83 N. Mobed, S. Das Gupta, and B.K. Jennings, Phys. Rev. C27, 1526 (1983).

Mek 77 A.Z. Mekjian, Phys. Rev. Lett. 38, 640 (1977).

Mek 78a A.Z. Mekjian, Phys. Rev. C17, 1051 (1978).

Mek 78b A.Z. Mekjian, Nucl. Phys. A312, 491 (1978).

Mek 80 A. Mekjian, Phys. Lett. 89B, 177 (1980).

Mek 82 A.Z. Mekjian, Nucl. Phys. A384, 492 (1982).

Men 77 Meng Ta-Chung, Phys. Rev. D15, 197 (1977).

Men 79 Meng Ta-Chung, Phys. Rev. Lett. 42, 1331 (1979).

Met+ 58 N. Metropolis, R. Bivins, M. Storm, J.M. Miller, G. Friedlander, and A. Turkevich, Phys. Rev. 110, 185 (1958).

Mey+ 80 W.G. Meyer, H.H. Gutbrod, Ch. Lukner, and A. Sandoval, Phys. Rev. C22, 179 (1980).

MGS 77 J.J. Murphy, II, H.J. Gehrhardt, and D.M. Skopik, Nucl. Phys. A277, 69 (1977).

MH 59 J.M. Miller and J. Hudis, Ann. Rev. Nucl. Sci. 9, 159 (1959).

Mil+ 74 L. Milazzo-Colli, G.M. Braga-Marcazzan, M. Milazzo, and C. Signorini, Nucl. Phys. A218, 274 (1974).

Min+ 82 R.W. Minich, S. Agarwal, A. Bujak, J. Chuang, J.E. Finn, L.J. Gutay, A.S. Hirsch, N.T. Porile, R.P. Scharenberg, B.C. Stringfellow and F. Turkot, Phys. Lett. 118B, 458 (1982).

MJD 81 N. Mobed, B.K. Jennings, and S. Das Gupta, Phys. Lett. 106B, 371 (1981).

MLS 78 D.J. Morrissey, W. Loveland, and G.T. Seaborg, Z. Phys. A289, 123

(1978).

MM 78a Meng Ta-Chung and E. Moeller, Phys. Rev. Lett. 41, 1352 (1978).

MM 78b H.B. Mathis and Meng Ta-Chung, Phys. Rev. C18, 952 (1978).

MMS 80 I.N. Mishustin, F. Myhrer, and P.J. Siemens, Phys. Lett. 95B, 361 (1980).

Mon+ 71 E.J. Moniz, I. Sick, R.R. Whitney, J.R. Ficenec, R.D. Kephart, and W.P. Trower, Phys. Rev. Lett. 26, 445 (1971).

Mor+ 78 D.J. Morrissey, W.R. Marsh, R.J. Otto, W. Loveland and G.T. Seaborg, Phys. Rev. C18, 1267 (1978).

Mor+ 79 D.J. Morrissey, L.F. Oliviera, J.O. Rasmussen, G.T. Seaborg, Y. Yariv, and Z. Fraenkel, Phys. Rev. Lett. 43, 1139 (1979).

Mor+ 80 D.J. Morrissey, W. Loveland, M. de Saint Simon, and G.T. Seaborg, Phys. Rev. C21, 1783 (1980).

MT 66 J.L. Matthews and W. Turchinetz, LNS Internal Report 110 (unpublished).

Muk 77 N.C. Mukhopadhyay, Phys. Rep. 30C, 1 (1977).

Mur+ 78 J.J. Murphy II, D.M. Skopik, J. Asai, and J. Uegaki, Phys. Rev. C18, 736 (1978).

MV 65 L. Meneghetti and S. Vitale, Nucl. Phys. 61, 316 (1965).

Mye+ 54 H. Myers, A. Odian, P.C. Stein, A. Wattenberg, Phys. Rev. 95, 576 (1954).

Mye 78 W.E. Myers, Nucl. Phys. A296, 177 (1978).

MZ 79 I. Montvay and J. Zimanyi, Nucl. Phys. A316, 490 (1979).

Nag+ 79 S. Nagamiya, L. Anderson, W. Brückner, O. Chamberlain, M.-C. Lemaire, S. Schnetzer, G. Shapiro, H. Steiner, and I. Tanihata, Phys Lett. 81B, 147 (1979).

Nag 80 S. Nagamiya, Nucl. Phys. A335, 517 (1980).

Nag+ 80 S. Nagamiya, M.-C. Lemaire, S. Schnetzer, H. Steiner, and I. Tanihata, Phys. Rev. Lett. 45, 602 (1980).

Nag 81 S. Nagamiya, Proceedings of the 5th High Energy Heavy Ion Study (LBL, 1981) Report No. LBL-12652, p. 141.

Nag+ 81 S. Nagamiya, M.-C. Lemaire, E. Moeller, S. Schnetzer, G. Shapiro, H. Steiner, and I. Tanihata, Phys. Rev. C24, 971 (1981).

Nag 82a S. Nagamiya in Proceedings of the Relativistic Heavy Ion Winter School, (Banff, 1982) [also LBL Report No. 14031].

Nag 82b S. Nagamiya, Phys. Rev. Lett. 49, 1383 (1982).

Nag+ 82 S. Nagamiya, H. Hamagaki, P. Hecking, S. Kadota, R. Lombard, Y. Miake, E. Moeller, S. Schnetzer, H. Steiner, I. Tanihata, S. Bohrmann, and J. Knoll, Phys. Rev. Lett. 48, 1780 (1982).

Nak+ 82 K. Nakai, O.Terasaki, T-A. Shibata, H. En'yo, and I. Arai, Phys. Rev. C25, 1992 (1982).

Nat+ 81 J.B. Natowitz, M.N. Namboodiri, L. Adler, R.P. Schmitt, R.L. Watson, S. Simon, M. Berlanger, and R. Choudhury, Phys. Rev. Lett. 47, 1114 (1981).

NG 83 S. Nagamiya and M. Gyulassy, Advances in Nuclear Physics, J.W. Negele and E. Vogt, editors, (Plenum, New York) in press.

Nix 80 J.R. Nix, Prog. Part. Nucl. Phys. 4, 5 (1980).

Nix+ 82 J.R. Nix, D. Strottman, Y. Yariv, and Z. Fraenkel, Phys. Rev. C25, 2491 (1982).

NS 81 J.R. Nix and D. Strottman, Phys. Rev. C23, 2548 (1981).

Nom+ 78 T. Nomura, H. Utsunomiya, T. Motobayashi, T. Inamura, and Y. Yanokura, Phys. Rev. Lett. 40, 694 (1978).

NY 81 T. Nakai and H. Yokomi, Prog. Theor. Phys. 66, 1328 (1981).

Odi+ 56 A.C. Odian, P.C. Stein, A. Wattenberg, B.T. Feld, and R. Weinstein,

Phys. Rev. 102, 837 (1956).

Ols+ 83 D.L. Olson, B.L. Berman, D.E. Greiner, H.H. Heckman, P.J. Lindstrom, and H.J. Crawford, Phys. Rev. C28, 1602 (1983).

Pal+ 67 H. Palevsky, J.L. Friedes, R.J. Sutter, G.W. Bennett, G.J. Igo, W.D. Simpson, G.C. Phillips, D.M. Corley, N.S. Wall, R.L. Stearns, and B. Gottschalk, Phys. Rev. Lett. 18, 1200 (1967).

Pan+ 83 A.D. Panagiotou, M.W. Curtin, H. Toki, D.K. Scott, and P.J. Siemens, Phys. Rev. Lett. (in press).

Pap+ 75 J. Papp, J. Jarus, L. Schroeder, J. Staples, H. Steiner, A. Wagner, and J. Wiss, Phys. Rev. Lett. 34, 601 (1975).

PBH 71 A.M. Poskanzer, G.W. Butler, and E.K. Hyde, Phys. Rev. C3, 882 (1971).

PDG 70 Particle Data Group, NN and ND Interactions (Above 0.5 GeV/c)--A Compilation, Lawrence Radiation Laboratory, Berkeley, Report UCRL-20000NN (1970).

Pee+ 68 R.W. Peelle, T.A. Love, N.W. Hill, and R.T. Santoro, Phys. Rev. 167, 981 (1968).

Por+ 79a N.T. Porile, D.R. Fortney, S. Pandian, R.A. Johns, T. Kaiser, K. Wielgoz, T.S.K. Chang, N. Sugarman, J.A. Urbon, D.J. Henderson, S.B. Kaufman, and E.P. Steinberg, Phys. Rev. Lett. 43, 918 (1979).

Por+ 79b N.T. Porile, S. Pandian, H. Klonk, C.R. Rudy, and E.P. Steinberg, Phys. Rev. C19, 1832 (1979).

Pos+ 75 A.M. Poskanzer, R.G. Sextro, A.M. Zebelman, H.H. Gutbrod, A. Sandoval, and R. Stock, Phys. Rev. Lett. 35, 1701 (1975).

PS 57 N.T. Porile and N. Sugarman, Phys. Rev. 107, 1410 (1957).

PS 78 P.B. Price and J. Stephenson, Phys. Lett. 78B, 197 (1978).

PS 79 H.J. Pirner and B. Schürmann, Nucl. Phys. A316, 461 (1979).

PSF 77 P.B. Price, J. Stevenson, and K. Frankel, Phys. Rev. Lett. 39, 177 (1977).

PT 64 N.T. Porile and S. Tanaka, Phys. Rev. 135, B122 (1964).

PT 65 N.T. Porile and S. Tanaka, Phys. Rev. 137, B58 (1965).

Rai+ 75 G.M. Raisbeck, P. Boerstling, R. Klapisch,and T.D. Thomas, Phys. Rev. C12, 527 (1975).

Ran 78 J. Randrup, Phys. Lett. 76B, 547 (1978).

Ran 79 J. Randrup, Nucl. Phys. A316, 509 (1979).

RC 75 P.G. Roos and N.S. Chant, Proceedings of the Second International Conference on Clustering Phenomena in Nuclei, College Park, 1975 D.A. Goldberg, J.B. Marion, and S.J. Wallace, editors (ERDA Technical Information Center,Oak Ridge).

Rem 75 E.A. Remler, Ann. Phys. (N.Y.) 95, 455 (1975).

Rem 79 E.A. Remler, Ann. Phys. (N.Y.) 119, 326 (1979).

Rem 81 E.A. Remler, Ann. Phys. (N.Y.) 136, 293 (1981).

Rem 82 E.A. Remler, Phys. Rev. C25, 2974 (1982).

RK 81 J. Randrup and S.E. Koonin, Nucl. Phys. A356, 223 (1981).

RMS 82 G. Röpke, L. Münchow, and H. Schulz, Nucl. Phys. A379, 536 (1982).

RO 73 I. Ribansky and P. Oblozinsky, Phys. Lett. 45B, 318 (1973).

Roo+ 77 P.G. Roos, N.S. Chant, A.A. Cowley, D.A. Goldberg, H.D. Holmgren, and R. Woody III, Phys. Rev. C15, 69 (1977).

Rop+ 83 G. Röpke, M. Schmidt, L. Münchow, and H. Schulz, Nucl. Phys. A399, 587 (1983).

Roy+ 81 G. Roy, L.G. Greeniaus, G.A. Moss, D.A. Hutcheon, R. Liljestrand, R.M. Woloshyn, D.H. Boal, A.W. Stetz, K. Aniol, A. Willis, N. Willis, and R. McCamis, Phys. Rev. C23, 1671 (1981).

RP 75 L.P. Remsburg and D.G. Perry, Phys. Rev. Lett. 35, 361 (1975).

RS 75 E.A. Remler and A.P. Sathe, Ann. Phys. (N.Y.) 91, 295 (1975).

RS 78 E.A. Remler and A.P. Sathe, Phys. Rev. C18, 2293 (1978).

Sak+ 80 H. Sakai, K. Hosono, N. Matsuoka, S. Nagamachi, K. Okada, K. Maeda, H. Shimizu, Phys. Rev. Lett. 44, 1193 (1980).

San+ 80a A. Sandoval, R. Stock, H.E. Stelzer, R.E. Renfordt, J.W. Harris, J.P. Brannigan, J.V. Geaga, L.J. Rosenberg, L.S. Schroeder, and K.L. Wolf, Phys. Rev. Lett. 45, 874 (1980).

San+ 80b A. Sandoval, H.H. Gutbrod, W.G. Meyer, R. Stock, Ch. Lukner, A.M. Poskanzer, J. Gosset, J-C. Jourdain, C.H. King, G. King, Nguyen Van Sen, G.D. Westfall, and K.L. Wolf, Phys. Rev. C21, 1321 (1980).

SB 77 I.A. Schmidt and R. Blankenbecler, Phys. Rev. D15, 3321 (1977).

SBM 77 W. Scobel, M. Blann, and A. Mignerey, Nucl. Phys. A287, 301 (1977).

SC 80 B. Schürmann and M. Chemtob, Z. Physik A294, 371 (1980).

Sch 51 L.I. Schiff, Phys. Rev. 83, 252 (1951).

Sch+ 74 W.O. Schröder, U. Jahnke, K. H. Lindenberger, G. Röschert, R. Engfer and H.K. Walter, Z. Phys. 268, 57 (1974).

Sch 79 B. Schürmann, Phys. Rev. C20, 1607 (1979).

Sch+ 79a W. Schimmerling, J.W. Kast, D. Ortendahl, R. Madey, R.A. Cecil, B.D. Anderson, and A.R. Baldwin, Phys. Rev. Lett. 43, 1985 (1979).

Sch+ 79b T.C. Schweizer, R.R. Doering, S.T. Thornton, L.C. Dennis, K.R. Cordell, and R.L. Parks, Phys. Rev. C19, 1408 (1979).

Sch+ 82 S. Schnetzer, M.-C. Lemaire, R. Lombard, E. Moeller, S. Nagamiya, G. Shapiro, H. Steiner, and I. Tanihata, Phys. Rev. Lett. 49, 989 (1982).

Sch+ 83 H. Schulz, G. Ropke, K.K. Gudima and V.D. Toneev, Phys. Lett. 124B, 458 (1983).

Sco 80 D.K. Scott, Prog. Part. Nucl. Phys. 4, 5 (1980).

Sco 81 D.K. Scott, Nucl. Phys. A354, 375c (1981).

SCW 56 N. Sugarman, M. Campos, and K. Wielgoz, Phys. Rev. 101, 388 (1956).

SE 73 R.M. Sundelin and R.M. Edelstein, Phys Rev. C7, 1037 (1973).

Seg+ 82 R.E. Segal, T. Chen, L.L. Rutledge, Jr., J.V. Maher, J. Wiggins, P.P. Singh, and P.T. Debevec, Phys. Rev. C26, 2424 (1982).

Ser 47 R. Serber, Phys. Rev. 72, 1114 (1947).

SG 66 L.W. Swenson and C.R. Gruhn, Phys. Rev. 146, 886 (1966).

SGB 81 H. Stöcker, M. Gyulassy, and J. Boguta, Phys. Lett. 103B, 269 (1981).

Shi+ 78 T. Shibata, H. Ejiri, J. Chiba,S. Nagamiya, K. Nakai, A. Anholt, H. Bowman, J.G. Ingersoll, E.A. Rauscher, and J.O. Rasmussen, Nucl. Phys. A308, 513 (1978).

Shi+ 83 T.A. Shibata, K. Nakai, H. En'yo, S. Sasaki, M. Sekimoto, I. Arai, K. Nakayama, K. Ichimaru, H. Nakamura-Yokota, and R. Chiba, Nucl. Phys. A408, 525 (1983).

Sim+ 70 W.D. Simpson, J.L. Friedes, H. Palevsky, R.J. Sutter, G.W. Bennett, B. Gottschalk, G. Igo, R.L. Stearns, N.S. Wall, D.M. Corley, G.C. Phillips, Nucl. Phys. A140, 201 (1970).

Sin 74 P. Singer, Springer Tracts Mod. Phys. 71, 39 (1974).

SK 79 P.J. Siemens and J.I. Kapusta, Phys. Rev. Lett. 43, 1486 (1979).

SM 82 B. Schürmann and N. Mankoc-Borstnik, Phys. Rev. C26, 519 (1982).

SMA 79 P. Singer, N.C. Mukhopadhyay, and R.D. Amado, Phys. Rev. Lett. 42, 162 (1979).

SMG 79 H. Stöcker, J.A. Maruhn, and W. Greiner, Z. Physik A293, 173 (1979).

SMG 80 H. Stöcker, J.A. Maruhn, and W. Greiner, Phys. Rev. Lett. 44, 725 (1980).

Smi+ 67 I.L. Smith, J. Garvey, J.G. Rutherglen, and G.R. Brookes, Nucl.

Phys. B1, 483 (1967).

SN 80 A.J. Sierk and J.R. Nix, Phys. Rev. C22, 1920 (1980).

SOG 81 H. Stöcker, A.A. Ogloblin, and W. Greiner, Z. Phys. A303, 259 (1981).

Sob+ 75 M. Sobel, P.J Siemens, J.P. Bondorf, and H.A. Bethe, Nucl. Phys. A251, 502 (1975).

SP 76 O. Scheidemann and N.T. Porile, Phys. Rev. C14, 1534 (1976).

SPF 77 J. Stevenson, P.B. Price, and K. Frankel, Phys. Rev. Lett. 38, 1125 (1977).

SR 79 P.J. Siemens and J.O. Rasmussen, Phys. Rev. Lett. 42, 880 (1979).

SS 75 M.M. Sternheim and R.R. Silbar, Phys. Rev. Lett. 34, 824 (1975).

ST 56 K. Strauch and F. Titus, Phys. Rev. 104, 191 (1956).

Sta 79 D. Stauffer, Phys. Rep. 54, 1 (1979).

Ste+ 60 P.C. Stein, A.C. Odian, A. Wattenberg, and R. Weinstein, Phys. Rev. 119, 348 (1960).

Ste 78 J.D. Stevenson, Phys. Rev. Lett. 41, 1702 (1978).

Ste 80 J.D. Stevenson, Phys. Rev. Lett. 45, 1773 (1980).

Sto+ 80a R. Stock, H.H. Gutbrod, W.G. Meyer, A.M. Poskanzer, A. Sandoval, J. J. Gosset, C.H. King, G. King, Ch. Lukner, Nguyen Van Sen, G.D. Westfall, and K.L. Wolf, Phys. Rev. Lett. 44, 1243 (1980).

Sto+ 80b H. Stöcker, J. Hofmann, J.A. Maruhn, and W. Greiner, Prog. Part. Nucl. Phys. 4, 133 (1980).

Sto+ 80c H. Stöcker, R.Y. Cusson, J.A. Maruhn, and W. Greiner, Z. Phys. A294, 125 (1980).

Sto 81 H. Stöcker, Lawrence Berkeley Laboratory Report 12302 (1981).

Sto+ 81 H. Stöcker, C. Riedel, Y. Yariv, L.P. Csernai, G. Buchwald, G. Graebner, J. A. Maruhn, W. Greiner, K. Frankel, M. Gyulassy,

B. Schürmann, G. Westfall, J.D. Stevenson, J.R. Nix, and D. Strottman, Phys. Rev. Lett. 47, 1807 (1981).

Sto+ 82 H. Stöcker, L.P. Csernai, G. Graebner, G. Buchwald, H. Kruse, R.Y. Cusson, J.A. Maruhn, and W. Greiner, Phys. Rev. C25, 1873 (1982).

Sto+ 83 H. Stöcker, G. Buchwald, G. Graebner, P. Subramanian, J.A. Maruhn, W. Greiner, B.V. Jacak, and G.D. Westfall, Nucl. Phys. A400, 63c (1983).

Sub+ 81 P.R. Subramanian, L.P. Csernai, H. Stöcker, J.A. Maruhn, W. Greiner, and H. Kruse, J. Phys. G7, L241 (1981).

Sug+ 66 N. Sugarman, H. Münzel, J.A. Panontin, K. Wielgoz, M.V. Ramaniah, G. Lange, E. Lopez-Menchero, Phys. Rev. 143, 952 (1966).

Sul+ 82 J.P. Sullivan, J.A. Bistirlich, H.R. Bowman, R. Bossingham, T. Buttke, K.M. Crowe, K.A. Frankel, C.J. Martoff, J. Miller, D.L. Murphy, J.O. Rasmussen, W.A. Zajc, O. Hashimoto, M. Koike, J. Peter, W. Benenson, G.M. Crawley, E. Kashy, and J.A. Nolen, Jr., Phys. Rev. C25, 1499 (1982).

Sut+ 67 R.J. Sutter, J.L. Friedes, H. Palevsky, G.W. Bennett, G.J. Igo, W.D. Simpson, G.C. Phillips, D.M. Corley, N.S. Wall, and R.L. Stearns, Phys. Rev. Lett. 19, 1189 (1967).

SW 81 N. Stelte and R. Weiner, Phys. Lett. 103B, 275 (1981).

SWW 82 N. Stelte, M. Weström, and R.M. Weiner, Nucl. Phys. A384, 97 (1982).

SY 81 H. Sato and K. Yazaki, Phys. Lett. 98B, 153 (1981).

SZ 63 A. Schwarzschild and C. Zupancic, Phys. Rev. 129, 854 (1963).

Tam+ 77 T. Tamura, T. Udagawa, D.H. Feng, and K.K. Kan, Phys. Lett. 66B, 109 (1977).

Tan+ 80 I. Tanihata, M.-C. Lemaire, S. Nagamiya, and S. Schnetzer, Phys. Lett. 97B, 363 (1980).

Tan+ 81a I. Tanihata, S. Nagamiya, S. Schnetzer, and H. Steiner, Phys. Lett. 100B, 121 (1981).

Tan+ 81b I. Tanihata, Y. Miake, H. Hamagaki, S. Kadota, Y. Shida, R. Lombard, E. Moeller, S. Nagamiya, S. Schnetzer, and H. Steiner, Proceedings of the 5th High Energy Heavy Ion Study (Lawrence Berkeley Lab. 1981) Report No. LBL-12652, p. 365.

Tan 83 I. Tanihata, University of Tokyo Report INS-Rep-482.

TB 78 S.F. Tsai and G.F. Bertsch, Phys. Lett. 73B, 247 (1978).

Tho+ 79 S.T. Thornton, K.R. Cordell, L.C. Dennis, R.R. Doering, and T.C. Schweizer, Phys. Rev. C19, 913 (1979).

TLU 81 T. Tamura, H. Lenske, and T. Udagawa, Phys. Rev. C23, 2769 (1981).

TW 80 H.H.K. Tang and C.Y. Wong, Phys. Rev. C21, 1846 (1980).

Ube 65 H. Uberall, Phys. Rev. 139, B1239 (1965).

Urb+ 80 J.A. Urbon, S.B. Kaufman, D.J. Henderson, and E.P. Steinberg, Phys. Rev. C21, 1048 (1980).

Var 78 J.P. Vary, Phys. Rev. Lett. 40, 294 (1978).

VKR 70 A.O. Vaisenberg, E.D. Kolganove, and N.V. Rabin, Yad. Fiz. 11, 830 (1970) [Sov. J. Nucl. Phys. 11, 464 (1970)].

VL 73 H.J. von Eyss and G. Lührs, Z. Phys. 262, 393 (1973).

Vog 68 E. Vogt, Adv. Nucl. Phys. 1, 261 (1968).

Vol+ 75 E.N. Volnin, G.M. Amalsky, D.M. Seleverstov, N.N. Smirnov, A.A. Vorobyov, and Yu. P. Yakavlev, Phys. Lett. 55B, 409 (1975).

VTB 80 J.W. Van Orden, W. Treux, and M.K. Banerjee, Phys. Rev. C21, 2628 (1980).

VV 69 G.L. Vysotskii and A.V. Vysotskaya, Yad. Fiz. 9, 1177 (1969) [Sov. J. Nucl. Phys. 9, 689 (1969)].

Wal+ 79 N.S. Wall, J.R. Wu, C.C. Chang, and H.D. Holmgren, Phys. Rev. C20,

1079 (1979).

War+ 83 A.I. Warwick, H.H. Weiman, H.H. Gutbrod, M.R. Maier, J. Peter, H.G. Ritter, H. Stelzer, F. Weik, M. Freedman, D.J. Henderson, S.B. Kaufman, E.P. Steinberg, and B.D. Wilkins, Phys. Rev. C27, 1083 (1983).

Wat+ 56 A. Wattenberg, A.C. Odian, P.C. Stein, H. Wilson, and R. Weinstein, Phys. Rev. 104, 1710 (1956).

WBG 67 J.W. Wachter, W.R. Burrus, and W.A. Gibson, Phys. Rev. 161, 971 (1967).

WC 76 J.R. Wu and C.C. Chang, Phys. Lett. 60B, 423 (1976).

WC 77 J.R. Wu and C.C. Chang, Phys. Rev. C16, 1812 (1977).

WC 78 J.R. Wu and C.C. Chang, Phys. Rev. C17, 1540 (1978).

WCH 79a J.R. Wu, C.C. Chang, and H.D. Holmgren, Phys. Rev. C19, 370 (1979).

WCH 79b J.R. Wu, C.C. Chang, and H.D. Holmgren, Phys. Rev. C19, 659 (1979).

WCH 79c J.R. Wu, C.C. Chang, and H.D. Holmgren, Phys. Rev. C19, 698 (1979).

Wei 76 R.M. Weiner, Phys. Rev. D13, 1363 (1976).

Wei 78 R. Weiner, Proc. of the Intl. Workshop on Reaction Models for Continuous Spectra of Light Particles, J. Ernst, editor, Bad Honnef/Bonn (1978).

Wes+ 76 G.D. Westfall, J. Gosset, P.J. Johanson, A.M. Poskanzer, W.G. Meyer, H.H. Gutbrod, A. Sandoval, and R. Stock, Phys. Rev. Lett. 37, 1202 (1976).

Wes+ 78 G.D. Westfall, R.G. Sextro, A.M. Poskanzer, A.M. Zebelman, G.W. Butler, and E.K. Hyde, Phys. Rev. C17, 1368 (1978).

Wes+ 82 G.D. Westfall, B.V. Jacak, N. Anantaraman, M.V. Curtin, G.M. Crawley, C.K. Gelbke, B. Hasselquist, W.G. Lynch, D.K. Scott, B.M. Tsang, M.J. Murphy, T.J.M. Symons, R. Legrain, and T.J. Majors,

Phys. Lett. 116B, 118 (1982).

Wes+ 83 G.D. Westfall, Z.M. Koenig, B.V. Jacak, L.H. Harwood, G.M. Crawley, M.W. Curtin, C.K. Gelbke, B. Hasselquist, W.G. Lynch, A.D. Panagiotou, D.K. Scott, H. Stöcker, and M.B. Tsang, Michigan State University Report MSUCL-428.

WGB 72 J.W. Wachter, W.A. Gibson, and W.R. Burrus, Phys. Rev. C6, 1496 (1972).

Whi+ 58 C. Whitehead, W.R. McMurray, M.J. Aitken, N. Middlemas, and C.H. Collie, Phys. Rev. 110, 941 (1958).

Whi+ 74 R.R. Whitney, I. Sick, J.R. Ficenec, R.D. Kephart, and W.P. Trower, Phys. Rev. C9, 2230 (1974).

Wil+ 79 B.D. Wilkins, S.B. Kaufman, E.P. Steinberg, J.A. Urbon, and D.J. Henderson, Phys. Rev. Lett. 43, 1080 (1979).

Win 80a L. Winsberg, Phys. Rev. C22, 2116 (1980).

Win 80b L. Winsberg, Phys. Rev. C22, 2123 (1980).

Win+ 80 L. Winsberg, E.P. Steinberg, D. Henderson, and A. Chrapkowski, Phys. Rev. C22, 2108 (1980).

WM 53 J.W. Weil and B.D. McDaniel, Phys. Rev. 92, 391 (1953).

WM 77 H.J. Weber and L.D. Miller, Phys. Rev. C16, 726 (1977).

WMW 75 C.Y. Wong, J.A. Maruhn, and T.A. Welton, Nucl. Phys. A253, 469 (1975).

Wol 78 R.M. Woloshyn, Nucl. Phys. A306, 333 (1978).

Wol+ 79 K.L. Wolf, H.H. Gutbrod, W.G. Meyer, A.M. Poskanzer, A. Sandoval, R. Stock, J. Gosset, C.H. King, G. King, N.V. Sen, and G.D. Westfall, Phys. Rev. Lett. 42, 1448 (1979).

Wol+ 82 K.L. Wolf, H.H. Gutbrod, W.G. Meyer, A.M. Poskanzer, A. Sandoval, R. Stock, J. Gosset, J-C. Jourdain, C.H. King, G. King, N.V. Sen,

and G.D. Westfall, Phys. Rev. C26, 2572 (1982).

WR 66 N.S. Wall and P.G. Roos, Phys. Rev. 150, 811 (1966).

Wu 80 J.R. Wu, Phys. Lett. 91B, 169 (1980).

WW 75 R. Weiner and M. Weström, Phys. Rev. Lett. 34, 1523 (1975).

WW 77 R. Weiner and M. Weström, Nucl. Phys. A286, 282 (1977).

WYC 78 L. Wilets, Y. Yariv, and R. Chestnut, Nucl. Phys. A301, 359 (1978).

Wyt+ 78 A. Wyttenbach, P. Baertschi, S. Bajo, J. Hadermann, K. Junker, S. Katcoff, E.A. Hermes, and H.S. Pruys, Nucl. Phys. A294, 278 (1978).

YF 79a Y. Yariv and Z. Fraenkel, Phys. Rev. C20, 2227 (1979).

YF 79b T. Yukawa and S. Furui, Phys. Rev. C20, 2316 (1979).

YF 81 Y. Yariv and Z. Fraenkel, Phys. Rev. C24, 488 (1981).

YK 78 F.B. Yano and S.E. Koonin, Phys. Lett. 78B, 556 (1978).

Zaj+ 81 W.A. Zajc, J.A. Bistirlich, R.J. Bossingham, H.R. Bowman, C.W. Clawson, K.M. Crowe, K.A. Frankel, O. Hashimoto, J.G. Ingersoll, M. Koike, J.P. Kurck, C.J. Martoff, W.J. Macdonald, J.P. Miller, D. Murphy, J.O. Rasmussen, J.P. Sullivan, P. Truol, and E. Yoo, Proceedings of the 5th High Energy Heavy Ion Study, Lawrence Berkeley Laboratory Report LBL-12652 (1981).

Zar+ 81 Z. Zarbakhsh, A.L. Sagle, F. Brochard, T.A. Mulera, V. Perez-Mendez, I. Tanihata, J.B. Carroll, K.S. Ganezer, G. Igo, J. Oostens, D. Woodard, and S. Sutter, Phys. Rev. Lett. 46, 1268 (1981).

ZE 78 J.G. Zabolitzky and W. Ey, Phys. Lett. 76B, 527 (1978).

Zeb+ 75 A.M. Zebelman, A.M. Poskanzer, J.D. Bowman, R.G. Sextro, and V.E. Viola, Jr., Phys. Rev. C11, 1280 (1975).

Table I. Projectile energy dependence K_p^δ of the inclusive cross section for an ejectile observed at 90° and 50 MeV in the proton induced reactions, and 50 MeV per nucleon in the neon reactions. From Boa 82a.

Reaction	δ(experiment)	δ(snowball)	δ(coalescence)
(p,p')	0.8	input	input
(p,^{4}He)	1.6	0.8	3.2
(p,^{6}Li)	2.2	0.8	4.8
(Ne,p)	0.6	n.a.	input
(Ne,d)	1.3	n.a.	1.2
(Ne,t)	1.6	n.a.	1.8

Table II. Coalescence and thermal model parameters determined in Lem+ 77

System	Energy(MeV/A)	Fragment	p_0 (MeV/c)	$\tilde{p}_0$ (MeV/c)	R(fm)
C + C	800	d	304	167	2.9
		t, ^{3}He	280	204	2.6
Ne + NaF	400	d	259	142	3.4
		t, ^{3}He	223	162	3.3
	800	d	259	142	3.4
		t, ^{3}He	260	189	2.8
	2100	d	259	142	3.4
		t, ^{3}He	212	154	3.5
Ar + KCl†	800	d	248	137	3.5
		t, ^{3}He	246	179	3.0

†Average values taken

Figure Captions

Fig. 1 - Estimated non-evaporative (pre-equilibrium) component of integrated fragment production cross sections for Ag(p,fragment)X at K_p=480 MeV. Data are tabulated in GKJ 83. The percentages quoted here are an average over all isobars measured.

Fig. 2 - Kinematical domain for the momentum of a nucleon produced in an elastic nucleon-nucleon collision (dashed curve) and in the collision of a nucleon with a very heavy nucleus (solid curve). The calculation used an incident energy of 800 MeV, and is plotted in the lab frame.

Fig. 3 - Measured values of the (p,p') reaction at 800 MeV at forward angles showing quasi-elastic scattering. The quasi-elastic scattering momenta are marked with an arrow. Data are from Tan+ 81.

Fig. 4 - Behavior of the parameter b in Eq. (1) as a function of bombarding energy in the lab frame. Data are from PDG 70.

Fig. 5 - Direct interaction model for nucleon emission.

Fig. 6 - Analyzing power measured for the Ni(p,p')X reaction shown as a function of the detected proton kinetic energy for several angles. The incident proton kinetic energy is 500 MeV. Data are from Roy+ 81.

Fig. 7 - Some contributors to energetic nucleon emission: (a) single scat-

tering from a high momentum off-shell nucleon, (b) single scattering from a transient cluster of nucleons, and (c) multiple scattering.

Fig. 8 - Calculation of the high momentum components of the single particle momentum distribution using the Hamada-Johston potential (dot-dash curve) and de Tourreil-Sprung super soft core B potential (dashed curve). The results without correlations (dotted curve) are shown for comparison. From ZE 78.

Fig. 9 - Comparison of direct knockout model predictions with $^{12}C(\gamma,p)X$ data for an end point energy (E_o) of 1.05 GeV. From BW 81.

Fig. 10 - Definition of variables used in multiple scattering calculation.

Fig. 11 - Momentum vectors in the direct knockout model.

Fig. 12 - Contours of constant mean differential multiplicity (in units of coincident protons/MeV·sr·1000 trigger protons) associated with fixed coplanar trigger protons observed at 90° on the opposite side of the beam. The contours are shown on a polar grid in energy and emission angle of the coincident proton. The dashed outline is either the limits of the experimental measurements or the kinematic limit. The arrow indicates the QTBS angle associated with the trigger proton energy of K_q=70 MeV. Kinetic energies are denoted by E in this figure. From Gre+ 83.

Fig. 13 - Comparison of nonrelativistic phase space with the differential multiplicity for the Be(p,2p) reaction shown as a function of forward proton kinetic energy K_f. The trigger proton energy and angle, as well as the forward proton angle, were held fixed at 110 MeV, 90° and 30° respectively. The theoretical curves were normalized to 9×10^{-3} at K_f=75 MeV. From BR 84.

Fig. 14 - Similar to Fig. 13, only now the forward angle is varied, while the forward energy is integrated over a finite range. Two trigger energies, 70 MeV (circles) and 110 MeV (triangles) are shown. Kinetic energy is denoted by E in this figure. From Gre+ 83.

Fig. 15 - Comparison of the direct knockout model prediction for the differential multiplicity measured in the Be(p,2p)X experiment at 300 MeV incident energy. From Gre+ 83.

Fig. 16 - Backward proton spectra for a variety of forward angle proton triggers. From Tan+ 81b.

Fig. 17 - Trend of the inclusive cross section per target nucleon for Li, Be and Ta targets. Data used to produce the curves are taken from Fra+ 78b.

Fig. 18 - Target mass dependence of (a) the single proton quasi-elastic scattering cross section and (b) the two-proton quasi-elastic scattering cross section. Curves shown are the result of calculations like Eq. (13). From Tan+ 81a.

Fig. 19 - Estimated nucleon mean free path in the nucleus from KK 68. The kinetic energy of the nucleon is measured from the bottom of the Fermi sea.

Fig. 20 - Schematic representation of the energy spectrum of particles emitted from a thermally equilibrated source (a) in the source's rest frame and (b) in the lab frame with the source moving in the forward direction.

Fig. 21 - Contours of constant Lorentz invariant cross section $E \frac{d^3\sigma}{d^3p}$ (in units of mb/sr-GeV^2) for the U(p,p')X reaction at K_p=1.041 GeV. From BR 84 with data from San+ 80b.

Fig. 22 - Source rapidities as determined by single source model analysis of proton emission in heavy ion reactions (in the target rapidity region) and proton induced reactions. From BR 84 (Heavy ion rapidities from Jac 83).

Fig. 23 - Source temperatures determined as in Fig. 22. From BR 84.

Fig. 24 - Source sizes estimated by analysis of the single source model results. See text for details of calculations. From BR 84.

Fig. 25 - Contours of constant k_{min} (labels on curves are in MeV/c) for an incident proton of kinetic energy equal to 500 MeV on a mass 100 target. From Boa 84.

Fig. 26 - Contribution of three collisions in a knockout model to $\Sigma \exp(-k_{min}/k_o)$ assuming an incident proton with 500 MeV in energy loses one-third of this energy per collision. From Boa 84.

Fig. 27 - Ratios of (n,n')/(p,p'), (n,p)/(p,p') and (p,n)/(p,p') cross sections predicted by the direct knockout model. The calculations were performed at an incident proton energy of 400 MeV (dashed curve) and 1 GeV (solid curve). From Boa 82b.

Fig. 28 - Kinematic labels for a μ^- capture in the nucleus.

Fig. 29 - Estimated reaction rates for n+n (pp and pn elastic scattering) and n+p (pn charge exchange) reactions. From Boa 84.

Fig. 30 - Estimated time evolution of the proton to neutron ratio for $\lambda_{ex}=(10^{-23}\ \text{sec})^{-1}$. From Boa 84.

Fig. 31 - Estimated charge exchange rates for heavy ion induced and proton induced reactions at the same bombarding energy per nucleon K_i. From Boa 84.

Fig. 32 - (a) Estimated rate of cooling of the central region of a hot spot from the diffusion equation approach. The radius of the gaussian describing the hot spot was chosen to be 3 fm, and the calculations were performed at normal nuclear matter density. (b) Central temperature divided by the rate of cooling shown in (a).

Fig. 33 - The trajectories T(ρ) of the hydrodynamical compression and expansion are shown for K_{lab}=0.2, 0.4 and 0.8 AGeV. The shaded areas indicate the temperature increase due to viscosity. Calculations are shown for two different equations of state: ρ (solid curve) and ρ^2 (dashed curve). From Sto 81.

Fig. 34 - Comparison of cascade and fluid dynamical calculations of inclusive proton spectra in central collisions of Ne+U at 393 AMeV. From Sto+ 81.

Fig. 35 - Behavior of the (p,p') differential cross section per target nucleon shown as a function bombarding energy. From Boa 82b.

Fig. 36 - Estimated mean fraction of energy lost per NN collision for elastic scattering. From BR 84.

Fig. 37 - Behavior of the two proton correlation function for r_o= 4 fm and τ=0. The momentum difference is $\Delta p \equiv (\vec{p}_1 - \vec{p}_2)/2$.

Fig. 38 - Two proton correlation function observed in 400 MeV $^{16}O+^{197}Au$ collisions. The theoretical calculations are as in the previous figure with τ=0. From Lyn+ 83.

Fig. 39 - Target rapidity fragments from several nuclear reactions. The histograms represent fits to the data found with a quantum statistical calculation described in Sec. 4.2. From JSW 83.

Fig. 40 - Example of the differential cross section in fragment emission. The solid curves are a cluster knockout model calculation which fit data from 20° to 160° simultaneously. From Boa+ 81.

Fig. 41 - Possible reaction mechanisms for fragment formation in (a) low and (b) high multiplicity reactions.

Fig. 42 - Logarithmic plot of differential cross sections from which momentum space volume is extracted. From Boa+ 81.

Fig. 43 - Target nucleon reduction factor F compared to G for uranium, shown as a function of target mass. From BS 82.

Fig. 44 - Projectile energy dependence of the inclusive cross section at fixed energy and angle for several reactions. From Boa 82b.

Fig. 45 - Several contributing reaction paths for alpha production. From Boa 82a.

Fig. 46 - Ratio of differential cross sections of alpha particle and proton induced reactions at the same energy per nucleon on a uranium target. From Boa 82b, with data from San+ 80b.

Fig. 47 - Energy spectra of light particles in reactions of 310 MeV ^{16}O on ^{197}Au. The open squares are the spectra predicted by the coalescence power law. From Awe+ 82.

Fig. 48 - Rapidity plots of constant invariant cross section for fragment emission in the p+Ag reaction at 480 MeV. From GKJ 83.

Fig. 49 - Variation of apparent source velocity v_s wih radial velocity v_r of the observed fragment in the source rest frame. From GKJ 83.

Fig. 50 - Ratio of differential cross sections for alpha production in proton and electron induced reactions. From BW 81.

Fig. 51 - Comparison of the average values of the differential mean multiplicities $\langle \frac{d^2m}{d\Omega dE} \rangle$ in the (p,pd) reaction over two selected summed energy intervals as a function of the forward proton angle θ_f for two deuteron momenta q. Only statistical errors are shown. The two energy intervals selected are the uppermost 25 MeV kinematically allowed (circles) and the 50 MeV region immediately below (triangles). From Hel+ 83.

Fig. 52 - Forward proton angles θ_m corresponding to maximal differential multiplicities plotted as a function of the wide angle ejectile momentum q. Angles for minimal residual system recoil momenta (QTBS angles) are shown for the two extreme angles θ_q subtended by the telescope centered at 90°. The points and uncertainties were extracted using a 5 parameter fit which assumes that the angular distributions are symmetric. From Hel+ 83.

Fig. 53 - Estimated forward proton multiplicity as a function of trigger momentum for wide angle deuteron triggers. The curve represents

the calculation given in the text for the pickup model contribution shown in Fig. 54. Data from Hel+ 83.

Fig. 54 - Some possible contributors to deuteron formation in proton induced reactions.

Fig. 55 - Spectra of protons observed in coincidence with 20 to 40 MeV deutrons at 90° in the Ar+Au reaction at 100 AMeV. The proton angle θ_p is positive on the opposite side of the beam from the deuteron trigger. From Cra+ 84.

Fig. 56 - Total isobaric cross sections observed in the bombardment of Ag with 480 MeV protons. The curve is a least squares power law fit. From GKJ 83.

Fig. 57 - Angle averaged element cross sections for ^{12}C induced reactions on Au at K=15 and 30 A MeV. The histograms show the result of the statistical emission calculation described in the text. From Chi+ 83.

Fig. 58 - Plots of contours of Lorentz invariant cross section as a function of $q_\perp/m$ and g for several carbon isotopes observed in the p+Ag reaction at 480 MeV. From GKJ 83.

Fig. 59 - Variation of apparent temperature with fragment mass. Data from GKJ 83.

Fig. 60 - Variation of apparent temperature with the reciprocal of the fragment mass. Data from GKJ 83.

Fig. 61 - Temperatures obtained from moving source fits to the fragment energy spectra, as a function of the fragment mass. Two points for a single mass are shown where two fragments of that mass were observed. From Jac+ 83.

Fig. 62 - Yields of intermediate rapidity fragments from 137 A MeV Ar+Au (Jac+ 83) and 393 A MeV Ne+U (Gos+ 77). The solid lines represent fits using a quantum statistical model as described in the text where fragments with $1 \leq A_F \leq 4$ are fitted in (a) and (b) while only fragments with $1 \leq A_F \leq 3$ are used in (c). From JSW 83.

Fig. 63 - Summary of entropies extracted from various projectile-target-ejectile combinations. The curves labelled 1.0 to 3.0 are the results of an entropy calculation described n the text, the numbers being the multiple of ρ_o taken for the density. From JSW 83.

Fig. 64 - Schematic representation of the time evolution of a system initially composed only of nucleons. From Boa 83a.

Fig. 65 - Fragment abundances found from the solution of rate equations with $t=4 \times 10^{-23}$ sec. The data are from the p+Kr reaction at 80-350 GeV (Hir+ 82). From Boa 83a.

Fig. 66 - Square well form assumed for the NN potential energy in estimating critical point of the nuclear equation of state. From Boa 83c.

Fig. 67 - Van der Waal's equation of state for nuclear matter.

Fig. 68 - Schematic phase diagram for nuclear matter. (After GKM 83)

Fig. 69. Ratio of probabilities for a 40 nucleon system being in the states B and C compared to the thermodynamically favored states A. The inset shows the state labels in the Maxwell construction in a liquid-gas equation of state. From Boa 83b.

Fig. 70 - (a) Temperature dependence of the exponent τ as given in Pan+ 83. See text for an explanation of the labels.
(b) Estimated dependence of τ on coulomb barrier tunnelling is given by the curve through the data. From Boa 83b.

Fig. 71 - Comparison of $d^2\sigma/dEd\Omega$ observed in the Ag(p,F)X reaction at $\theta_F=90°$ for F=^{7}Li and ^{7}Be. The data are taken from GKJ 83.

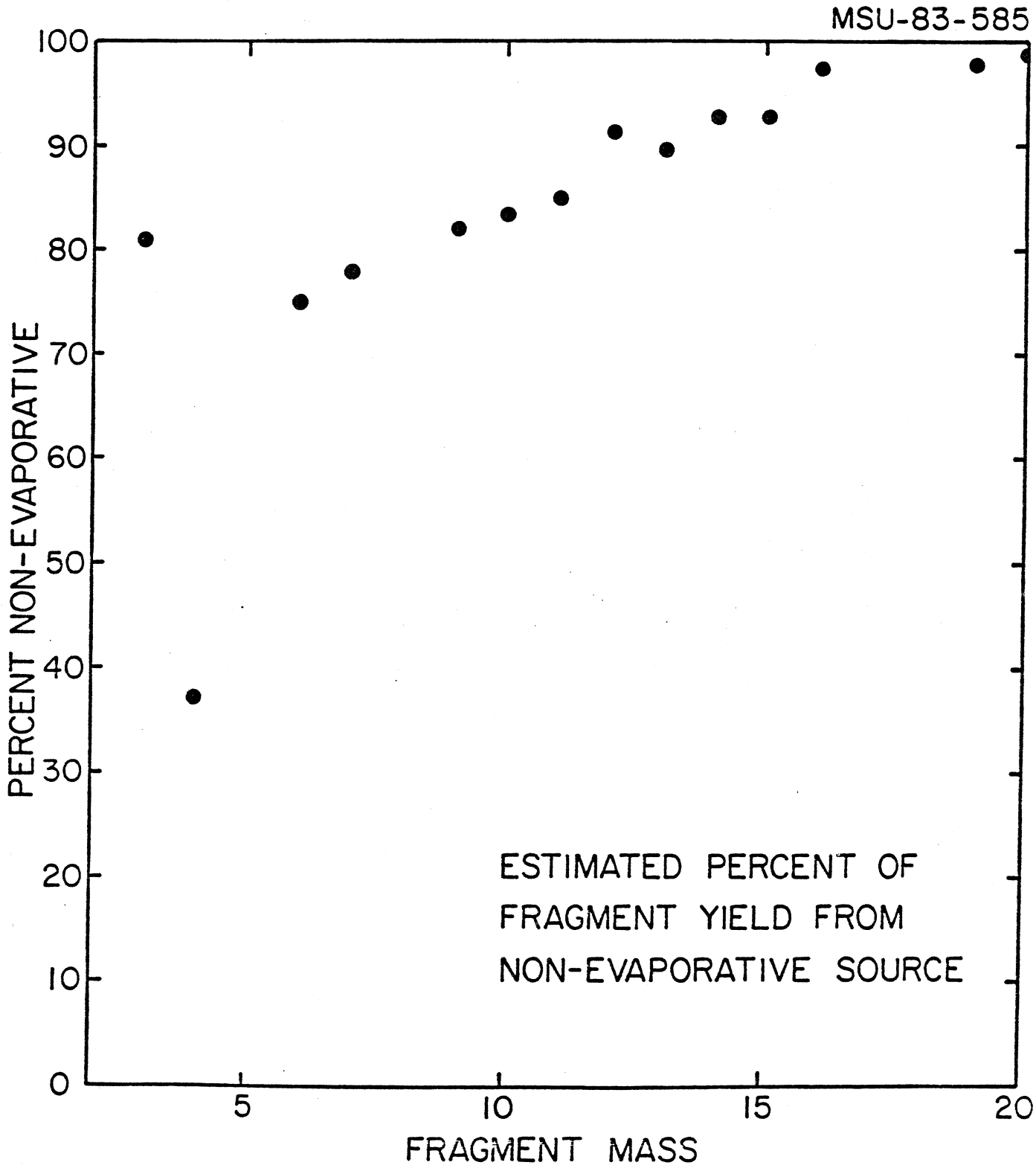
MSU-83-585
100
90
80
70
60
50
40
30
20
10
0
PERCENT NON-EVAPORATIVE
5
10
15
20
FRAGMENT MASS
ESTIMATED PERCENT OF
FRAGMENT YIELD FROM
NON-EVAPORATIVE SOURCE

Figure 1

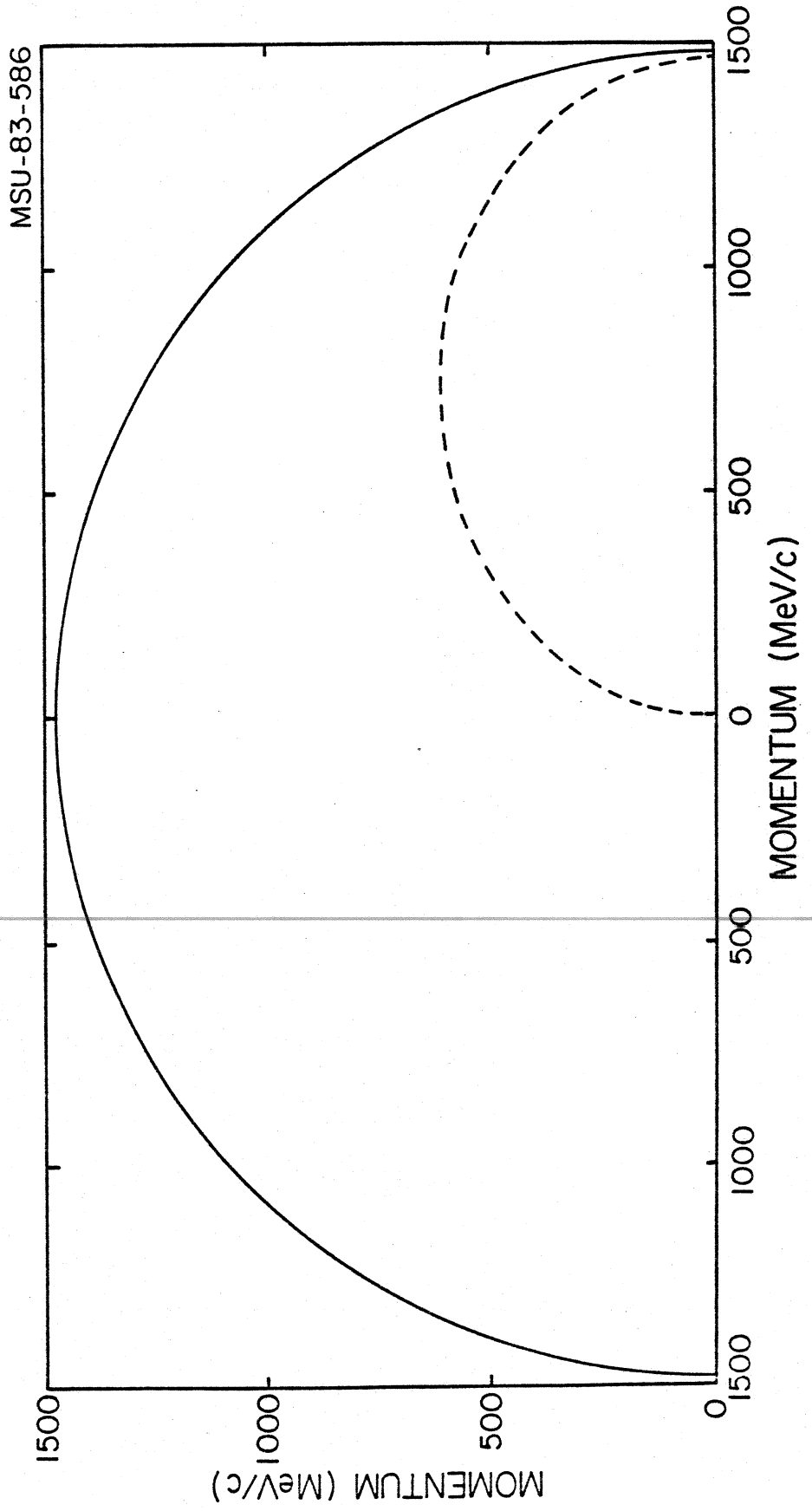
MSU-83-586
MOMENTUM (MeV/c)
0
500
1000
1500
MOMENTUM (MeV/c)
1500
1000
500
0

Figure 2

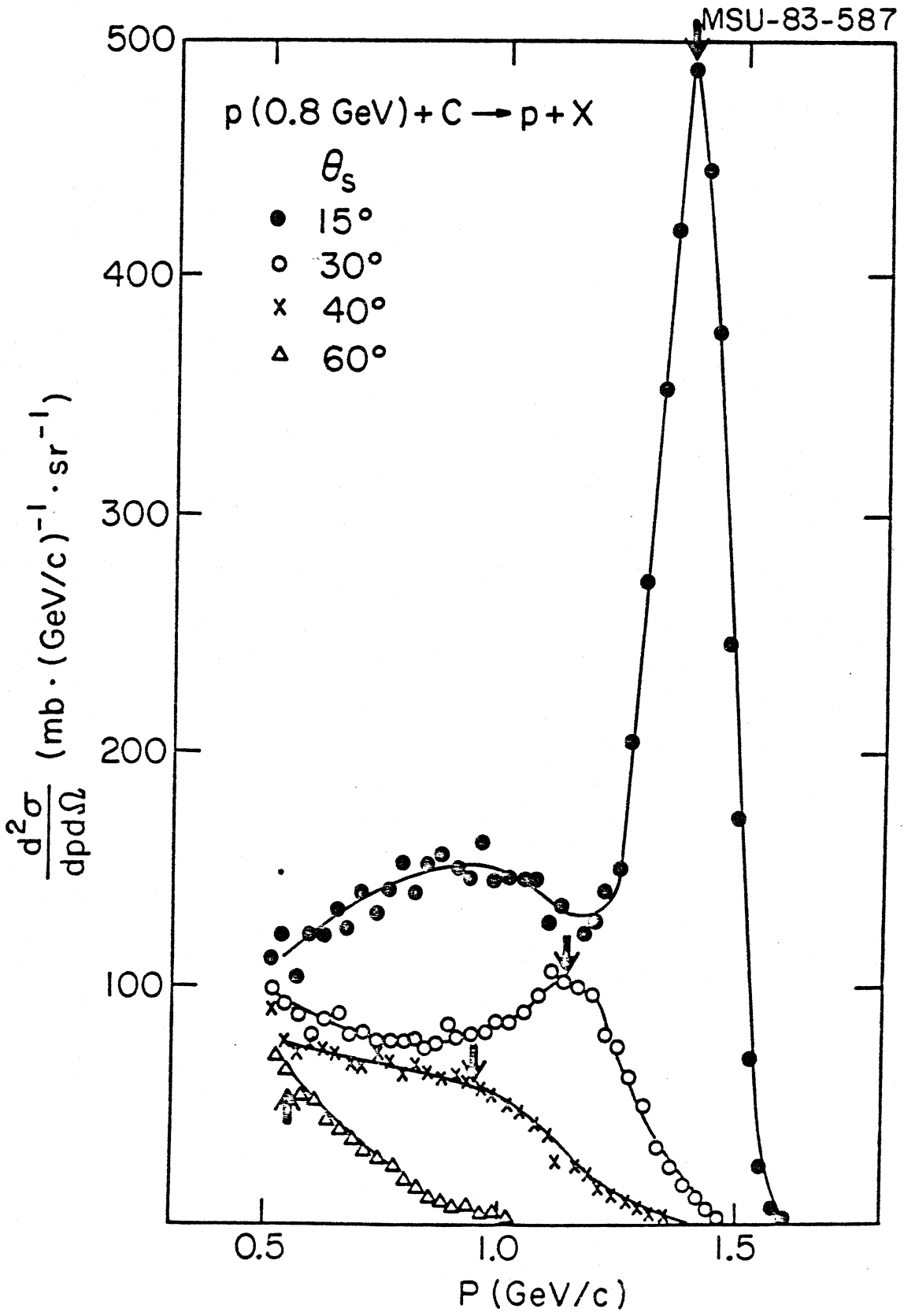
MSU-83-587
p (0.8 GeV) + C → p + X
θ_s
15°
30°
40°
60°
$\frac{d^2\sigma}{dpd\Omega}$ (mb · (GeV/c)$^{-1}$ · sr^{-1})
500
400
300
200
100
0.5
1.0
1.5
P (GeV/c)

Figure 3

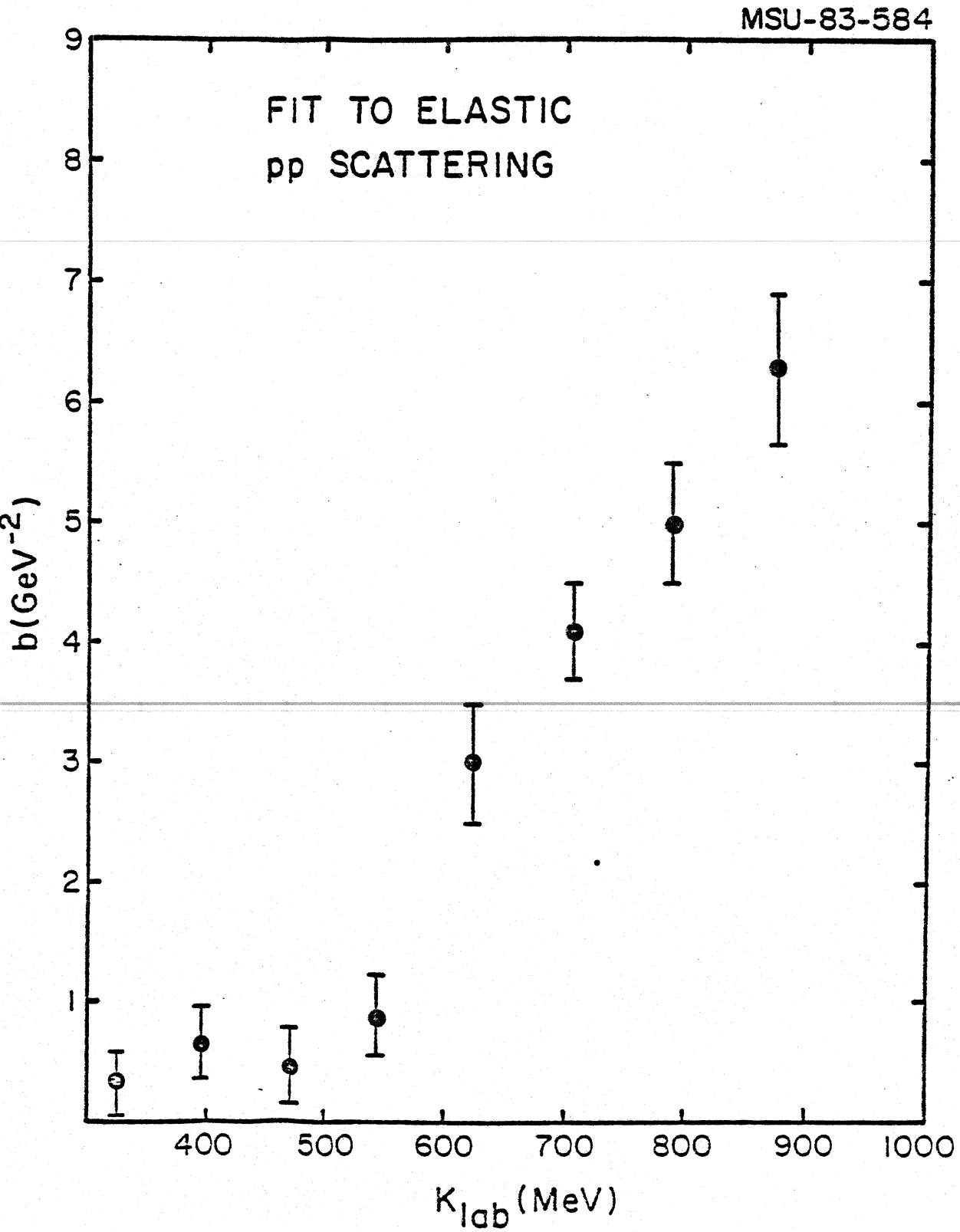
MSU-83-584
FIT TO ELASTIC
pp SCATTERING
b(GeV^{-2})
K_{lab} (MeV)
1
2
3
4
5
6
7
8
9
400
500
600
700
800
900
1000

Figure 4

MSU-83-588

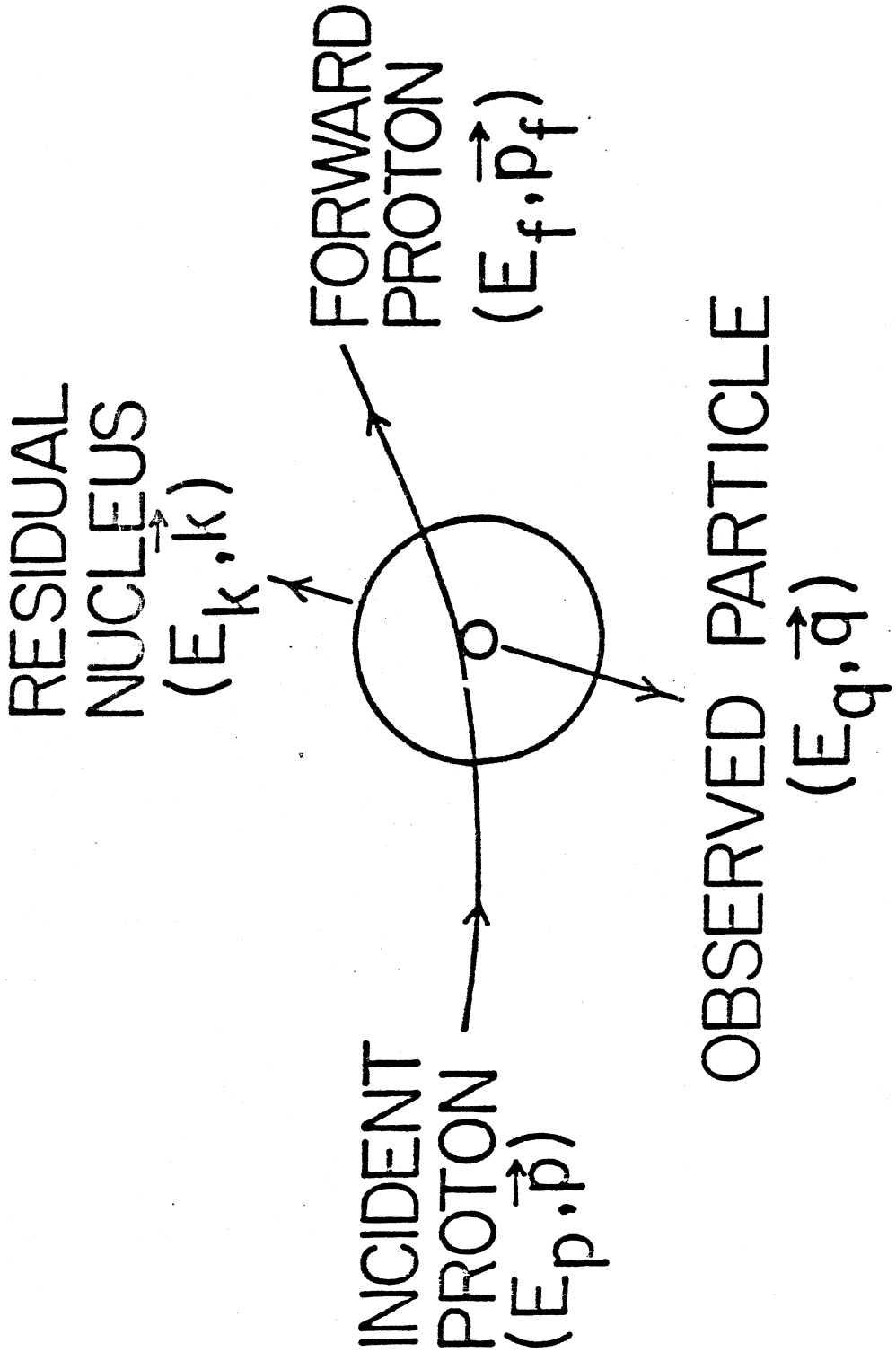

Figure 5

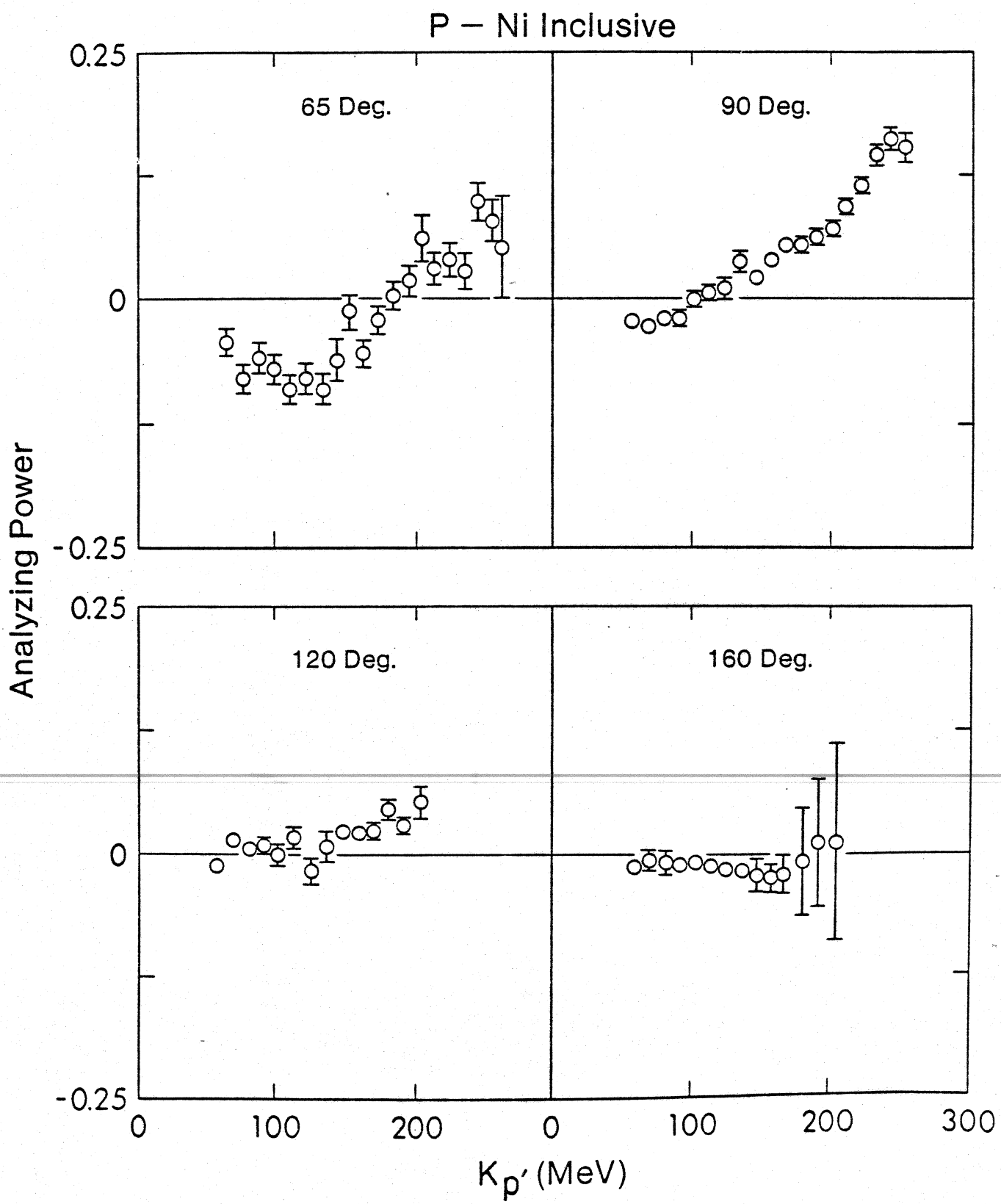
P — Ni Inclusive
65 Deg.
90 Deg.
120 Deg.
160 Deg.
0.25
0
-0.25
Analyzing Power
0
100
200
300
$K_{p'}$ (MeV)

Figure 6

MSU-83-583

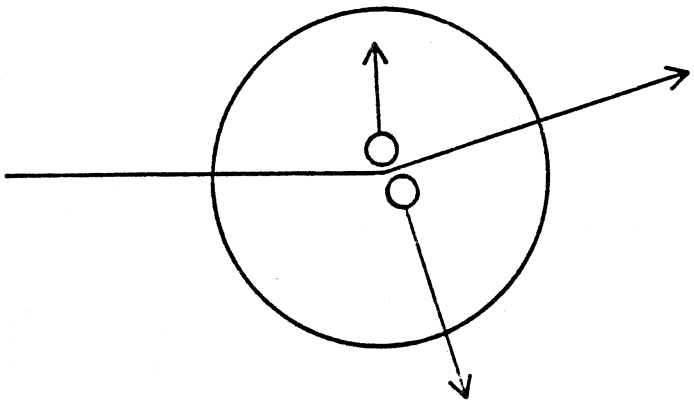

(a)

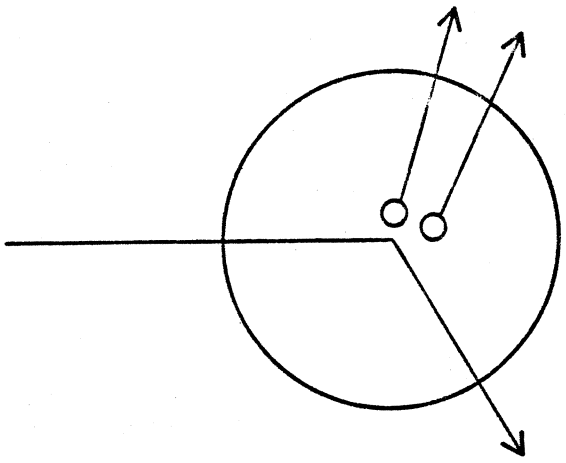

(b)

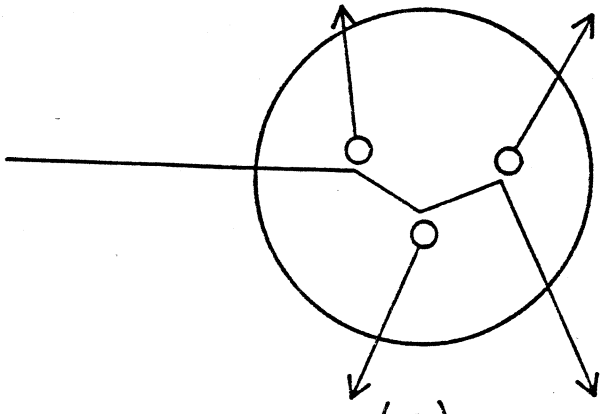

(c)

Figure 7

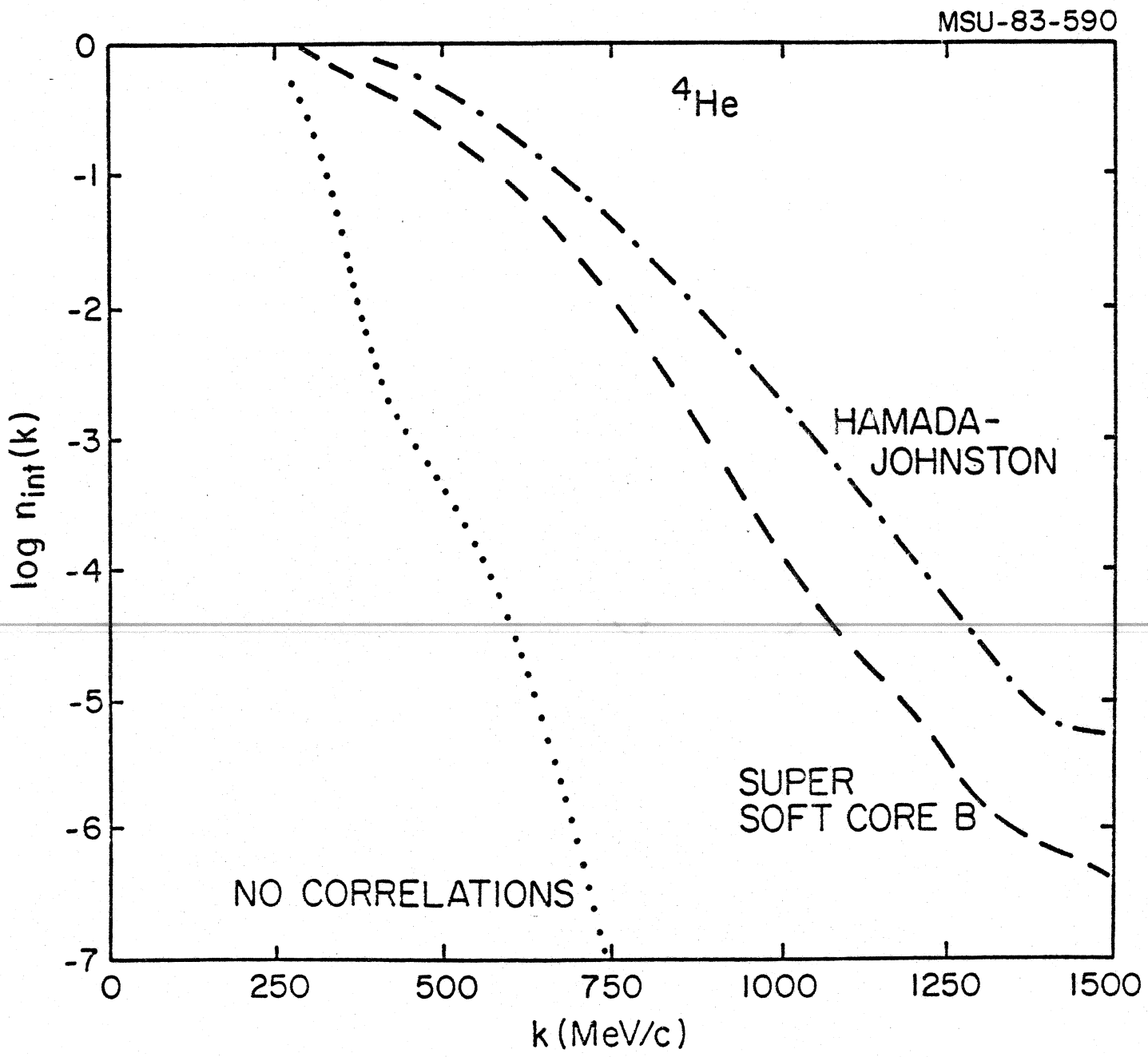
MSU-83-590
^{4}He
HAMADA-
JOHNSTON
SUPER
SOFT CORE B
NO CORRELATIONS
log $n_{int}(k)$
k (MeV/c)
0
-1
-2
-3
-4
-5
-6
-7
0
250
500
750
1000
1250
1500

Figure 8

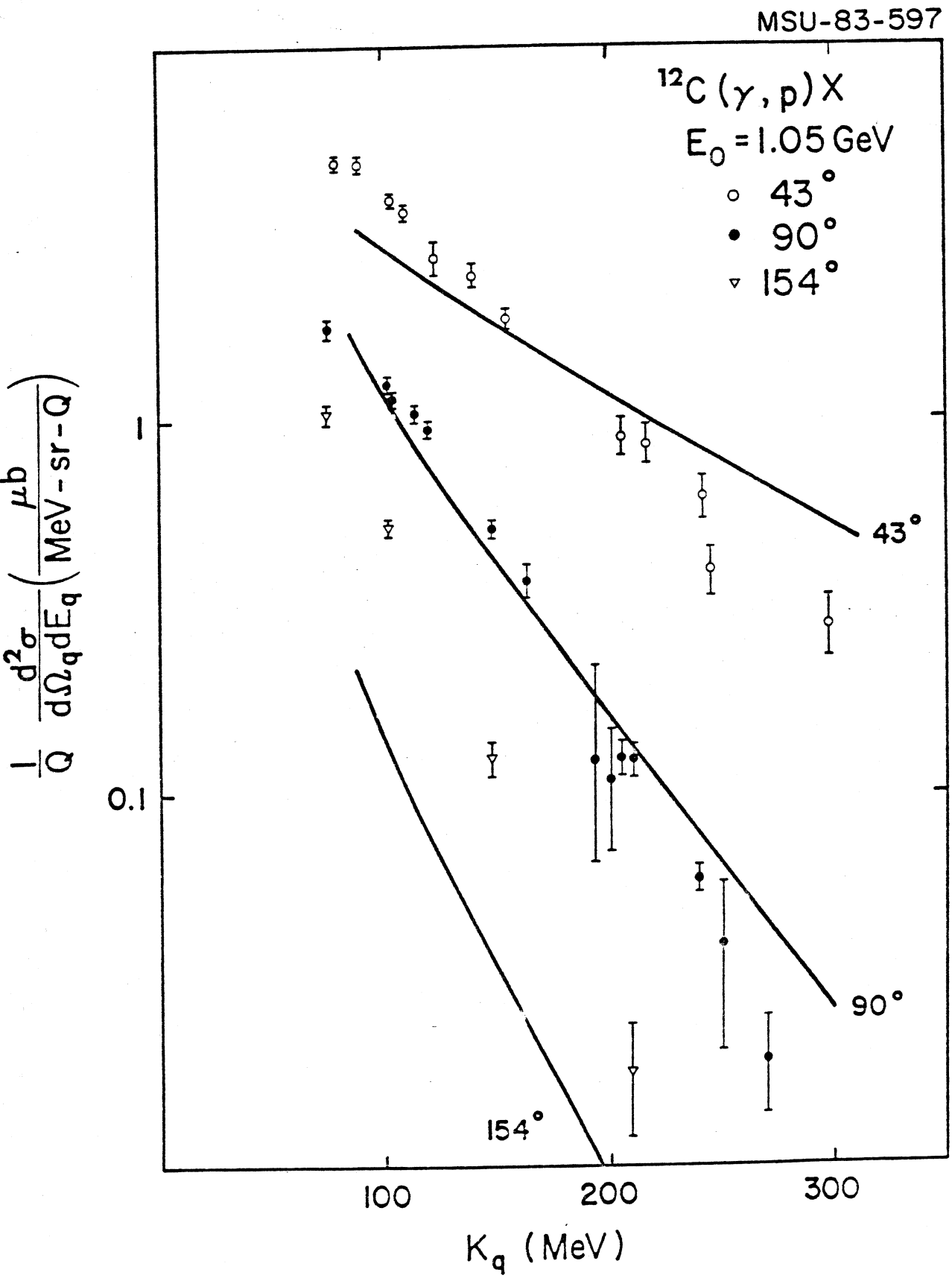
MSU-83-597
$^{12}C(\gamma, p)X$
$E_0 = 1.05$ GeV
43°
90°
154°
43°
90°
154°
$\frac{1}{Q}\frac{d^2\sigma}{d\Omega_q dE_q}\left(\frac{\mu b}{MeV\text{-}sr\text{-}Q}\right)$
1
0.1
100
200
300
K_q (MeV)

Figure 9

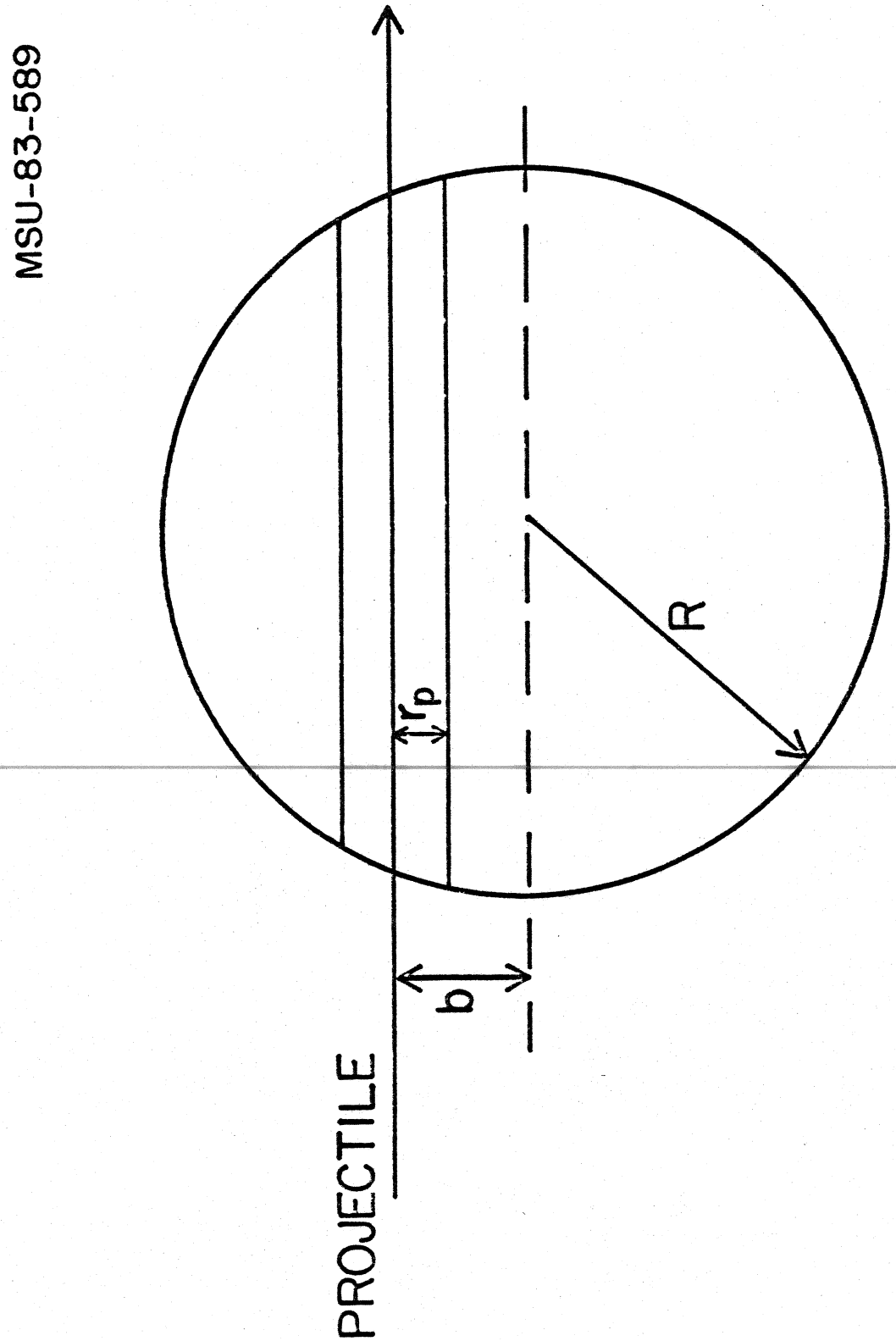

Figure 10

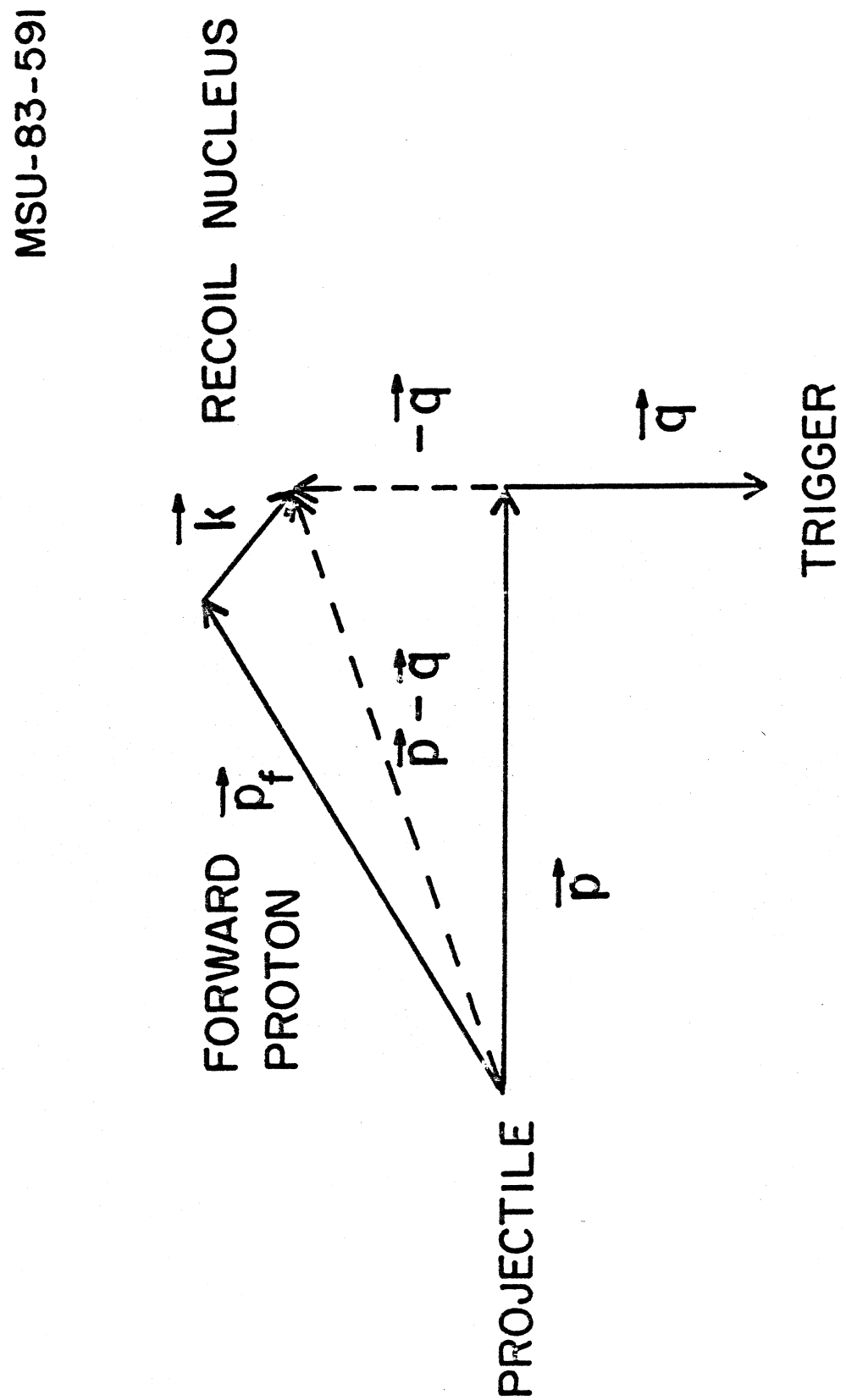
MSU-83-591
RECOIL NUCLEUS
$-\vec{q}$
$\vec{q}$
$\vec{k}$
TRIGGER
$\vec{p}-\vec{q}$
$\vec{p}_f$
FORWARD PROTON
$\vec{p}$
PROJECTILE

Figure 11

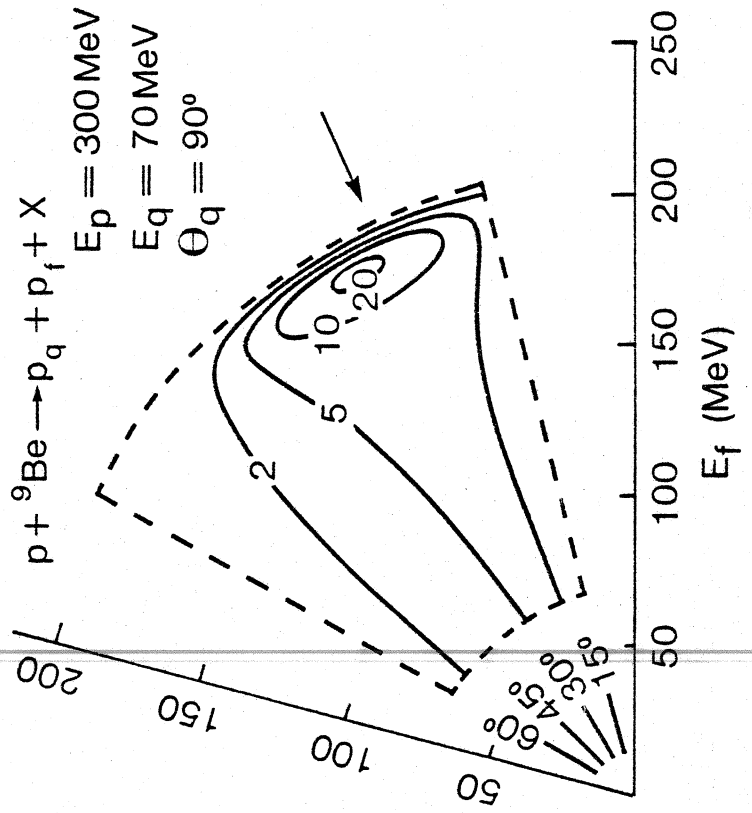
p + ^{9}Be → p_q + p_f + X
E_p = 300 MeV
E_q = 70 MeV
θ_q = 90°
2
5
10
20
50
100
150
200
250
E_f (MeV)
200
150
100
50
60°
45°
30°
15°

Figure 12

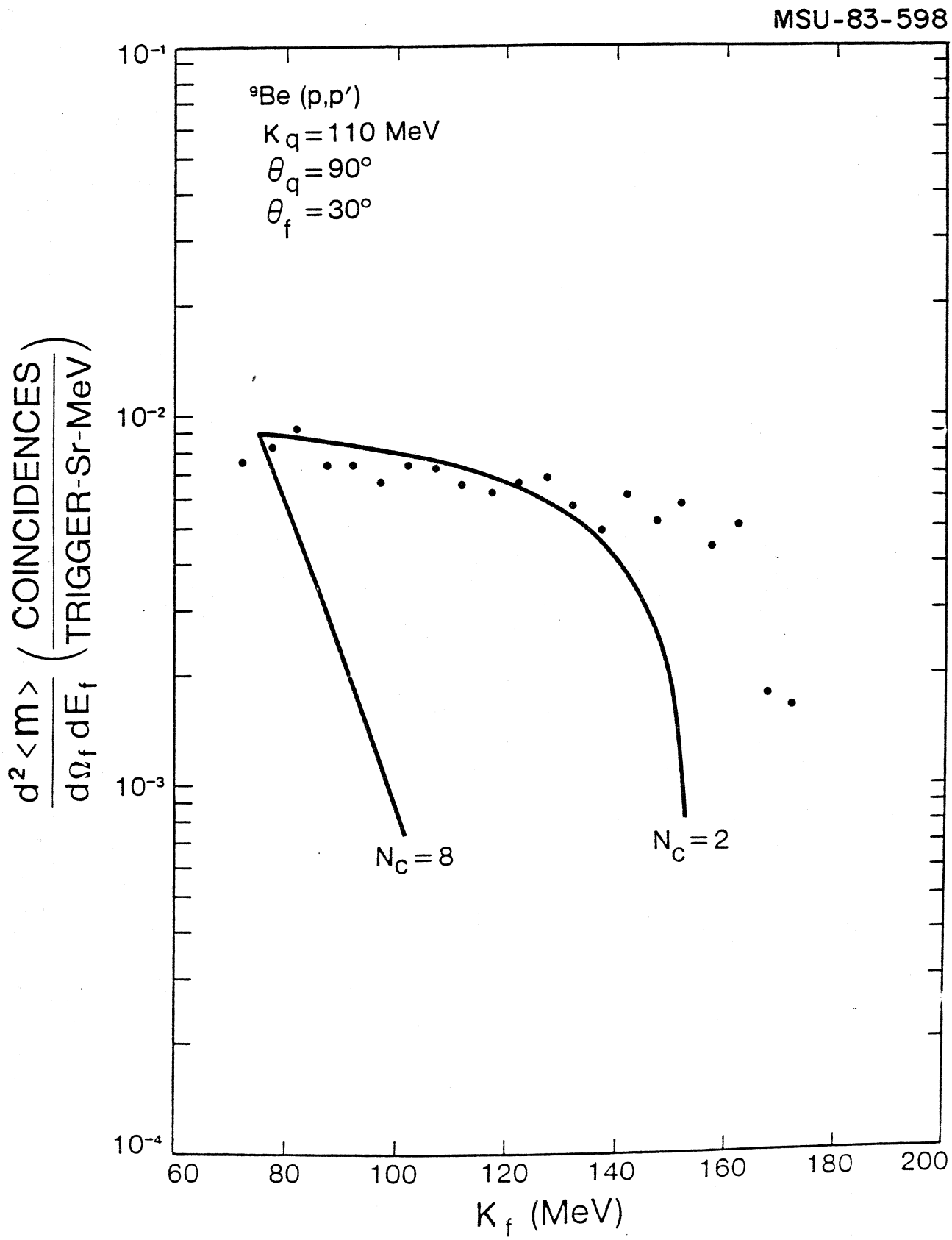
MSU-83-598
^{9}Be (p,p')
$K_q = 110$ MeV
$\theta_q = 90°$
$\theta_f = 30°$
$N_c = 8$
$N_c = 2$
$\frac{d^2\langle m \rangle}{d\Omega_f\, dE_f}\left(\frac{\text{COINCIDENCES}}{\text{TRIGGER-Sr-MeV}}\right)$
10^{-1}
10^{-2}
10^{-3}
10^{-4}
60
80
100
120
140
160
180
200
K_f (MeV)

Figure 13

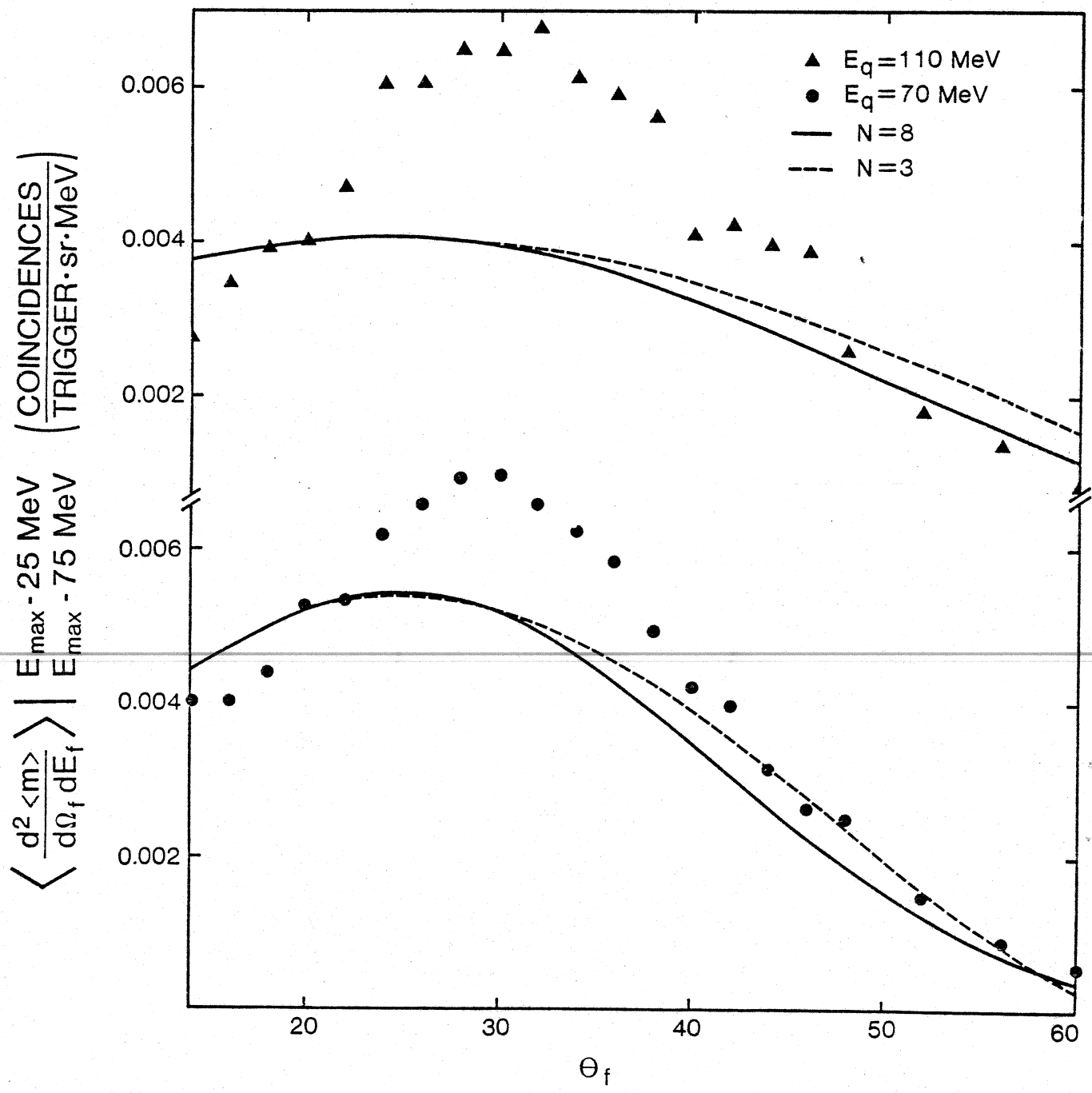
$\left\langle \frac{d^2\langle m\rangle}{d\Omega_f\, dE_f} \right\rangle \Big|_{E_{max}-75\ MeV}^{E_{max}-25\ MeV} \left(\frac{COINCIDENCES}{TRIGGER \cdot sr \cdot MeV}\right)$
0.006
0.004
0.002
0.006
0.004
0.002
E_q=110 MeV
E_q=70 MeV
N=8
N=3
20
30
40
50
60
Θ_f

Figure 14

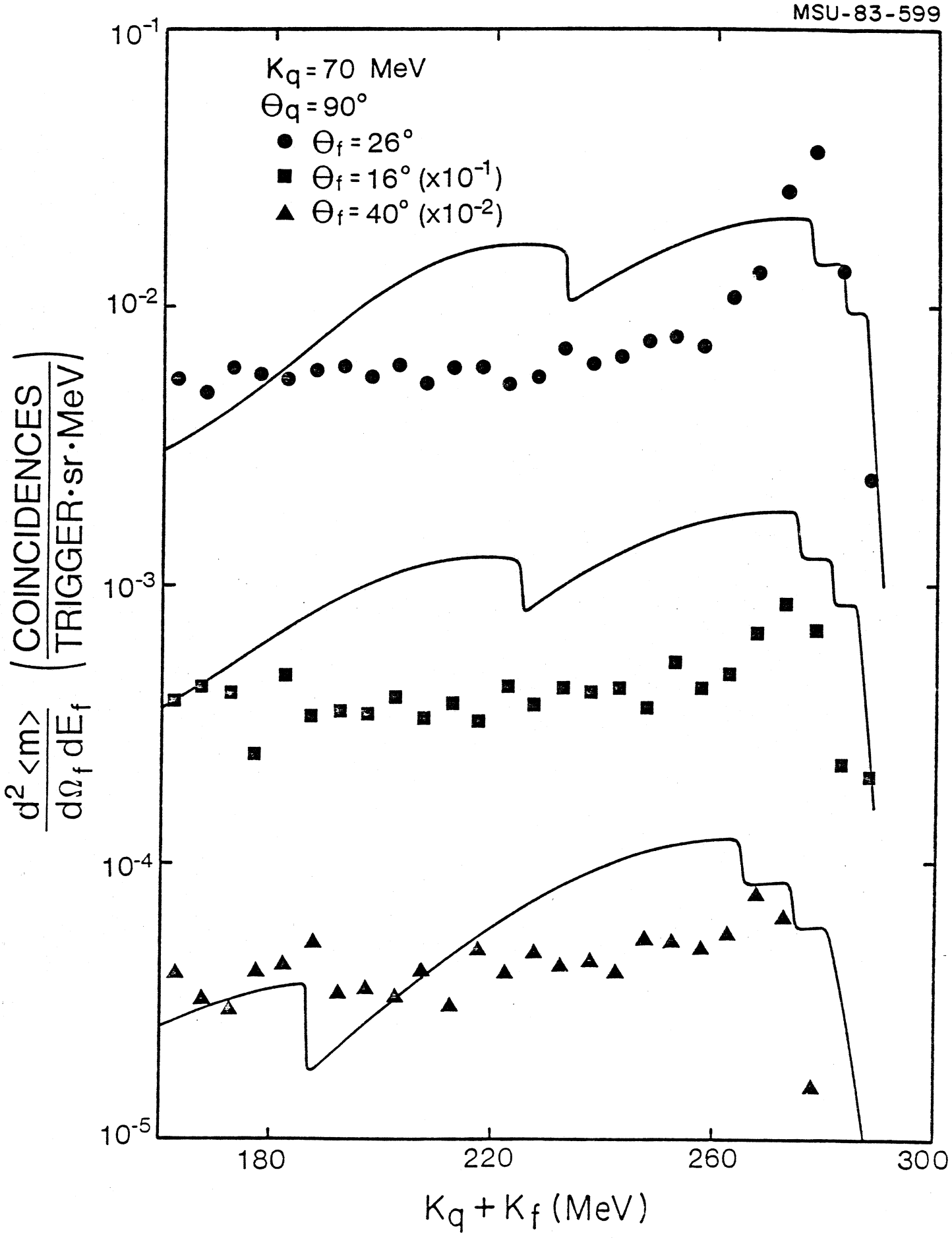
MSU-83-599
$K_q = 70$ MeV
$\Theta_q = 90°$
$\Theta_f = 26°$
$\Theta_f = 16°$ ($\times 10^{-1}$)
$\Theta_f = 40°$ ($\times 10^{-2}$)
10^{-1}
10^{-2}
10^{-3}
10^{-4}
10^{-5}
$\frac{d^2\langle m\rangle}{d\Omega_f\, dE_f}\left(\frac{\text{COINCIDENCES}}{\text{TRIGGER}\cdot sr\cdot MeV}\right)$
180
220
260
300
$K_q + K_f$ (MeV)

Figure 15

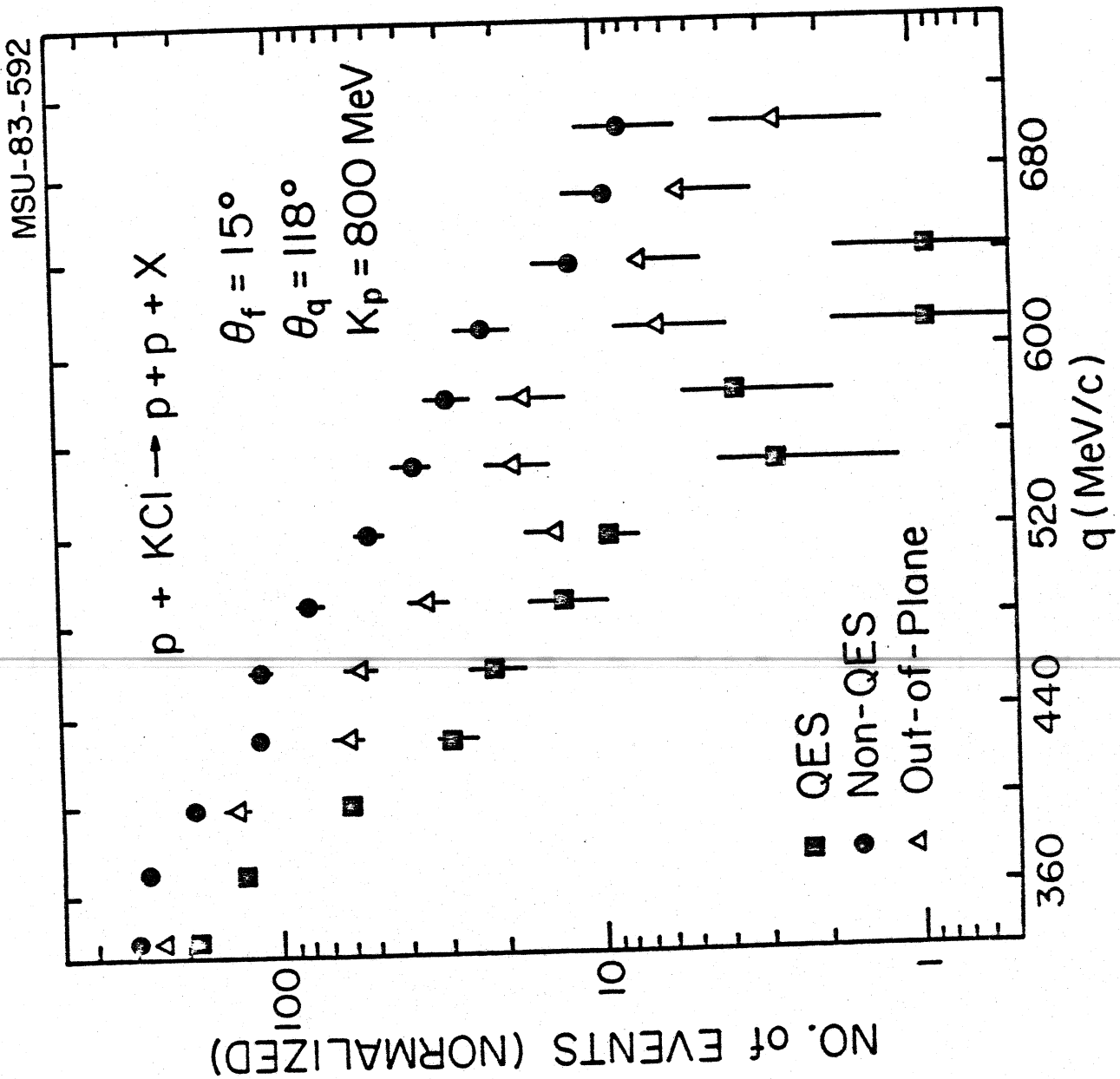
MSU-83-592
p + KCl → p+p + X
θ_f = 15°
θ_q = 118°
K_p = 800 MeV
QES
Non-QES
Out-of-Plane
NO. of EVENTS (NORMALIZED)
100
10
1
360
440
520
600
680
q (MeV/c)

Figure 16

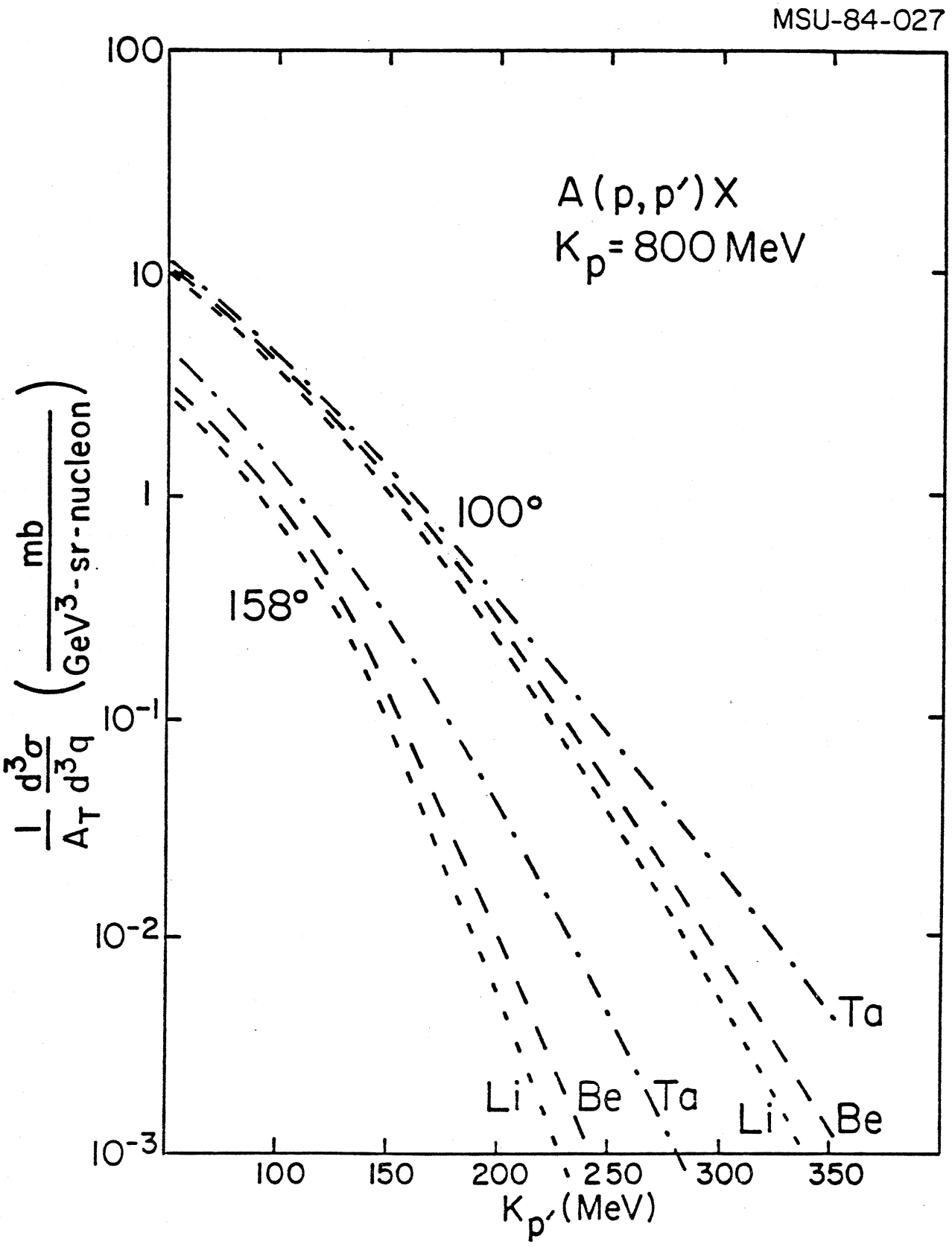
MSU-84-027
A(p,p')X
K_p= 800 MeV
100°
158°
Ta
Be
Li
Ta
Be
Li
100
150
200
250
300
350
$K_{p'}$ (MeV)
100
10
1
10^{-1}
10^{-2}
10^{-3}
$\frac{1}{A_T}\frac{d^3\sigma}{d^3q}\left(\frac{mb}{GeV^3\text{-}sr\text{-}nucleon}\right)$

Figure 17

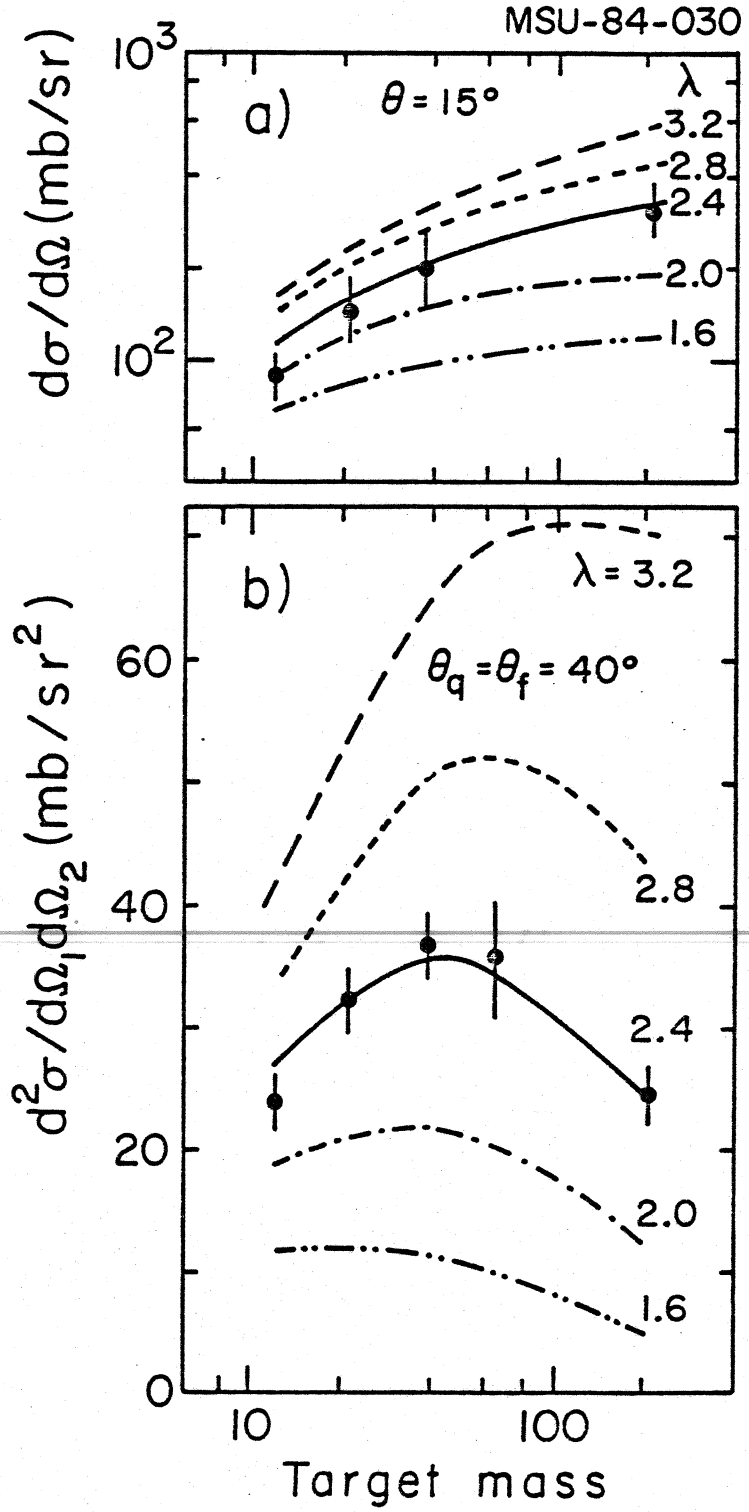
MSU-84-030
a)
θ = 15°
λ
3.2
2.8
2.4
2.0
1.6
dσ/dΩ (mb/sr)
10³
10²
b)
λ = 3.2
θq = θf = 40°
2.8
2.4
2.0
1.6
d²σ/dΩ1dΩ2 (mb/sr²)
60
40
20
0
10
100
Target mass

Figure 18

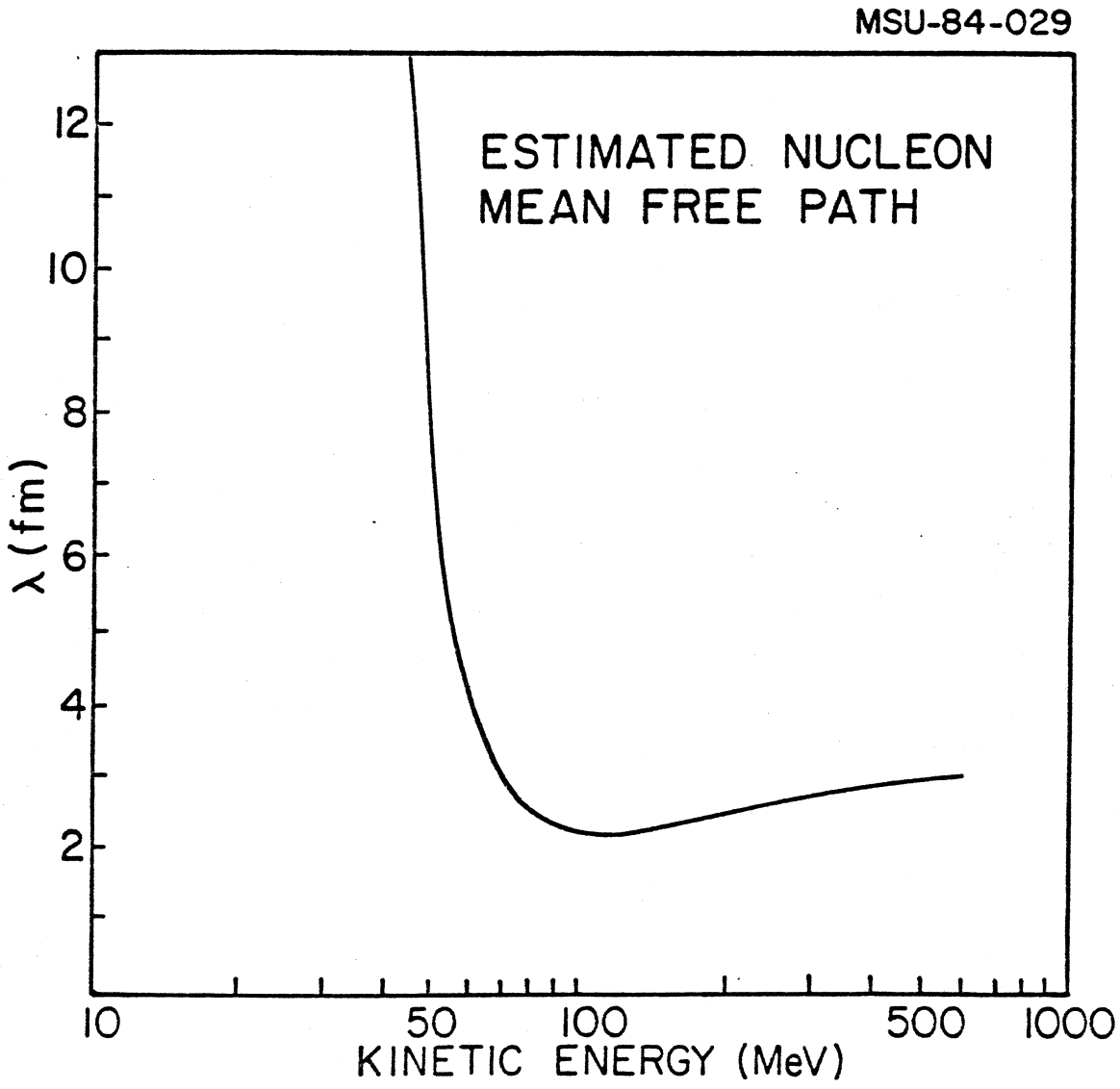
MSU-84-029
ESTIMATED NUCLEON
MEAN FREE PATH
λ (fm)
12
10
8
6
4
2
10
50
100
500
1000
KINETIC ENERGY (MeV)

Figure 19

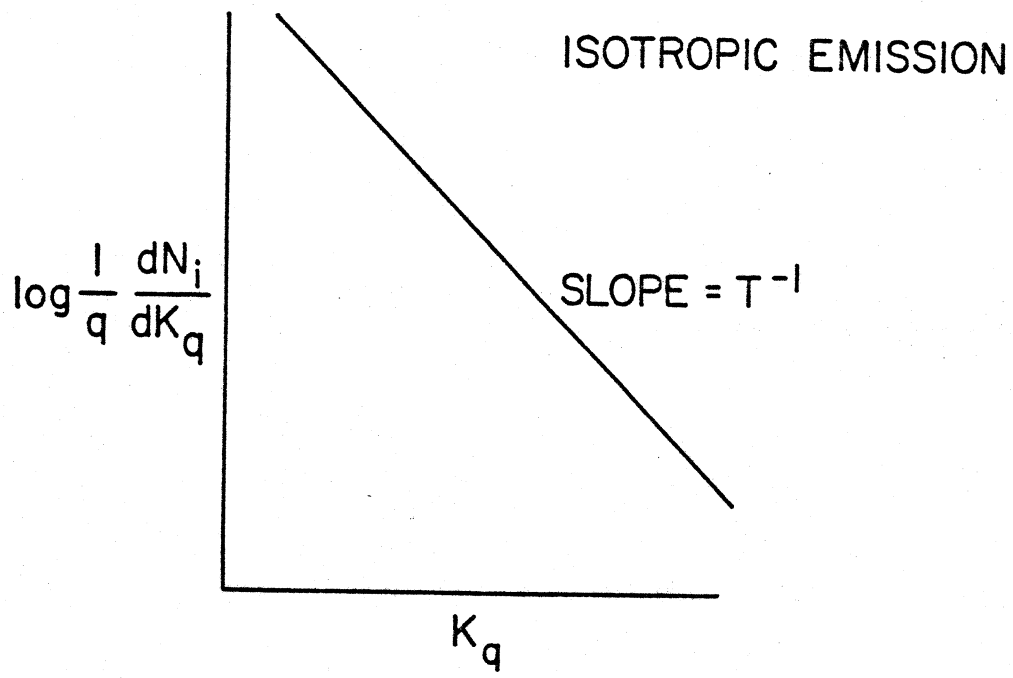
ISOTROPIC EMISSION
SLOPE = T⁻¹
log (1/q) (dN_i/dK_q)
K_q

(a)

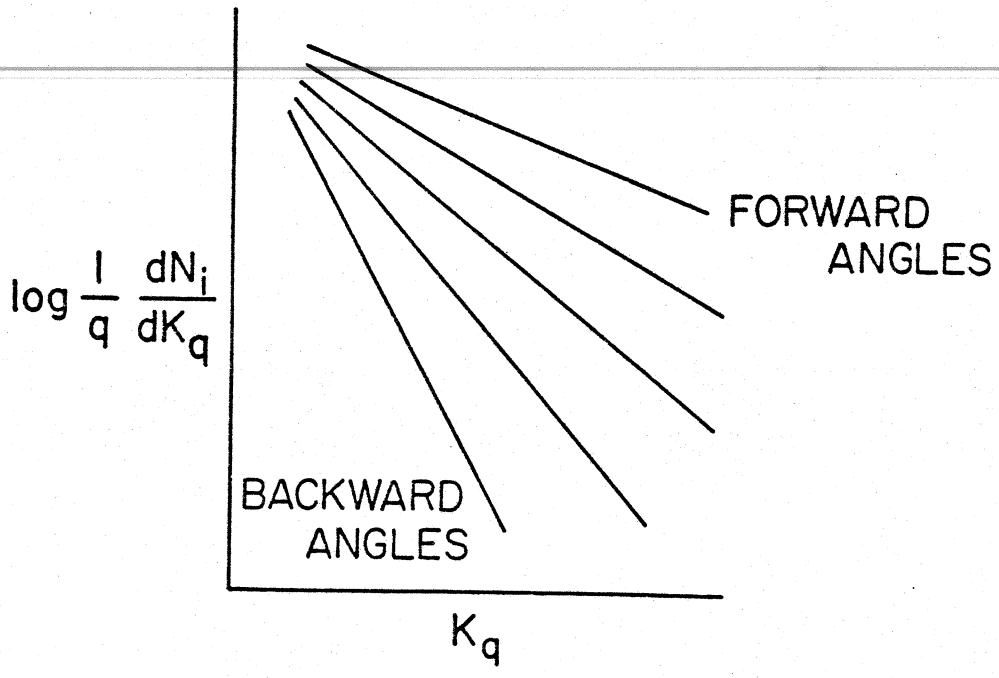
FORWARD ANGLES
BACKWARD ANGLES
log (1/q) (dN_i/dK_q)
K_q

(b)

Figure 20

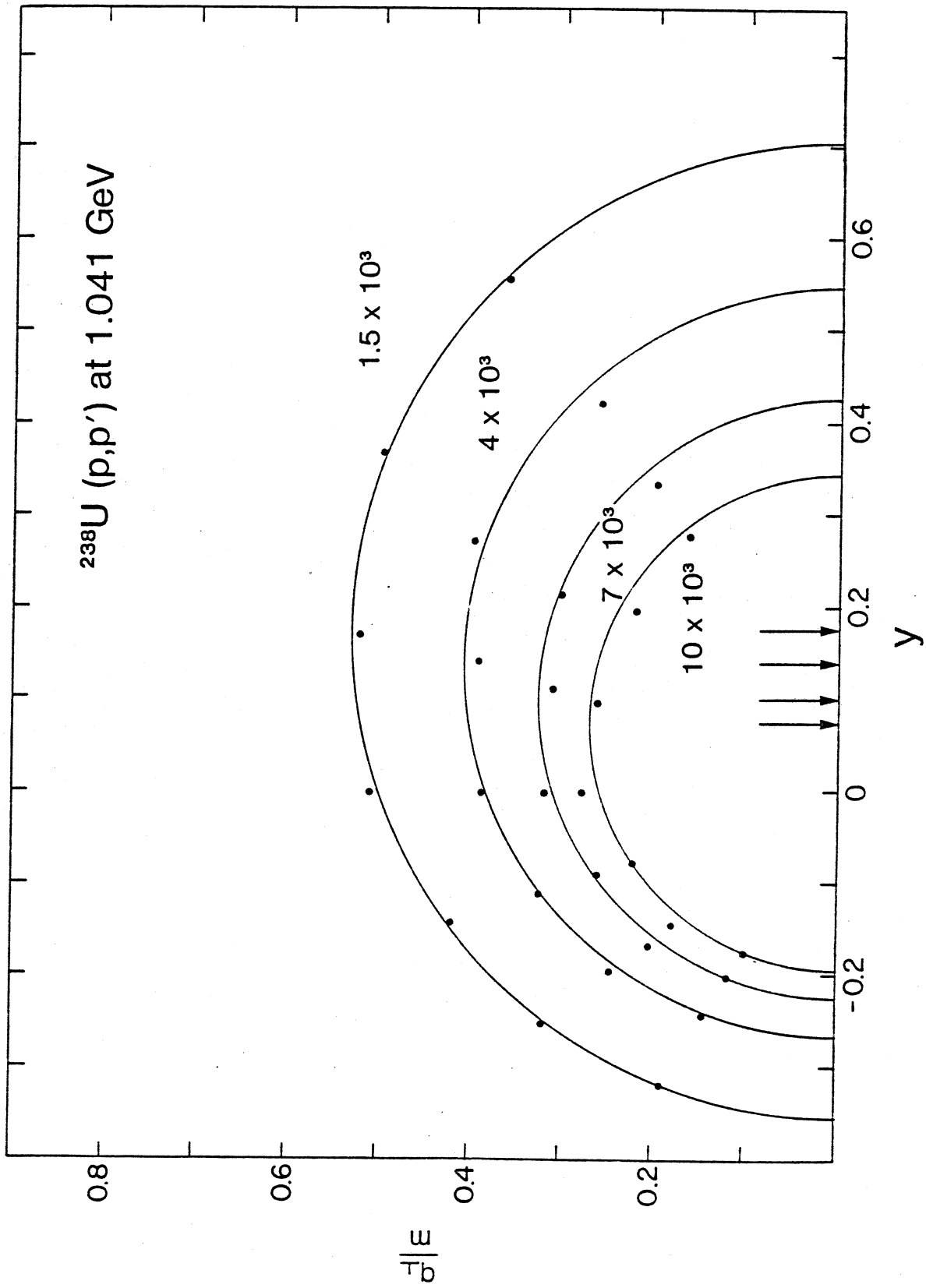
^{238}U (p,p′) at 1.041 GeV
1.5 x 10³
4 x 10³
7 x 10³
10 x 10³
0.8
0.6
0.4
0.2
-0.2
0
0.2
0.4
0.6
y
$\frac{q_L}{m}$

Figure 21

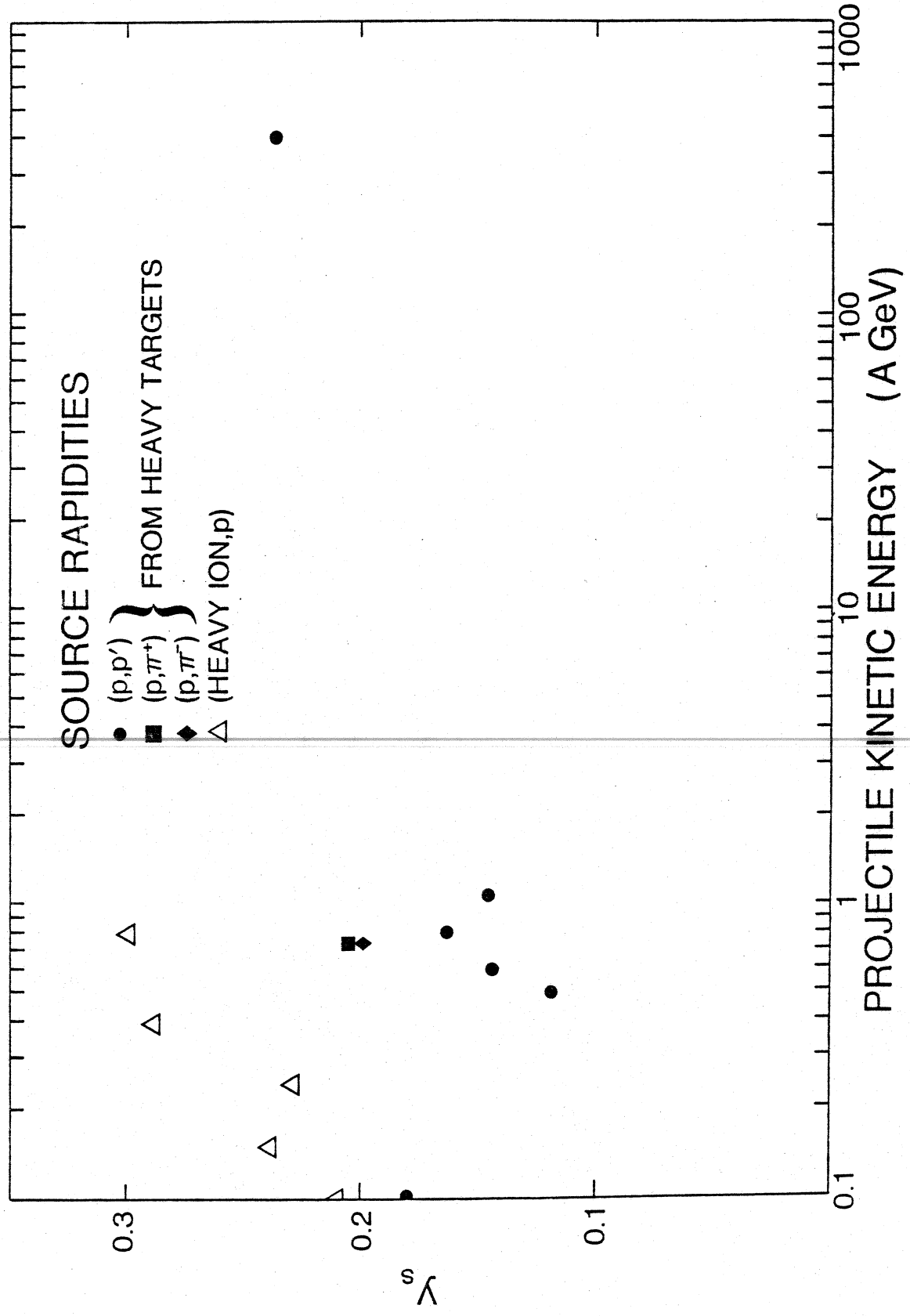
SOURCE RAPIDITIES
(p,p')
(p,π+)
(p,π−)
FROM HEAVY TARGETS
(HEAVY ION,p)
0.3
0.2
0.1
y_s
0.1
1
10
100
1000
PROJECTILE KINETIC ENERGY (A GeV)

Figure 22

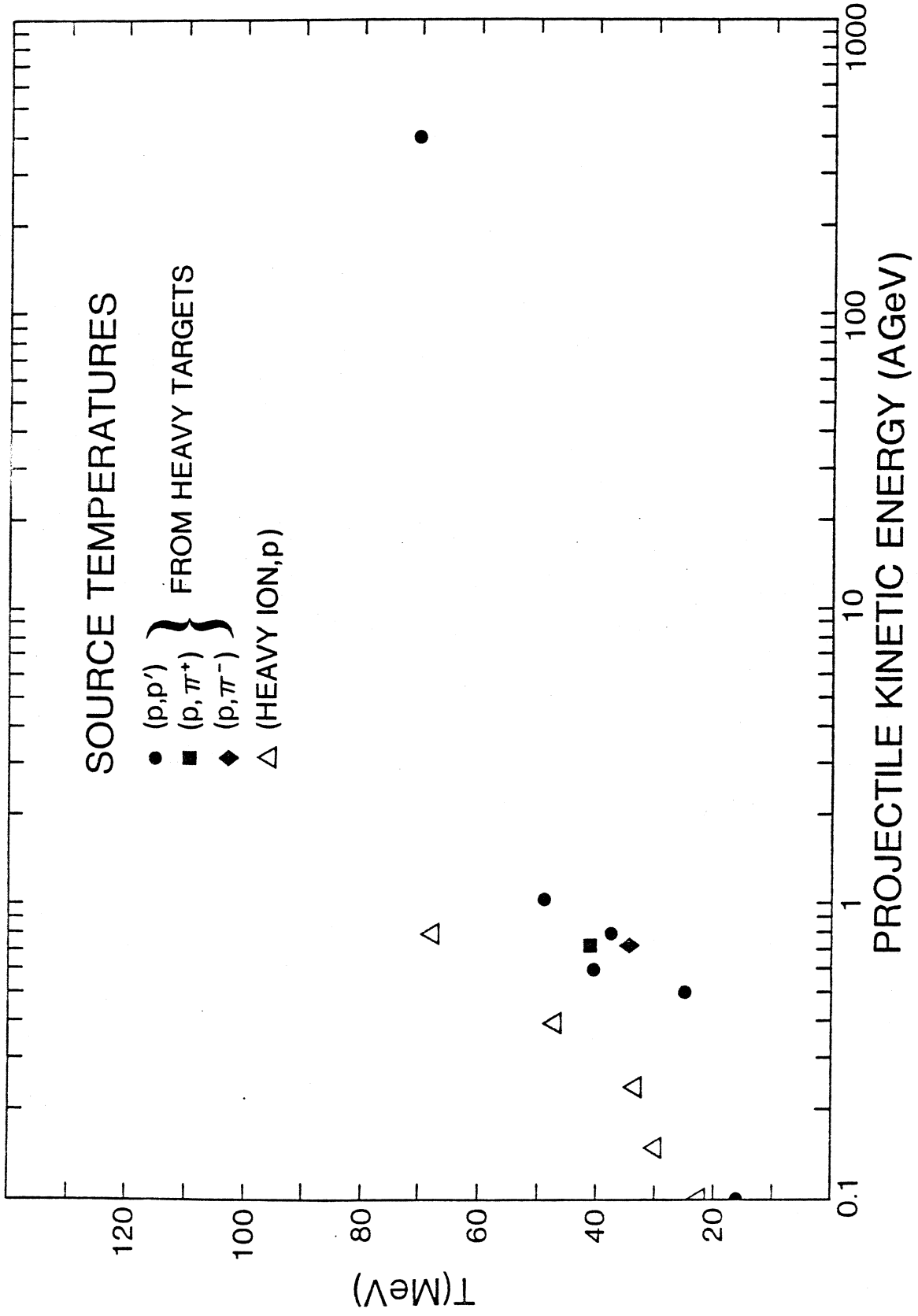
SOURCE TEMPERATURES
(p,p')
(p,π+)
(p,π-)
FROM HEAVY TARGETS
(HEAVY ION,p)
T(MeV)
120
100
80
60
40
20
0.1
1
10
100
1000
PROJECTILE KINETIC ENERGY (AGeV)

Figure 23

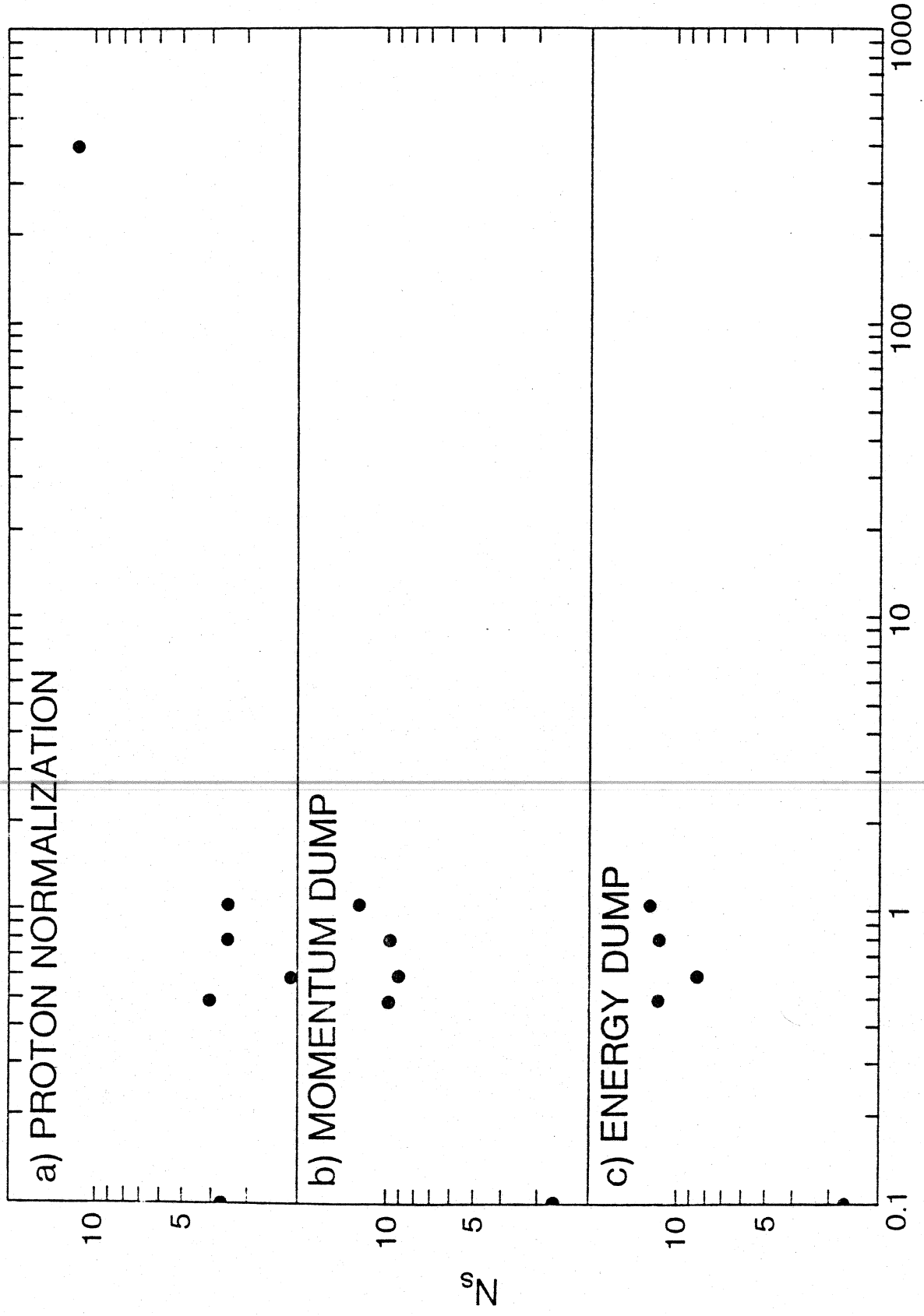
a) PROTON NORMALIZATION
b) MOMENTUM DUMP
c) ENERGY DUMP
N_s
10
5
10
5
10
5
0.1
1
10
100
1000
T_p (GeV)

Figure 24

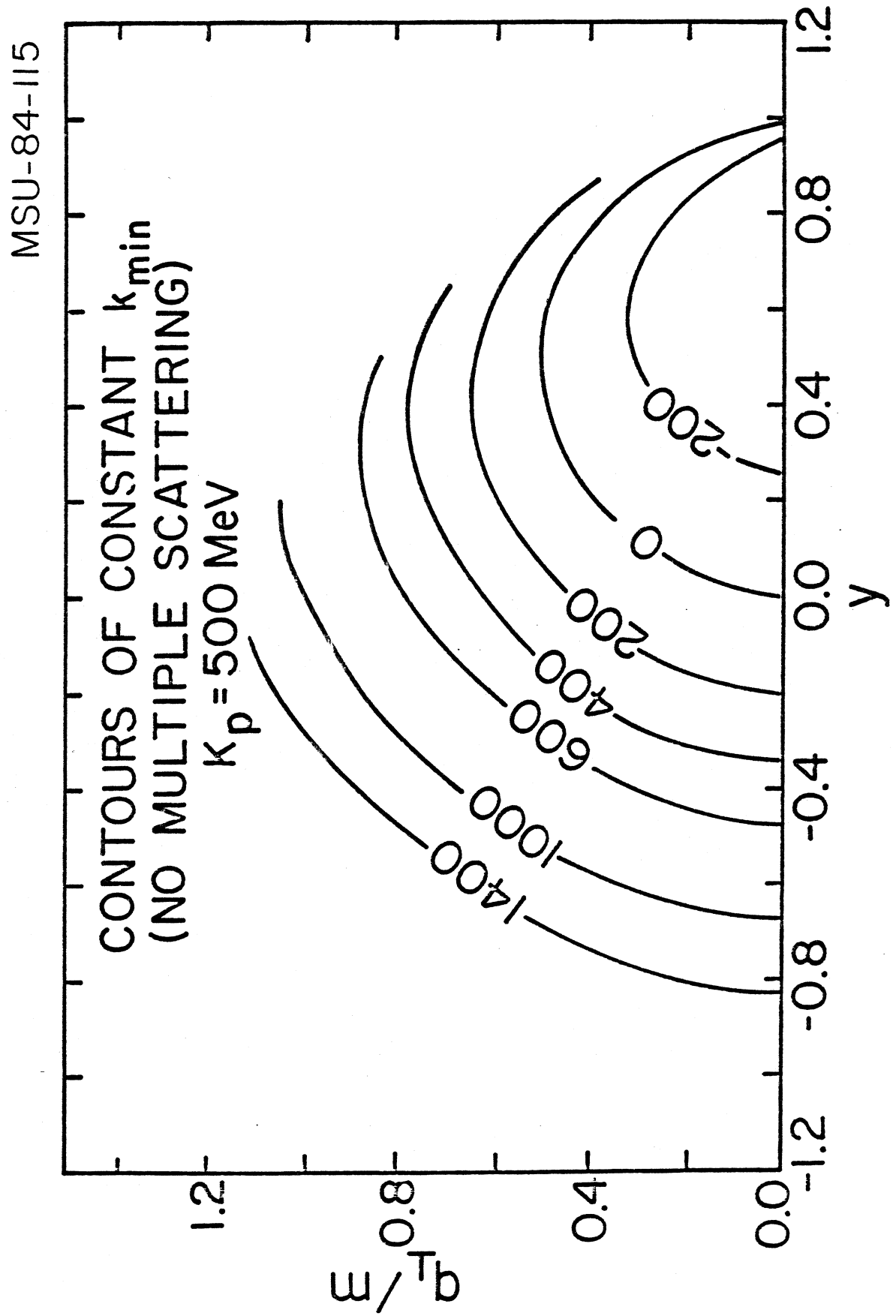
MSU-84-115
CONTOURS OF CONSTANT k_{min}
(NO MULTIPLE SCATTERING)
K_p=500 MeV
-200
0
200
400
600
1000
1400
y
1.2
0.8
0.4
0.0
-0.4
-0.8
-1.2
ω/T_b
1.2
0.8
0.4
0.0

Figure 25

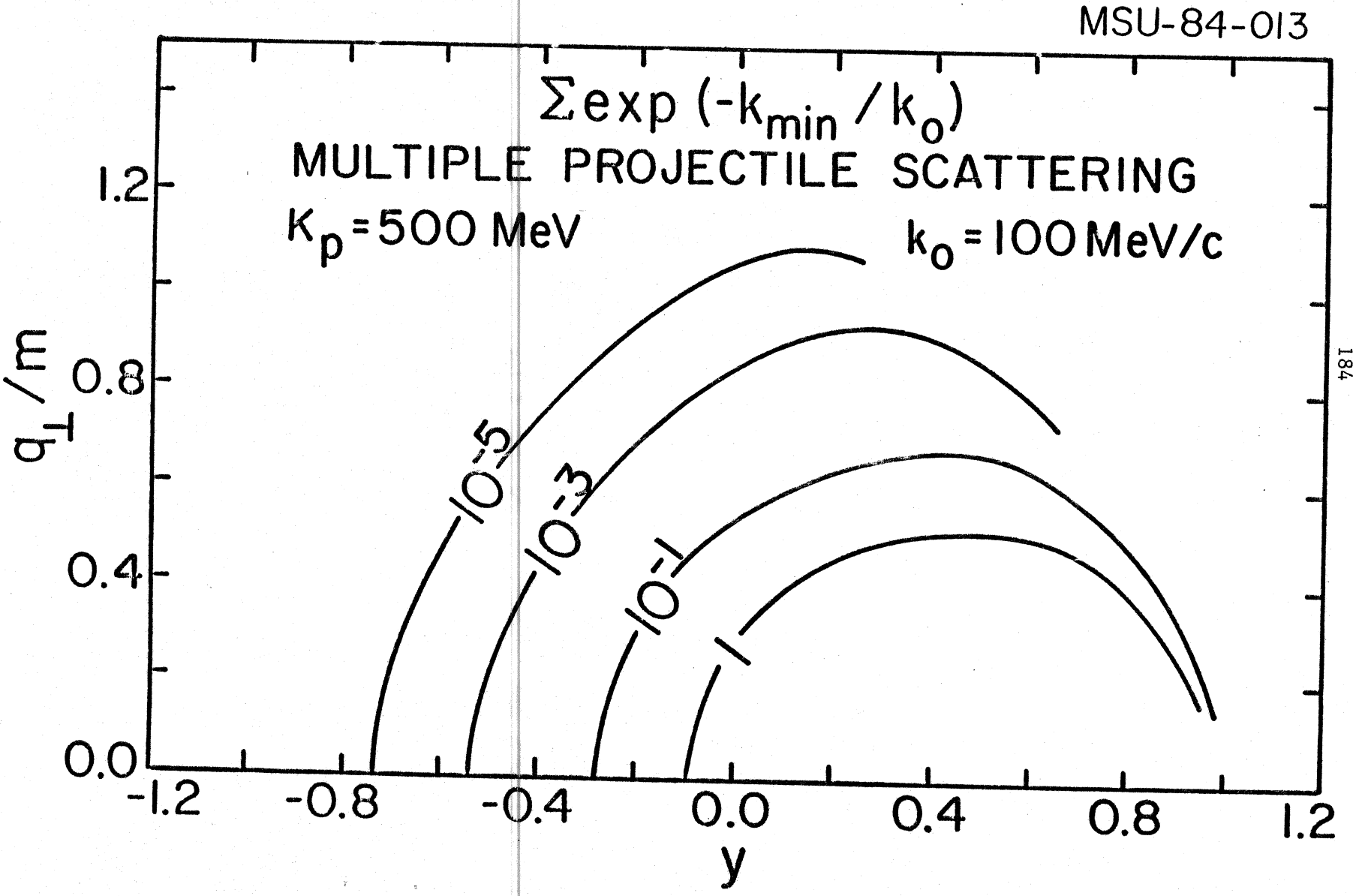
MSU-84-013
Σexp (-k_min / k_o)
MULTIPLE PROJECTILE SCATTERING
K_p = 500 MeV
k_o = 100 MeV/c
10^-5
10^-3
10^-1
1
q_T / m
y
0.0
0.4
0.8
1.2
-1.2
-0.8
-0.4
0.0
0.4
0.8
1.2

Figure 26

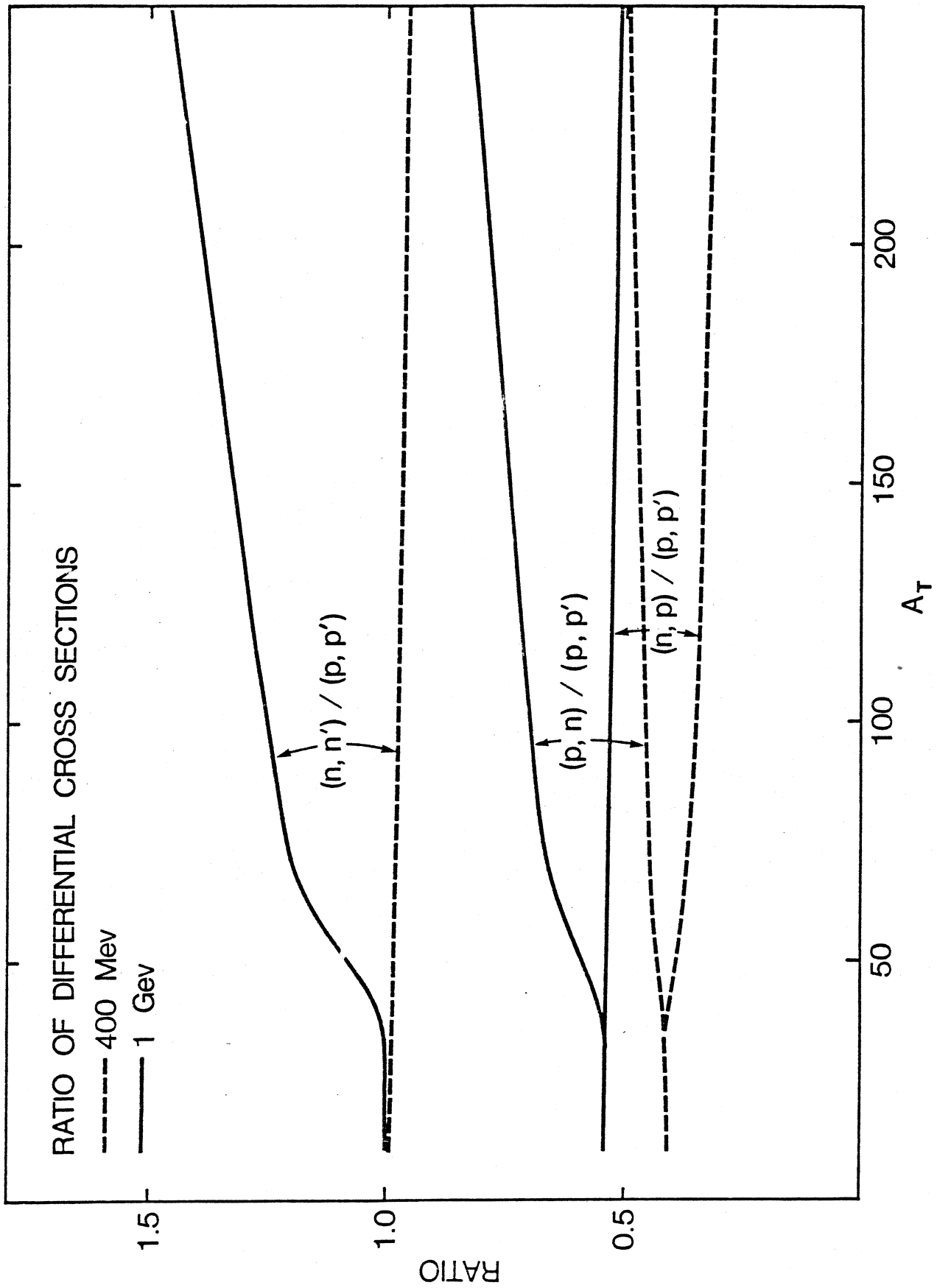
RATIO OF DIFFERENTIAL CROSS SECTIONS
400 Mev
1 Gev
(n, n') / (p, p')
(p, n) / (p, p')
(n, p) / (p, p')
RATIO
1.5
1.0
0.5
50
100
150
200
A_T

Figure 27

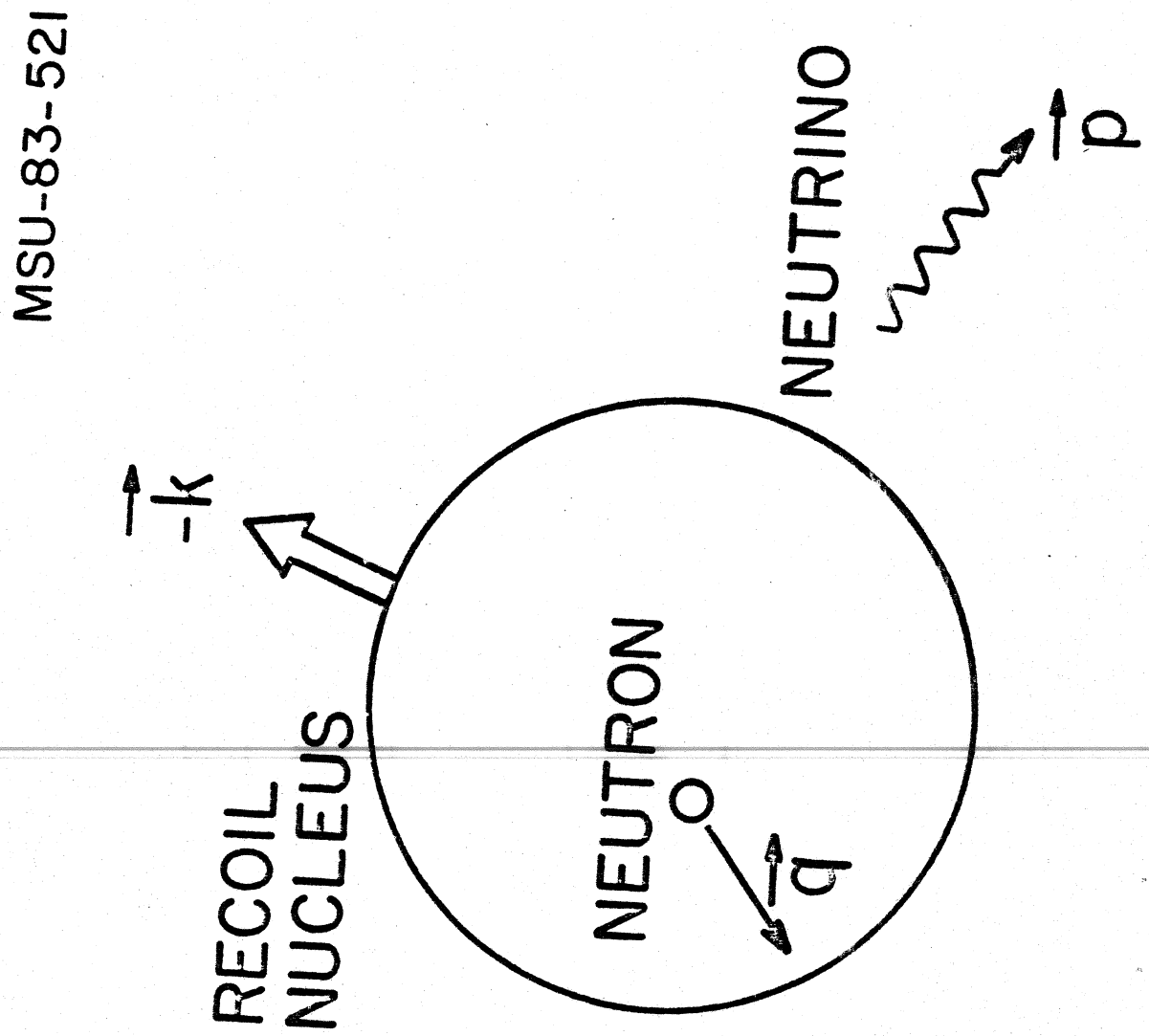

Figure 28

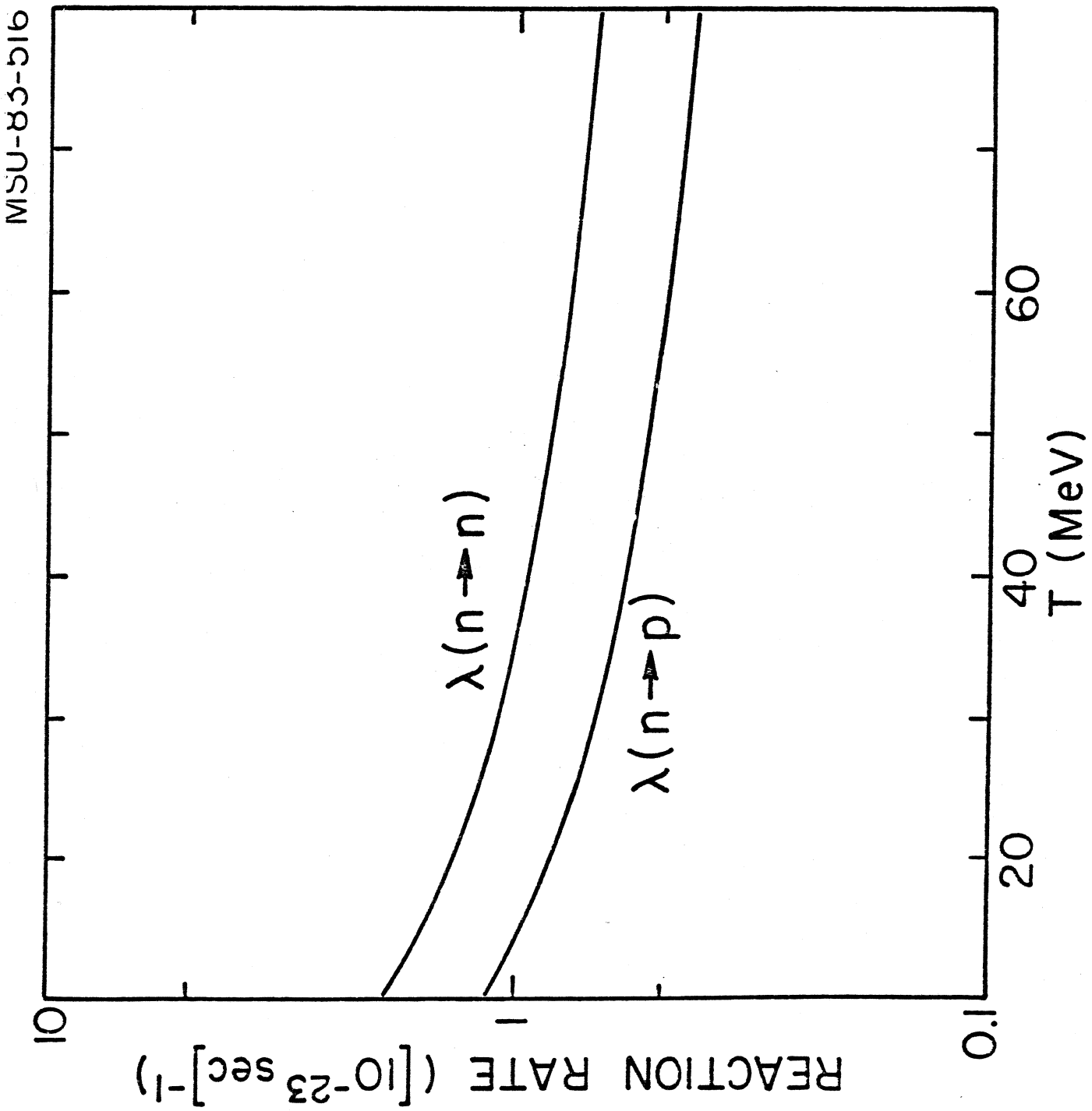

Figure 29

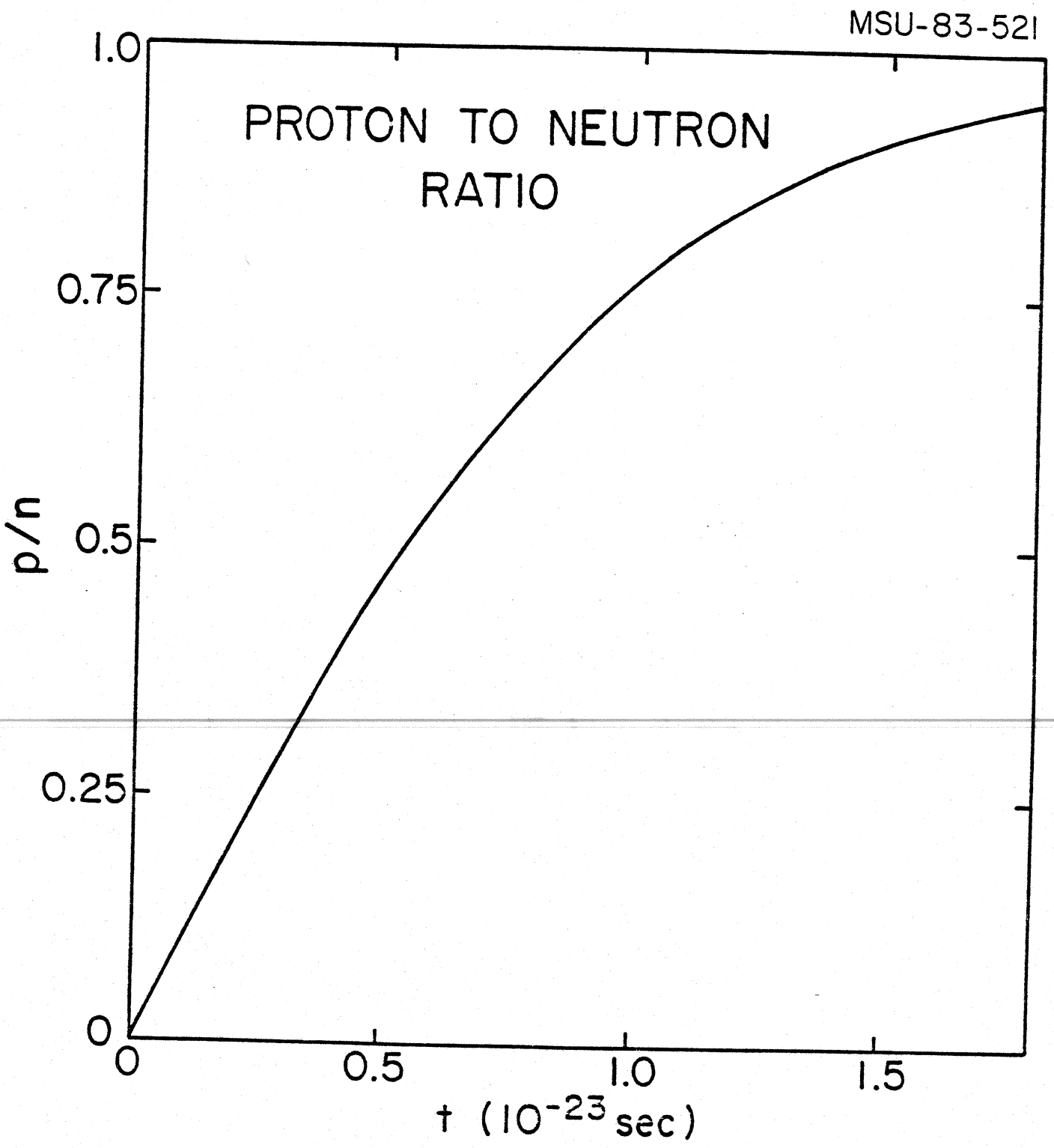
MSU-83-521
PROTON TO NEUTRON RATIO
1.0
0.75
0.5
0.25
0
p/n
0
0.5
1.0
1.5
t (10^-23 sec)

Figure 30

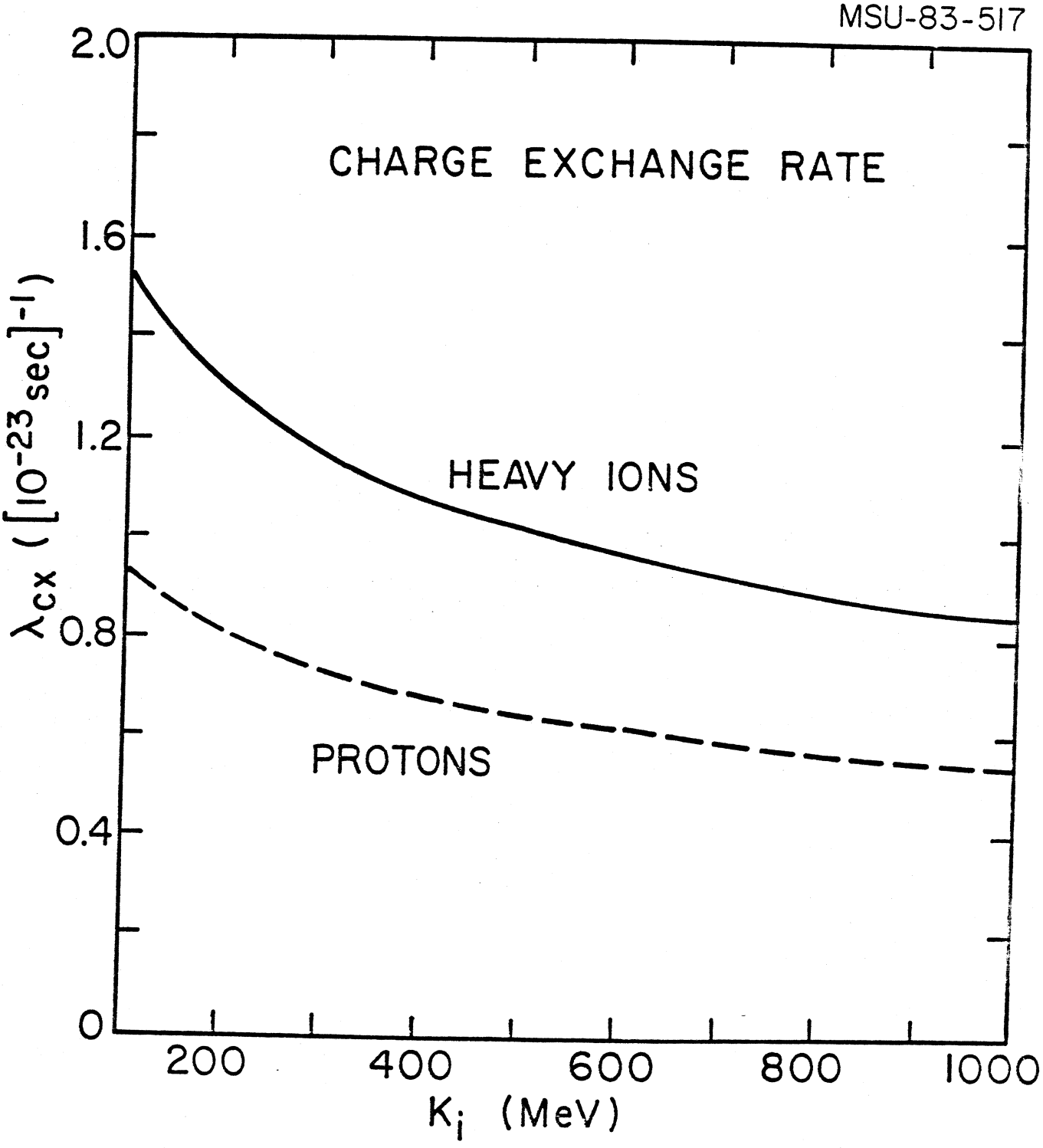
MSU-83-517
CHARGE EXCHANGE RATE
HEAVY IONS
PROTONS
2.0
1.6
1.2
0.8
0.4
0
200
400
600
800
1000
λ_{cx} ([10^{-23} sec]$^{-1}$)
K_i (MeV)

Figure 31

MSU-84-002

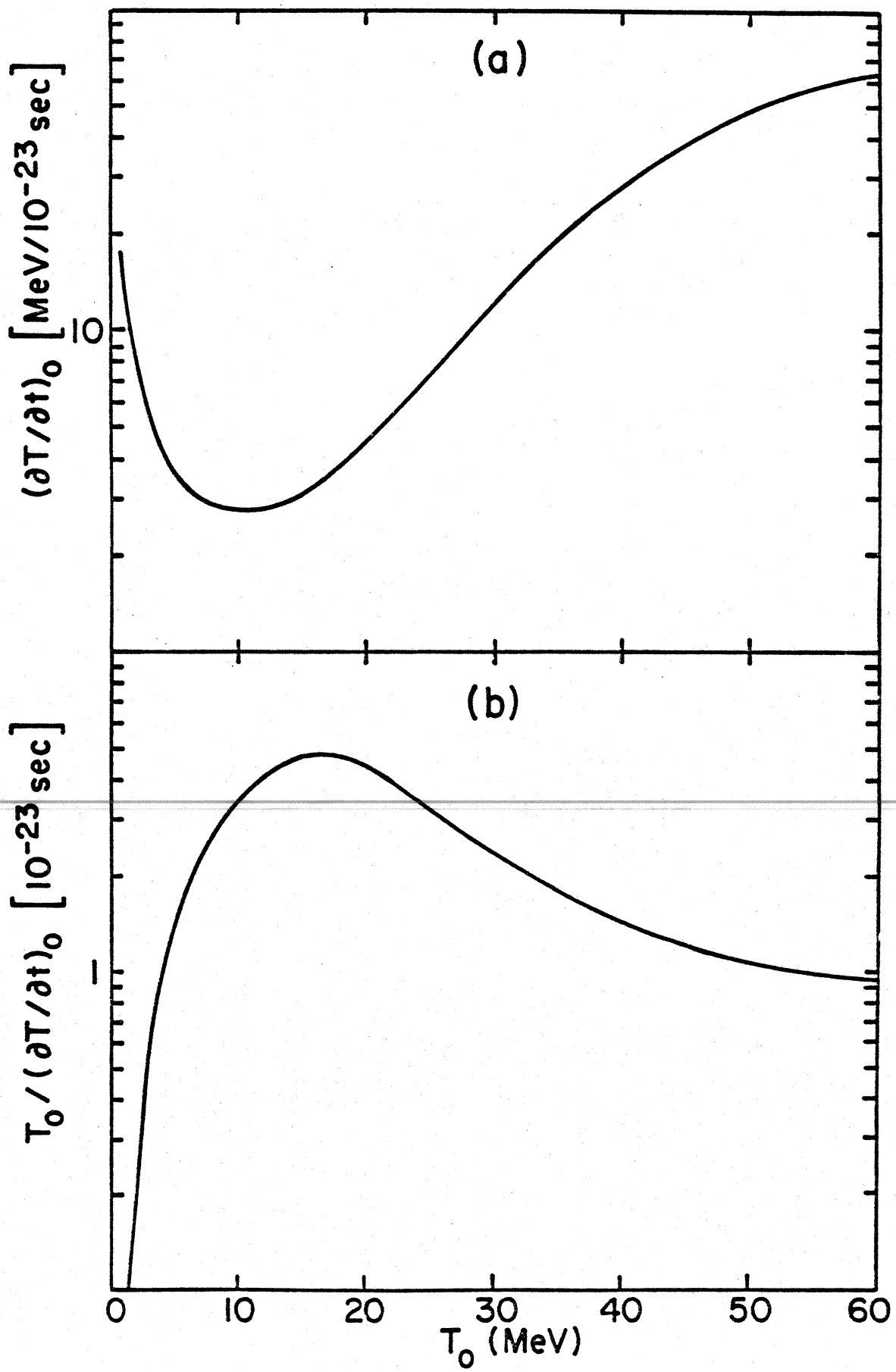

Figure 32

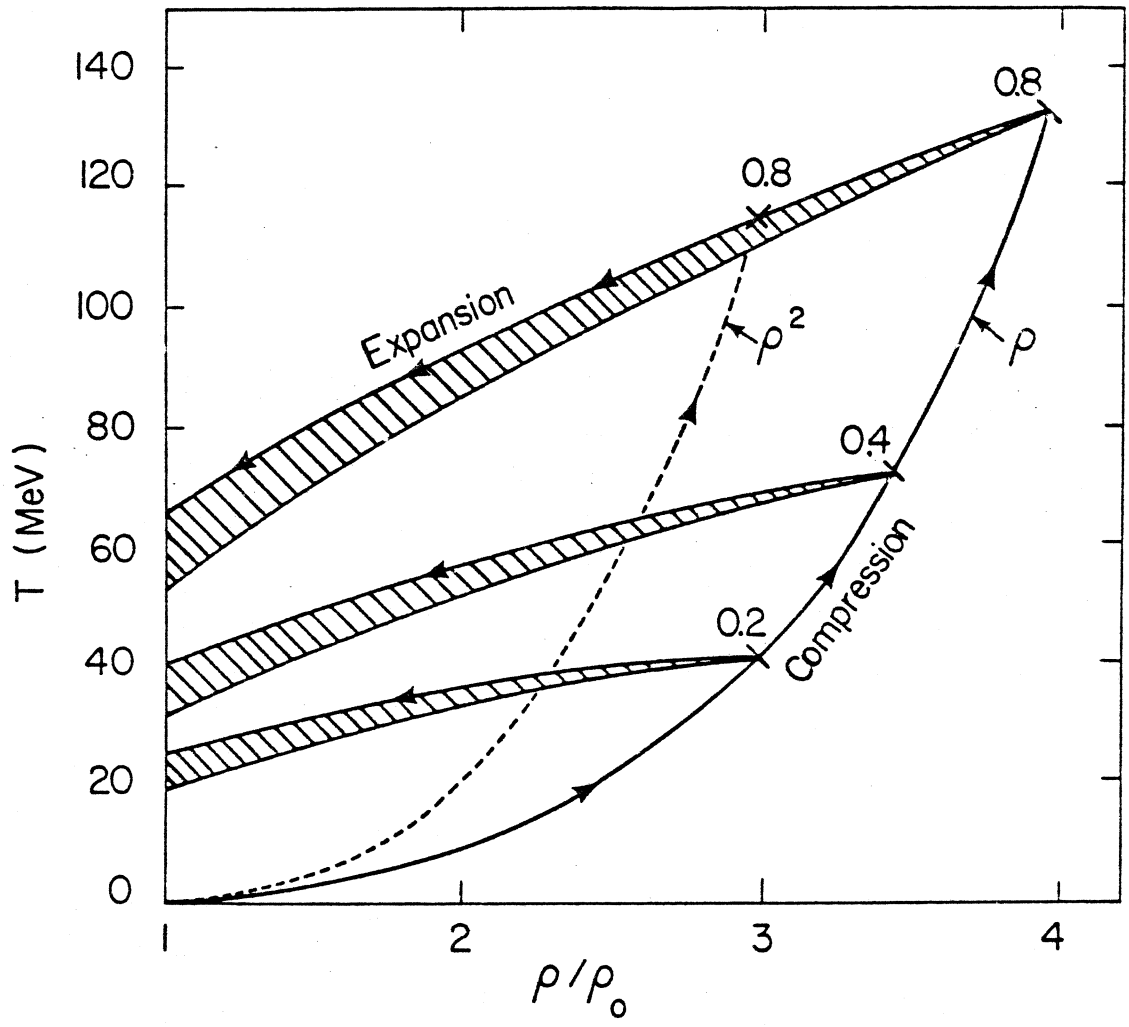
140
120
100
80
60
40
20
0
T (MeV)
1
2
3
4
ρ/ρ0
0.8
0.8
Expansion
ρ2
ρ
0.4
0.2
Compression
XBL 813-427

Figure 33

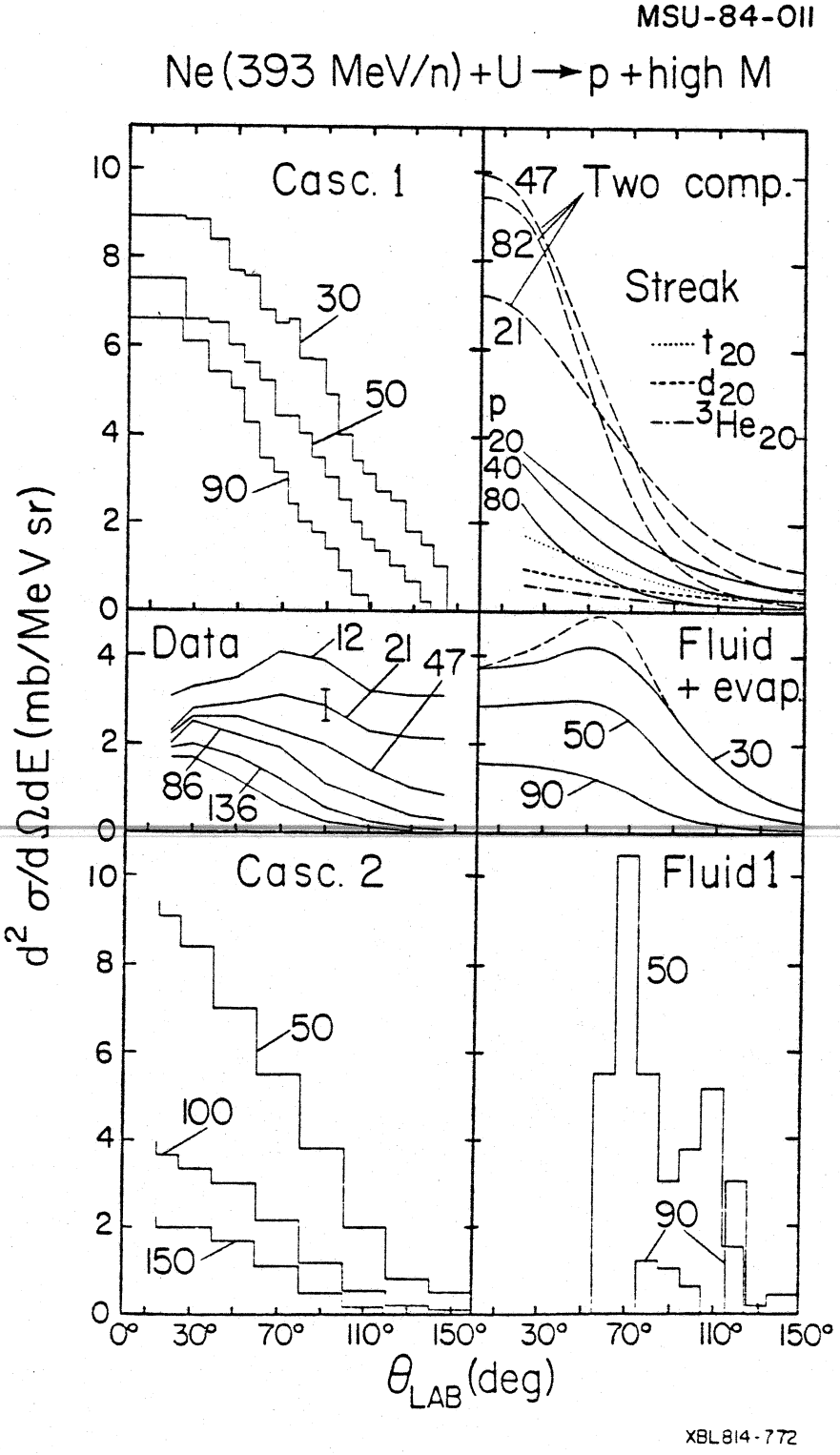
MSU-84-011
Ne(393 MeV/n)+U → p+high M
Casc. 1
30
50
90
47 Two comp.
82
Streak
21
t_{20}
d_{20}
$^3He_{20}$
p
20
40
80
Data
12
21
47
86
136
Fluid
+ evap.
50
30
90
Casc. 2
50
100
150
Fluid1
50
90
$d^2\sigma/d\Omega dE$ (mb/MeV sr)
0° 30° 70° 110° 150° 30° 70° 110° 150°
θ_{LAB} (deg)
XBL814-772

Figure 34

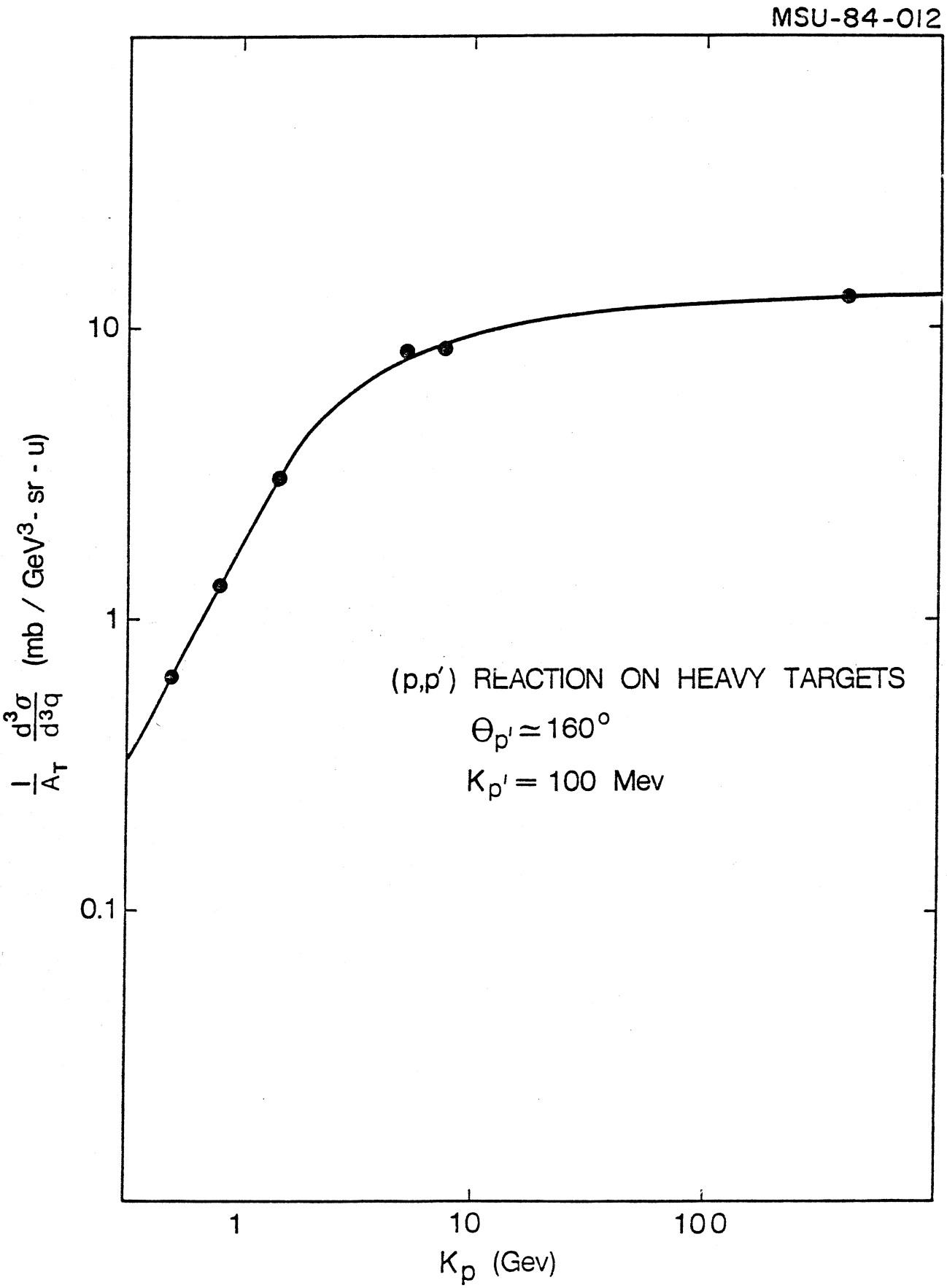
MSU-84-012
10
1
0.1
$\frac{1}{A_T}\frac{d^3\sigma}{d^3q}$ (mb / GeV^3 - sr - u)
(p,p′) REACTION ON HEAVY TARGETS
$\Theta_{p'} \simeq 160°$
$K_{p'} = 100$ Mev
1
10
100
K_p (Gev)

Figure 35

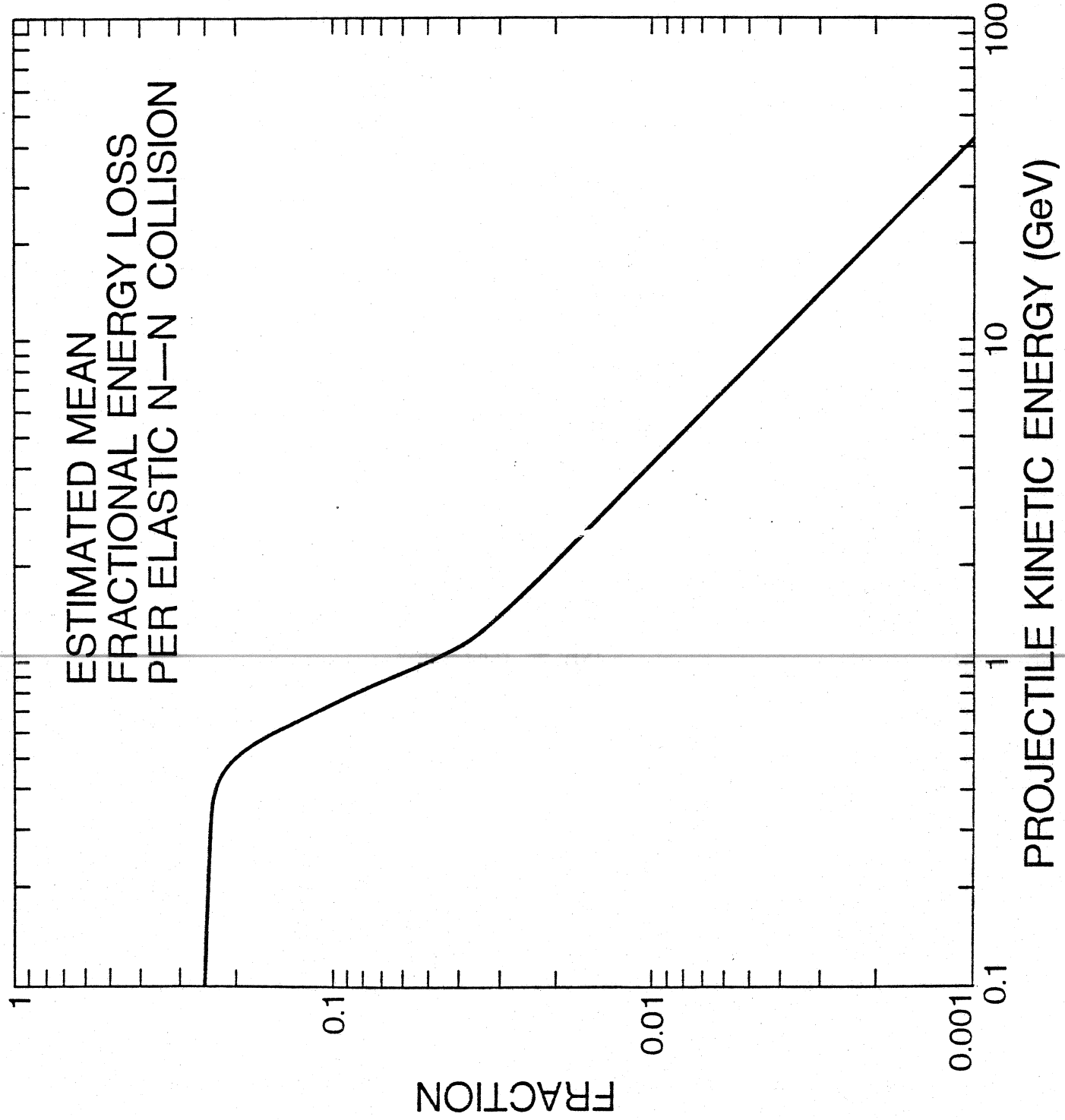
ESTIMATED MEAN
FRACTIONAL ENERGY LOSS
PER ELASTIC N—N COLLISION
FRACTION
1
0.1
0.01
0.001
0.1
1
10
100
PROJECTILE KINETIC ENERGY (GeV)

Figure 36

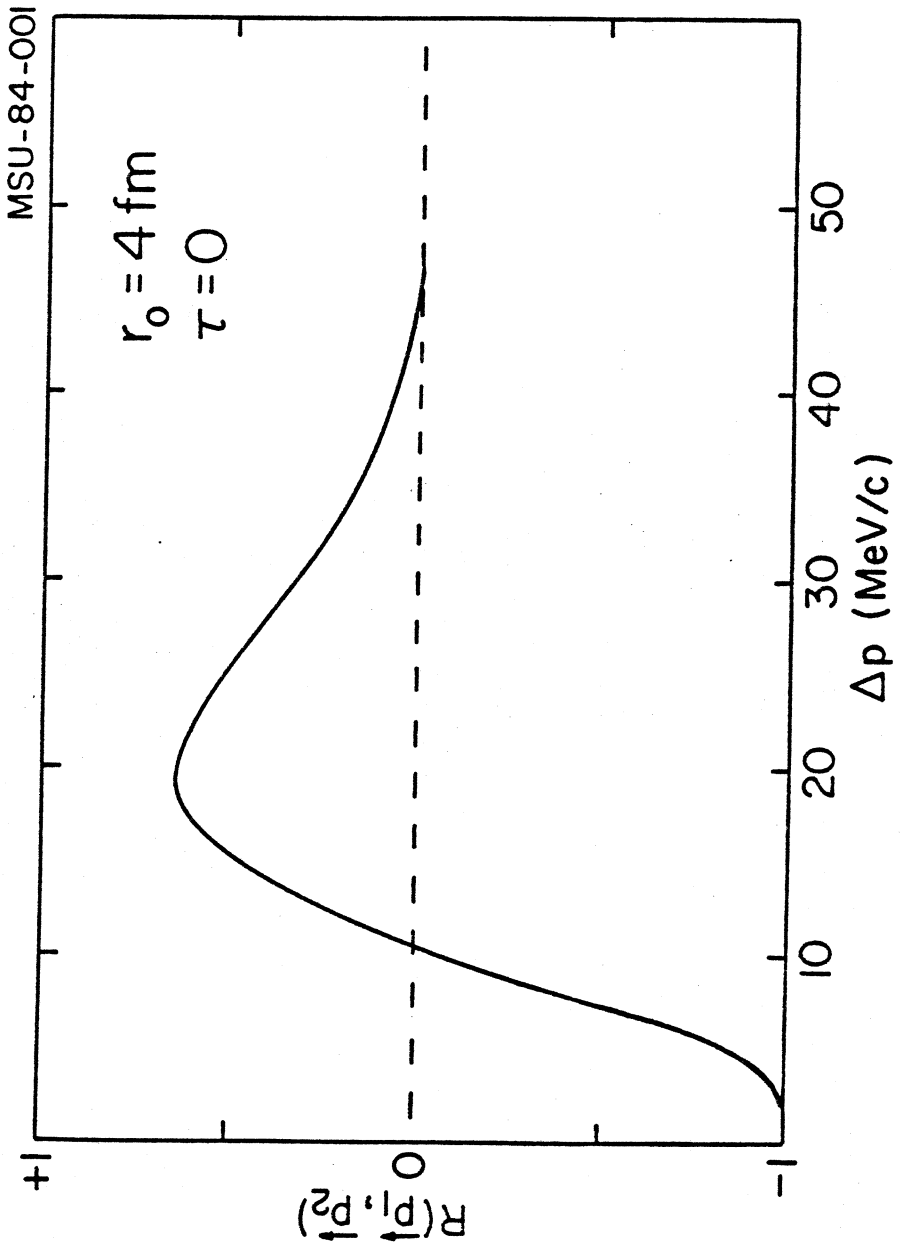

Figure 37

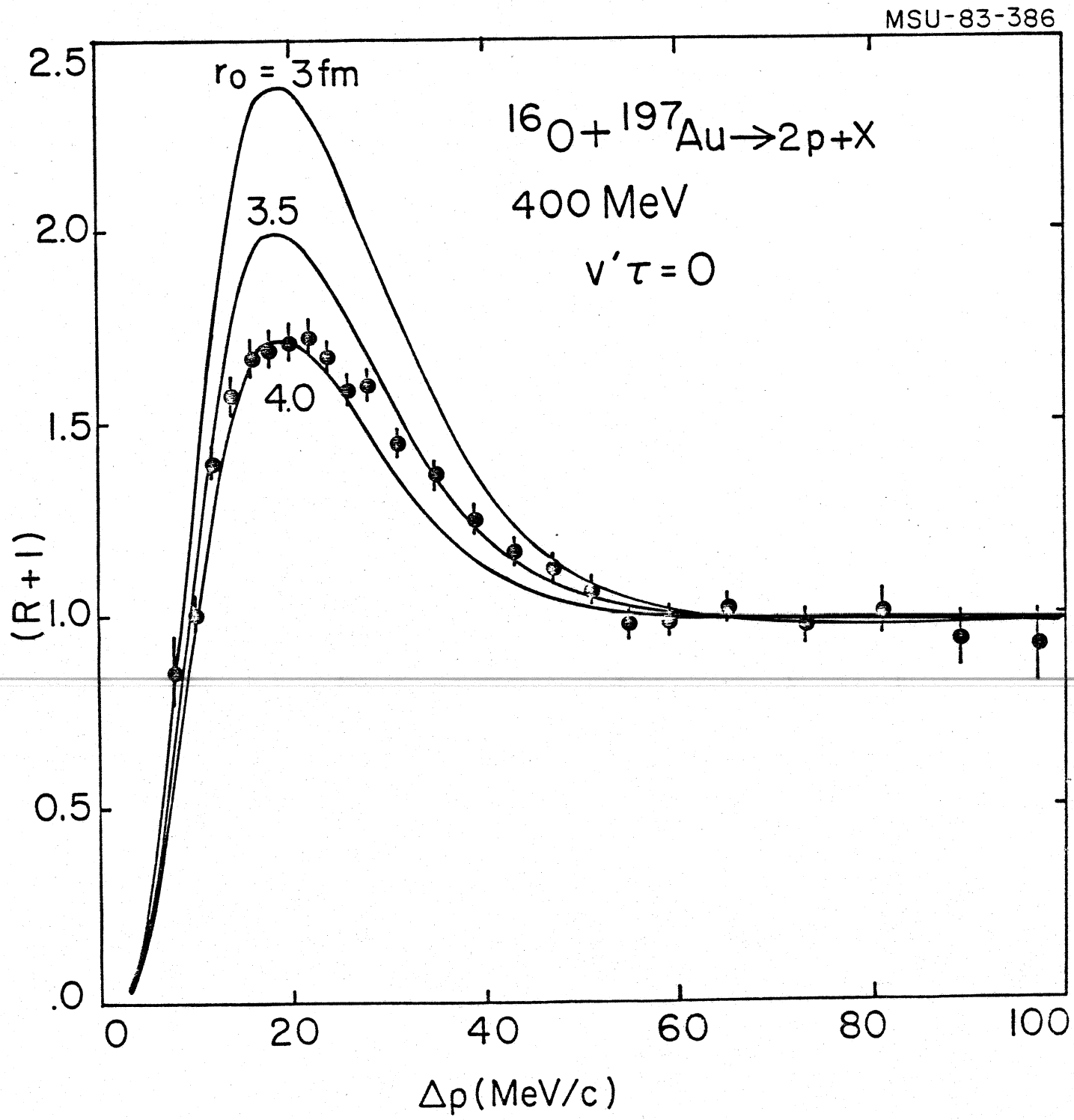
MSU-83-386
r_0 = 1 3fm
3.5
4.0
$^{16}O + ^{197}Au \rightarrow 2p + X$
400 MeV
$v'\tau = 0$
(R+1)
2.5
2.0
1.5
1.0
0.5
.0
0
20
40
60
80
100
Δp(MeV/c)

Figure 38

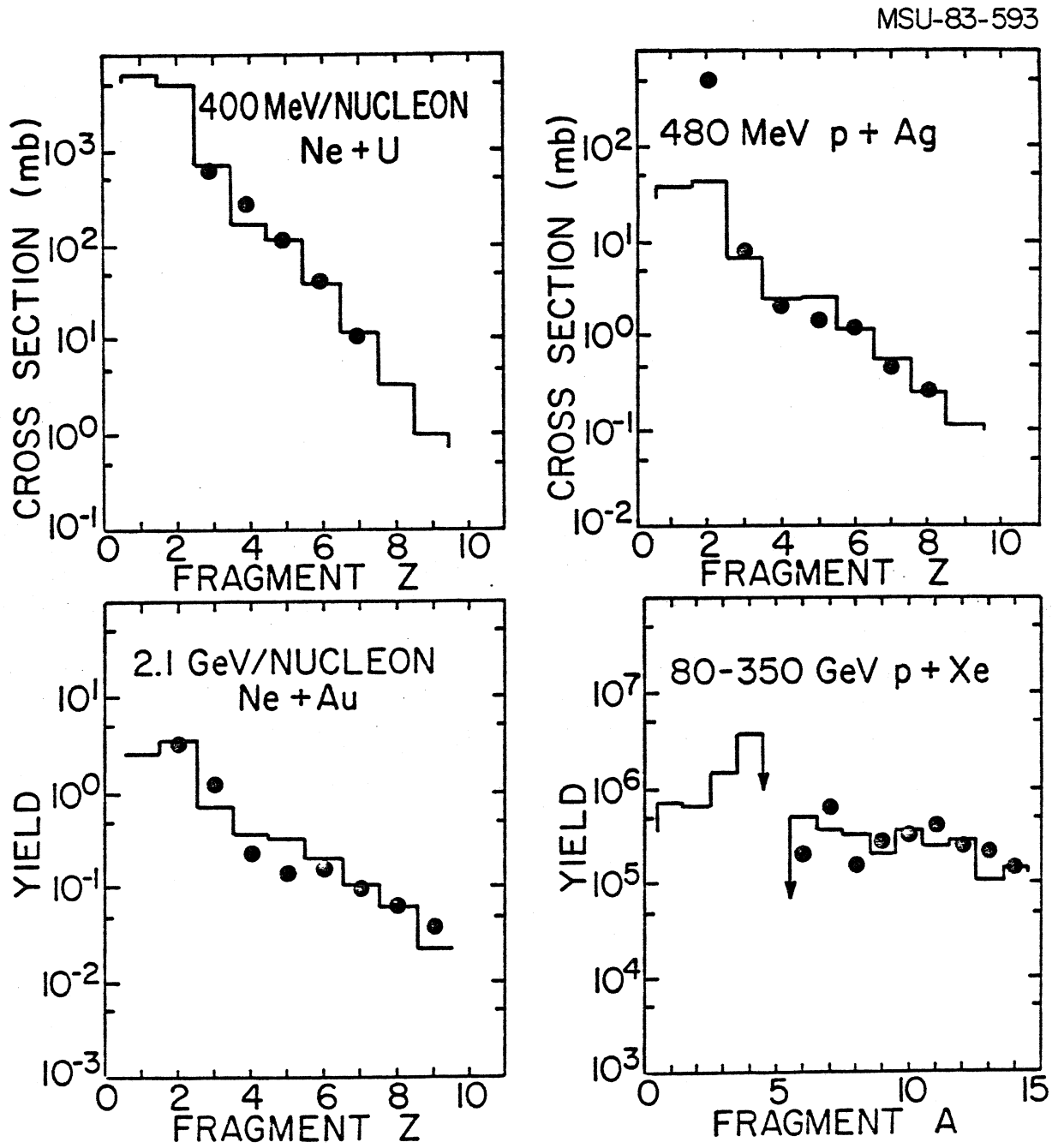
MSU-83-593
400 MeV/NUCLEON
Ne + U
CROSS SECTION (mb)
FRAGMENT Z
480 MeV p + Ag
CROSS SECTION (mb)
FRAGMENT Z
2.1 GeV/NUCLEON
Ne + Au
YIELD
FRAGMENT Z
80-350 GeV p + Xe
YIELD
FRAGMENT A

Figure 39

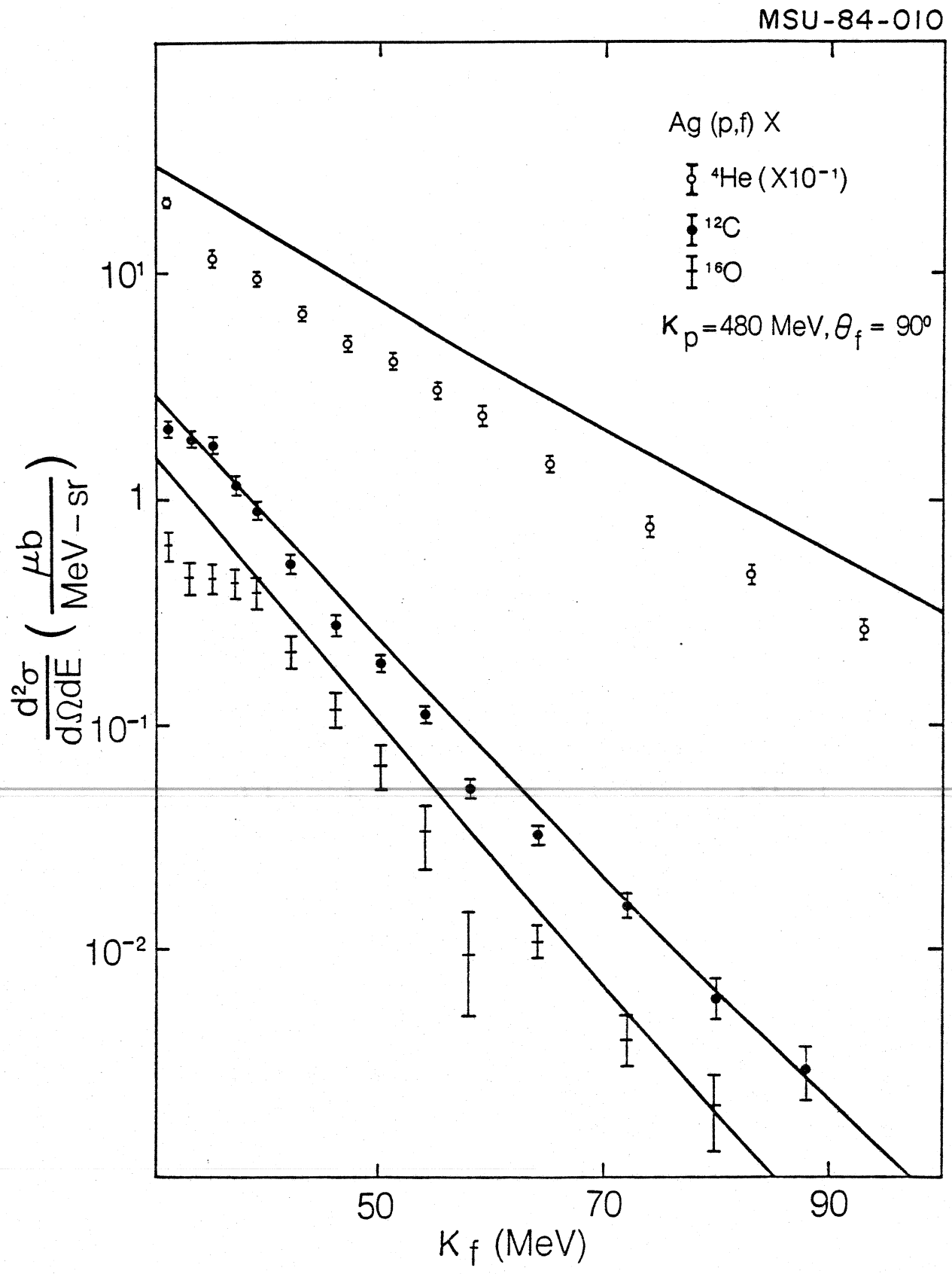
MSU-84-010
Ag (p,f) X
⁴He (X10⁻¹)
¹²C
¹⁶O
K p=480 MeV, θ f = 90°
d²σ/dΩdE (μb/MeV-sr)
10¹
1
10⁻¹
10⁻²
50
70
90
K f (MeV)

Figure 40

(a)

LOW MULTIPLICITY

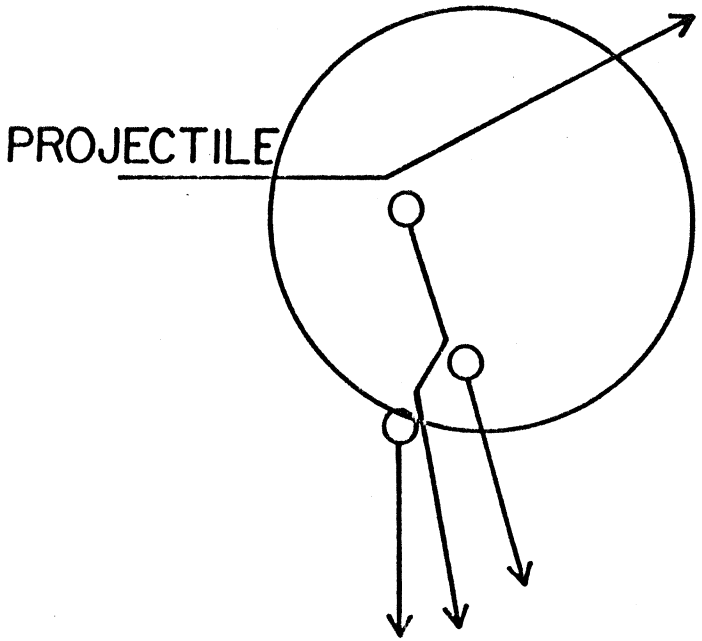

PICK-UP TO
FORM FRAGMENT

(b)

HIGH MULTIPLICITY

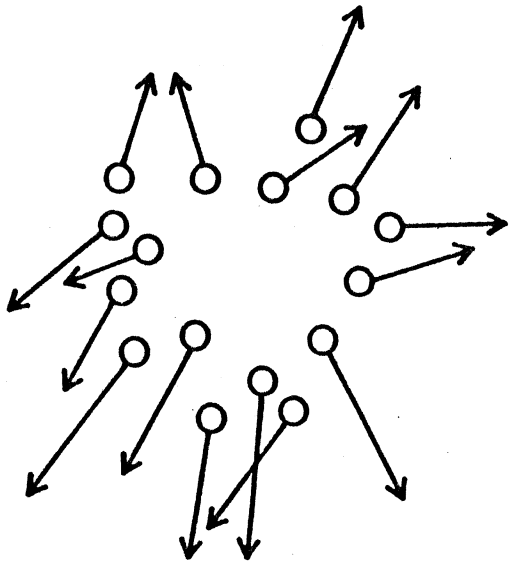

COALESCENCE TO
FORM FRAGMENT

Figure 41

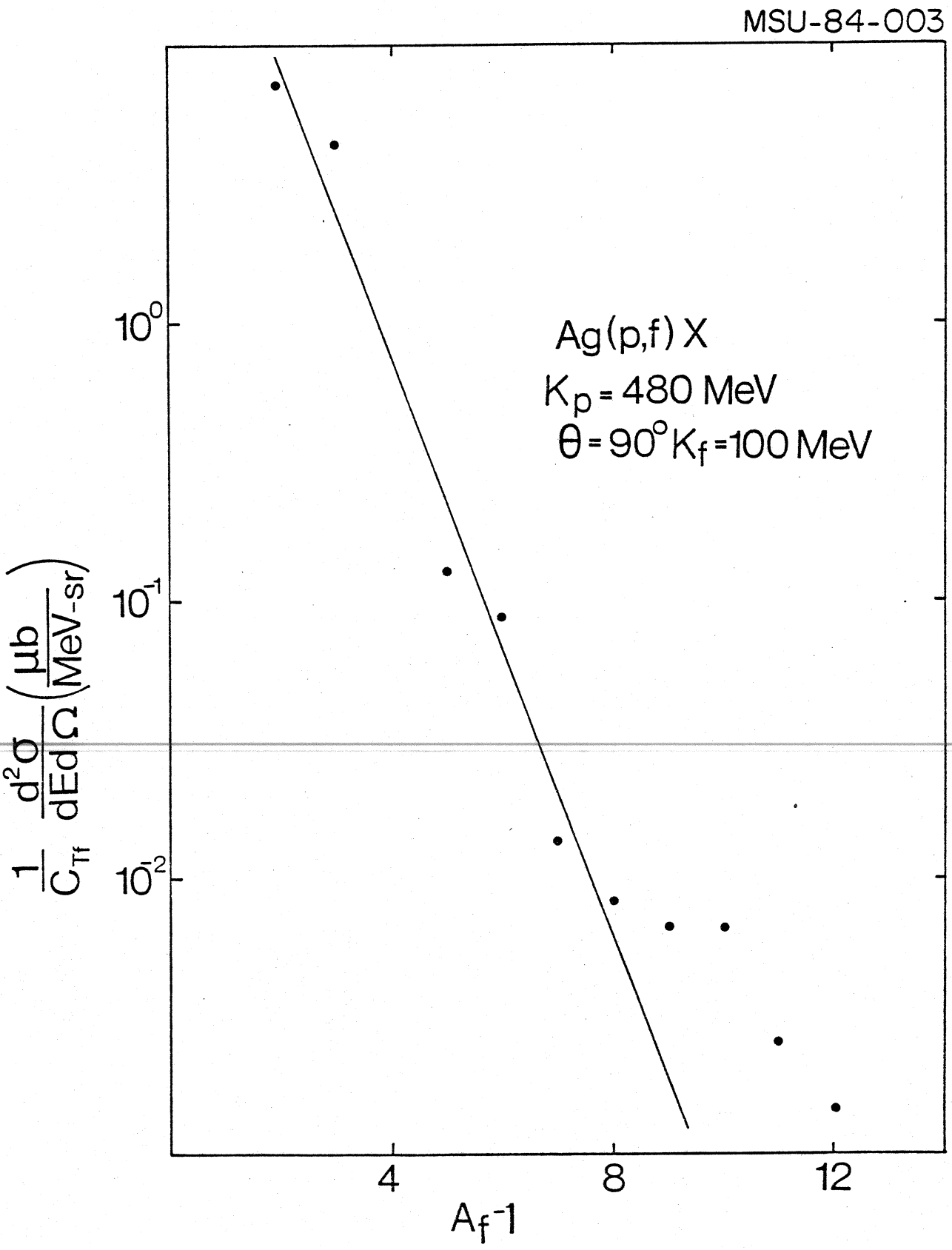
MSU-84-003
Ag(p,f) X
K_p = 480 MeV
θ = 90° K_f = 100 MeV
$\frac{1}{C_{Tf}} \frac{d^2\sigma}{dEd\Omega} \left(\frac{\mu b}{MeV\text{-}sr}\right)$
10^0
10^{-1}
10^{-2}
4
8
12
A_f^{-1}

Figure 42

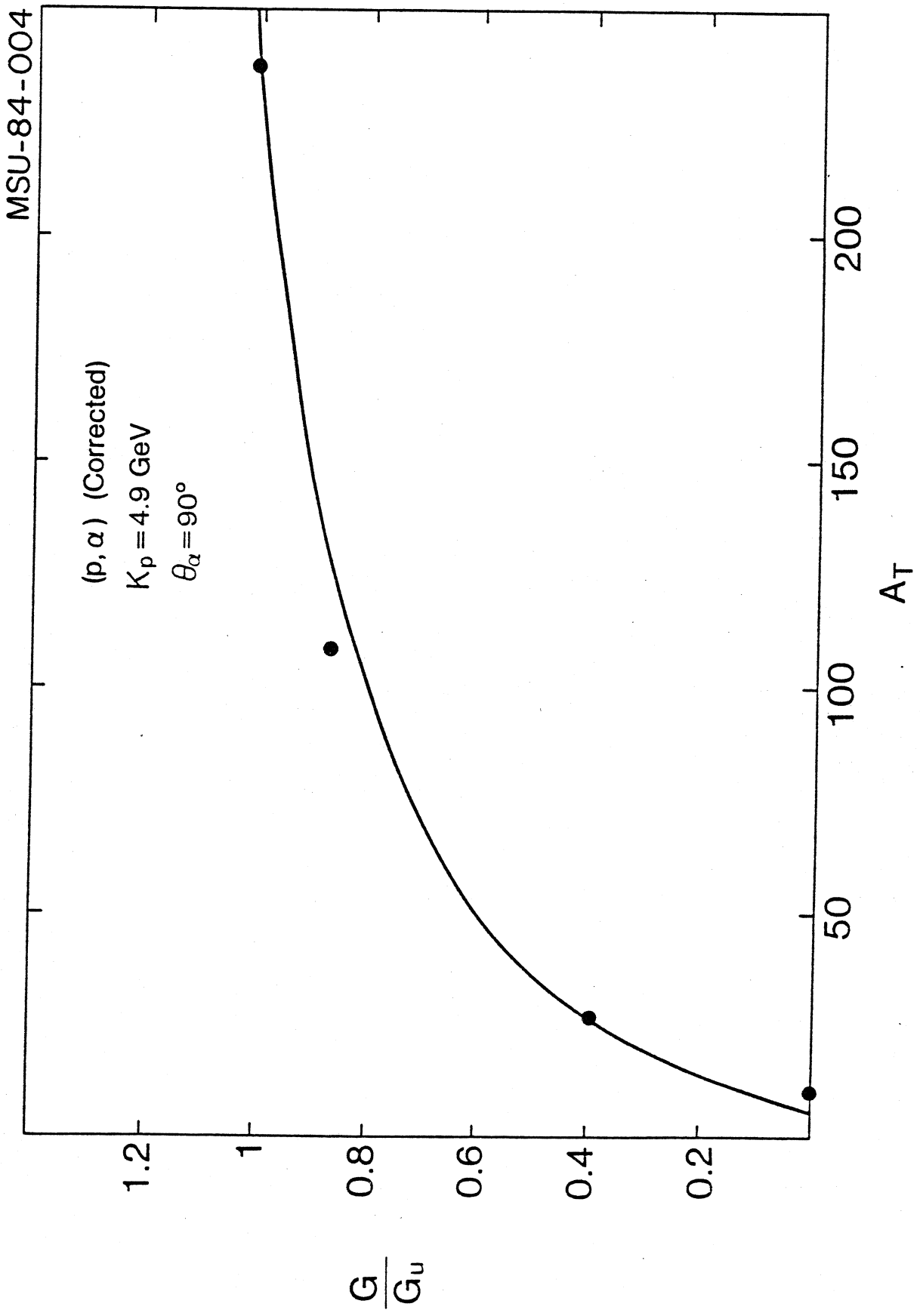
MSU-84-004
(p, α) (Corrected)
$K_p = 4.9$ GeV
$\theta_\alpha = 90°$
G/G_u
1.2
1
0.8
0.6
0.4
0.2
50
100
150
200
A_T

Figure 43

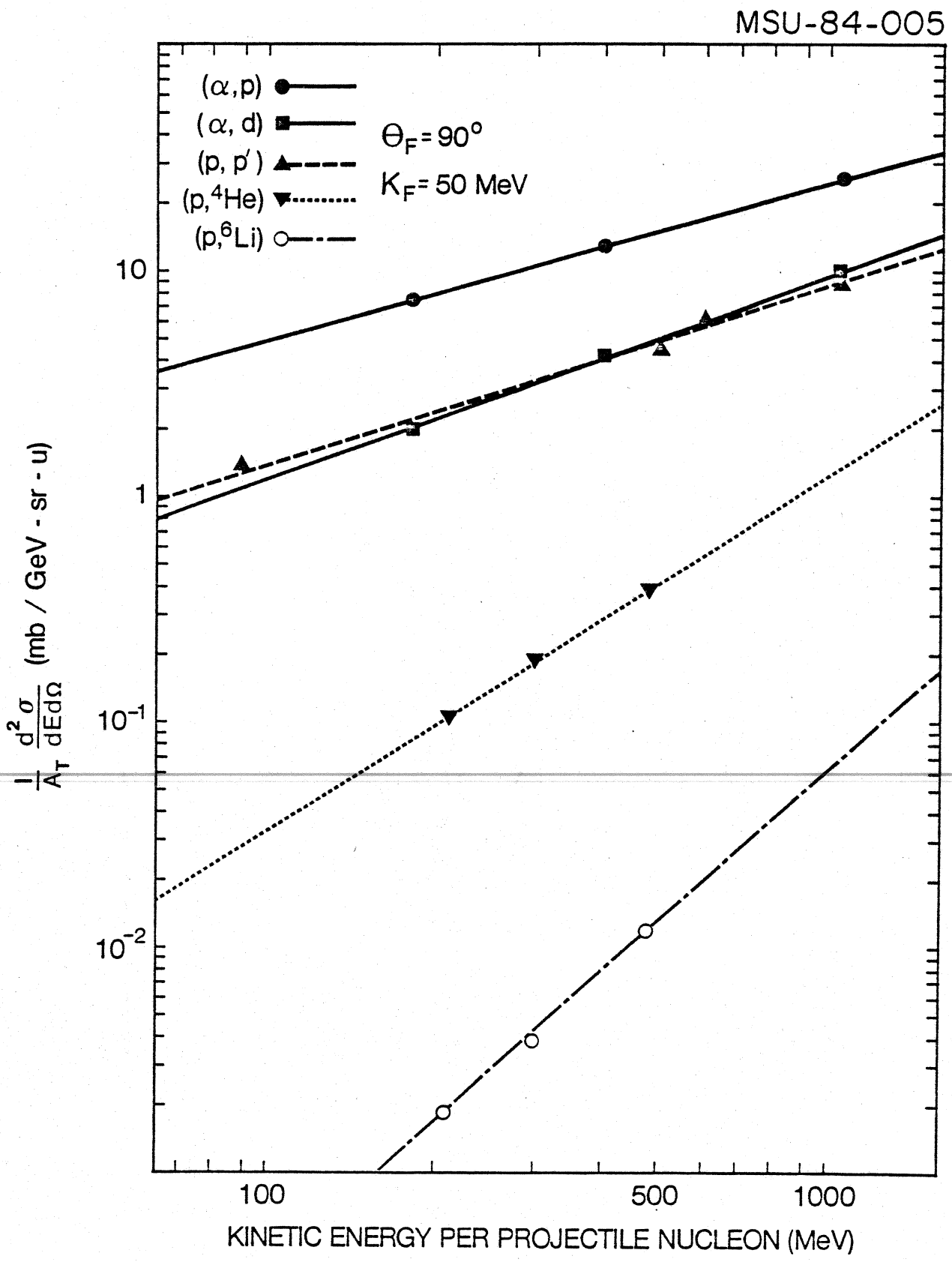
MSU-84-005
(α,p)
(α, d)
(p, p′)
(p,⁴He)
(p,⁶Li)
Θ_F = 90°
K_F = 50 MeV
10
1
10⁻¹
10⁻²
100
500
1000
KINETIC ENERGY PER PROJECTILE NUCLEON (MeV)
1/A_T d²σ/dEdΩ (mb / GeV - sr - u)

Figure 44

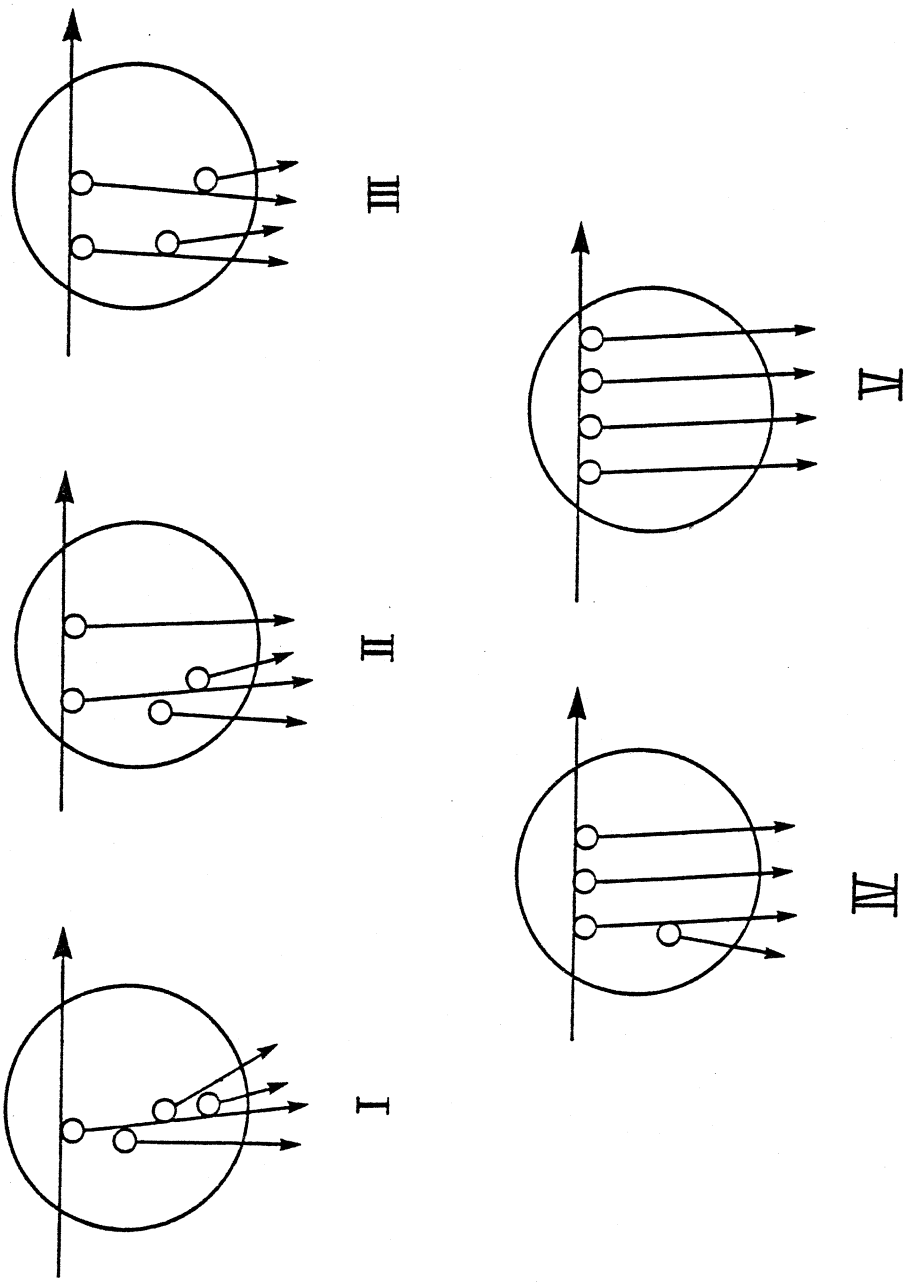

Figure 45

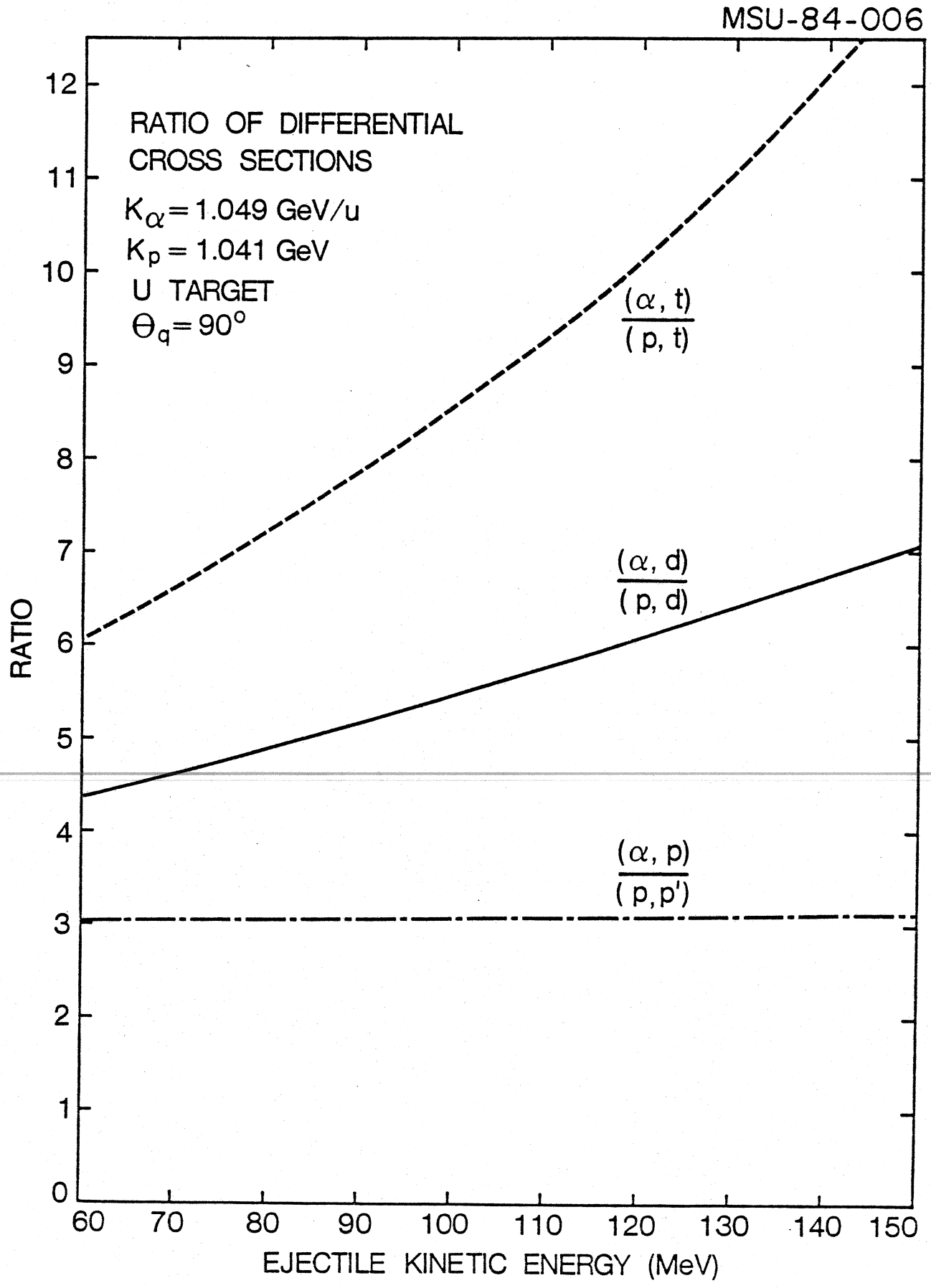
MSU-84-006
RATIO OF DIFFERENTIAL
CROSS SECTIONS
$K_\alpha = 1.049$ GeV/u
$K_p = 1.041$ GeV
U TARGET
$\Theta_q = 90^\circ$
$\frac{(\alpha, t)}{(p, t)}$
$\frac{(\alpha, d)}{(p, d)}$
$\frac{(\alpha, p)}{(p, p')}$
RATIO
EJECTILE KINETIC ENERGY (MeV)
0
1
2
3
4
5
6
7
8
9
10
11
12
60
70
80
90
100
110
120
130
140
150

Figure 46

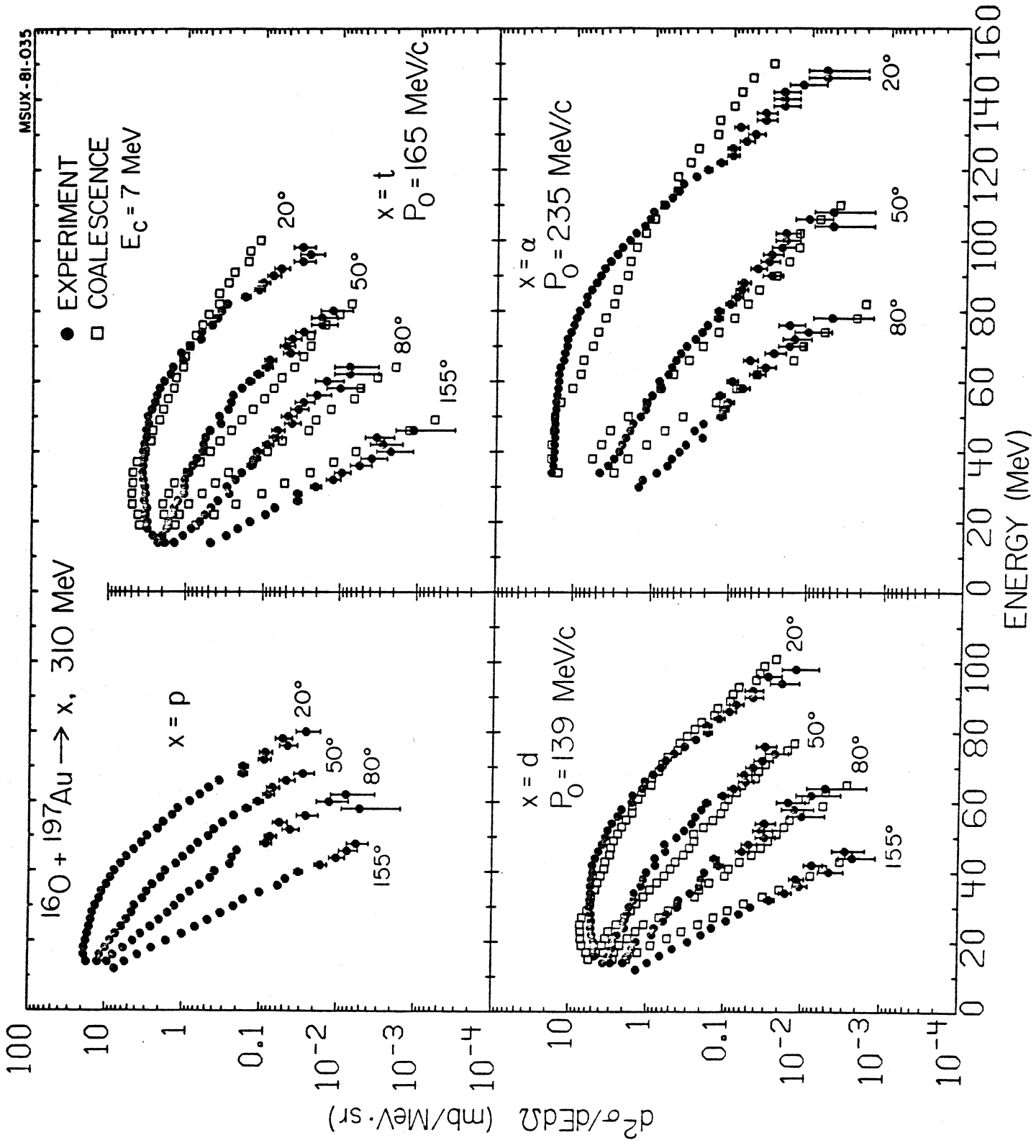
MSUX-81-035
$^{16}O + ^{197}Au \rightarrow x$, 310 MeV
● EXPERIMENT
□ COALESCENCE
E_c = 7 MeV
x = p
x = t
P_0 = 165 MeV/c
x = d
P_0 = 139 MeV/c
x = α
P_0 = 235 MeV/c
20°
50°
80°
155°
$d^2\sigma/dE d\Omega$ (mb/MeV·sr)
ENERGY (MeV)

Figure 47

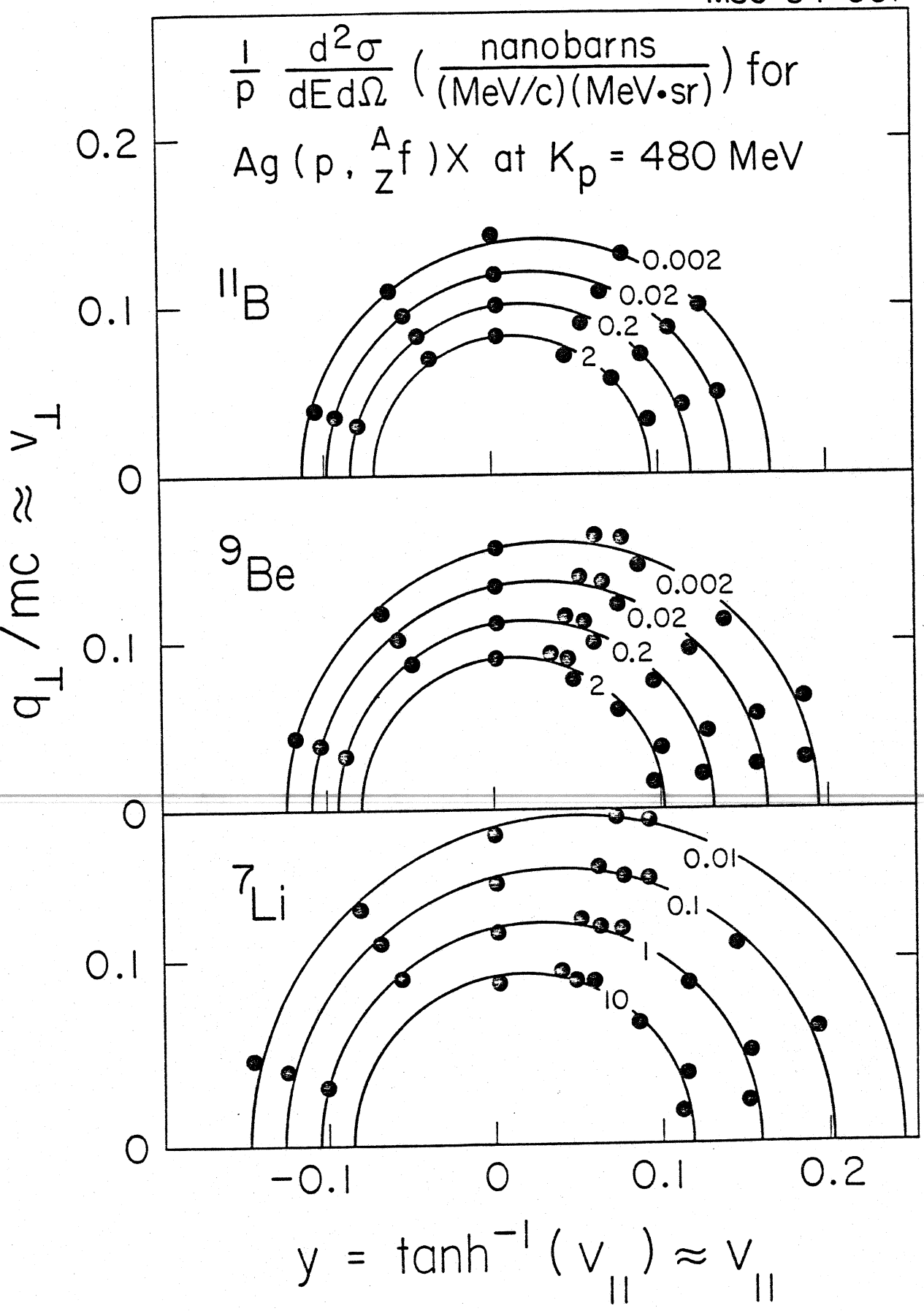
$\frac{1}{p}\frac{d^2\sigma}{dE\,d\Omega}\left(\frac{\text{nanobarns}}{(\text{MeV/c})(\text{MeV}\cdot\text{sr})}\right)$ for
Ag (p , $^{A}_{Z}$f) X at K_p = 480 MeV
^{11}B
0.002
0.02
0.2
2
^{9}Be
0.002
0.02
0.2
2
^{7}Li
0.01
0.1
1
10
0.2
0.1
0
0.1
0
0
0.1
−0.1
0
0.1
0.2
$q_\perp/mc \approx v_\perp$
$y = \tanh^{-1}(v_{\parallel}) \approx v_{\parallel}$

Figure 48

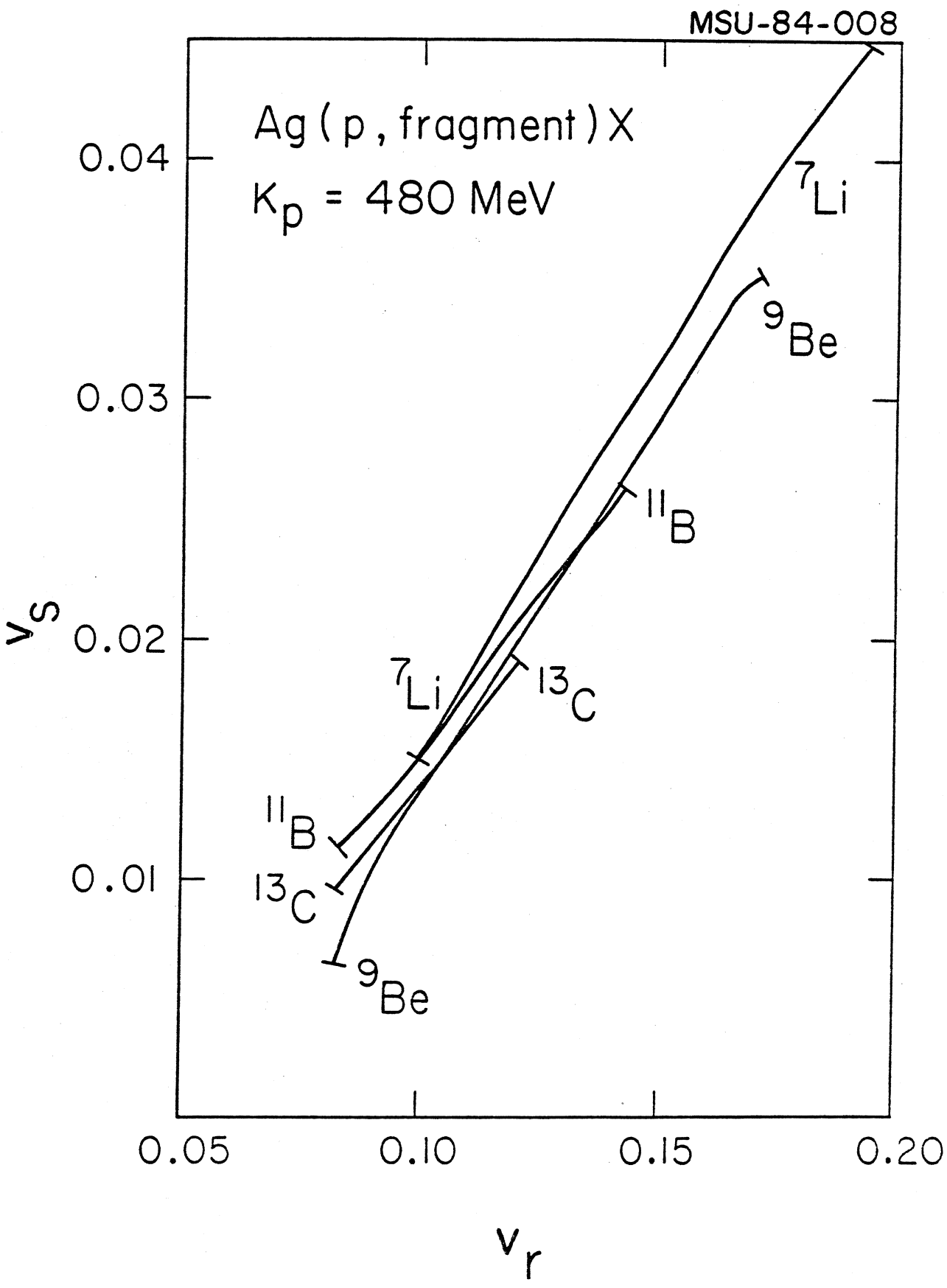
MSU-84-008
Ag (p , fragment) X
K_p = 480 MeV
0.04
0.03
0.02
0.01
v_s
0.05
0.10
0.15
0.20
v_r
^{7}Li
^{9}Be
^{11}B
^{13}C
^{7}Li
^{13}C
^{11}B
^{9}Be

Figure 49

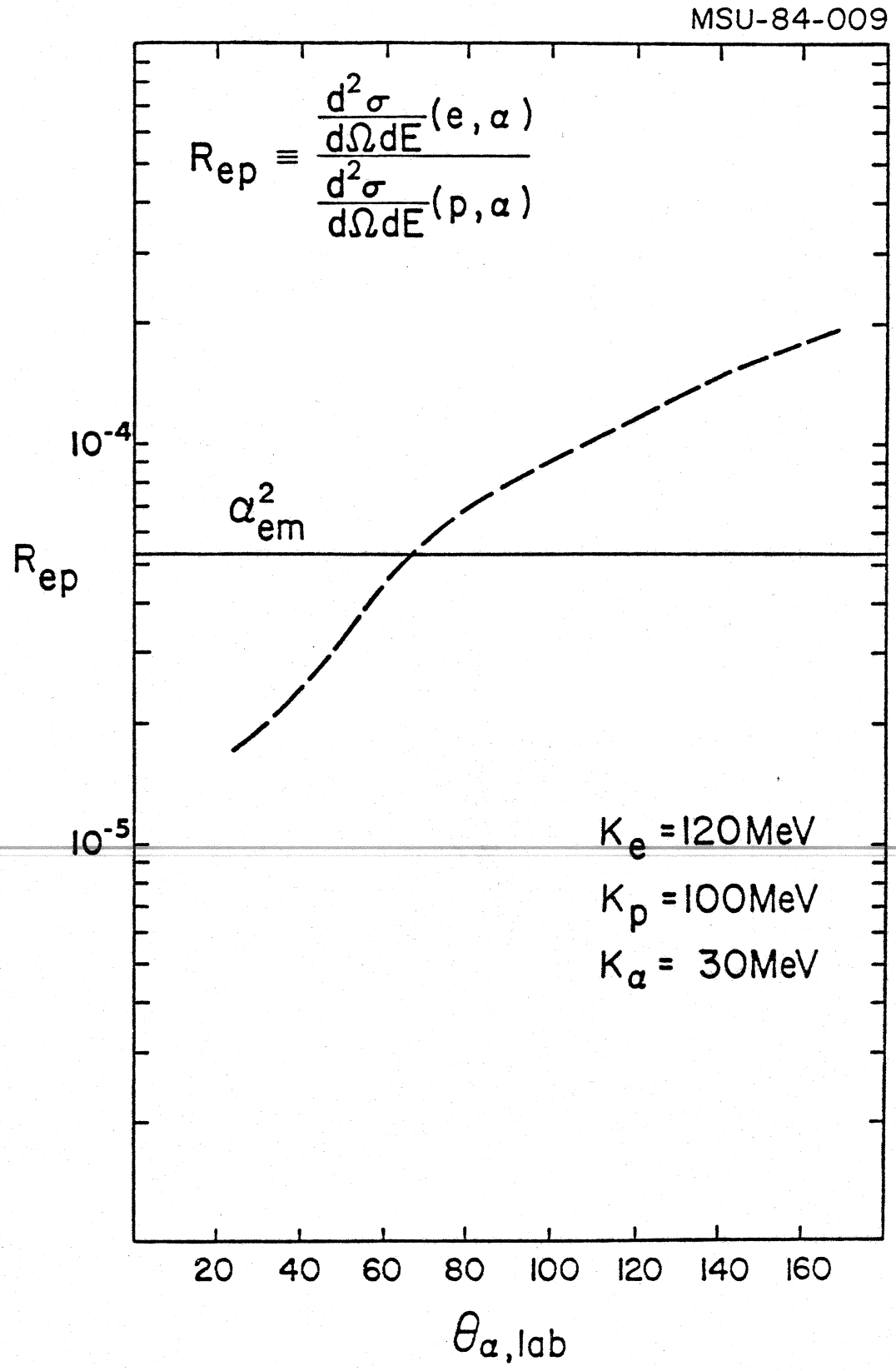
MSU-84-009
$R_{ep} \equiv \frac{\frac{d^2\sigma}{d\Omega dE}(e,\alpha)}{\frac{d^2\sigma}{d\Omega dE}(p,\alpha)}$
10^{-4}
α^2_{em}
R_{ep}
10^{-5}
K_e = 120MeV
K_p = 100MeV
K_α = 30MeV
20
40
60
80
100
120
140
160
$\theta_{\alpha,lab}$

Figure 50

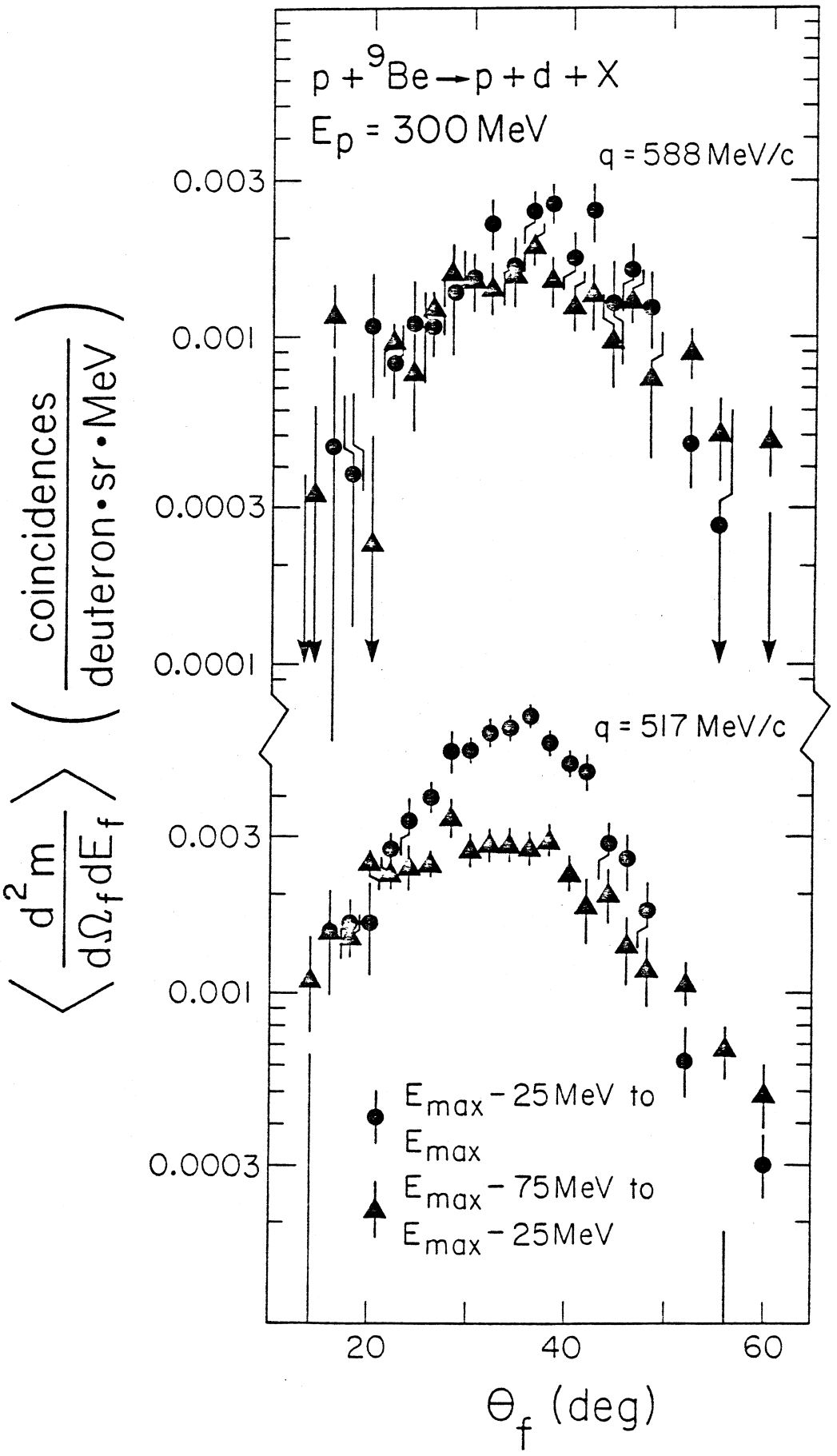
p + 9Be → p + d + X
Ep = 300 MeV
q = 588 MeV/c
q = 517 MeV/c
0.003
0.001
0.0003
0.0001
Emax - 25 MeV to Emax
Emax - 75 MeV to Emax - 25 MeV
20
40
60
θf (deg)
⟨ d²m / dΩf dEf ⟩ (coincidences / deuteron • sr • MeV)

Figure 51

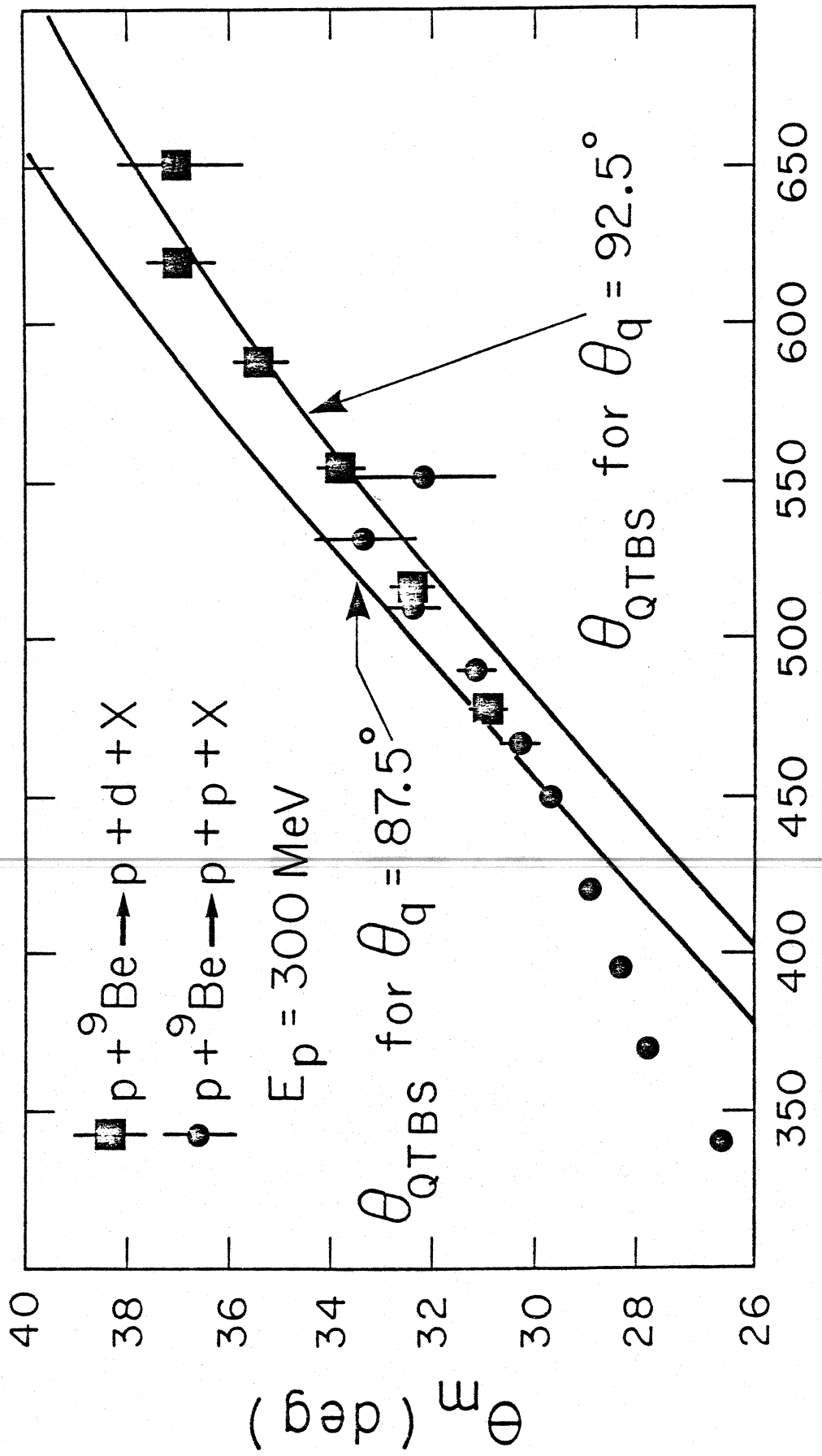
Θ_m (deg)
40
38
36
34
32
30
28
26
q (MeV/c)
350
400
450
500
550
600
650
$p + {}^9Be \rightarrow p + d + X$
$p + {}^9Be \rightarrow p + p + X$
$E_p = 300$ MeV
θ_{QTBS} for $\theta_q = 87.5°$
θ_{QTBS} for $\theta_q = 92.5°$

Figure 52

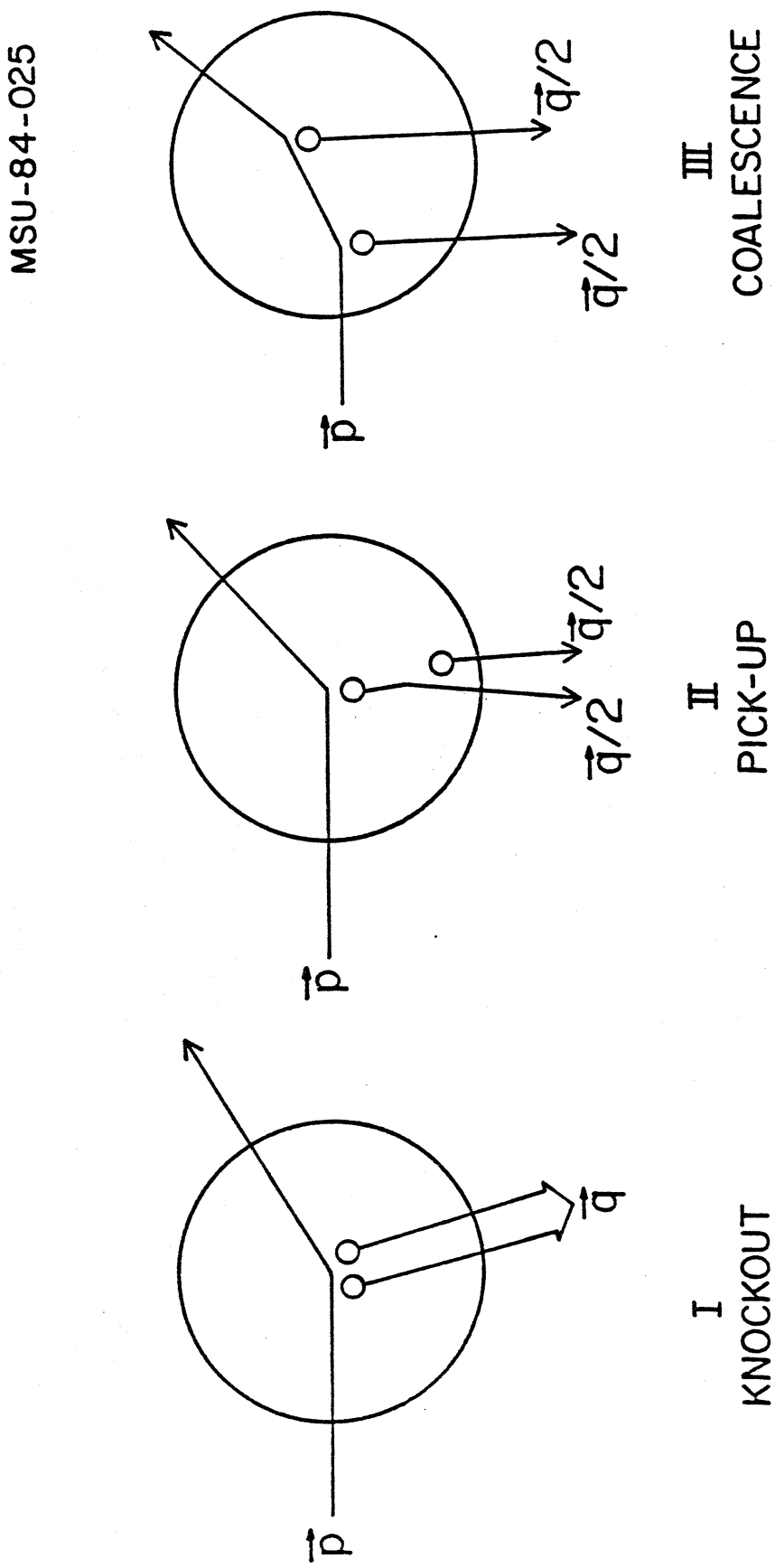
MSU-84-025
III
COALESCENCE
II
PICK-UP
I
KNOCKOUT
p
q/2
q/2
q/2
q/2
p
q
p

Figure 54

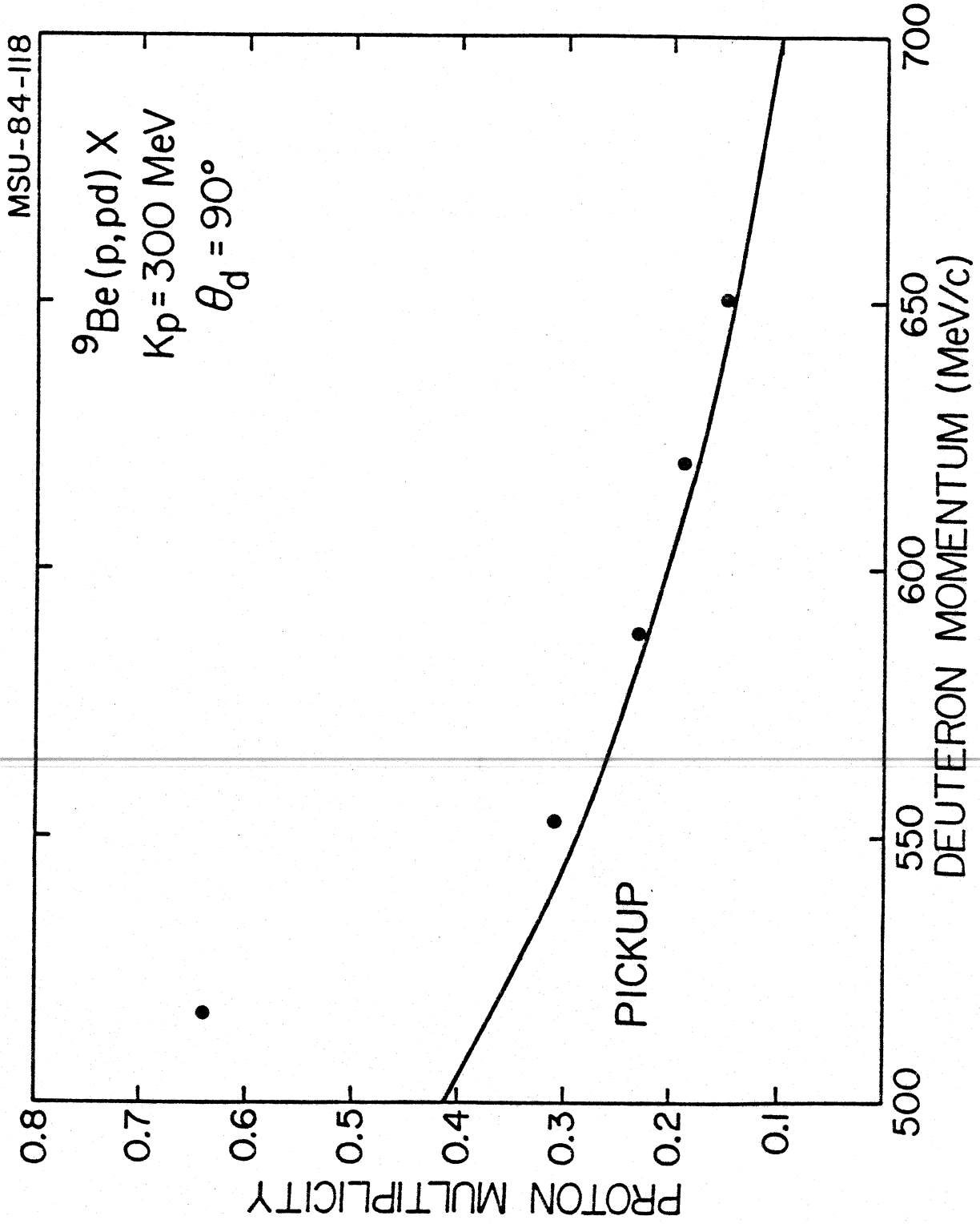
MSU-84-118
^{9}Be(p,pd) X
Kp = 300 MeV
θ_d = 90°
PICKUP
PROTON MULTIPLICITY
DEUTERON MOMENTUM (MeV/c)
0.8
0.7
0.6
0.5
0.4
0.3
0.2
0.1
500
550
600
650
700

Figure 53

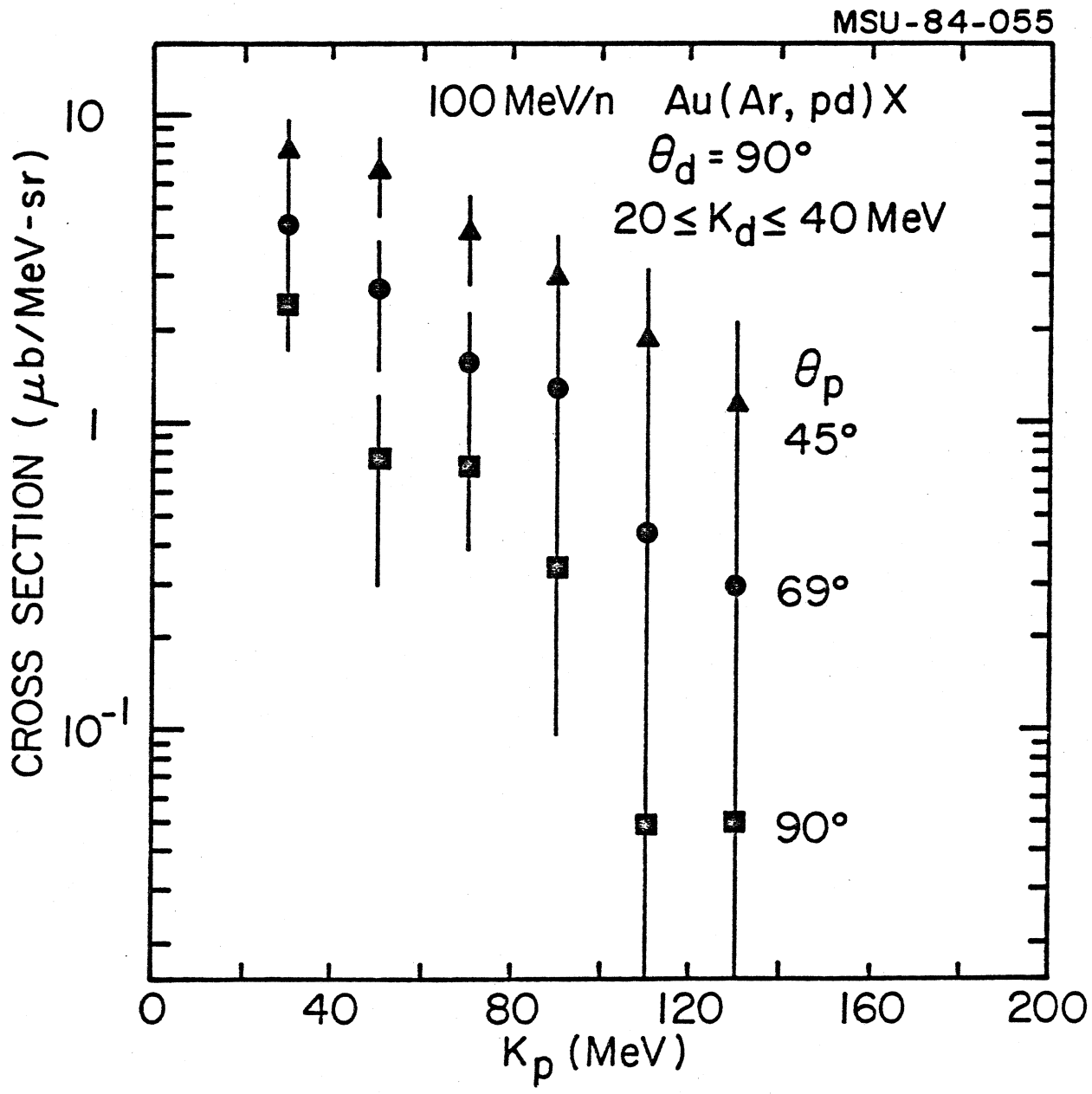
MSU-84-055
100 MeV/n Au(Ar, pd) X
$\theta_d = 90°$
$20 \leq K_d \leq 40$ MeV
θ_p
45°
69°
90°
CROSS SECTION (μb/MeV-sr)
10
1
10^{-1}
0
40
80
120
160
200
K_p (MeV)

Figure 55

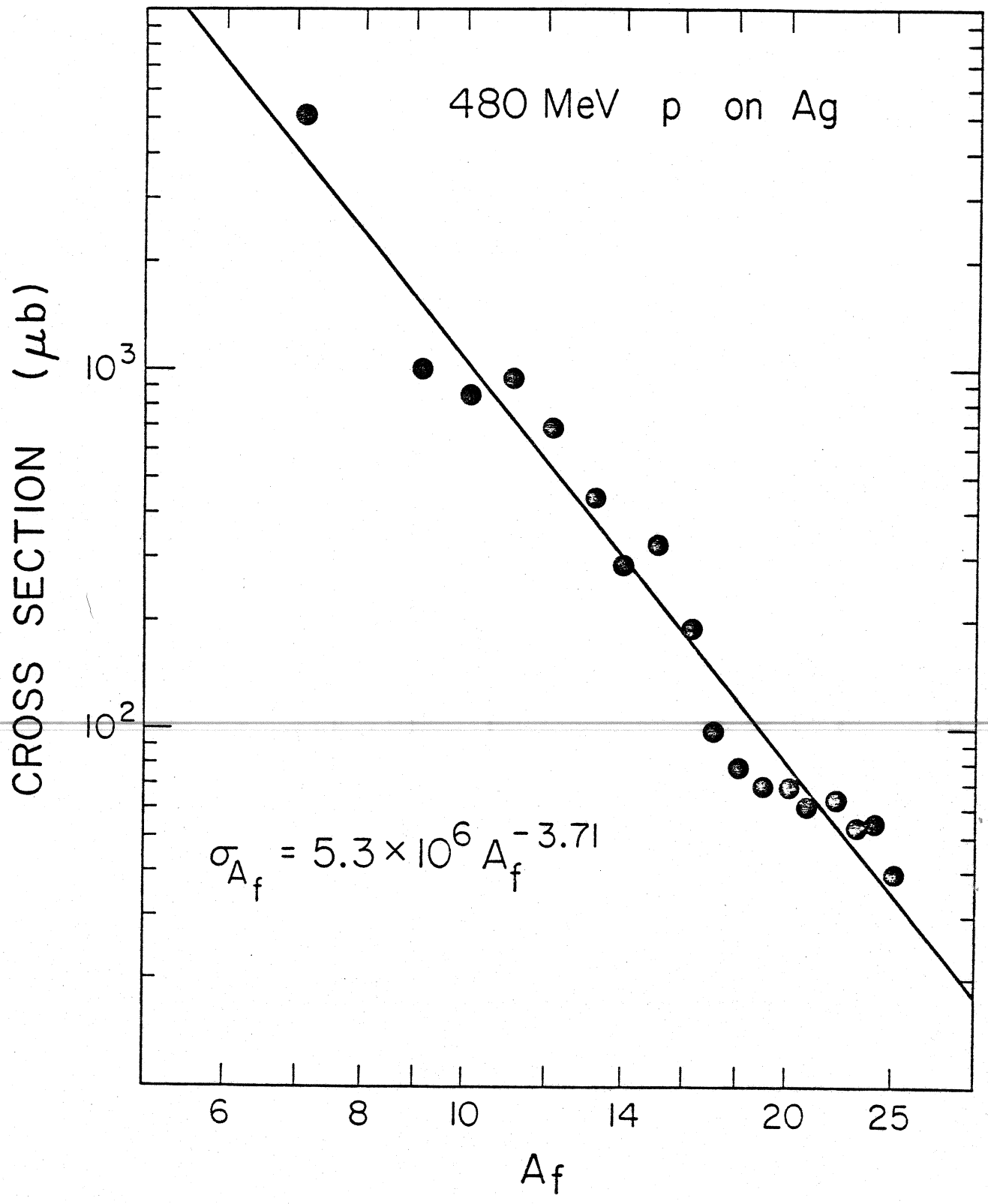
480 MeV p on Ag
CROSS SECTION (μb)
10^3
10^2
$\sigma_{A_f} = 5.3 \times 10^6 A_f^{-3.71}$
6
8
10
14
20
25
A_f

Figure 56

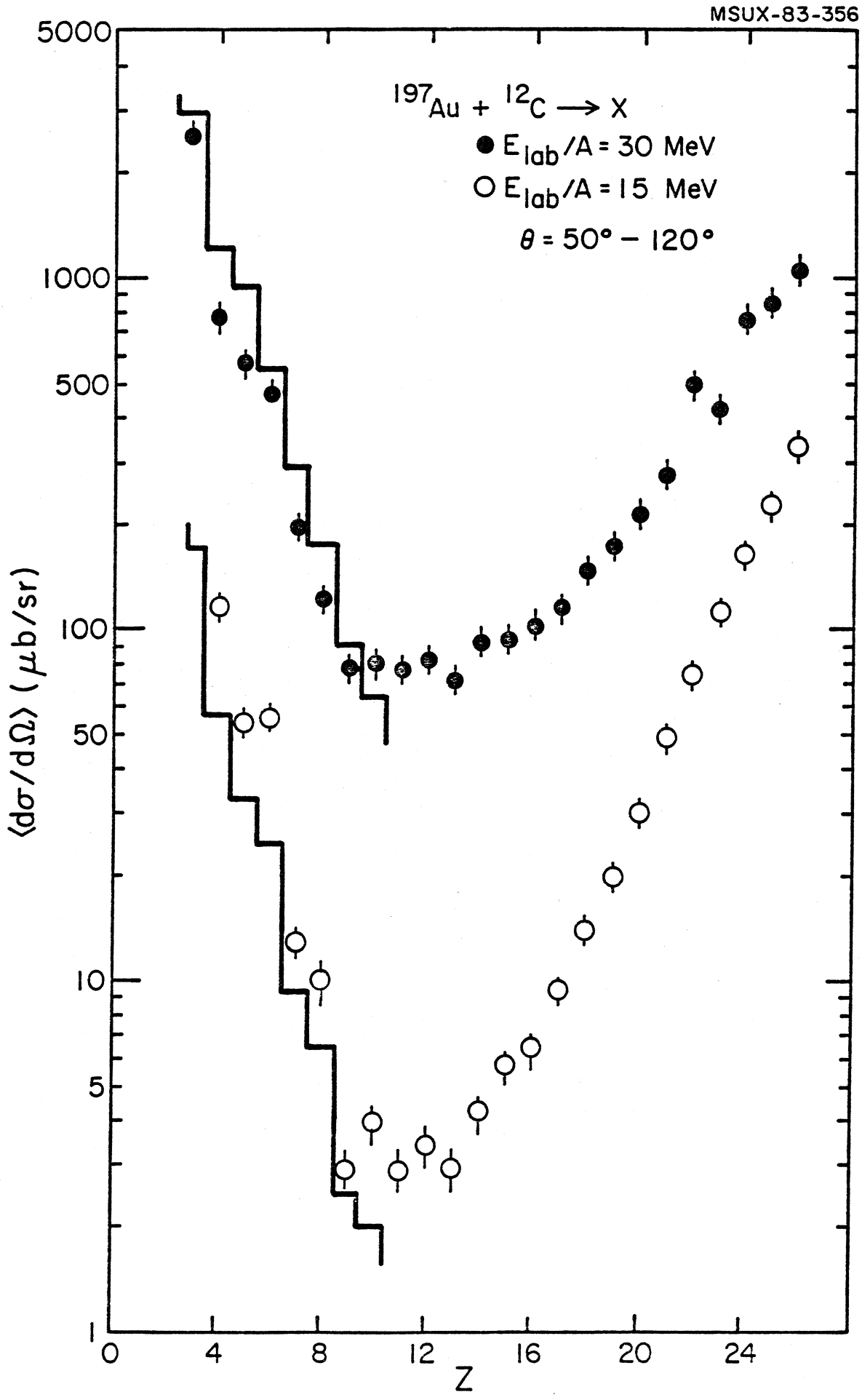
MSUX-83-356
$^{197}Au + ^{12}C \rightarrow X$
● $E_{lab}/A = 30$ MeV
○ $E_{lab}/A = 15$ MeV
$\theta = 50° - 120°$
$\langle d\sigma/d\Omega \rangle$ (μb/sr)
5000
1000
500
100
50
10
5
1
0
4
8
12
16
20
24
Z

Figure 57

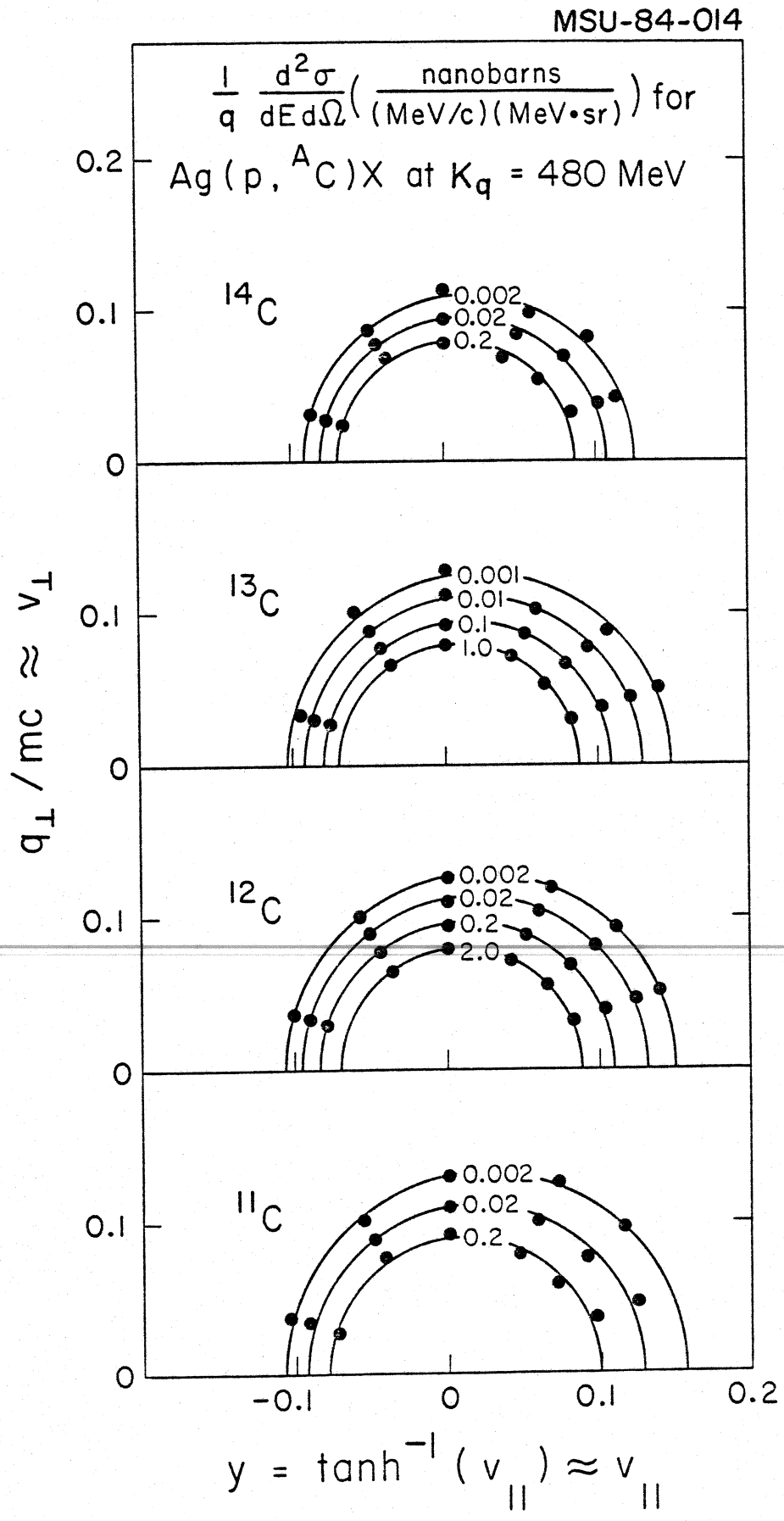
MSU-84-014
$\frac{1}{q}\frac{d^2\sigma}{dE\,d\Omega}\left(\frac{\text{nanobarns}}{(\text{MeV/c})(\text{MeV}\cdot\text{sr})}\right)$ for
Ag(p, ^{A}C)X at K_q = 480 MeV
^{14}C
0.002
0.02
0.2
^{13}C
0.001
0.01
0.1
1.0
^{12}C
0.002
0.02
0.2
2.0
^{11}C
0.002
0.02
0.2
0.2
0.1
0
-0.1
$q_\perp/mc \approx v_\perp$
$y = \tanh^{-1}(v_{\parallel}) \approx v_{\parallel}$

Figure 58

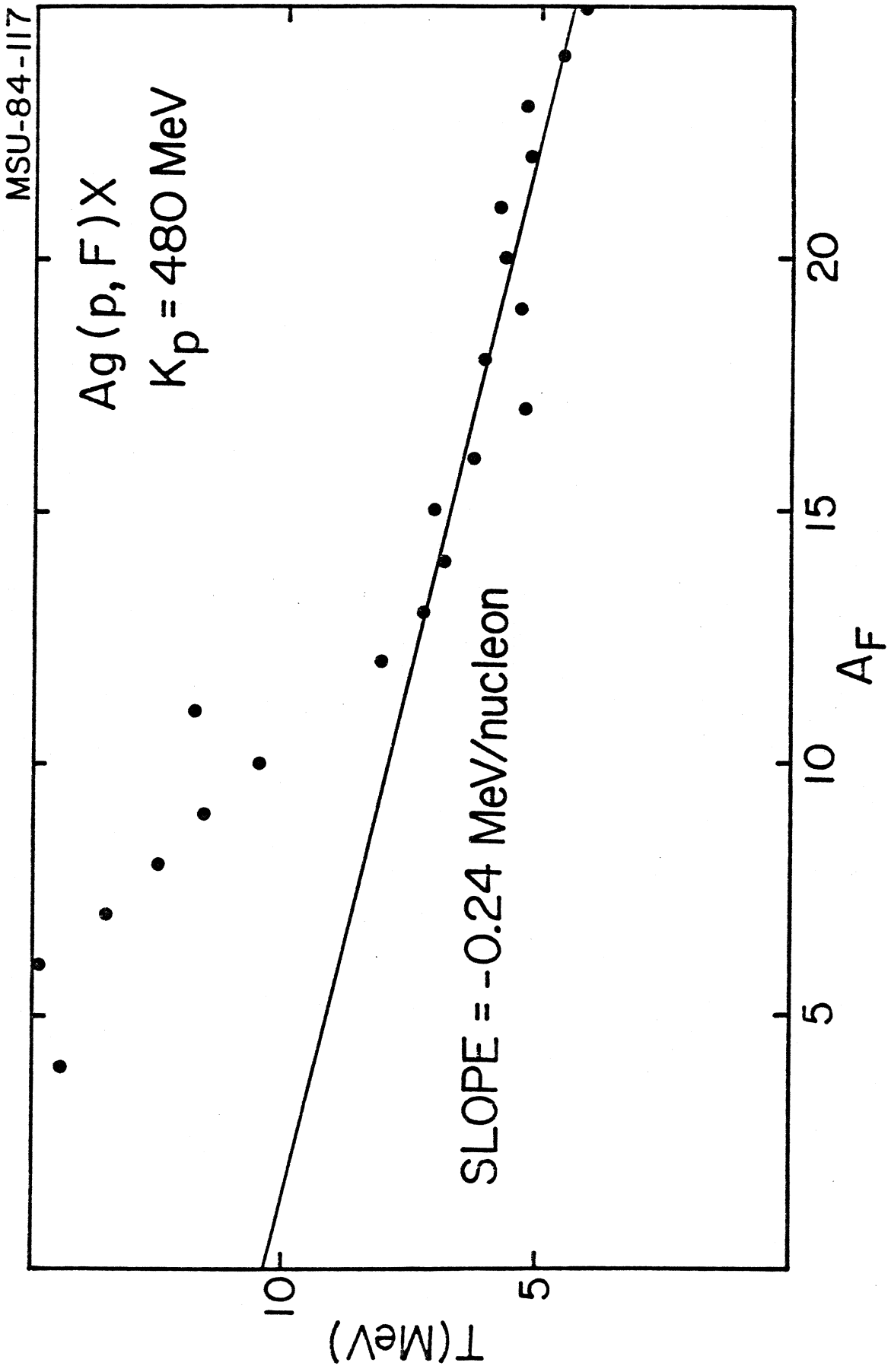
MSU-84-117
Ag(p, F)X
K_p = 480 MeV
SLOPE = -0.24 MeV/nucleon
T(MeV)
A_F
10
5
5
10
15
20

Figure 59

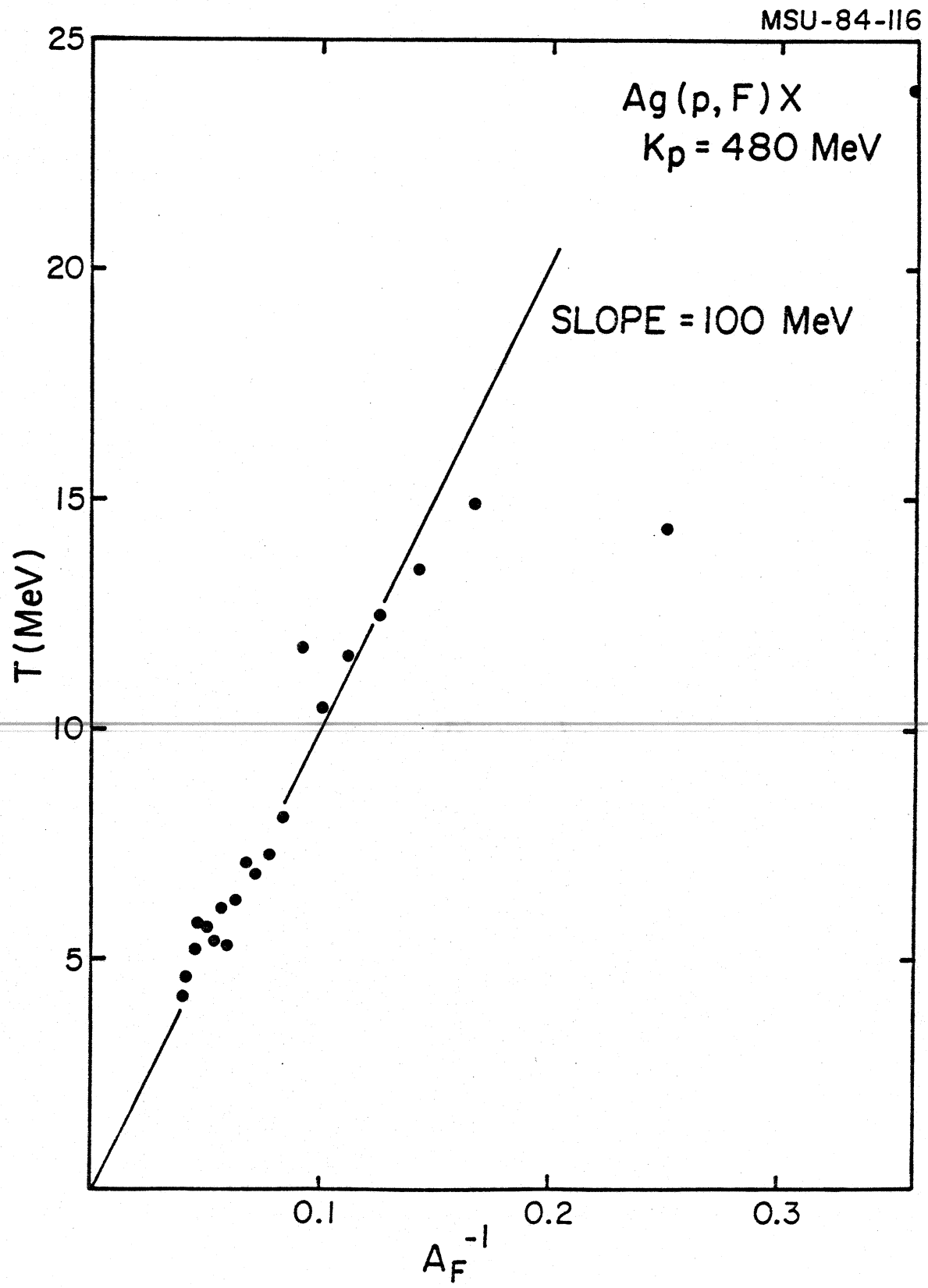
MSU-84-116
Ag (p, F) X
Kp = 480 MeV
SLOPE = 100 MeV
T (MeV)
25
20
15
10
5
0.1
0.2
0.3
A_F^{-1}

Figure 60

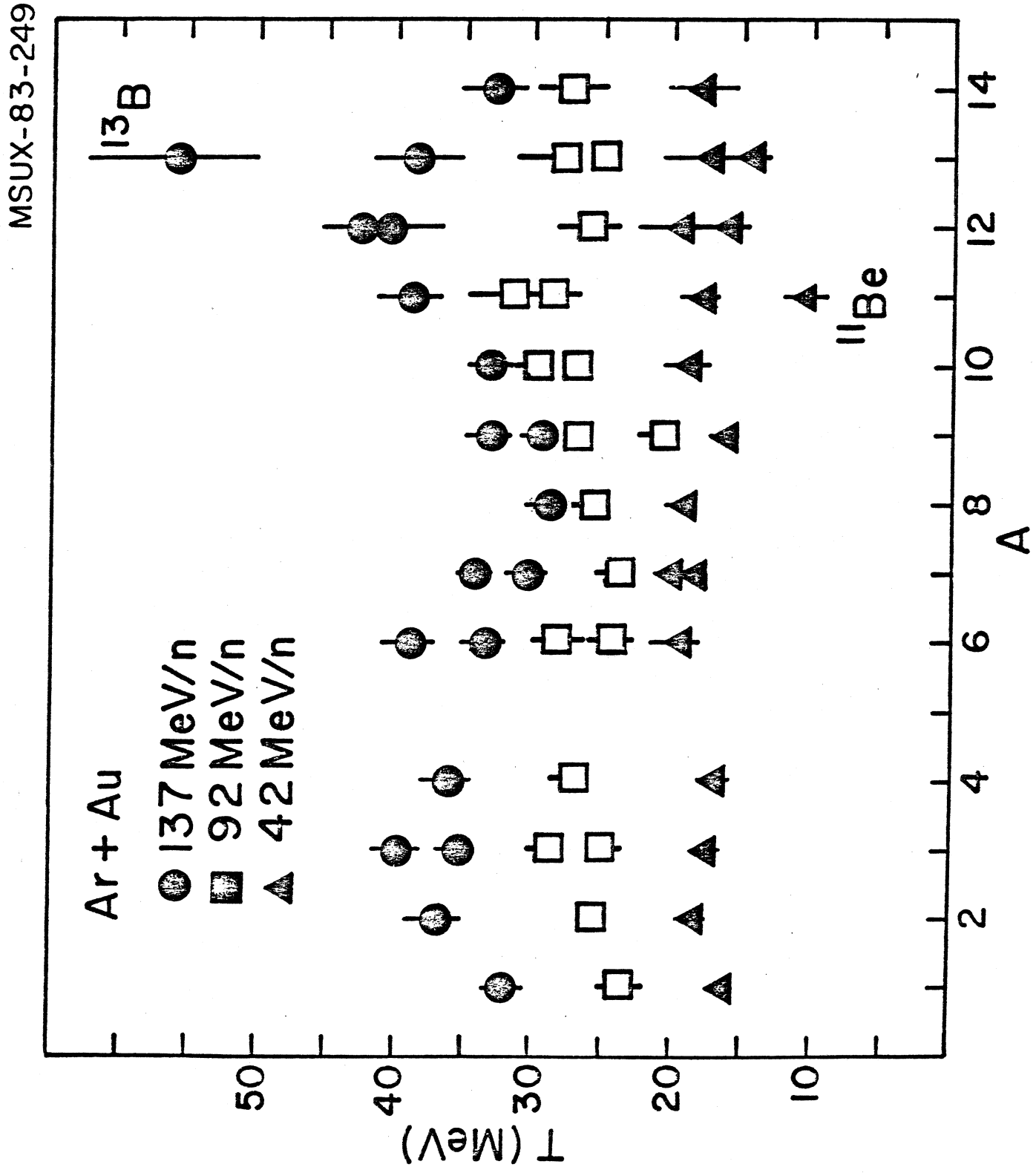
MSUX-83-249
Ar + Au
137 MeV/n
92 MeV/n
42 MeV/n
^{13}B
^{11}Be
T (MeV)
A
50
40
30
20
10
2
4
6
8
10
12
14

Figure 61

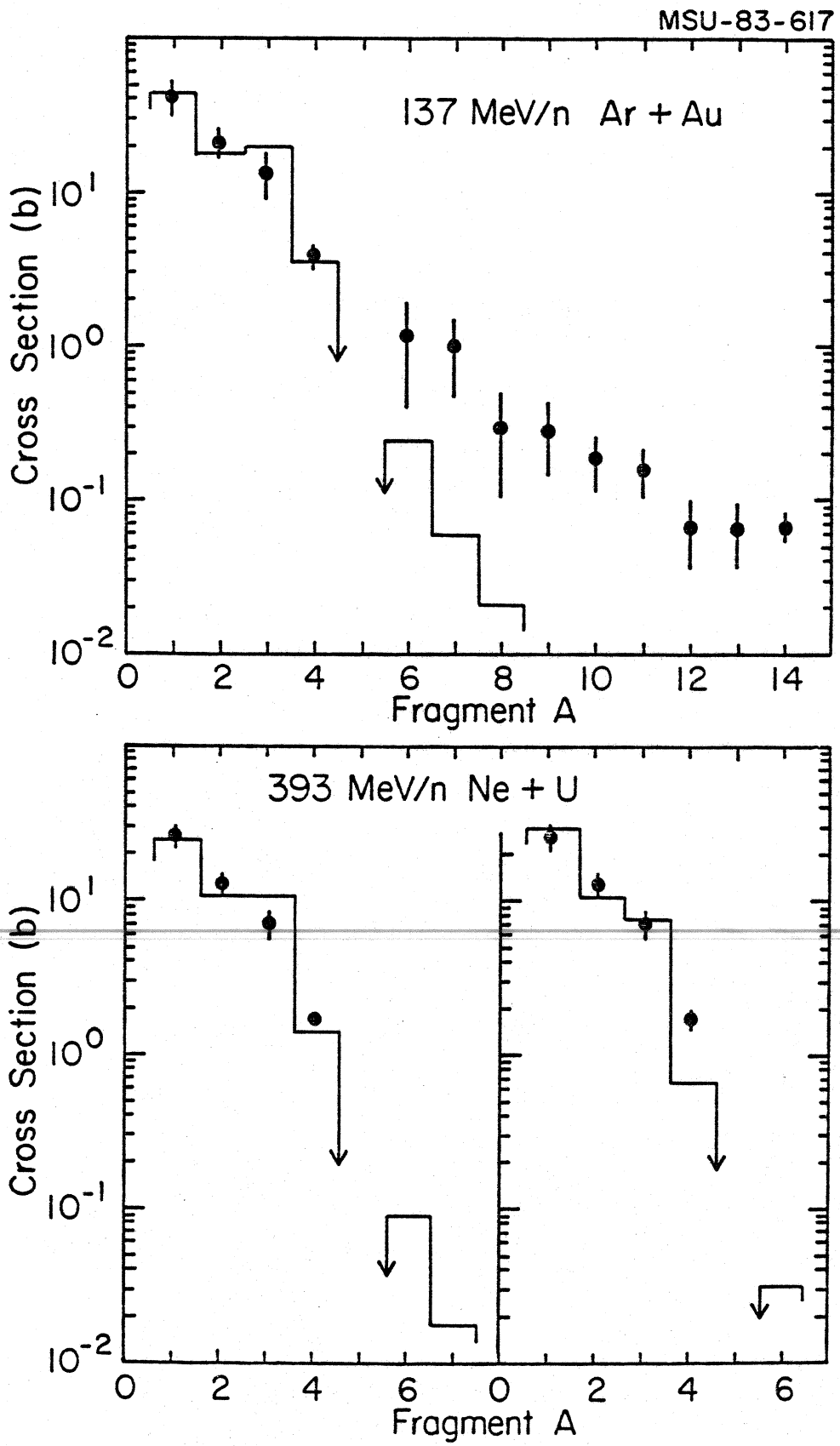
MSU-83-617
137 MeV/n Ar + Au
Cross Section (b)
10^{1}
10^{0}
10^{-1}
10^{-2}
0 2 4 6 8 10 12 14
Fragment A
393 MeV/n Ne + U
Cross Section (b)
10^{1}
10^{0}
10^{-1}
10^{-2}
0 2 4 6 0 2 4 6
Fragment A

Figure 62

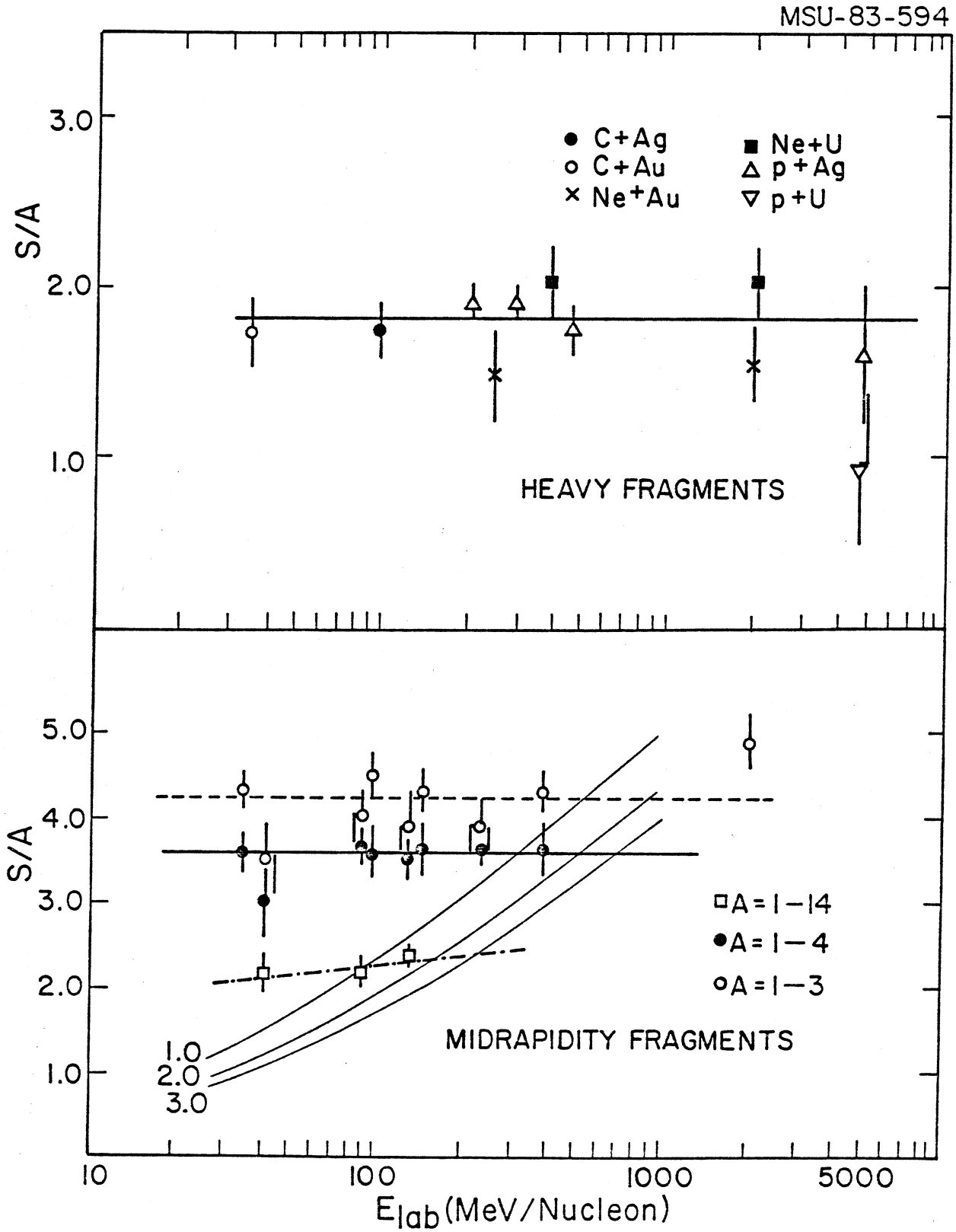
MSU-83-594
S/A
3.0
2.0
1.0
C+Ag
C+Au
Ne+Au
Ne+U
p+Ag
p+U
HEAVY FRAGMENTS
5.0
4.0
3.0
2.0
1.0
A=1-14
A=1-4
A=1-3
MIDRAPIDITY FRAGMENTS
1.0
2.0
3.0
10
100
1000
5000
Elab(MeV/Nucleon)

Figure 63

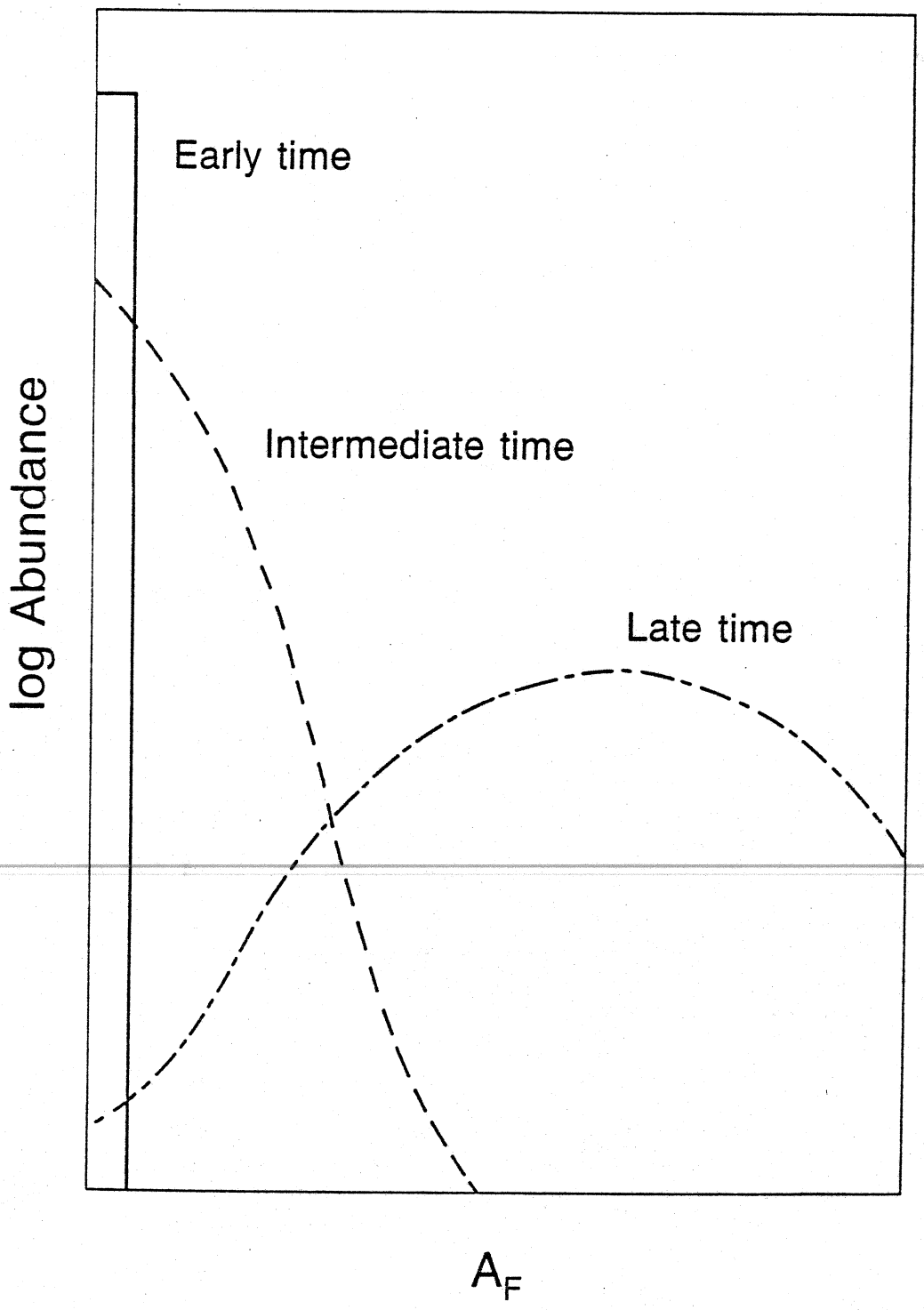
Early time
Intermediate time
Late time
log Abundance
A_F
XBL 838-3126

Figure 64

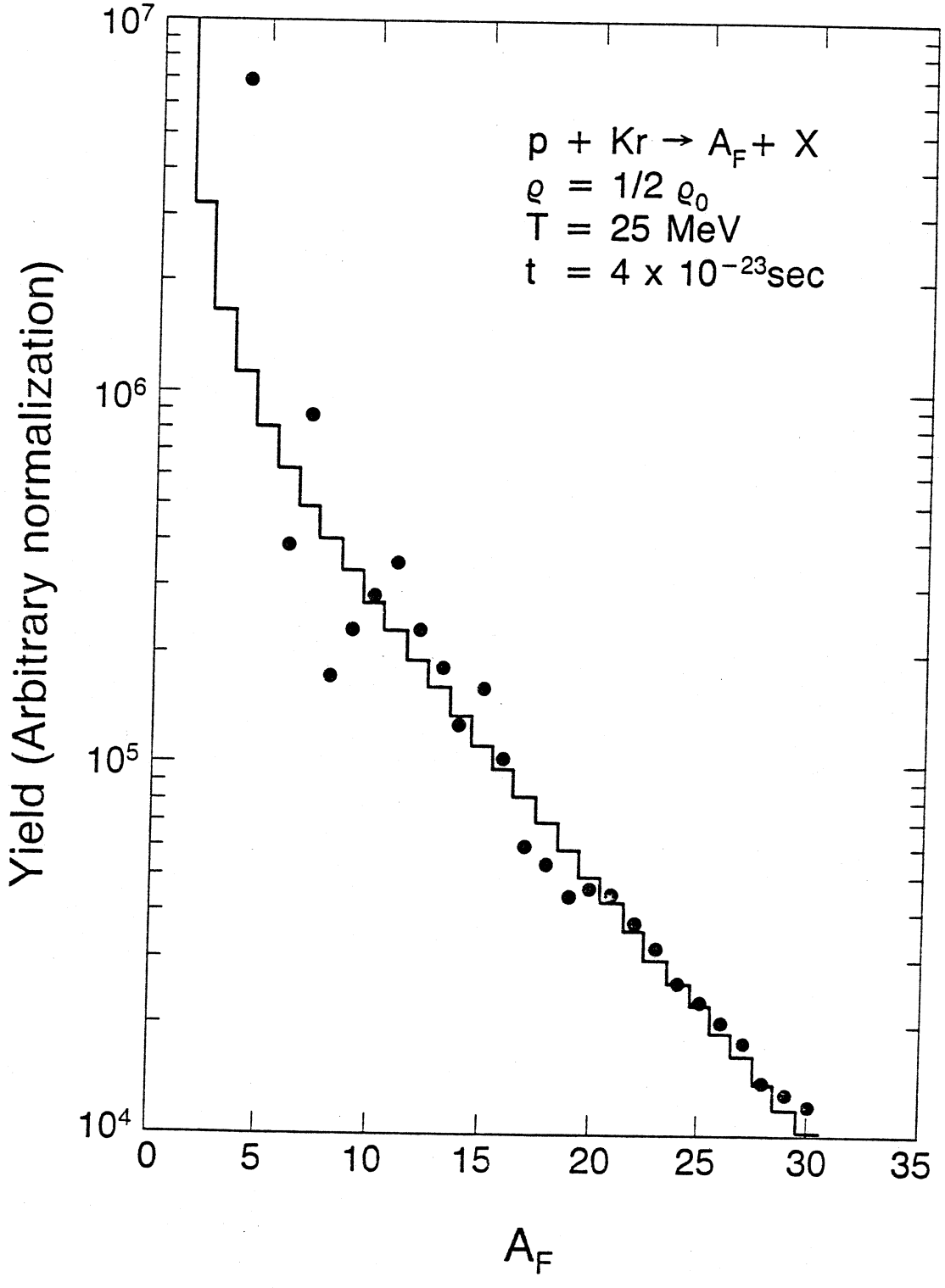
10^7
10^6
10^5
10^4
Yield (Arbitrary normalization)
p + Kr → A_F + X
ϱ = 1/2 $ϱ_0$
T = 25 MeV
t = 4 x 10^{-23}sec
0
5
10
15
20
25
30
35
A_F
XBL 838-3127

Figure 65

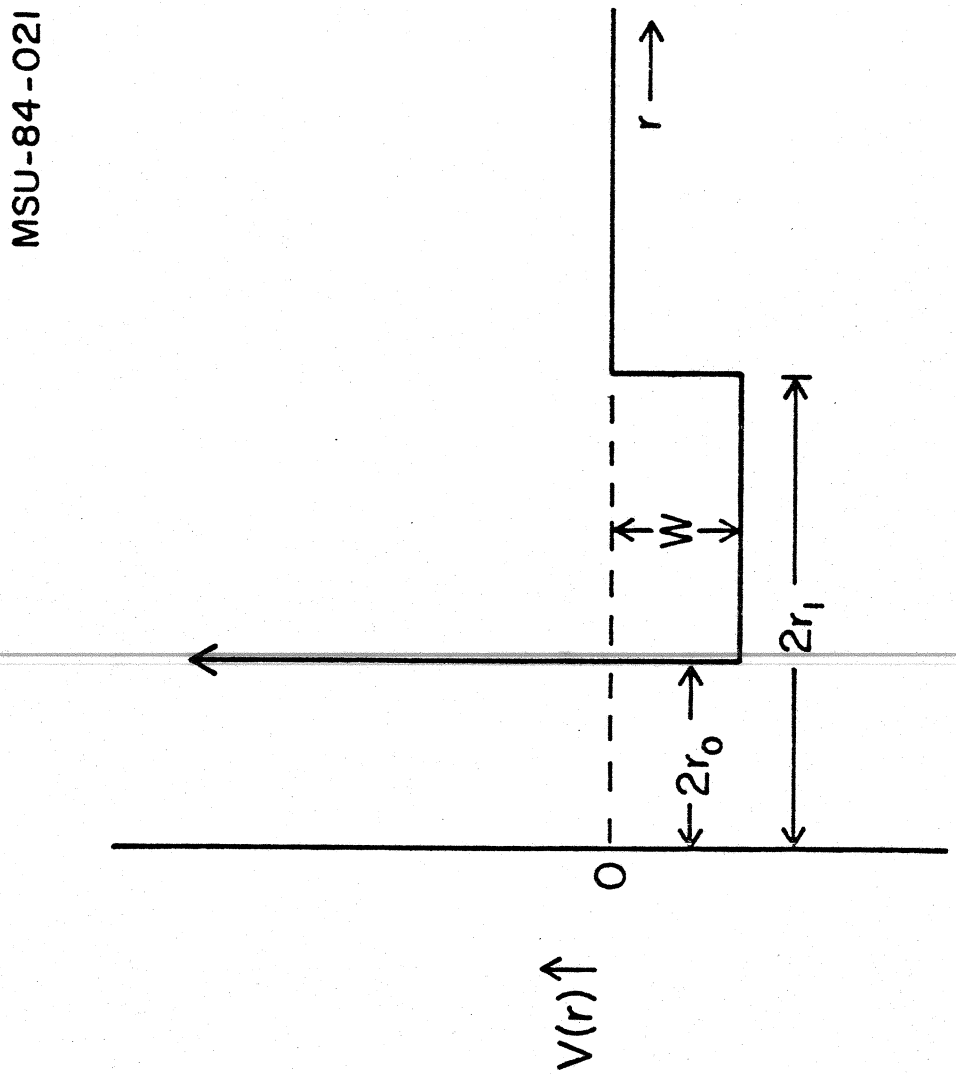

Figure 66

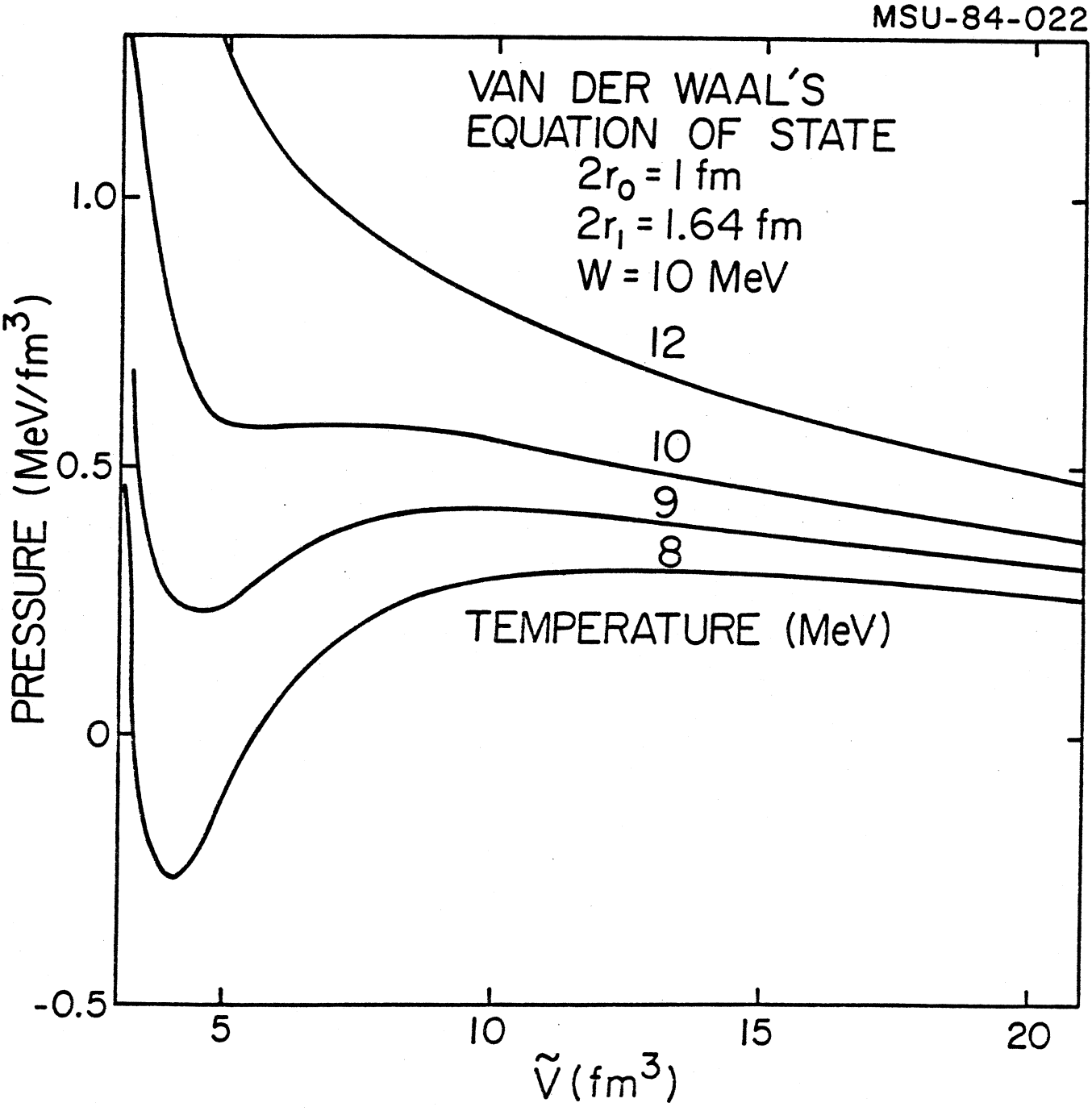
MSU-84-022
VAN DER WAAL'S
EQUATION OF STATE
$2r_0$ = 1 fm
$2r_1$ = 1.64 fm
W = 10 MeV
12
10
9
8
TEMPERATURE (MeV)
PRESSURE (MeV/fm^3)
1.0
0.5
0
-0.5
5
10
15
20
$\tilde{V}$ (fm^3)

Figure 67